Fatigue behaviour of glass fibre reinforced polyurethane acrylate.

Abidin, Mohd. Hanafiah Bin

FATIGUE BEHAVIOUR OF GLASS FIBRE REINFORCED POLYURETHANE ACRYLATE

By

Mohd. Hanafiah Bin Abidin
B.Sc. (Hons) (Malaya)
M.Sc. (Warwick UK)

Thesis submitted to the University of Wales for the degree of Doctor of Philosophy

September 2002

Department of Materials Engineering
Faculty of Engineering
University of Wales Swansea
Swansea

DECLARATION AND STATEMENTS

DECLARATION

This work has not previously been accepted in substance for any degree and is not being concurrently submitted in candidature for any degree.

Signed _____(candidate)
Date 1/9/2002

STATEMENT 1

This thesis is the result of my own investigations, except where otherwise stated. Other sources are acknowledged by footnotes giving explicit references. A bibliography is appended.

Signed _____(candidate)
Date 1/9/2002

STATEMENT 2

I hereby give consent for my thesis, if accepted, to be available for photocopying and for inter-library loan, and for the title and summary to be made available to outside organisations.

Signed _____(candidate)
Date 1/9/2002

ACKNOWLEDGEMENTS

I would like to express my special appreciation to Dr. D. H. Isaac who served as supervisor during the course of this work. His continuing support, expert supervision and reliable advice were essential ingredients in the successful completion of this research study.

I wish to thank to Dr C. Arnold and Dr M. Bache for their help and good advice, Mr. J. Morgan and all technical staffs who have provided vital back up especially to Mr. B. Watkins for his help with the fatigue machine and to SEM experts, Mr. A. Brooks and Mr. P. Davies for their help with my microstructural work.

I would also like to express my gratitude to the Universiti Teknologi MARA, Malaysia for providing the financial support for the duration of this research programme.

I would also to thank Mr. T.Yakub, Mr I. Badri, Mr. S. Som, Mr. C. Jusoh, Mr. S. Fauzi, Mr. Z. Samicho and Mrs. Teh Ah Kau for their advice, help and supporting me through writing-up the thesis.

Finally, I am indebted to my beloved wife Najemiah Amir Husin and my beloved children Mohd. Nazri, Nazliah, Muhammad Nazreen, Muhamad Nazmi and Nursyafinaz, without whose patience, love encouragement and constant support this postgraduate study might never have been completed. I, therefore, gratefully dedicate this thesis to them.

ABSTRACT

A comprehensive study of the fatigue behaviour of a polyurethane acrylate resin and glass fibre reinforced composites has been undertaken.

In the first part, three types of resins were tested: polyurethane vinyl ester, polyester and polyurethane acrylate, which was formulated to have superior properties. Three different types of glass fibre cloth were used for reinforcement, a woven roving and two novel stitch bonded Ulticloths. The $[0/90]_{2S}$ and $[\pm 45]_{2S}$ lay-ups were prepared in order to investigate the effects of matrix, cloths and lay-up on fatigue strength and life time. Polyurethane acrylate composites proved to be superior to the polyester resin. The study on damage mechanisms also showed that the first damage was matrix cracking followed by interfacial failure, debonding, delamination and fibre fracture which accumulate from the initial cycles until failure.

The second part of this study concentrated only on polyurethane acrylate resin reinforced with Ulticloth $[90/0]_{2S}$ and Biaxial Ulticloth $[\pm 45]_4$ lay-ups. The data were produced to compare the effect of environment such as air, distilled water and seawater on the composite with tension-tension and tension-compression loading. With the $[90/0]_{2S}$ lay-up the fatigue strength and lifetime were reduced by the presence of distilled water and seawater. Once again, during fatigue testing with R=0.1, microscopic observations showed that these composites suffered severe damage. Samples tested in seawater had more damage compared with samples tested in air and distilled water.

The last part of this research was to investigate the modulus degradation during the fatigue life. This investigation revealed that the modulus degradation on all laminates was dependent on stress ratio and lay-up. The modulus of $[90/0]_{2S}$ lay-ups was degraded during fatigue tests and this modulus degradation curve could be divided into three stages. The most clear damage occurring in $[\pm 45]_4$ was delamination which happened at both types of stress ratio, R=0.1 and R=-1. Analysis of some microscopic fractography has been carried out to support the observations.

CONTENTS

CHAPTER

1

INTRODUCTION

Composite materials are gaining increased recognition as materials suitable for both structural and non-structural components. The applications of polymer composites have increased for a number of reasons. These include: reduced cost due to part consolidation and lower tooling investment, reduced weight due to high strength and stiffness to density ratio, and increased design freedom compared with metals.

Composites are currently in use in a number of automotive structural components and marine/boat building components. Due to high strength and stiffness to density ratio, composites also have been used in aerospace industry components. These components, along with other potential applications of structural composites, can be exposed to fatigue loading. An understanding of fatigue behaviour of polymer composites is necessary to ensure that structural components are properly designed. The superior strength and stiffness of composite materials can be used to full advantage in structural applications only when the behaviour of these materials under different loading and environmental conditions is properly understood. Several major damage mechanisms initiate, grow, and interact to alter the state of the material, change strength, and define life. The amount of damage activity, the chronology of damage

events, the interaction of damage mode, and the cumulative effect on stiffness, strength, and life are dependent on material system, geometry, loading, and environment.

The ability of a composite structure to satisfy performance requirements will be affected by damage induced by cycling loads. Damage, as used here, is a generic term, which describes the collective state of individual damage modes in composites, including matrix cracks, fibre matrix debonds, delamination, and fibre fracture. There is a great need to improve our understanding of relationships between loads, materials properties, damage, and long-term performance of composite materials.

This project sets out to characterise the fatigue behaviour, fractographic features and damage mechanisms in polyurethane acrylate matrix composites under tension-tension and tension-compression loading. It has also looked at the effects of different fibre lay ups and various environments so as to examine the microstructure of the laminates with particular emphasis on matrix morphology and fibre lay-up. The other investigation in this research was to identify and monitor the modulus degradation accumulation during fatigue.

CHAPTER

2

REVIEW OF LITERATURE

2.1 INTRODUCTION

A fibre-reinforced composite is not simply a mass of fibres dispersed within a polymer, metal, or ceramic matrix but consists of fibres embedded in or bonded to a matrix with distinct interfaces between the two constituent phases. The fibres are usually of high strength and modulus and serve as the principal load carrying members.

In considering the formulation of a composite material for a particular type of application, it is important to consider the properties exhibited by the potential constituents. The mechanical properties of particular interest are the stiffness, strength and toughness. Density also has a great significance in many situations, since the mass of the component may be of critical importance.

Glass fibre reinforced polymer (GRP) laminates consist of glass fibres embedded in polymer matrix. These materials are ideal for building the hull and superstructure of

marine vessels because they are relatively easy to fabricate, are not prone to corrosion or degradation by marine organisms, and have lightweight combined with high strength and stiffness.

2.1.1 The description of laminates

Continuous fibre composites are highly anisotropic, so optimum mechanical properties can be achieved if all the fibres are aligned in one direction and these properties decrease rapidly in directions away from the fibre direction. A laminate is fabricated by stacking a number of thin layers of fibres and matrix, and consolidating them into the desired thickness. Fibre orientation in each layer as well as the stacking sequence of various layers can be manipulated to produce a wide range of physical and mechanical properties. Therefore, the description of composite materials has to identify the construction of laminates, including ply orientation with respect to control axis and the number of such laminates [Cervenka (1988)]. A set of bracket [ ] indicates a repeated sequences while a numerical suffix indicates the number of times that the sequence is repeated. The suffix S indicates that lay up is symmetrical about central axis. For example, $[90/0]_{2S}$ indicates a stacking sequence of [90/0|90/0|0/90|0/90].

Symmetry about a central axis is very important to the construction of laminates from highly anisotropy products such as prepreg tape, otherwise, thermal stresses may cause distortion. All composites based on continuous fibres exhibit strong anisotropy, so that longitudinal properties or transverse properties must be defined in the description of basic mechanical properties of composites.

2.2 FACTORS WHICH DETERMINE COMPOSITES PROPERTIES

There are a lot of factors which determine composite properties. These various factors can have large effects on the mechanical and physical properties of composites. Properties of composites are strongly influenced by the properties of their constituent materials, their distribution and the interaction among them. The static properties of these materials have been studied widely [Hitchen et al. (1995)]. Factors such as the

fibre length and orientation, the individual properties of the fibre and matrix, and the behaviour of the fibre-matrix interface have being shown to influence the mechanical behaviour.

2.2.1 Fibres

A great majority of materials are stronger and stiffer in the fibrous form than as a bulk material. According to Jang (1994), the well-known rule of mixture equation can be applied to a unidirectional continuous fibre composite to give:

$$Ec = E_f V_f + E_m V_m \tag{2.1}$$

For an advanced fibre composite, where,

$$E_m << E_f \text{ and} \tag{2.2}$$

$$V_f \geq V_m \tag{2.3}$$

Equation 2.1 can be written as:

$$Ec \approx E_f V_f \tag{2.4}$$

where E_C is the modulus of the composite, E_m the modulus of the matrix, E_f the modulus of the fibres and V_m and V_f the volumetric fraction of the matrix and the fibres respectively. This suggests that the longitudinal modulus of a unidirectional composite is practically dictated by axial modulus of the fibres.

For discontinuous fibre composites, a high fibre aspect ratio (length: diameter ratio) permits very effective transfer of load via matrix material to the fibres, thus taking advantage of their excellent properties. Therefore, fibres are very effective and attractive reinforcement materials. The structure and properties of the fibre play a major role in the mechanical and physical properties of composite materials. A wide variety of fibres are available for use in composites. Composites can differ in the amount of fibre, fibre type, fibre length and fibre orientation. Fibre is available in a wide range of sizes. Diameters of commonly used fibres vary from a few microns to more than one hundred

micron. Fibre lengths range from long continuous fibres through chopped short fibres to sub-micrometer whiskers. The most commonly used fibres in polymer matrices are various types of carbon, glass, and aramid fibres. Boron fibres are expensive and are used currently in military and aerospace applications only. Alumina, silicon carbide, mullite, silicon nitride and other ceramic fibres and metal wires also still in limited use. Many of these fibres can be fabricated with a wide range of properties. The unique combinations of properties available in these fibres provide the outstanding structural characteristics of fibre reinforced composites [Jang (1994)].

Although glass is the most widely used reinforcement for polymers in general, both carbon and aramid are employed to obtain composites with different characteristics which are required for certain applications. Fibres, since they cannot transmit loads from one to another, have limited use in engineering applications. When they are embedded in a matrix material, to form a composite, the matrix serves to bind the fibres together, transfer loads to the fibres, and protect them against environmental attack and damage due to handling.

The fabrication and properties of composites are strongly influenced by the proportions and properties of the matrix and the reinforcement. The proportion can be expressed either via weight fraction, which is relevant to fabrication, or via the volume fraction, which is common in property calculations. Fibre orientation directly affects the distribution of load between the fibres and the matrix. The contribution of the fibres to the composite properties is maximum only when they are parallel to the loading direction [Denial and Ishai (1994), Echtermeyer et al. (1991)].

A large variety of fibres are available as reinforcement for composites. The desirable characteristic of most reinforcing fibres are high strength, high stiffness and relatively low density. Glass fibres are the most commonly used ones in low to medium performance composites because of their tensile strength and low cost. They have a somewhat limited high performance in composite applications because of their relatively low stiffness, low fatigue endurance, and rapid property degradation with

exposure to severe hygothermal conditions. David and Jamie (1982) concluded after extensive investigations that, high modulus fibres such as graphite and aramid exhibit outstanding fatigue properties in unidirectional composites. This is because matrix strains in these composites are very low, resulting in fatigue performance almost totally dominated by the fibres.

Most glass fibres are based on silica (SiO_2), with additions of oxides of calcium, boron, sodium, iron and aluminium. These glasses are usually amorphous, although some crystallisation may occur after prolonged heating at high temperatures, leading to a reduction in strength. Hull and Clyne (1996) noted that the strength of the glass fibres depends on processing conditions and test environment. The strength falls in humid air, owing to the adsorption of water on the surface.

To obtain the best performance from a fibre, it is necessary:

(i) That the fibres act co-operatively and that stresses can be transferred into and out of the fibres.
(ii) To protect the fibres from damaging one another and from moisture and chemical attack.
(iii) To keep the fibres in the positions required giving desired performance.
(iv) To provide resistance to shear and transverse stresses.

2.2.2 Matrix

The matrix materials in fibre composites are extensive and varied in properties. The most common polymers used in high performance fibre composites are thermosetting resins converted from low molecular weight species, with low viscosity, to three-dimensional cross-linked networks that are infusible and insoluble. Cross-linking can be accomplished with the application of heat and or by chemical reaction. Thermoplastic polymers, although used to a lesser extent, are gaining increasing acceptance in composite applications. Metal matrix composites have been tested with many metals,

but the most important are aluminium, titanium, magnesium, and copper alloys. Ceramic-based composites are particularly suitable for applications where elevated temperature or chemical stability is a concern.

The matrix acts as a load transfer medium between fibres, and in less ideal cases where loads are complex, the matrix may even have to bear loads transverse to the fibre axis. Since the matrix is generally more ductile than the fibres, it is the source of composite toughness. The matrix also serves to protect the fibres from environmental damage before, during, and after composite processing. In composites, both fibres and the matrix largely retain their identities and yet result in many properties that cannot be achieved with either of the constituents acting alone.

The characteristics of the cure process and the final properties of thermosetting polymeric composites are strongly influenced by the properties of the matrix. One of the most critical variables is the resin viscosity, which can vary with temperature, flow conditions and time owing to complexity of the molecular distribution of the thermosetting macromolecules.

A suitable matrix material requires several properties including the ability to infiltrate between the fibres without disturbing their position or causing physical damage and to solidify when required, the ability to bond to the fibre but not interact chemically in such a way that the fibre or matrix is weakened or a definite interface is created, a low specific gravity, high toughness and good fatigue characteristics.

In a previous study [Sloan and Seymour (1992)], the influence of various polyester and vinyl esters on the fatigue properties of composites was investigated. Polymers are the most widely used matrix materials for fibre composites. Their chief advantages are low cost, easy processing ability, good chemical resistance and low specific gravity. On the other hand, low strength, low modulus, and low operating temperatures limit their use. For general use, the polymers tend to be thermosetting resins such as epoxies, phenolics, melamine or polyesters due to the ease of processing of these materials.

Polyester resins are relatively inexpensive and have low viscosity, which is a benefit in many fabrication processes.

A polyester resin is unsaturated polyester dissolved in a polymerisable monomer. Unsaturated polyesters are long chain linear polymers containing a number of carbon double bonds. They are made by a condensation reaction between a glycol (ethylene, propylene, and diethylene glycol) and an unsaturated dibasic acid (maleic or fumaric). The polymerisable monomer such as styrene, which also contains carbon double bonds, acts as a crosslinking agent by bridging adjacent polyester molecules at their unsaturation points. The monomer also acts as a diluent, reduces viscosity, and makes it easier to process. The curing or crosslinking process is initiated by adding a small quantity of a catalyst such as organic peroxide or an aliphatic compound. Since there is no by-product of the reaction, the curing is done at room temperature or elevated temperature with or without application of pressure. A typical polyester resin made from the reaction of maleic acid and diethyene glycol is shown below:

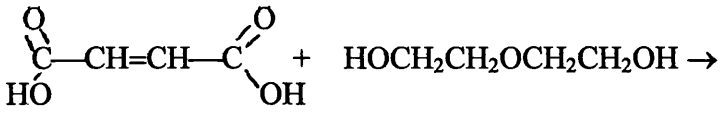

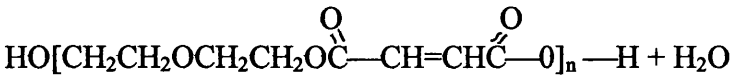

The length of the molecule or degree of polymerisation may vary. The resin will generally be a solid but is dissolved in a monomer such as styrene. The solution viscosity can be controlled by the percent styrene and is generally quite fluid. The conversion from liquid to solid occurs through the use of a free radical initiator or curing agent. The styrene monomer cross-links or reacts with the double bond in the polyester backbone to form a network polymer. The reaction does not produce a by-product and is an exothermic reaction. In the last few years, thermoplastics such as

poly(aryl-ether-ether-ketone) (PEEK) have also been used as matrix materials in fibre reinforced composites, due to their greater toughness.

Many resin manufacturers have sought to improve the performance of matrix materials. The principal goal has been increased toughness without detriment to the high temperature properties, particularly after moisture absorption. This had led to improvements in static strength, but usually poorer fatigue behaviour [Matthew and Rawlings (1994)].

The type of matrix used depends on the desired properties of the composite. Ceramics are potentially high strength materials, which retain their strength at very high temperatures. Unfortunately, they are very brittle and highly notch sensitive and are usually reinforced in an effort to increase their toughness. The most common reinforced ceramic systems are silicon carbide reinforced glass for high temperature applications such as turbine blades and fibre reinforced cement for use in the building industry, with fibres ranging from asbestos to combinations of glass and carbon. Metals in general have a greater ductility and toughness than ceramics although their temperature resistance is lower. They also tend to have high strengths and their properties without reinforcement are sufficient for most structural applications, although metal matrix composites (MMC) are becoming more widely used.

Polymers are the preferred matrix materials due to their low densities, good chemical resistance, relatively low cost and ease of processing, although their temperature resistance is low. There are two types of polymers: thermoplastics and thermosets. Thermoplastics have greater toughness but due to their high molecular weight and molecular entanglements, are difficult and expensive to process. Thermosets are more brittle from the crosslinks that occur between polymer chains on solidification, but easier to process. The most common polymer matrices are three thermosetting resins; polyesters, epoxies and phenolics. Each resins type has advantages and disadvantages associated with its chemical nature and they therefore tend to be used in distinct areas. Polyester resins are very versatile and impart to fibre composites a variety of favourable properties at moderate cost. They are used mainly where a good balance is

required between mechanical properties and chemical resistance at moderate or ambient temperatures. Their disadvantages are:

- Relatively high shrinkage on curing.
- Sensitivity to some solvents and chemicals especially under alkaline conditions.
- Appreciable water absorption under certain conditions.

Epoxy resins have good adhesion characteristics with aramid, glass and carbon fibres resulting in remarkable success as the matrix in composites. They also have a good balance of physical, mechanical, and electrical properties and have a lower degree of cure shrinkage than other thermosetting resin. Other attractive features for composite application are relatively good hot/wet strength, chemical resistance, dimensional stability, and ease of processing and low material costs. Epoxies may be more expensive than polyester resins and may not perform as well at elevated temperatures.

Cyanate ester resin matrix composites reinforced with glass or aramid fibres established their presence in the application for multi-layer electric circuit boards as early as the late 1970s. The use of cyanate ester resins was led by the following considerations [Connell (1992)]:

- their glass transition temperature (Tg) which exceeds those of epoxy resins and matches molten solder temperature (220-270°C).
- low dielectric loss properties
- excellent (epoxy-like) processability.

Lee and Holl (1996) reported that currently available cyanate ester resins for structural composites offer a desirable combination of high resistance to moisture absorption, reasonably good fracture toughness, and acceptable processability. In the case of epoxy resin matrix composites, moisture absorption has been shown to relieve the residual stresses by matrix swelling and temporarily increase the resistance to matrix/interface cracking [Lee et al. (1978), Haener et al. (1979)].

A wide spectrum of chemical compositions and microstructural arrangements are possible in each matrix category. All the fibres can be incorporated into a matrix either in continuous lengths or in discontinuous lengths. The features of low fibre density and high strengths and moduli with specific matrices give rise to high strength and specific stiffness properties of composites.

The property requirements for a matrix material are different than those for reinforcement. Since the fibres must serve as the principal load bearing members in a composite, they must be of high strength and stiffness. With some exceptions, reinforcement fibres are usually of low ductility. In contrast, matrix materials usually have relatively low modulus and strength values and comparable or higher ductility values. When the composite is under a compressive load, the matrix also plays a critical role in avoiding micro buckling of fibres, a major compressive failure mechanism in continuous fibre composites. The matrix provides the composite with interlaminar fracture toughness, damage tolerance, and impact resistance.

Jang (1994) suggested that when selecting a particular resin for a specific composite application, service environment parameters such as temperature, stresses, moisture, chemical effects, and possibly radiation dosage must be considered. The processability and the processing history of the matrix must be taken into account, since it directly influences the formation of flaws and microstructure in the matrix, residual stresses, and fibre matrix interface. These factors ultimately determine the properties of a composite. In practical fibre composites, the proportion of fibre present will vary between about 10% (in dough compounds) and 70% (in high performance composites), and crack resistance effects directly attributable to the matrix material may not be significant except perhaps in composites reinforced with relatively low volume fractions V_f of short fibres. However three specific effects might be listed:

- The effective toughness of a non-brittle matrix, such as thermoplastic, will be reduced by the presence of a high V_f.

- The effective toughness of a low toughness, flexible matrix may be increased by the presences of low V_f
- The effective toughness of low toughness matrix may be increased by the presence of fibres as a result of the slowing up of crack growth in the neighbourhood of the filler.

2.2.3 Interfaces and interphases.

Interface and interphase are defined as regions where the fibre and matrix phases are chemically or mechanically combined or otherwise indistinct. The properties of a composite depend critically on the microstructure and properties of the interface and interphase between the fibre and the matrix. Leach and Grover (1982) noted for thermosetting matrix composites, a weak interface between the matrix and reinforcement is deliberately designed to optimise the toughness. The structure and properties of the fibre-matrix interface play a major role in the mechanical and physical properties of composite materials [Cox (1952), Kelly and Tyson (1965), Hull (1981), Swain (1992)]. Although the properties of a composite depend on the properties of the fibres and the matrix, it is increasingly being recognised that the fibre-matrix interface region also plays an important role in defining the composite properties. The strength of the interface determines how much of the applied stress can be transferred to the load bearing fibres and this interfacial strength is largely determined by the degree to which the fibres and matrix are intimately contacted and the level of adhesion at those contact points. The load acting on the matrix has to be transferred to the reinforcement via the interface. The reinforcing fibres must be strongly bonded to the matrix if their high strength and stiffness are to be imparted to the composite. The interfacial condition controls the propagation mode of microcracks at the fibre ends. When a strong bond exists between the fibre and matrix, the cracks do not propagate along the length of the fibres.

Stress can only be transferred across an interface between two materials if they are in intimate molecular contact, separated only by about the same distance as the

molecules inside bulk materials. A mass of indirect evidence already cited [Parkyn (1970)] suggests that properties of composites, particularly mechanical properties are often limited by failure at the interface, and this is supported by direct evidence of separation at the interface by visual observation, light microscopy and electron microscopy.

Moisture induced interfacial failure is often cited as the culprit for this degradation. Interfacial degradation however, can also lead to enhanced crack growth resistance due to fibre bridging [Sloan and Seymour (1992), Chiou and Bradley (1995)]. Recent experimental results [Subramaniam et al. (1995)] indicate that the region near the fibre surface, called the interface, could possess elastic properties that are significantly different from those of the bulk matrix material. Small changes in properties of the interface could lead to significantly altered fatigue performance. Subramaniam et al. (1997) have shown that by varying the local properties at the fibre matrix interface level, the fatigue life can alter significantly. They have also reported on varied damage mode and failure mechanisms in cross ply laminates, which have the same fibre and matrix, but different fibre-matrix interface.

The bond between the fibre and matrix is of prime importance to the performance of composite materials since this controls stress transfer to, and distribution between, the fibres. It also governs mechanisms of damage accumulation and propagation [Mashall (1991)]. It is clear from the experience reported [Reifsnider (1994)] here, and from much additional information in the literature, that the interphase region between the fibre and matrix in continuous fibre reinforced composites can greatly alter strength and life, even for properties normally thought of as 'fibre controlled'.

The interface has a strong influence on the properties of composite materials. An important consideration in the design of a composite material for any application, but particularly in aerospace, is its reaction to the environment to which it will be subjected in service. However, environmental studies have primarily considered prepregs or laminates. It has been shown that long-term exposure to high temperature and humidity

degrades the composite by plasticising the matrix, thus degrading the mechanical properties. Also the interface can be damaged. Buxton and Baillie (1994) have studied the debonding that occurs more easily with a pre-soak in water.

2.2.4 Voids

The void content of a composite may significantly affect some of its mechanical properties. Higher void contents usually mean lower fatigue resistance and greater susceptibility to water penetration and weathering. Good composites should have less than 1 % voids, whereas a poorly made composite can have as much as 5% void content.

Voids can be found in composite materials in many shapes and sizes and there are two principal causes. The first is air entrapment in the composite during the initial manufacturing stage, due either to air bubbles being trapped in viscous resin formulations during their preparation or to poor wetting of the filaments. Poor wetting tends to be aggravated by high viscosity resins, which make it difficult for the matrix to penetrate bundles of fibres and displace all the air. Secondly, voids may be formed by volatile components or contaminants, which vaporise during the high temperature part of the composites, cure cycle. In fibre reinforced polymer composites these voids have been shown to reduce mechanical properties such as interlaminar shear strength, longitudinal and transverse strength and modulus and fatigue resistance [Thomason (1995a), Thomason (1995b)]. The theoretical analysis of Woo and Piggott (1988) indicates that voids have diffusivity 15 times greater than that of the composite matrix. Thomason (1995b) concluded that the major factor influencing water uptake in polymer composites was found to be the composite void content and the water absorption. Results also indicated that the density of the matrix is lowered by the presence of the glass fibres, perhaps because of the formation of an interphase region.

2.2.5 Fibre volume

Fibre volume fraction of composites is an important factor in determining the mechanical properties. The ultimate tensile strength of fibre composites in the longitudinal direction has traditionally been predicted by the rule of mixture more or less successfully. The basic approach is to consider the mode of failure of the composite, evaluate each contribution of the fibres and the matrix at the point of failure. The modulus of the composite is the sum of the contributions according to their relative volumetric proportions as mentioned earlier in Equation 2.1 stated:

$$E_C = E_f V_f + E_m V_m \tag{2.5}$$

If the composite has zero porosity, fibre volume fraction can be obtained from the density of the composite and the constituents by the following equation:

$$V_f = (\rho_c - \rho_m) / (\rho_f - \rho_m) \tag{2.5a}$$

Where ρ_c, ρ_m and ρ_f are the densities of composite, matrix and fibre respectively.

In order to have a reinforcing effect, the fibre volume has to exceed a certain critical proportion depending on the properties of the composite system. For most common composites this critical fibre volume is of the order of a few percent and is exceeded in all practical applications [Karam (1991)]. Evans et al. (1996) reported that an increase in fibre volume fraction significantly improves fatigue crack growth propagation resistance.

2.2.6 Environmental

Environmental influences, for example moisture absorption, can have a significant effect on the behaviour of polymers. Polyester resin can absorb up to 4-5% by weight of water if exposed to 100% relative humidity or immersed in water.

Moisture can also have a significant effect on most polymer matrix materials. There has been a growing interest in using fibre reinforced polymeric composites in offshore applications where long term durability in a marine environment is essential. To realise the full potential of polymeric composites in marine applications, it is important to develop a better understanding of the magnitude and mechanisms of seawater degradation. Fibre reinforced polymer matrix composites, which form various structural components of aircraft, are subjected to a complex history of temperature, moisture and other environmental conditions. Their effects, particularly the effects of moisture absorption and thermal cycling have been extensively studied since the early 1970s [Thomason (1995b), Lee and Holl (1996)]. According to Morgan (1987) the most critical performance deterioration mechanisms for carbon and Kevlar 49 fibres used in high performance polymer matrix composites are their decrease in strength with increasing temperature and in the case of Kevlar 49 fibres, moisture induced physical and chemical modifications.

Absorption of moisture in composites can result in plasticisation of the matrix, swelling, and degradation of the fibre-matrix interface. Water absorption has been shown to lead to a general reduction in the mechanical properties of composites and this has been attributed, in part, to degradation of the fibre-matrix interfacial bond [Lee and Peppas (1983), Ishai (1975), Mashall et al. (1982)]. These mechanisms can lead to reduced static loading performance and, hence, reduced fatigue performance of the composites. The effects of moisture are more severe for matrix dominated fatigue conditions than for fibre dominated fatigue. A gaseous or liquid environment may produce profound changes in properties of composite materials. Exposure to any

chemical, which can attack the polymer matrix material or the fibre-matrix interface, can also have an effect on fatigue performance [David and Jamie (1982)]. Mac Kague et al. (1975) found that absorbed moisture can have undesirable effects upon epoxy matrix composites, and some of these effects have been documented.

Moisture is absorbed directly from the atmosphere. When exposed to constant temperature/constant humidity conditions, moisture is absorbed at a rate determined by the exposure temperature. Accelerated environmental testing of materials is commonly used to enable completion of tests within a short time frame. However, it is often found that accelerated testing does not reveal the true long-term behaviour, or even provide the correct ranking of candidate materials [Chester and Baker (1996)]. The main environmental attacks are related to temperature, moisture, radiation and contact with various types of chemicals [Selzer and Friedrich (1997)]. These factors can affect the thermal and mechanical properties of the composites in different ways. Several investigations in the open literature verify that moisture influences the properties of reinforced polymers, but such studies only look at some basic mechanical properties. In the research carried out on three carbon fibre reinforced polymers: two with toughness-modified epoxy and one with a thermoplastic matrix, poly(aryletheretherketone) (PEEK), in water baths of different temperature, Selzer and Friedrich (1997) reported that the properties of epoxy-based composites were influenced by the absorbed moisture only in specimens in which fibres were orientated perpendicular to load direction. The values for CF/PEEK were not affected by moisture, which can be explained by the low moisture uptake of the PEEK matrix. They also found that the water temperature had no influence on mechanical properties of the material used.

The problem of moisture absorption in materials has received attention in experimental studies on composite systems as well as from the theoretical point of view. In the case of glass fibre reinforced epoxy composites it has been shown that the sensitivity of certain mechanical properties to water can be reduced by the use of organosilane coupling agents as a fibre treatment [Emadipour et al. (1982),

Plueddemann (1982), Boudreau (1982)]. Many researchers reported that the aims of their research were [Chester and Baker (1996)]:

- to determine the equilibrium moisture absorption level of the composite material,
- to examine the environmental durability of the materials used and
- to investigate the influence of exposure and type on the environmental durability.

Intensive research work was performed to introduce new thermosetting resins with a reduced tendency of moisture absorption without penalising the processability. One important example of the achievement in this direction was the synthesis of polycyanurate, or so-called cyanate ester, which was reported by Wolff (1993) to exhibit an equilibrium level of water absorption as low as 0.7% at 100°C.

Thomason (1995a) noted that water absorption in polymers is often analysed in terms of Fickian diffusion, which requires that the results be plotted as weight gain (as a percentage of dry weight) versus square root of time. Moisture diffusion behaviour of fibre-reinforced composites can deviate from Fick's law for the following reasons:

(1) the development of cracks or delamination altering the structure of the material
(2) moisture propagation along the fibre-matrix interface,
(3) voids in the matrix, and
(4) non-Fickian behaviour of the matrix itself without defects.

The microscopy study showed that the composite specimens in the dry state are virtually void free and well compacted. However, on exposure to moist-heat for 50 days, the composite underwent extensive cracking of the matrix/interface region. The damage took the form not only of delamination between the plies, but also translaminar cracking within plies. Weakening of fibre-matrix bonding has been confirmed by the failure analysis in conjunction with the decrease of in plane shear strength of the composites. This was confirmed based on SEM [Lee and Holl (1996)].

In seawater environments composite structures are subjected to moisture absorption and fatigue wave loading. Springer (1981) cited that composite materials are known to exhibit some degree of degradation due to moisture absorption. Several studies have examined the fatigue performance of polymeric composites in seawater [Macabder et al. (1979), Sandifier (1982), Dyer (1996)].

2.3 FABRICATION OF COMPOSITES

The fabrication or shaping of composites into finished products is often combined with the formation of the material itself during the fabrication process. The formation of the composite involves the combination of the matrix and fibre such that the matrix impregnates, surrounds, and wets the fibres. Fabrication and processing of composites is often done by conventional methods used in the plastics or metals industry. With regard to polymeric matrix composites, the processing methods for thermosetting matrix materials typically involves material formation during final moulding. In some cases, material formation is accomplished separately from forming or shaping, but because of the curing nature of thermosetting resins, final curing always occurs during final formation. In thermoplastic matrix composites, it is more common to form the composites first and form or mould a shape in a second operation. However, in this latter step, the composite properties can still be substantially influenced.

The choice of a fabrication process is strongly influenced by the chemical nature of the matrix and the temperature required to form, melt, or cure the matrix. The various composite forming and fabrication methods are described in the following sections.

2.3.1 Fabrication of Thermosetting Resin Matrix Composites

Thermosetting resin systems, by chemical reaction become hard when cured and further heating does not soften them; the hardening is irreversible. During curing they undergo a chemical change or reaction called polymerisation, the linking of monomer or prepolymers to form network polymers. This reaction is accomplished in the presence of catalysts or curing agents usually selected to give a desired combination of time and

temperature to complete the reaction suitable for a particular product. Further, the curing can be staged so that impregnation of composite forming can be accomplished separately from the final moulding process.

Fabrication processes for thermosetting resin matrix composites can be broadly classified as wet forming processes and processes using premixes or prepregs. In the wet forming processes, the final product is formed while the resin is quite fluid and the curing process is usually completed in one step. Compounding is done during forming. The wet processes include hand lay-up, filament winding, pultrusion, and bag moulding. In the processes using premixes, as the name suggests, compounding is separated from lay-up or moulding. Compounding is done to make such premixes as bulk moulding compounds, sheet moulding compounds, and prepregs. The matrix material in some of the premixes is thickened so that it is tack free or slightly tacky, does not flow, and can be handled easily. Thickening is achieved by the use of a thickening agent and by advancing the cure of the resin. In the latter case, they must be stored and transported at low temperatures, typically 10-15°C. Premixes are subsequently used for product lay-up and final curing completed under heat and pressure. The use of premixes makes manufacturing more simple and increases the possibility of automation. High fibre volume fractions can be achieved with uniform fibre distribution.

2.3.1.1 Hand lay-up Technique

The hand lay-up technique is the oldest, simplest, and most commonly used method for the manufacture of both small and large reinforced products. A flat surface, a cavity (female) or a positive (male) shaped mould, made from wood, metal, plastics, reinforced plastics, or a combination of these materials may be used. Fibre reinforcements and resin are placed manually against the mould surface. Thickness is controlled by the layers of the materials placed against the mould.

This technique, also called contact lay-up, is an open mould method of moulding thermosetting resins in association with fibres, usually glass fibre mat, fabric, or woven

roving. A chemical reaction initiated in the resin by a catalytic agent causes hardening to a finished part. Hand lay-up techniques are best used in applications where production volume is low and other forms of production would be prohibitive because of costs or size requirements. Typical applications include boat and boat hulls, radomes, ducts, pools, tanks, furniture, and corrugated and flat sheets.

2.3.1.2 Bag Moulding Processes

Bag moulding is one of the oldest and most versatile of the processes used in manufacturing composite parts. The laminae are laid up in a mould and resin is spread or coated, covered with a flexible diaphragm or bag, and cured with heat and pressure. After the required curing cycle, the materials become an integrated moulded part shaped to the desired configuration.

The quality of part is dependent on the skill and know-how of the workers laying up and bagging the part. The size of a part that can be made by bag moulding is limited only by the curing equipment, specifically, the size of the curing oven or autoclave. The general process of bag moulding can be divided into three basic moulding methods: pressure bag, vacuum bag and autoclave. Vacuum bag and autoclave methods are used to produce most bag-moulded parts. Their main advantages are that the tooling is relatively inexpensive and the basic curing equipment can be used for an unlimited variety of shaped parts. The disadvantage of pressure bag system is that the tooling is relatively expensive because it is combined with the curing pressure system and can be used only for the specific part for which it is designed.

2.3.1.3 Filament winding

Filament winding is a technique used for the manufacture of surfaces of revolution such as pipes, tubes, cylinders, spheres, and is frequently used for the construction of large tanks and pipework for the chemical industry. High-speed precise lay down of continuous reinforcement in predescribed pattern is the basis of the filament winding

method. Continuous reinforcements in the form of rovings are fed from a multiplicity of creels. A creel is a metallic shelf holding roving packages at desired intervals and designed for pulling roving from the inside of the package. The reinforcement goes from the creels to a resin bath and may be gathered into a band of given width and wound over a rotating male mandrel. The winding angles and the placement of the reinforcements are controlled through specially designed machines, traversing at speeds synchronised with the mandrel rotation. The reinforcements may be wrapped in adjacent bands that will step the width of the band, and which eventually cover the entire mandrel surface. The technique has the capacity to vary the winding tension, wind angle, or resin content in each layer of reinforcement until the desired thickness and resin content of the composite are obtained.

2.3.1.4 Pultrusion

Pultrusion is an automated process for manufacturing composite materials into continuous, constant cross section profiles. This technique has some similarities to aluminium extrusion or thermoplastic extrusion. In pultrusion, however, the product is pulled from the die rather than forced out by pressure. A large number of profiles such as rods, tubes, and various structural shapes can be produced using appropriate dies. Profiles may have high strength and stiffness in the length direction, with fibre content as high as 60-65% by volume.

The pultrusion process generally consists of pulling continuous roving and/or continuous glass mats through a resin bath or impregnator and then into preforming fixtures where the section is partially shaped and excess resin and/or air is removed. Then it goes into a heated die where the section is cured continuously. The basic pultrusion machine consists of the following elements: (1) creels (2) resin bath or impregnator, (3) heated dies, (4) puller or driving mechanism, and (5) cut-off saw. A diagram of a pultrusion scheme is given in Figure 2.1

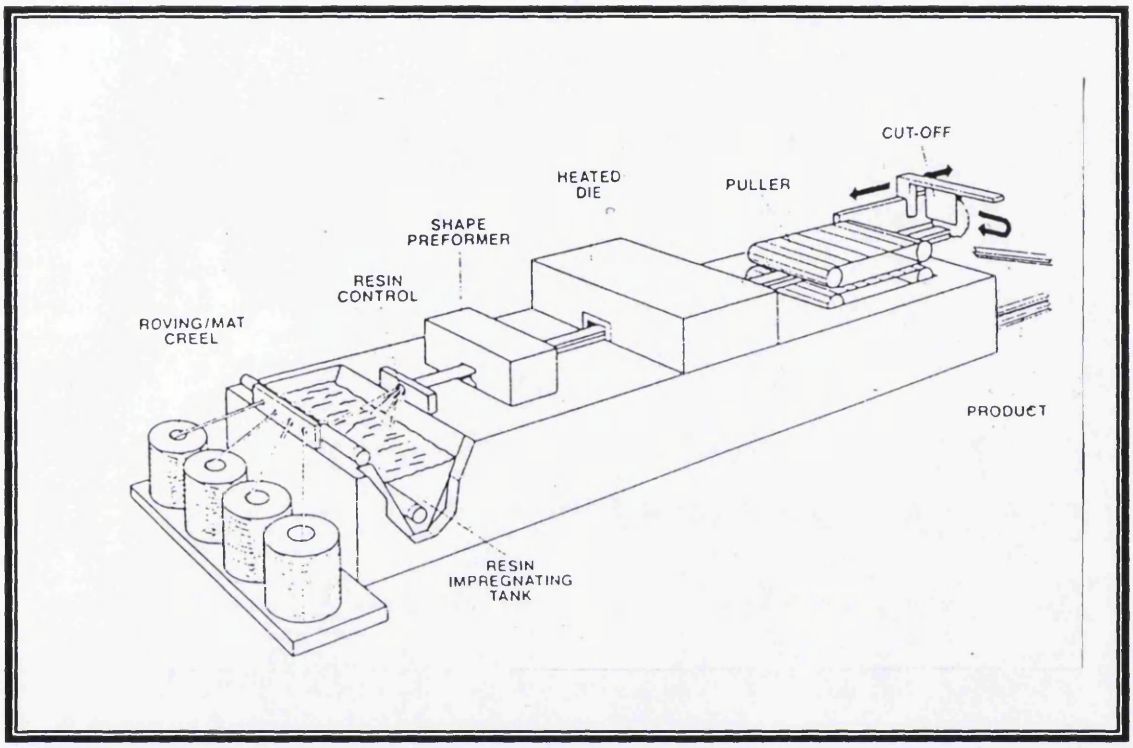

Figure 2.1: Pultrusion Scheme
[Bhagwan and Broutman (1990)]

The pultrusion process is most suitable for thermosetting resins that cure without producing a condensation by-product (polyester and epoxy). The reinforcement used consists of continuous fibres such as roving or chopped strand mat or a combination of the two, depending on the strength and rigidity required in the moulded profile. Thermoplastic resins may be used but special impregnation equipment is required in order to melt or soften the resin.

2.3.1.5 Preformed Moulding Compounds

A large number of reinforced thermosetting resin products are made by matched die moulding processes such as hot press compression moulding, transfer moulding and injection moulding. Matched die moulding can be a wet process but it is most convenient to use a preformed moulding compound or premix to which all necessary ingredients have been added. Moulding compounds can be divided into three broad categories: dough moulding compound (DMC), sheet moulding compound (SMC), and prepregs.

2.3.2 Fabrication of Thermoplastic Resin Matrix Composites

The principal method used for the production of parts with short fibre reinforced thermoplastics is injection moulding. The raw material used for injection moulding of reinforced thermoplastics is a moulding compound of the resin and fibres in a pelletised form. The compounding is carried out as a separate process prior to the injection moulding. The compounding method aims at achieving the following:

- Total enclosure of each fibre by the matrix
- Uniform dispersion of fibres throughout the matrix
- Low fibre breakage so that a high aspect ratio (fibre length: diameter) is maintained for effective stress transfer.

2.4 FATIGUE TESTING

2.4.1 The process of Fatigue

There have been many cases of catastrophic failure in engineering structures reported [Saib (1991)]. The phenomenon of fatigue is contributory in more than 80% of these, normally in conjunction with other processes such as creep or corrosion, depending on the application.

Fatigue failure can be defined as failure that occurs as a result of cyclic loading. The levels of stress imposed during fatigue are significantly lower than would be expected to cause static failure of the material. Fatigue is the process whereby mechanical damage, caused by repetitive or fluctuating stresses, results in a material failure at lower stress levels than would be required under static loading. Fatigue damage in isotropic metals typically occurs from the initiation and growth of a single crack, and thus damage is localised. Fatigue of composite materials differs from that of more isotropic metals in that the damage mechanisms are more complex, and may exhibit a synergistic damage effect from several micro-failure mechanisms. These multiple damage mechanisms can blunt the stress concentration effect of a notch or crack on the load bearing fibres, resulting in good fatigue behaviour of composites [Jang (1994)].

The damage that progresses during fatigue results in a reduction of laminate stiffness and load-carrying capability frequently observed in fatigued laminates. Many materials exhibit a fatigue limit for stress, and if this is not exceeded no fatigue failure of the material will occur. Because of their unique microstructure, composite materials may or may not have a fatigue limit depending on the material combination chosen. Fibre reinforced composites laminates can sustain fatigue damage by matrix cracking, fibre matrix debonding, ply cracking, delamination and fibre breakage. Fatigue of all materials depends upon a large number of important external variables. Three of these variables are most critical to the extent of fatigue damage. They are a maximum tensile

or compressive stress (or strain) of sufficient magnitude, a variation or fluctuation in the applied stress (or strain) cycles and stress ratio R (minimum load / maximum load). Other variables, which play a role in the extent of fatigue damage, include stress concentrations, temperature, environment, stress fluctuation frequency, overloading stresses, the material composition and structure, residual stresses and combined stresses.

Hitchen et al. (1995) studied the effect of fibre length on the fatigue of a random short carbon fibre/epoxy composite containing 1, 5, or 15 mm length fibres. All laminates gave a sloping S-N curve with longer fatigue lives obtained at decreasing peak stresses. They concluded that the fatigue life was independent of fibre length at any peak strain. According to Bhagwan and Broutman (1990) short fibre composites are less resistant to fatigue damage because the weaker matrix is required to sustain a much greater proportion of the cyclic load. In aligned short fibre composites, the fibre ends and weak interfaces can become sites for fatigue crack initiation. An important aspect of fatigue of short fibre composites is the local failures in the matrix and at the interface can destroy the integrity of the composite even though the fibres remain undamaged.

For the $[45/0/-45/90]_S$ carbon/epoxy laminate studied by Chiou and Bradley (1995), seawater absorption did not significantly reduce the maximum available strain energy release rate or accelerate the growth of edge cracking in fatigue. There is probably a moisture-induced degradation of the interfacial strength of the laminate.

According to Shah Khan and Mouritz (1996), fatigue performance for the stitched composite was degraded when the laminates were fatigued at relatively low cyclic stresses. This reduction was caused by fatigue failure of the stitch/GRP interfaces and by damage to the glass fibres incurred during stitching. Consequently, stitched laminates exhibit much shorter lives when subjected to in plane zero to tension fatigue loading.

2.4.1.1 The Types of Fatigue Testing

When considering fatigue testing, it is also essential to know how the test was performed [Jang (1994)]. There are three types of fatigue tests often encountered in laboratory: load control, energy control and strain control. Each type of test control exhibits certain unique stress loading and will, therefore, affect the type and extent of the damage to the laminate.

Load control testing maintains a constant magnitude cyclic stress on the tested samples. As damage in the sample occurs, the strain increases to accommodate the constant stress on the damaged laminate. This increases the strain-energy per cycle applied as the test progresses. Load controlled fatigue life is typically the shortest of the three control methods.

Energy control fatigue testing, the magnitude of the stress applied will decrease as the sample is damaged. However, the strain energy per cycle remains constant throughout the test. Fatigue life is greater than with load control tests but less than with strain control tests. This type of test may better represent the fatigue life of a structure in service than do other test methods.

In strain controlled fatigue testing, maximum and minimum extension limits are maintained at constant values. The strain energy per cycle decreases as the test proceeds. This method of testing generally exhibits longer fatigue lives than load or energy control methods.

2.4.2 Frequencies

Several researchers [Dally and Broutman (1967), Zhuo (1995), Kujawski and Ellyin (1995)] have studied the effects of test frequency. Dally and Broutman have found a modest decrease in fatigue life with increasing frequency up to 40 Hz for cross plies as well as quasi isotropic (QI) E glass/epoxy composites. According to Zhuo (1995), there

was little effect on the fatigue life of waisted QI, PEEK/CF specimens with loading frequency varied from 0.5 Hz to 1 Hz. However, it has been reported that there are significant effects when the frequency changes to 5 Hz or 10 Hz, the fatigue life of PEEK/CF composites either QI or $[\pm 45]_{4S}$ lay-ups is reduced following a frequency change from 0.5 Hz to 5 Hz under tension tension loading and is associated with a temperature rise of the specimen.

With viscoelastic materials such as polymers, low frequencies are chosen to prevent the specimens heating up. An increase in temperature, leading to thermal failures, during fatigue testing of polymers is a major problem.

As with polymers themselves, the most obvious external variable is frequency of cycling. Polymers are viscoelastic and exhibit mechanical hysteresis even at moderate strains. Thus, under cyclic loading, some of this inelastic deformation energy will be dissipated as heat in each cycle resulting in a specimen temperature rise and reduction in stiffness. The temperature rise per unit time is a function of test frequency and the stress amplitude imposed. Owing to the presence of a large proportion of polymer, short fibre composites are likely to exhibit similar behaviour in terms of heat build up. However, the effect of frequency is considered negligible for most unidirectional continuous fibre composites tested in the fibre direction [Jang 1994)].

2.4.3 Mean Stress and Stress Concentration

The stress waveform created in fatigue testing is usually sinusoidal or triangle or square wave form as seen in Figure 2.2 . Stress may also be expressed in terms of a pair of variables such as the mean stress (σ_m) and the stress amplitude (σ_a). Goodman's linear law and Gerber parabolic relationship have been applied in the assessment of the effect of mean stress on fatigue performance of materials [Madayag (1969)]. According to Goodman's linear law (Figure 2.3), when a material is subjected to a mean tensile or compressive stress, the stress range must be decreased to preserve the same N_f (number of cycles to failure). Specimens with notches or holes are usually designed to study

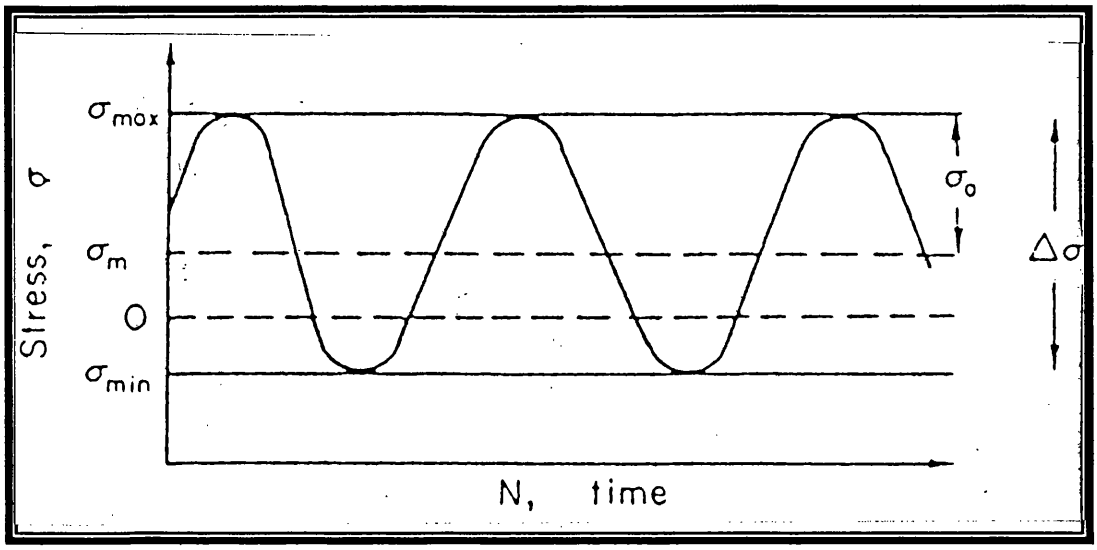

Figure 2.2: Sinusoidally wave in fatigue testing.
[after Ashby and Jones (1981)]

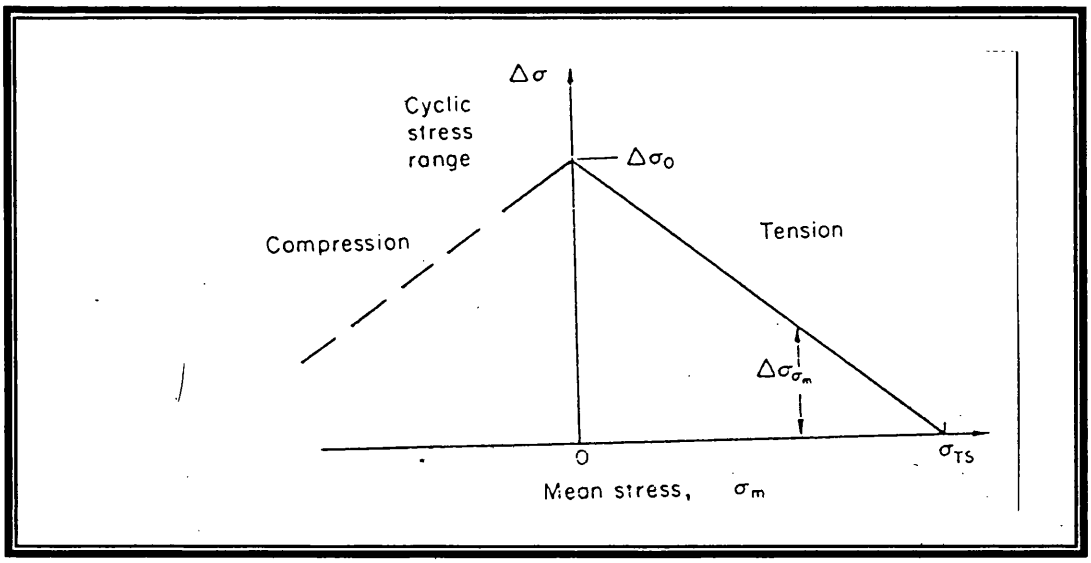

Figure 2.3: Goodman's Rule- the effect of non zero mean stress on initiation controlled fatigue.
[after Ashby and Jones (1981)]

stress concentration effects on fatigue behaviour of materials. The ratio of the peak stress in the notched specimen to that of a corresponding unnotched specimen is termed the theoretical stress concentration. Mechanical properties of materials are strongly influenced by repeated stress such as stress spectrum and stress distribution, stress body including materials and structures and environment [Zhuo (1995)].

2.4.4 Fatigue life (S/N) testing

Fatigue life testing is normally carried out using plain, unnotched specimens. Applied cyclic stress and the number of cycles to failure are recorded. Data is normally presented on a graph relating applied stress, S or σ to log number of cycles to failure (N). For applications where component geometry and surface finish are controlled and defect populations are known to be low or negligible, S/N curves have proved to be useful. For design purposes, the mean S/N curve is adjusted by applying a safety factor [Karam (1991)]. This accounts for scatter, resulting from variations in material properties and stress amplification due to the presence of stress concentrating features in the component.

2.4.5 Fatigue Performance

There are different types of fatigue stressing commonly applied. The stress states include tension-tension, tension-compression, compression-compression, and flexure. The tension-tension state is the most frequently used for composites. The compression states are not common, primarily because of the difficulty in gripping the specimens to prevent buckling failure of thin laminates.

2.4.5.1 Tension-tension Fatigue

Owen and Morris (1971) have reported data on the tension-tension and flexure fatigue of high modulus carbon fibre reinforced epoxy and polyester composites. The tension-tension S-N curves for unidirectional composites are almost horizontal and fall within the scatter band of the static tensile strength. The fatigue effect is said to be slightly greater for relatively low modulus carbon fibre reinforced composites. Unidirectional 0-degree Boron and Kevlar-49 fibre composites also exhibit very good fatigue strength in tension-tension.

2.4.5.2 Flexural Fatigue

In general, the flexural fatigue resistance of fibre composites is inferior to the corresponding tension-tension response. For high modulus carbon fibre composites, it has been reported that the slope of the flexural S-N curve is higher than that of the tension-tension S-N curve [Owen and Morris (1971)]. The lower flexural fatigue strength is generally ascribed to the weakness of laminates on the compression side [Mallick (1988)].

2.4.5.3 Compressive Fatigue

In compression, the fibres are the principal load-bearing constituents, but they must be supported from becoming locally unstable, undergoing buckling failure. This support is provided by the matrix and the fibre-matrix interface, which both play a more important role in compressive loading than tensile loading. Local resin and interfacial damage lead to fibre instability in compressive loading. The need to support the specimen from undergoing macro buckling, combined with the limitations imposed on specimen geometry by the anisotropic nature of the materials, has made it very difficult to conduct compressive tests. According to Echtermeyer et al. (1994), in order to prevent buckling in compression an antibuckling device similar to the support jig of

ASTM 695 was used. The dimensions of the device had to be changed to fit the specimen for the investigation of glass/phenolic and glass/polyester under fatigue.

Many laminates, without fibres in the loading direction, develop intraply damage, which causes local ply delamination at relatively short lifetimes. Tensile-induced damage of this type can lead to local ply instability and buckling when the laminate is in compression during cycling.

With continuous fibre composites, the fibres form the bulk of the structure (i.e. very high fibre volume fractions). The matrix is present essentially as a bonding agent to protect the delicate fibres and ensure better utilisation of the inherently high levels of mechanical properties of the fibres than would otherwise be the case. Mechanical properties are fibre dominated when loading is in the fibre direction. However, the importance of the matrix (and the fibre-matrix bond) cannot be underestimated where the loading is not parallel to the fibre axis. Since continuous fibre composites have been extensively used in applications involving cyclic loads, a vast amount of literature has built up and the subject of fatigue in continuous and thermoset matrix composites has been reviewed by several workers [O'Brien and Reifsnider (1981), Stinchcomb and Bakis (1990), and Reifsnider (1991)].

2.4.6 Fatigue Modulus Concept

Broutman and Sahu (1969) observed the continuous reduction of elastic modulus of composites during fatigue testing. The secant modulus degradation during fatigue test was investigated by Hahn and Kim (1976) and by O'Brien and Reifsnider (1981). Wang and Chim (1983) proposed a fatigue damage model defined by elastic modulus. They assumed that the fatigue damage degradation rate is a power function of fatigue cycles, n, and proportional to a parameter, which is a function of damage. Lagace (1989) reported that there was one main difference between the residual strength degradation and the modulus degradation approaches as the failure criterion. Usually, in the residual strength degradation method, the only failure condition is that failure occurs when the

residual strength degrades to the applied stress. To predict fatigue life by modulus degradation methods, another failure condition is needed in addition to the above condition.

Due to degradation of composite materials under cyclic loading, the stress-strain curve changes as the cycling continues (Figure 2.4). A line-applied stress and resultant strain represent fatigue modulus at a specific loading cycle, n. Fatigue modulus is a slope of a line $0n'$. Therefore,

$$F(n,r) = \frac{\sigma_a}{\epsilon(n)} = \sigma_u \frac{r}{\epsilon(n)} \qquad (2.6)$$

Where;

$F(n,r)$ = fatigue modulus at n loading cycle,

ϵ (n) = resultant strain at n loading cycle,

σ_a = applied stress, and

r = ratio of applied stress, σ_a, to ultimate strength, σ_u

Fatigue modulus, F, of a material is a function of loading cycle, n, and applied stress, r.

Initial and final conditions give the following relations:

$$F(0,r) = F_o \cong E_o \qquad (2.7)$$

$$F(N,r) = F_f \qquad (2.8)$$

Fatigue modulus at zero cycle, F_o, is assumed to be the same as elastic modulus, E_o, and fatigue modulus at fracture is defined as F_f at the number of cycles to failure, N.

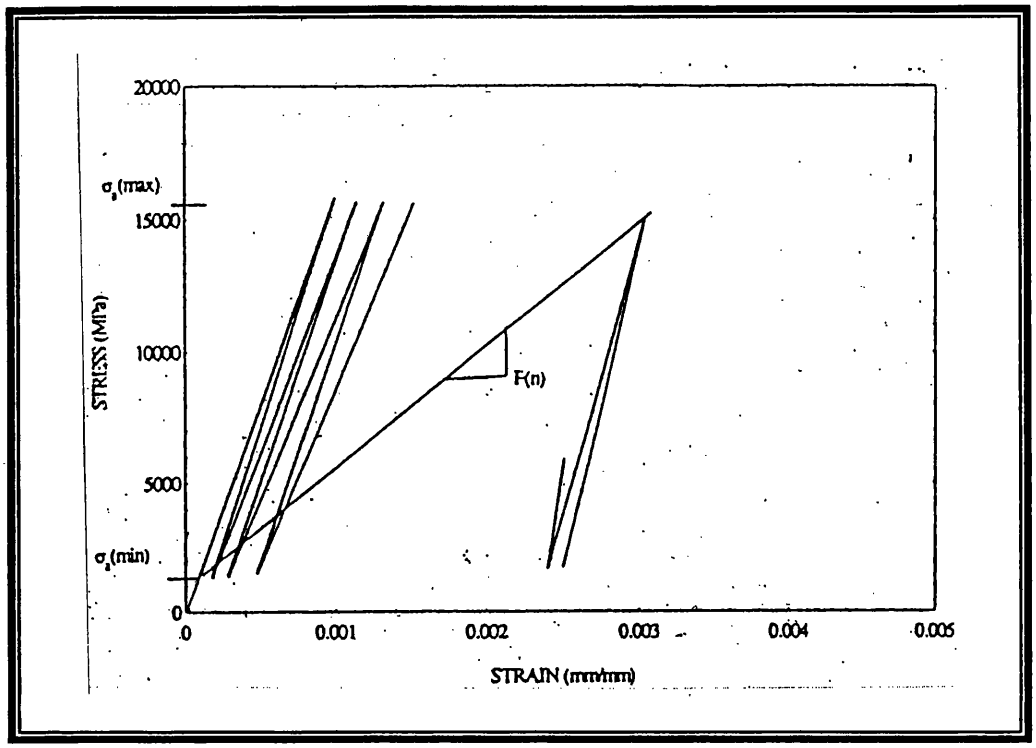

Figure 2.4: Stress-strain curve under cyclic loading.
[after Mahfuz et al. (2000)]

F_o should be constant regardless of applied stress, while F_f depends on the applied stress.

To make further derivation simple, it is reasonable to assume that applied stress has a linear relation with resultant strain at any arbitrary loading cycle if the specimen undergoes constant maximum loading. This assumption follows:

$$\sigma_a = F(n_i) \in (n_i) \tag{2.9}$$

where $F(n_i)$, fatigue modulus at nth cycle, is assumed to be constant. Using this assumption, it is concluded that for a single-stress level fatigue test, fatigue modulus is not a function of applied stress but rather a function of loading cycle only, that is,

$$F = F(n) \tag{2.10}$$

It is expected that fatigue modulus and conventional secant modulus differ a lot for short fibre composites. For unidirectional composites, difference will be small. However, fatigue modulus concept and some assumptions have to be verified by experiment.

2.4.6.1 Fatigue Life Prediction Model

According to Mahfuz et al. (2000), fatigue modulus, F, of composite material ideally is a function of loading cycle, n, applied stress, σ and thickness, t;

$$F = f(n, \sigma, t) \tag{2.11}$$

This equation can be expressed by a power function of the number of the fatigue cycle as

$$\frac{dF}{dn} = - ACn^{C-1} \tag{2.12}$$

Where, A and C are the material parameters.

Integration of equation (2.12) from n_1 to n_2 gives

$$F(n_2) - F(n_1) = - A(n_2^C - n_1^C) \qquad (2.13)$$

Substituting $n_2 = n$ and $n_1 = 0$, one can write

$$F(n) - F(0) = - An^C \qquad (2.14)$$

equation (2.14), can be written as

$$F_f - F_0 = - AN_f^C \qquad (2.15)$$

Where,

N_f = number of cycles to failure

F_f = fatigue modulus at fracture

i.e.,

$$N_f = \left[\frac{1}{A}\left(F_0 - F_f\right)\right]^{\frac{1}{C}} \qquad (2.16)$$

$$= \left[\frac{F_0}{A}\left(1 - \frac{F_f}{F_0}\right)\right]^{\frac{1}{C}} \qquad (2.17)$$

$$= \left[B\left(1 - \frac{F_f}{F_0}\right)\right]^{\frac{1}{C}} \qquad (2.18)$$

where,

$$\frac{F_0}{A} = B \qquad (2.19)$$

From strain-failure criterion, it can be stated as;

$$\frac{F_f}{F_0} = \frac{\sigma_a}{\sigma_u} = r \qquad (2.20)$$

where,

r = ratio of applied stress level / ultimate tensile strength

F_0 = tensile modulus

σ_a = applied stress

σ_u = ultimate tensile strength

Substituting in Equation (2.18),

$$N_f = [\, B\,(1 - r)\,]^{\frac{1}{C}} \qquad (2.21)$$

Where, B and C are assumed to remain constant with respect to r and t. Fatigue life of composite materials can be predicted as long as the material parameter B and C are known.

In this model, B and C are expected to vary with stress level r. Fatigue modulus F is determined by using test data at two cycle numbers n_1 and n_2 for any particular stress level. Equation (2.14) is then utilised at two n's and at a particular r to solve for A and C. If fatigue moduli are denoted by $F(n_1)$ and $F(n_2)$ at cycle numbers n_1 and n_2, respectively, one can derive that

$$\Rightarrow \quad F(n_2) - F_0 = -An_2^C \qquad (2.22)$$

$$\Rightarrow \quad F(n_1) - F_0 = -An_1^C \qquad (2.23)$$

$$\frac{equation(2.22)}{equation(2.23)} \Rightarrow$$

$$\frac{F(n_2)-F_0}{F(n_1)-F_0} = \frac{-An_2^{\,C}}{-An_1^{\,C}} \tag{2.24}$$

Taking log on both side,

$$\Rightarrow \quad \ln\frac{F(n_2)-F_0}{F(n_1)-F_0} = \ln\frac{n_2^{\,C}}{n_1^{\,C}} \tag{2.25}$$

$$= \ln n_2^{\,C} - \ln n_1^{\,C} \tag{2.26}$$

$$= C\left[\ln\frac{n_2}{n_1}\right] \tag{2.27}$$

$$\Rightarrow \quad C = \frac{\ln\dfrac{F(n_2)-F_0}{F(n_1)-F_0}}{\ln\dfrac{n_2}{n_1}}$$

$$\Rightarrow \quad C = \frac{\ln\left(\dfrac{\dfrac{F(n_2)}{F_0}-1}{\dfrac{F(n_1)}{F_0}-1}\right)}{\ln\left(\dfrac{\dfrac{n_2}{n_f}}{\dfrac{n_1}{n_f}}\right)} \tag{2.28}$$

When (2.22) – (2.23),

$$\Rightarrow \qquad F(n_2) - F_0 - F(n_1) + F_0 = -An_2{}^C + An_1{}^C \tag{2.29}$$

$$F(n_2) - F(n_1) = A(n_1{}^C - n_2{}^C) \tag{2.30}$$

$$\therefore \text{ A } = \frac{F(n_2) - F(n_1)}{n_1{}^C - n_2{}^C} \tag{2.31}$$

From $B = \frac{F_0}{A}$, we can derive,

$$B = \frac{F_0(n_1{}^C - n_2{}^C)}{F(n_2) - F(n_1)}$$

$$\Rightarrow \qquad B = \frac{n_f{}^C \left[\left(\frac{n_2}{n_f} \right)^C - \left(\frac{n_1}{n_f} \right)^C \right]}{\frac{F(n_1)}{F_0} - \frac{F(n_2)}{F_0}} \tag{2.32}$$

Equation (2.28) and (2.32) had been simplified to be used to determine B and C at each stress level.

2.5 S-N CURVE

The fatigue life of all materials depends on a number of external variables. Three factors have a critical effect on the extent of fatigue damage. These are the maximum stress (or strain), the variation or fluctuation in the applied stress (or strain), and the number of stress (or strain) cycles. By plotting the number of cycles to failure against its maximum stress of each cycle (S-N curve) predictions can be made of composite lifetime. An alternative method of presenting fatigue data is to plot a peak strain-fatigue life curve. According to Hitchen et al. (1995), this type of diagram is often preferred because during fatigue cycling of continuous fibre composites both the fibre and matrix are subjected to the same strain, whereas the stresses in the two phases will differ depending on the fibre volume fraction.

Fatigue life prediction of composite materials has been the subject of many investigations during the past two decades. Fatigue damage results in a change of strength, stiffness and other mechanical properties of the composite. Talreja (1987) noted that for polymeric composites, damage mechanisms under various loading conditions can vary significantly; for example, crack propagation due to fibre breakage and matrix crack propagation at high stress load result in catastrophic failure of composites. More details of the failure mechanisms will be discussed later.

Takeda et al. (1995) proposed the use of fatigue life diagrams for a systematic understanding of the fatigue performance of composites. The fatigue life diagram shows the number of cycles at which a certain damage mode occurs under a certain strain. Lee et al. (1989) experimentally determined the use of S-N curves for 0° and 90° laminates to predict the property degradation and fatigue life of laminates.

2.5.1 Fatigue life prediction by S-N data

Fatigue life prediction of composite materials has been the subject of many investigations during the past two decades. Lagace (1989) reported that the residual

strength degradation and modulus degradation approaches have been frequently used to predict fatigue life of composite materials.

Simple approaches for predicting fatigue life have been developed to give an analytical representation of S-N curves for the fatigue of composite materials. On the whole scale ($N_f = 1 - 10^7$), the relationship between the maximum stress (σ_m) and the cycles to failure (N_f) is usually non-linear, thus the prediction models are various, such as exponential, logarithmic, trigonometric and order, etc. varying with individual set of SN data. But in the portion of high cycles ($N_f = 10^3 - 10^7$), the relationship between σ_{max} and $\log(N_f)$ is likely to be linear. Therefore, many of these approaches are based on linear extrapolations of fatigue data. One such relationship is [Mallick (1988)]:

$$\sigma_{max} = \sigma_u (m \log N_f + b) \qquad (2.33)$$

Where σ_{max} is the maximum fatigue stress, N_f is the number of cycles to failure, σ_u is the static strength, and m and b are constant.

Fatigue is described as a process, which causes damage in materials and structures under fluctuating loads of a magnitude less than the static failure load. Accumulated damage may result in a gradual or significant decrease of mechanical properties and lead to crack growth and finally cause a complete failure or collapse. There are two types of fatigue tests often encountered in the laboratory: stress control and strain control. Fibre reinforced plastics are also susceptible to thermal failure during fatigue loading. This can occur from testing at high temperature where creep effects combine with fatigue to cause early failure of the sample. They can also occur from inherent materials variables such as crack tip heating from interfacial friction and various external test variables. Frequency is the rate at which the sample is cycled. Very slow frequencies tend to be around one cycle per second; this frequency is typical for polymers. Low frequencies were chosen to prevent the specimens heating up [Echtermeyer et al. (1995)].

2.5.2 Scatttering of Results of Fatigue Tests

It is well known that the number of loading cycles that cause failure, determined in identical conditions, is different for each specimen tested. The scattering of such experimental results is greater the smaller the stress amplitude or deformation [Puškár and Golovin (1985)]. According to McClintock (1955) there are three groups of factors that affect the scattering of results of fatigue tests:

- Microscopic sources of scattering, such as differences in stress concentration in the region of grain boundaries, differences in stresses around inclusions, differences in strength of different phases of material. These factors cannot be completely removed.

- Heterogeneity among pieces, such as the difference in thermal processing of parts of pieces, difference in surface flatness and the occurrence of inclusions of larger dimensions. These factors can be removed or significantly suppressed.

- Sources of scattering caused by differences of production conditions for specimens, such as differences in thermal processing, different preceding mechanical processing, different chemical composition of pieces, differences in machining, grinding or polishing. These factors of scattering of results can be removed or significantly suppressed.

2.6 FAILURE MECHANISMS

2.6.1 Introduction

In general, two major types of failure mode can be identified for fibre reinforced plastic composites, namely fibre dominated failure and matrix dominated failure. Laminates with sufficient 0^{o} layers, that is, layers with fibres oriented in the load direction, will exhibit the fibre dominated failure mode. This type of failure is essentially independent of the rate/frequency of loading. On the other hand, the matrix dominated failure mode is a rate/frequency dependent phenomenon due to the viscous matrix behaviour. The viscous dependent matrix behaviour plays an essential role in fatigue performance of polymeric composites [Sturgeon (1978), Rotem (1993), and Stinchcomb et al. (1975)]. In the failure mechanism study special emphasis was placed on stiffness loss during fatigue. Stiffness is not only an important engineering parameter, but also is seen as an indicator of damage. Matrix cracking has been identified as the cause of stiffness reduction in static and fatigue tests. It has been observed that the stiffness of the laminate reduces during the process of damage accumulation in laminated composites [Subramaniam et al. (1995), Echtermeyer et al. (1995)]. Four main damage mechanisms have been observed in laminated composites under fatigue loading matrix cracking, fibre-matrix debonding, delamination, and fibre fracture.

Fatigue damage in continuous and discontinuous fibre composites is different. In discontinuous fibre composites, matrix crack initiation can occur at the fibre ends as a result of stress concentration in these areas. Cracking and fibre-matrix debonding can also occur at low stress levels if the discontinuous fibres are not adequate lengths to support the applied load. Fibre distribution and orientation are also important factors in damage resistance. The fatigue life of discontinuous fibre composites exhibits slower crack growth initially, followed by rapid growth near failure [Jang (1994)].

2.6.2 Fatigue Damage Accumulation Mechanisms

Four main damage modes have been observed [Hull (1981), Reifsnider et al. (1983), Talreja (1987), Subramaniam et al. (1995)] in laminated composites under fatigue loading, namely matrix cracking, fibre-matrix debonding, delamination, and fibre fracture. Fatigue in composite materials produces both microscopic and macroscopic damage mechanisms at various stages in the fatigue process. Typically, matrix cracking and delamination occur early in the life, where fibre-matrix debonding and fibre fractures initiate during the beginning of the life and accumulate rapidly towardly the end, leading to final failure [Razvan and Reifsnider (1991), Subramaniam et al. (1995)].

Reifsnider (1991) noted that for laminate that have off axis plies, $[0/90/\pm45]_S$ quasi-isotropic, the first damage mode observed is matrix cracking. While for the cross ply laminate $[0/90m/0]_S$, where m = 4, 8 and 12, Takeda et al.(1995) found that the first damage observed is transverse cracking, which runs through the thickness of the 90° plies. As the number of cycles increases, delamination initiates from the tips of the transverse cracks.

Several major damage mechanisms initiate, grow, and interact to alter the state of the material, change strength, and define life. The amount of damage activity, the chronology of damage events, the interaction of damage modes, and the cumulative effect on stiffness, strength, and life are dependent on material system, geometry, loading, and environment. If eventual failure due to cyclic loading occurs, then damage must have developed in the laminate during the fatigue lifetime and caused degradation of properties such as strength and stiffness. The damage process in composite laminates consists of the initiation and growth of several different damage modes and complex interactions between damage modes. Figure 2.5 [Reifsnider et al. (1983)] illustrates a schematic representation of an S-N curve with damage development and residual strength variations superposed.

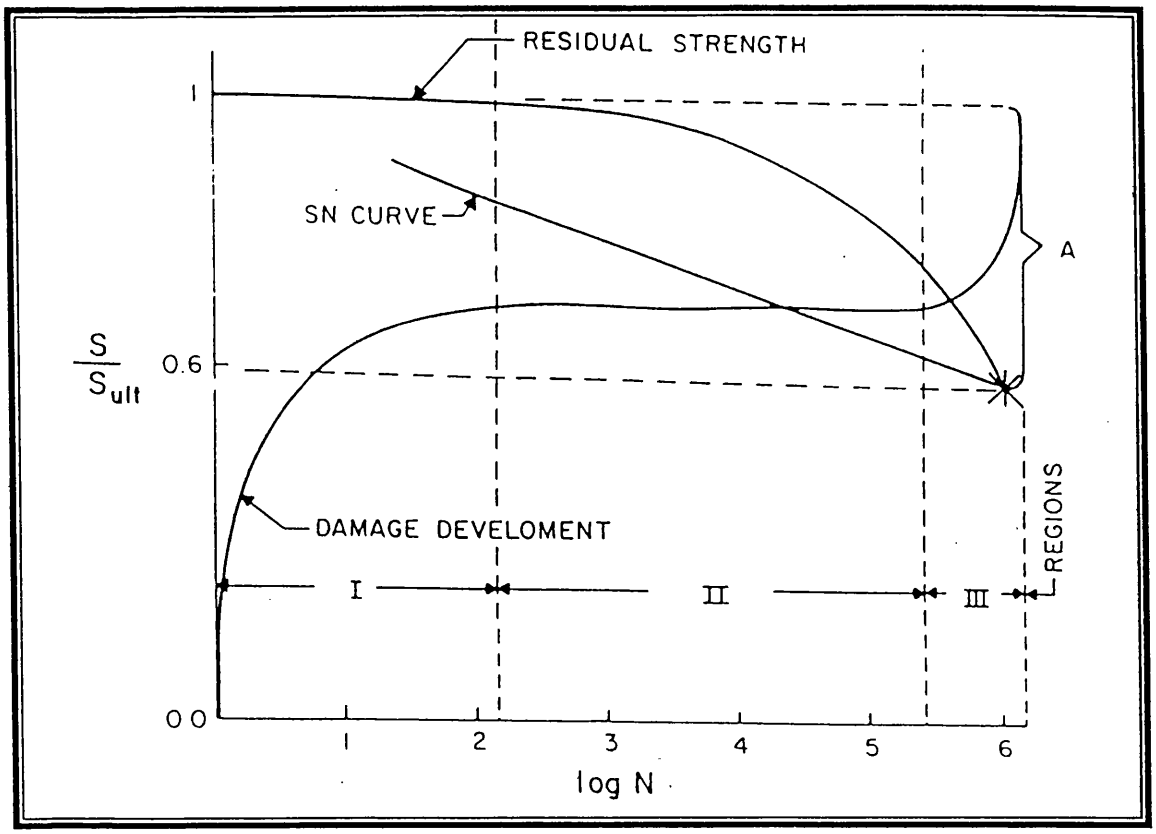

Figure 2.5 : Long-term behavior diagram showing three regions of development, after Reifsnider [1983]

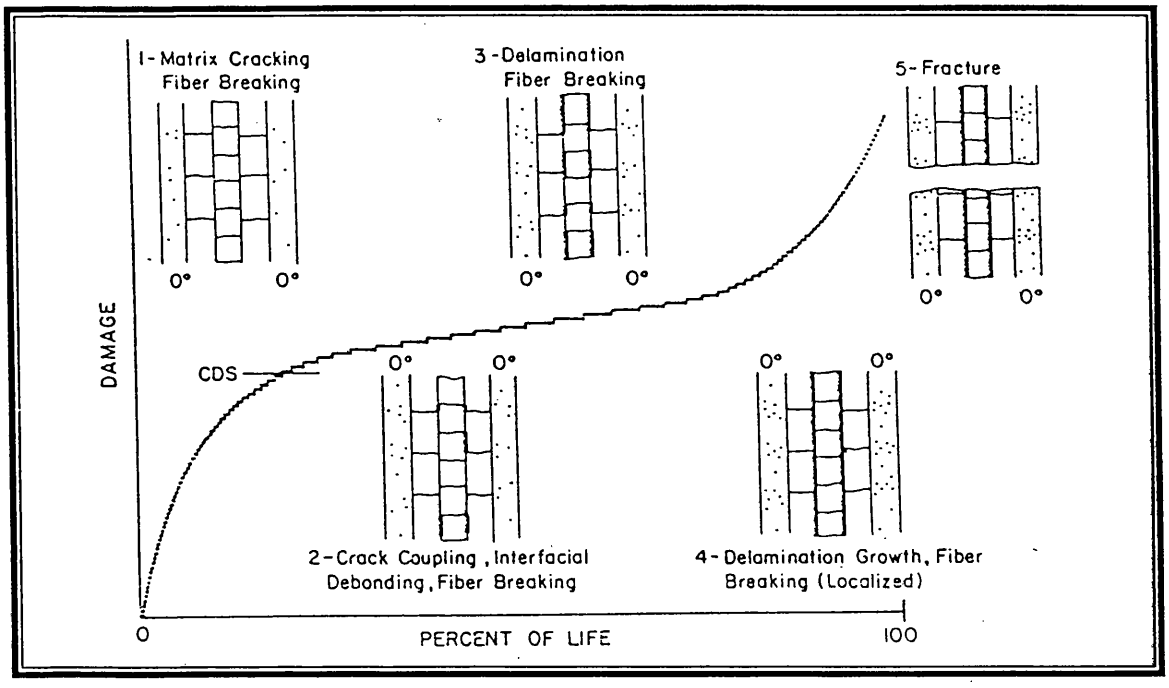

Figure 2.6 : Schematic representation of the development of damage during fatigue life of composite laminate, after Reifsnider [1991]

The damage process can be considered in three stages. Stage I occurs during the first 10-15% of life, during which damage develops at a very rapid rate. Stage II corresponds to the next 70-80% of the fatigue life, during which time damage continues to initiate and grow, but at a slower rate than during stage I. However, at the end of stage II, the laminate is severely damaged to the level where continued cyclic loading accelerates the damage process during stage III, the final 10-15% of life.

The major damage during stage I is matrix cracking: numbers of fibre fractures have been observed during the early stage of fatigue life. Matrix cracks will appear in some plies on the first cycle if the ply level tensile stress perpendicular to the fibres is sufficiently large to produce so called first ply failure. Matrix cracks initiate in the off axis plies at low values of applied stress relative to the laminate strength, but the initial cracks are few in number and are widely spaced.

Throughout stage I, the number and density of matrix cracks increase until a uniform, saturation spacing is reached. This state of damage is known as the Characteristic Damage State (CDS), Figure 2.6.

Generally, matrix cracking occurs early in the weakest ply. Crack multiplication then dominates most of the fatigue life with cracks initiating in the progressively stronger plies. As cracks intersect each other, areas of delamination can occur. At some later stage, the fibres break in the loading direction causing the laminate to fail. Both SEM and optical micrographs may be taken periodically to detect which damage mechanisms is dominant.

According to Chiou and Bradley (1995), the first damage found as a result of seawater absorption on fatigue of samples of quasi-isotropic $[45/0/-45/0]_S$ graphite with epoxy novolac resin was transverse cracking in 90° and 45° plies. Transverse cracking in 90° plies almost always led to the initiation of -45/90 interply edge cracking at the point where the transverse cracks intersects the -45° ply.

It is widely believed that compression induced damage is of a different nature in notched graphite/epoxy laminates than tension induced damage [Phillips (1981)]. The rate of damage development has been observed to be highest for tension-compression fatigue loading when compared to equal peak amplitudes or stress ranges of tension-tension or compression-compression or both [Bakis and Stinchcomb (1986)].

2.6.2.1 Matrix Cracking

Matrix cracking is characterised by the microscopic cracks that form predominantly in the matrix area of a laminate under loading. Their orientation may be in any direction depending on applied stress. In a multidirectional laminate, matrix cracks will appear first in the weakest ply layer. As the laminate is further stressed, cracking will subsequently occur from the weakest to the strongest layers. Matrix cracks are initiated early in the fatigue process. The majority of the fatigue life of a laminate is spent in the crack multiplication stage where the density of cracks increases [Jang (1994)]. As the crack increases, cracks begin to grow into each other forming larger cracks. As cycling continues, the cracking extends within the laminates.

Matrix cracks have been observed by many authors, in both static and fatigue testing, to occur in and between plies. Stiffness is an indicator of damage. Matrix cracking has been identified as the cause of loss of stiffness [Echtermeyer et al. (1995)].

When the laminate is still further loaded, the crack density will be increased to a limiting value where stress redistribution would limit the initiation of new cracks. At this point, matrix cracking becomes a macroscopic form of damage that could dictate the initiation of other damage mechanisms. The subsequent damage is usually delamination, and then fibre breakage.

On the other hand, resistance to crack growth in composites mainly arises from two mechanisms. The first, and usually the most important, is the bridging of the crack. The second one is the trapping of the crack due to the reinforcement ahead of the crack front

[Botsis and Zhao (1997)]. Another mechanism that may contribute to fracture resistance is due to energy dissipation in the matrix material.

2.6.2.2 Fibre-Matrix Debonding

Debonding, the separation of fibre from the matrix is followed by the development of a crack along the interface. It depends on the interfacial bond strength between the fibre and the matrix. High interfacial bond strengths will permit little or no fibre matrix debonding. In contrast, laminates with low bond strength may exhibit large areas of debonding that either combines with or intensify other damage mechanisms to speed up laminate failure. Agarwal and Broutman (1990) noted that the damage first initiates by the separation of the fibres from the matrix and called debonding in the fibre rich regions of the plies in which the fibre lie perpendicular or at a large angle to the loading direction. Fatigue damage by this mechanism is dependent on the interfacial bond strength between the fibre and the matrix.

2.6.2.3 Delamination

According to Jang (1994), delamination is the separation of plies in laminates, usually induced by high interlaminar stress. It occurs under conditions of high interlaminar shear or in a combined stress state such as occurs on the edge of a laminate, in the vicinity of voids and at the base of cracks [Goetchius (1987)]. Delaminations also may occur at several locations in a given component or structure. Delaminations will typically initiate at edges, holes, and ultimately, matrix cracks [O'Brien (1993)].

These local stresses occur near free edges of a composite. Their magnitude depends upon the materials used, stacking sequence, laminate shape and type of stress loading. During fatigue loading, delamination begins early in the life and progresses as the fatigue cycles increase. Other damage mechanism may also influence the extent and propagation of delamination in a fatigued laminate.

As matrix cracks accumulate, and as delaminations form and grow, the stiffness of the laminate decreases. Laminates stiffness is the ratio of the remote stress to the global strain in the laminate. This global strain is typically measured using an extensometer or linear voltage displacement transducer (LVDT), which yields the displacement of the laminate over a fairly long gauge length relative to the laminate's length. As damage forms and grows in the laminate under a constant maximum cyclic stress, corresponding to a constant applied maximum cyclic load, the global strain in the laminate increases. The amount of stiffness loss associated with matrix cracking depends upon the ply orientation of the cracked ply, the laminate lay-up, the relative moduli of the fibre and the matrix, and the crack spacing, or density of cracks, in the ply.

The amount of stiffness loss due to delamination also depends on the laminate lay-up and the relative stiffness of the fibre and the matrix. Delamination starting from matrix cracks will affect laminate stiffness differently from delaminations growing from the straight edge. The ply interface position where two cracks cross also creates a region of local delamination [Donat (1970)]. The extent and progression of delamination are influenced by other damage mechanisms. As delamination is dependent on the geometry of the interlaminar matrix layer, it is also dependent on the uniformity and resin content of the laminate, the presence of strong fibres on lamina surfaces and the laminate stacking sequence [Russell (1987)]. The effect of moisture on delamination cracking resistance is critical to the durability of composite materials in seawater environment because delamination crack growth has been identified as the most dominant failure mechanism in the fatigue life of fibre reinforced composites [Chiou and Bradley (1995)].

Due to the complexity of the effect of moisture on long term durability, however, a variety of results have been reported on the effect of moisture on delamination cracking resistance of composite materials [Marom (1989)].

2.6.2.4 Fibre Fracture

When enough stress is applied, a fibre will break at its weakest point. Depending on the properties of the constituent, these fibre breaks produce different types of failure. Not all fibres fail simultaneously, but isolated single fibre breaks occur at weak points. As the load increases the single fibre breaks increase in density and interact to produce adjacent fibre breaks. These localised failures interact and eventually come together to produce catastrophic failure.

Hull and Clyne (1996) noted that, in tension, most fibres tend to fracture in a brittle manner, without any yield or flow. Carbon, glass and ceramic are almost completely brittle and fracture without any reduction in cross sectional area. The failure process of advanced composite laminates under static and fatigue loading is known to involve a sequential accumulation of damage in the form of matrix dominated cracking.

Laminates subjected to both tensile and compressive cyclic loads may exhibit either tensile or compressive fracture modes, depending on the response of competing damage modes to the magnitudes of the loads and the material system (Stinchcomb and Bakis (1990)]. Under cyclic tensile loads, laminate fracture is coincident with the catastrophic fracture of the major load bearing plies. Under cyclic compressive loads, failure occurs when the laminate stiffness degrades to such an extent that the laminate cannot support the applied loads. Failure is usually due to buckling or micro buckling and subsequent shear crippling, dependent on constraint conditions.

2.7 DAMAGE TOLERANCE AND MODULUS DEGRADATION

A large number of previous studies on fatigue behaviour of composites involved measurement of stiffness reduction during fatigue loading [Charewicz and Daniel (1986), O'Brien (1990), Razvan and Reifsnider (1991), Hitchen et al. (1995), Subramaniam et al. (1995), Zhuo (1995)]. Subramaniam et al. ((1995) noted that in their research, a $[0,90_3]_S$ cross-ply epoxy laminate, most of the stiffness reduction

occurs during the first 10% of the life of the laminate. During this stage, the crack density increases in the 90° ply and reaches a saturation value. Most of the stiffness reduction is due to damage in the 90° ply, and there is very little stiffness reduction in the 0° of the laminate. Razvan and Reifsnider (1991) have observed that the stiffness of laminate reduces during the beginning of the life and accumulate rapidly towards the end, leading to final fracture. O'Brien and Reifsnider (1981) and Camponeschi and Stinchcomb (1982) have shown that changes in the components of stiffness are indications of tensile fatigue damage in thin composite laminates and, in some instances, may be used to predict damage growth. The amount of change in a given stiffness component will depend on the direction of load, the directional growth of damage, and the direction in which the particular stiffness component is measured.

The emergence of new toughened matrix composites with improved durability has resulted in the need to understand the influence of increased toughness on long-term damage tolerance. Hitchen et al. (1995) studied the effect of damage accumulation during fatigue cycling in terms of residual strength and modulus reduction. On damage accumulation tests with laminates containing 1, 5 or 15 mm length fibres, they found that no significant modulus reduction could be detected, and damage accumulation during fatigue cycling, based on modulus reduction during fatigue cycling, indicated that final catastrophic failure is the result of a sudden death mode of failure. Recent research [O'Brien (1990)] has focused heavily on this issue in developing damage tolerance criteria that will satisfy the safety requirements of current military aircraft.

It was concluded that long term behaviour and damage tolerance are controlled by a number of interacting factors such as matrix toughness, fibre architecture, loading level, and damage types and distributions [Bakis et al. (1990)]. Subsequently, open hole compression tests and compression after impact tests have been used to evaluate the damage tolerance of composite material. Interlaminar fracture toughness, open hole compressive strength, and post impact compressive strength are measured during short term, monotonic loading tests. Under such conditions, toughened epoxy and

thermoplastic matrix composites appear to be attractive materials for structural application where damage tolerance must be satisfied.

Damage measurements stiffness change, residual strength, and life data are used to compare and contrast the long-term behaviour and damage tolerance of these materials.

2.7.1 Modulus Degradation

Composite laminates under fatigue loading exhibit an accumulation of damage, consisting of matrix cracking in off-axis plies, delamination between layers, fibre breakage and debonding. These cause deterioration of the material mechanical properties such as strength and stiffness. Modulus degradation can be monitored and used to evaluate damage progression of laminates during the fatigue process. Fatigue of composites causes a loss of stiffness and development of damage before ultimate failure. Research has been done by Echtermeyer et.al.(1995) to compare the effect of phenolic and polyester resins reinforced by five layers of woven roving chopped strand combination glass mat.

Change in stiffness of a composite laminate as a result of cyclic loading is a repeatable characteristic of the type of material and lamination arrangement. The changes take place in three distinct stages, as illustrated in Figure 2.7 for $[0/90_2]_S$ graphite epoxy laminate [Jamison and Reifsnider (1991)] subjected to tension-tension (stress ratio, R=0.1) cyclic loading.

Stage I is characterised by an initial rapid decrease in stiffness caused by matrix cracking and some early fibre fracture. Stage II is an intermediate but long period of stiffness reduction, which results from additional matrix cracking in off-axis, and on-axis plies, crack coupling along ply internal delamination and interfaces. Stage III is characterised by a rapid decrease in stiffness as a result of an increase in damage growth rates, including coalescence and fibre fracture.

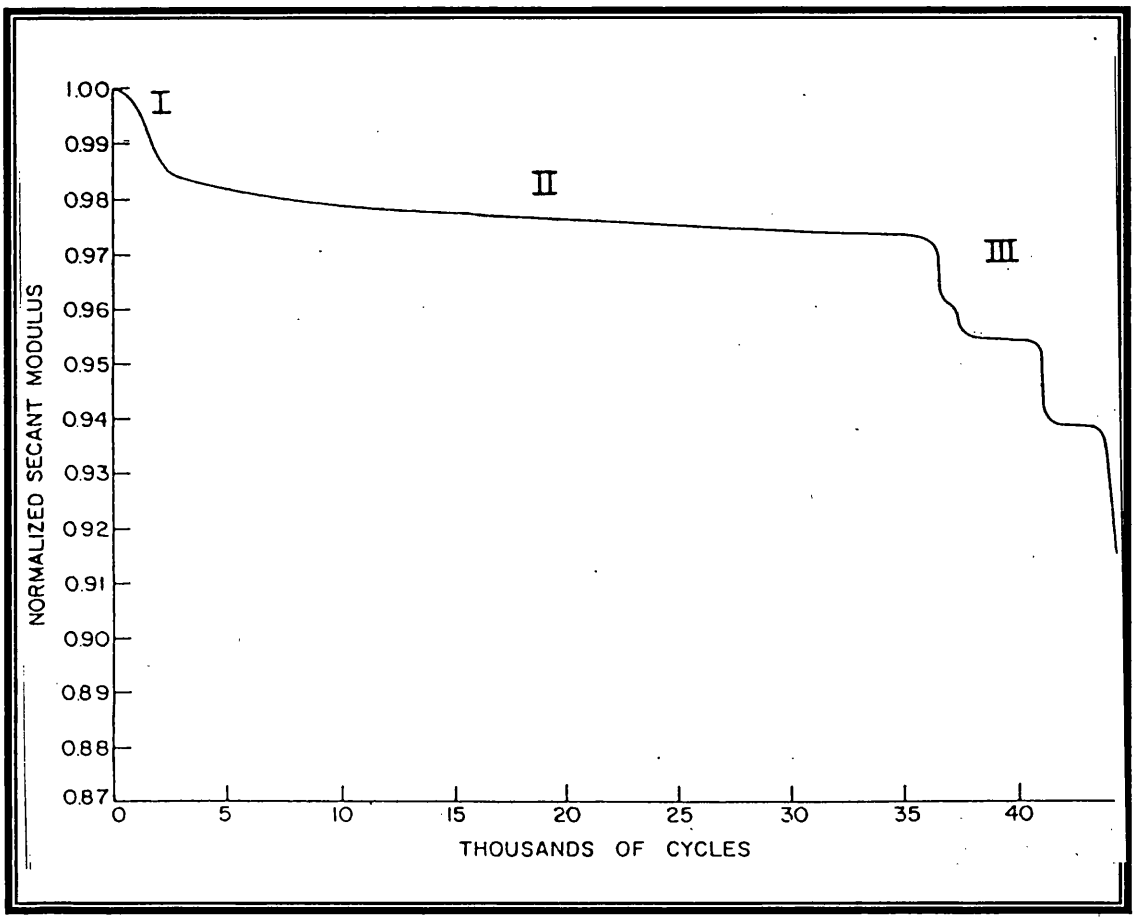

Figure 2.7: Stages of stiffness reduction during fatigue life of a $[0,90_2]_S$ graphite epoxy laminate.
[after Jamison and Reifsnider (1982)

Reifsnider (1991) and Yang et al. (1987) noted that the stiffness changed because of cyclic loading depending on material and loading. Stiffness change data can also be normalised with respect to initial (undamaged) stiffness and plotted versus cycles or percentage of fatigue life. The transition between stage I and stage II response, as indicated by change in stiffness data occurs between 10 and 15% of life at both stress levels. Transition between stage II and stage III occurs between 90 and 95% of life at both stress levels.

Yaniv et al. (1990) concluded that for the graphite/epoxy laminates under tension-tension fatigue loading cycles (stress ratio R=0.1), the shear modulus is more sensitive to longitudinal cracks in the 0^{o} plies than the commonly measured axial modulus. Subramaniam et al. (1995) have studied the tensile fatigue behaviour of $[0/90_3]_S$ cross-ply Apollo fibre laminates and toughened epoxy matrix. The results indicated that most of the stiffness reduction occurs during the first 10 percent of the life of the laminate due to damage in the 90^{o} ply, and there is very little stiffness reduction in the 0^{o} ply of the laminates. Furthermore, according to Echtermeyer et al., the compressive stiffness does not change during the majority of the fatigue process (it only drops just before final failure).

Dyer (1996) reported that stiffness reduction changes could be directly related to stress redistribution from internal damage. It involves taking regular stiffness measurement throughout a fatigue test and correlating them with the damage as it is seen to occur. The author also mentioned other studies on stiffness reduction during the fatigue of carbon polyimide and found three stages of stiffness reduction. It was noted that in stage I, stiffness reduction was due to the formation of transverse cracks in the off-axis plies and that this was followed by delamination in stage II which reduced the contribution of the off-axis plies to the stiffness. The author also noted that stage III was characterised by extensive fibre breakage.

2.8 FRACTOGRAPHY: OPTICAL MICROSCOPY AND SCANNING ELECTRON MICROSCOPY (SEM)

It is becoming more evident that direct observation of the fracture surface is not always sufficient to describe the mechanisms of fracture and in some cases such observation alone may be misleading. It is important to examine specimens for structures that are representative and relate to the problem and then correlate them with the relevant properties of the material [Roulin-Moloney (1989)].

Sectioning of samples close to the fractured surface exposes the damage, which is not visible on the fracture surface. Because of the limited resolution and magnification, the optical microscope is not usually suitable for observation of detailed structures at high magnifications.

In cutting out the desired sample, it is important to remember that regardless of cutting method, the cutting process induces damage to the material adjacent to the cut. It if beneficial to use an original sample (without any testing) for comparison prior to sectioning. Composites, such as samples used in this research are prepared by metallographic polishing methods. This method include grinding, to remove roughness and damage due to cutting, and polishing to remove grinding damage and create a polished reflective surface suitable for observation.

The most common abrasive used for grinding is silicon carbide powder, which is usually bonded to paper with a waterproof adhesive. Grit sizes 240, 320, 400 and 600 are standards. With some polymers and many composites, excessive grinding damages the surface. In these cases, grinding time should be minimised to the time it takes to remove previous scratches. It is important that both the sample and hands be thoroughly washed between stages to avoid scratches due to contamination. Often it is only necessary to use the finer grits, 400 and 600 when possible.

The purpose of polishing is to create a smooth reflective surface with minimum amount of scratches. According to Hemsley (1984), the most common abrasives for polymers and composites are synthetic diamond pastes. They come in a number of different mesh sizes measured in μm. Polishing is usually done on cloths mounted on rotating wheels.

An early report on the study of in situ fracture of polymeric systems in the scanning electron microscopy (SEM) was the work of Hearle et al. (1972) who studied the deformation of fibres. However, early investigations on bulk polymers were published by Smith et al. (1976) who investigated the ductile fracture of poly(vinylchloride).

Samples preparation for SEM involves glueing the sample onto an aluminium stub using a colloidal solution of silver. Coating the sample with a thin layer of metal such as gold, silver or aluminium not only provides a conducting film but also gives enhanced electron emission from the sample surface and reduces the effects of radiation damage.

2.9 CONCLUSION OF LITERATURE REVIEW

It has been seen from the literature review that some areas have been comprehensively studied. These areas include the basic fatigue properties of composites. Although these research studies have produced large amounts of literature, there are still a few areas, which need further study. These include an in depth study on the final cause of failure of composites for new materials such as polyurethane acrylate during fatigue.

To compare the properties of this new resin, some investigations have been carried out, such as the effect of environmental conditions on fatigue testing. This investigation also includes the damage accumulation due to the environment. The study has also been extended by using other values of R (stress ratio), not only for tension-tension loading (R positive) but also for tension-compression (R negative). This investigation has used similar parameters and techniques to those used in previous investigations to compare

the strength, failure accumulation and effects on fatigue process of different environments such as seawater and distilled water. The other study that has been carried out is the characterisation of modulus degradation in the laminates during fatigue testing. As mentioned earlier, previous results have suggested that the modulus reduction has three stages prior to fracture and hopefully this investigation will show whether this new composite, either [90/0] or [±45], will have the same type of modulus reduction as the other composites.

Using fractography observation, investigations have been made to see whether this new composite shows the same pattern of macroscopic and microscopic damage as other polymer composites during fatigue testing. Other areas that have been further studied include the modulus degradation during the fatigue process using different values of R.

CHAPTER

3

AIMS OF PROGRAMME

A review of the available literature shows that polymer composites are widely used in marine, automotive and aerospace industries for component and structures operating at high temperature and stress. Under these conditions, fatigue damage is an important element in determining the life expectancy of particular components and an early detection of microstructural changes due to fatigue damage would be of great benefit for safe operation and assessing the useful remaining life of the components.

Among others, this research work has objectives as follows: -

- To evaluate the progression and interaction of damage modes in glass/polyurethane acrylate laminate subjected to tension-tension and tension-compression cyclic

loading.

- To identify damage mechanisms/accumulation and explore the role of fibre and matrix in the fatigue process for a few different lay-ups.
- To determine any relationships between the damage state and the strength, stiffness (modulus) and life of the laminate through fatigue testing and to identify and monitor the modulus degradation accumulation during fatigue and to evaluate damage progression for several types of laminates under various stress conditions.
- To identify the effects of various environments on this polyurethane acrylate composite through fatigue testing such as in air, distilled water and seawater. To generate fatigue life data under a range of experimental conditions and to analyse scatter of the resultant data.
- To investigate any differences between $[90/0]_{2S}$ and $[\pm 45]_4$ laminate through fatigue testing.
- To identify the damage mechanisms using fractography methods such as SEM and to examine the microstructure of the laminates.

CHAPTER

4

EXPERIMENTAL PROCEDURES

4.1 Introduction

The experiments carried out in this investigation were tailored with respect to the aims of this research project as mentioned in the previous chapter. In this chapter, details of the materials used and the procedure adopted will be explained; meanwhile the results obtained will be discussed in Chapter 5.

Most of the experiments were carried out in the laboratories within Materials Engineering Department at room temperature of 23°C and humidity of about 50 percent.

4.2 Materials

In the first set of experiments, three types of resins were used to identify the characteristics of the S-N graph for each polymer composite. The resins, were a standard isophthalic polyester resin and the other two were more specialised resins, a polyurethane vinyl ester (PUVE) and a polyurethane acrylate (PUA). Table 4.1 shows

some typical mechanical properties of the three resins. All the resins were provided by Scott Bader Co. Ltd. The isophthalic polyester resin was prepared by condensing a glycol with an unsaturated acid, isophthalic acid. The unsaturated acid provided the sites for subsequent crosslinking with the crosslinks sites being fumarate ester groups for this resin. The polyurethane vinyl ester resin was also supplied in diluent styrene. In this case, the main chains included aromatic urethane groups, which lead to higher chain stiffness and higher Tg (glass transition temperature). Crosslinks were formed with the methacrylate ester groups and the styrene, which had the added advantage of capping the polymer chains ends.

Property	Polyurethane vinyl ester	Polyester	Polyurethane acrylate
Elongation at break (%)	3.0	5.0	12
Tensile strength (MPa)	50	75	46
Tensile modulus (MPa)	3600	3500	2270
Volumetric shrinkage (%)	8.3	8.3	9.3

Table 4.1: Typical comparative mechanical properties of the resins
[from Scott Bader Technical Data Sheets]

Table 4.1 shows that the polyurethane acrylate resin has the lowest tensile strength and modulus compared with the other two resins.

These resin were reinforced with the following three types of E-glass fibre fabrics, provided by Flemings Laces.

(i) Woven Roving: WR/600/100
(ii) Ulticloth : UC/600/PB/100
(iii) Biaxial Ulticloth : BUC/600/LS/140

Tables 4.2 and 4.3 shows some basic typical comparative mechanical properties of the glass fibre cloths that were used in this research. The woven roving and Ulticloth

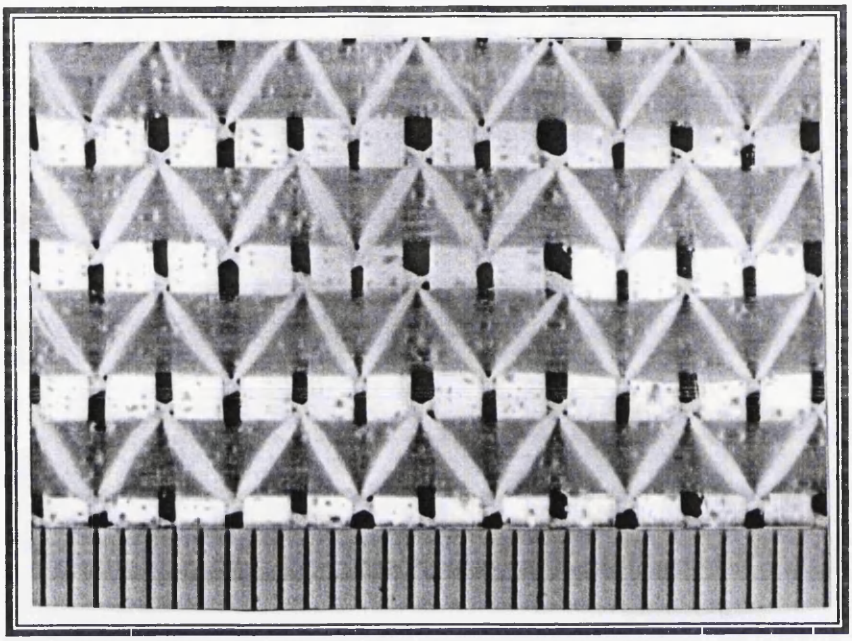

Figure 4.1: Ulticloth [90/0] used in this research

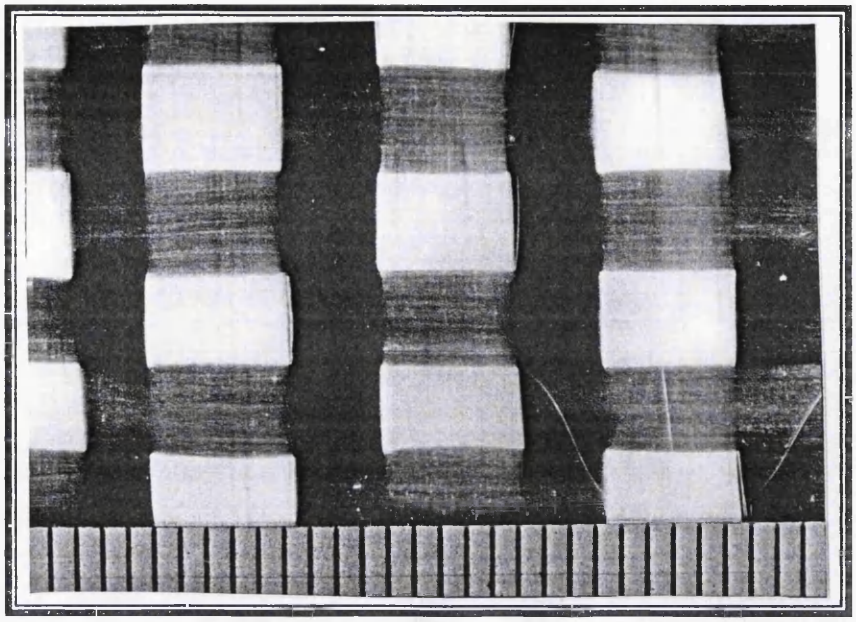

Figure 4.2: Woven Roving Cloth

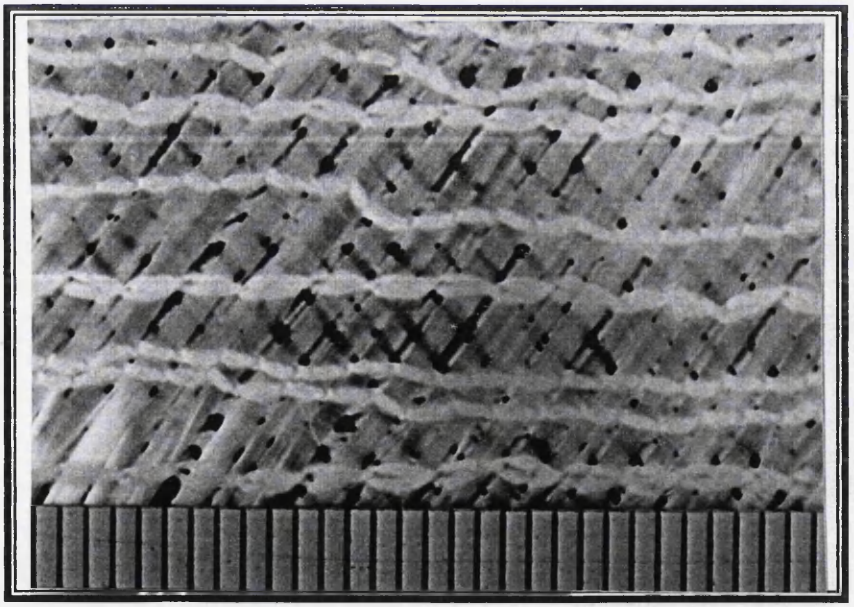

Figure 4.3: Biaxial-Ulticloth

consisted of fibres in the 0° and 90° directions, while the Biaxial Ulticloth consisted of fibres in the -45° and +45° directions. Both Ulticloth fabrics were stitch-bonded. All three cloths had a silane finish applied. Additionally, the woven roving and Ulticloth had a powder binder of polyester bisphenol, the content of which was between 4% and 5%.

Cloth	Total Weight(g/m^2)	Warp (g/m^2)	Weft (g/m^2)
Woven roving	600	300	300
Ulticloth	600	354	246
Biaxial Ulticloth	600	300	300

Table 4.2: The basic properties of the cloths
(from Fleming Industrial Fabrics Technical Data Sheets)

Property	Ulticloth	Woven Roving
Ultimate Tensile Strength , UTS (MNm^{-2})	310	240
Tensile Modulus (GNm^{-2})	16.3	12.9
Flexural Strength (MNm^{-2})	502	230
Flexural Modulus (GNm^{-2})	15	11

Table 4.3: Typical comparative mechanical properties of the laminate using polyester resin (from Fleming Industrial Fabrics Technical Data Sheets)

For each of the resin types, the following three different lay-ups of the cloth were used (see Figure 4.1-Figure 4.3):

(i) $[0/90]_{2S}$ Ulticloth

(ii) $[0/90]_{2S}$ Woven Roven

(iii) $[\pm 45]_{2S}$ Biaxial Ulticloth

The second set of experiments, was designed to determine the properties of polyurethane acrylate resin, with E glass used as reinforcement. The effects on these composites of various environments such as, air, distilled water and seawater were also investigated. The two stitch bonded Ulticloths described above were used in two arrangements. These arrangements consisted of four layers of the same cloth giving $[90/0]_{2S}$ (Ulticloth) and $[\pm 45]_4$ (Biaxial Ulticloth). Only the first arrangement was symmetrical. For comparison of properties and the results obtained by the previous researchers [Dyer (1996)], the non-symmetrical arrangement of Biaxial Ulticloth was used. This arrangement of Biaxial Ulticloth was also used with the other type of resin, to compare the mechanical properties.

4.2.1 Preparation of Samples

Table 4.4 shows the various proportions of resin, catalyst and accelerator used in mixing the formulations, as well as the cure times and post curing regimes.

Resin	Catalyst	Accelerator	Cure Time	Post Curing
150 ml. Polyurethane vinyl ester	4.5 ml. Trigonox R239	4.5 ml accelerator E	RT 24 hrs.	80° C 3 hrs.
150 ml. Polyester	3.0 ml catalyst M	3.0 ml accelerator E	RT 24 hrs.	80° C 3 hrs.
150 ml Polyurethane acrylate	3.0 ml catalyst M	Already has acce-lerator in resin	RT 24 hrs.	40° C 16 hrs.

RT = room temperature

Table 4.4: The resins formulation as used in laminates fabrication

Early on in the project, some time was spent in finding a good, reproducible method of fabricating the samples. Initially, a hand lay up technique was adopted where four layers of glass cloth were impregnated with resin and laid up in a symmetrical manner, about the central axis. This was done in a steel window frame mould. Each time, 150 ml

of resin were used. About 45 ml premixed resin was initially poured into the centre of the frame mould and the balance of the resin was added in stages. As may be seen in Table 4.4, the polyurethane vinyl ester and polyester resins required the addition of catalyst and accelerator while, for polyurethane acrylate resin, only catalyst was needed. This was because the polyurethane acrylate resin already had accelerator inside it. Catalysts and accelerators were used in order to speed up the curing process.

The steel frame mould was covered with PET film to aid release of the laminate. The first cloth layer was added and the resin was allowed to wet the cloth using a soft brush. A roller was used to expel as much air as possible from between layers. The moulding was left for about thirty seconds to allow the air bubbles to rise to the surface before the second layer was added. This process was repeated for the remaining two layers. Once all of the layers of cloth had been added, a second PET release film was then placed on the top of the moulding to ensure a good and smooth surface and to aid mould removal. A small stick was used to push out excess resin and trapped air bubbles. A steel plate was placed above the PET film and two weights totalling twenty kilograms were placed on the top, in order to expel excess resin.

Once the sample had gelled sufficiently (after about two hours), the weight and the steel frame were carefully removed. The plaque was left between the PET sheets for about twenty-four hours at room temperature. Resulting plaques were checked using an optical microscope to ensure that no fibre fibre contact could be observed. Finally, the polyester and polyurethane vinyl ester plaques were postcured at 80°C for three hours and for the polyurethane acrylate lay-ups at 40°C for sixteen hours, as recommended by Scott Bader Co. Ltd.

These combination of temperature, and time were recommended by the supplier to give optimum properties to the resin. Dyer (1996) reported that the tensile strength and modulus were optimised when polyurethane vinyl ester was post cured at 80°C. At higher temperatures, it was noted that degradation started to occur with a corresponding

reduction in mechanical properties. A similar fabrication technique was used to produce some pure resin samples.

The plaques were cut into parallel-sided samples of the required dimensions using a band saw. The edges were carefully polished to remove any signs of mechanical damage. Aluminium tabs were then glued onto both pre-roughened ends of the samples using Araldite 2005, a high peel strength glue. This helped to prevent grip failure in tensile and fatigue testing.

There were two main sample shapes used for this research as shown in Figure 4.4. The parallel sided geometry was used for tensile and basic fatigue characterisation. These were 20 mm wide to ensure a sufficient average number of fibre bundle were in the loading direction. The length of the samples was 140 mm for the $[90/0]_{2S}$ and 125 mm length for the $[\pm 45]_4$ samples.

The thickness of all samples was typically about 2.5 mm thick but there were small variations due to different cloth thicknesses. The waisted shaped samples were used for modulus decay measurement. This design was previously established by Curtis et al. (1991) to ensure that damage and failure only occurs in the central waisted region, which was monitored with an extensometer.

4.3 Materials Characterisation

Several techniques have been used to characterise the materials used in this research. These included fibre weight fraction measurements in order to find the percentage of the fibres in each plaque, tensile testing, to determine the strength and stiffness of the materials, and fracture toughness testing to compare the toughness of the resins.

A: sample of $[90^o/0^o]_{2S}$

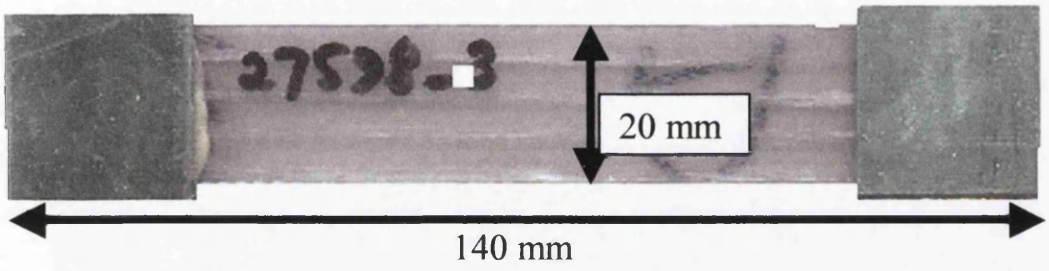

B: sample of $[\pm 45^o]_4$

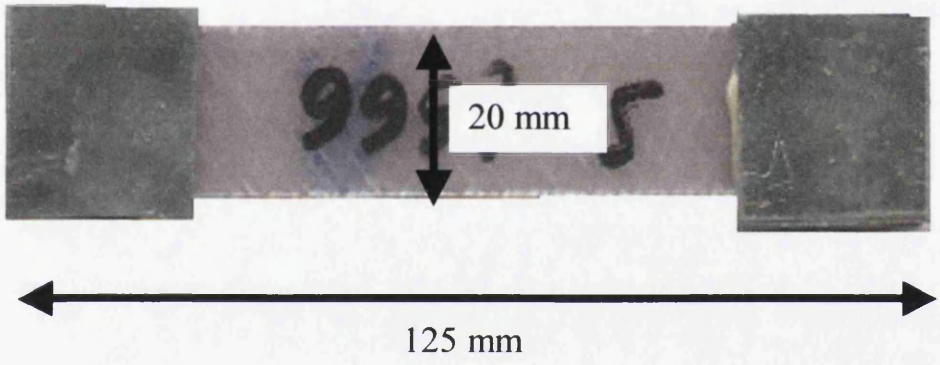

C: Modulus Degradation samples, $[90^o/0^o]_{2S}$ and $[\pm 45^o]_4$

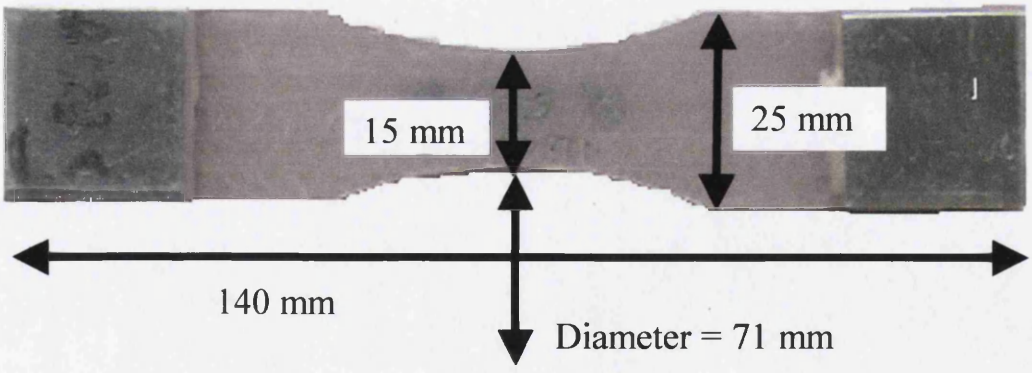

Figure 4.4 : Samples dimension,

4.3.1 Fibre Weight Fraction

Each plaque was checked to ensure that the fibre weight fraction of each lay up remained fairly constant, allowing results from different plaques to be compared. The fibre weight fraction was found by taking a large sample, size 80 mm x 80 mm from each plaque. This was then weighed before the sample was placed in a furnace at 650°C for approximately one hour until all the resin decomposed. After the sample had cooled, the weight of the fibres was determined; this was divided by the weight of the original sample and made into a percentage to give the fibre weight fraction.

$$\text{Fibre Weight Fraction } (\%) = \frac{(\text{weight of fibres and crucible}) - (\text{weight of crucible})}{(\text{weight of sample and crucible}) - (\text{weight of crucible})} \times 100\% \quad (4.1)$$

4.3.2 Tensile Testing

The tensile tests for the composite laminates were performed on the samples with an approximate thickness of 2.5 to 3.5 mm All dimensions were measured with a micrometer screw gauge with accuracy of 0.01 mm. The machine used was a Nene modified Instron Model 1602 tensile tester, which was operated with a crosshead speed of 1 $mm.min^{-1}$. Parallel sided coupon specimens were used for the $[90/0]_{2S}$ and $[\pm 45]_4$ lay ups, as described in Section 4.2.1. Tensile testing for the pure resins (polyester, polyurethane vinyl ester and polyurethane acrylate) was carried out on an ESH servo-hydraulic machine using parallel-sided coupons and an extensometer located at the middle of the sample.

Samples from the composite laminates were placed in the bottom set of grips which were then tightened. A set square was used to ensure that the samples were in a vertical position and the sample axis and loading directions coincided. The load was then zeroed before tightening the top set of grips. The test was then conducted with the crosshead moving at the rate of 1 $mm.min^{-1}$. The information from each test was recorded on a Nene computer, which provided a graph of load versus displacement. The ultimate

tensile strength (UTS) of the sample was taken as the maximum stress (i.e peak load/original cross sectional area) achieved during the tensile test.

The tensile modulus was calculated, using the initial slope of the curve and Equation 4.2.

$$\text{Tensile Modulus} = \frac{\text{Original Length of the sample x Load}}{\text{Extension x Area of The sample}} \qquad (4.2)$$

4.3.3 Single Edge Notch Tension (SENT) Fracture Toughness Testing

Single edge notch tension fracture toughness testing on the three pure resins i.e polyester, polyurethane vinyl ester and polyurethane acrylate was carried out in this research using the procedures outlined by Brown and Srawley (1966) to compare fracture toughness values, K_{IC}. Specimens with the dimensions as shown in Figure 4.5 were used for these tests. The dimension fitted the criteria that the thickness, B, was sufficient to ensure plane strain, while, the width, (W) minus the crack length (a), (W-a) was sufficient to avoid excess plasticity. W/B was approximately equal to 2 but not greater than 4. Also the crack length was approximately equal to the thickness and a/W was between 0.2 and 0.4, ($0.2<a/W<0.4$). A sharp natural crack was introduced into the sample at the machined notch tip using a razor blade.

Samples were placed in a NENE tensile machine and loaded at a rate of 1 $mm.min^{-1}$. Then the load was plotted against displacement on the connected printer. The resultant graphs showed a linear increase in load with time followed by an abrupt drop of load to zero. This allows the determination of K_Q, the invalidated fracture toughness, from the maximum load, P_Q. The crack length, a, was determined from the fracture surface after testing using a reflected light microscope. An average measurement was used for the determination of K_Q, with measurement taken from the centre of the front crack, and

Figure 4.5: Sample Dimension for Fracture Toughness

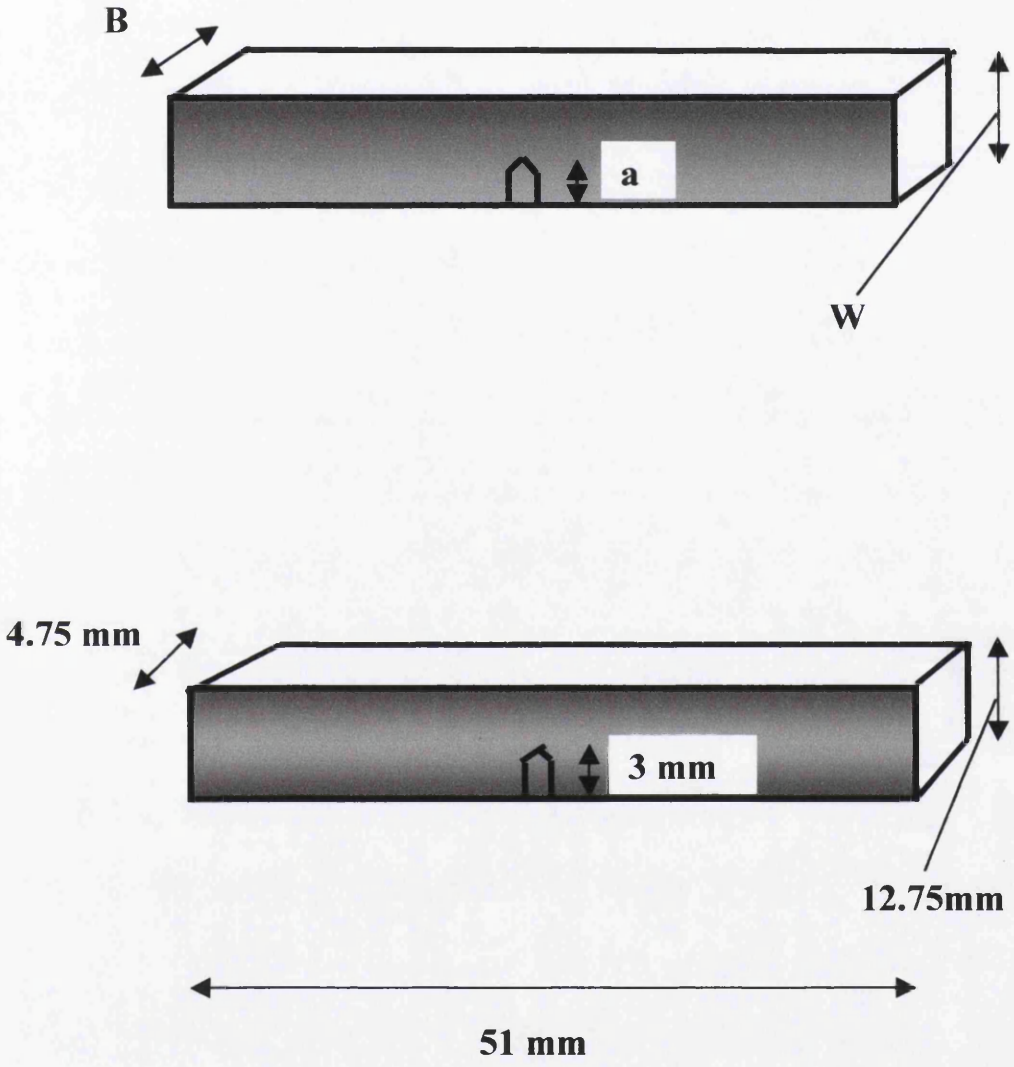

from the end of the front crack on each surface of the specimen. The obtained values were substituted into the following equation: -

$$K_Q = Y\frac{P_Q}{BW}\, a^{1/2} \quad (K_Q \text{ in of unit MPa.m}^{1/2}) \tag{4.3}$$

$$Y = 1.99 - 0.41(\alpha) + 18.7(\alpha)^2 - 38.48(\alpha)^3 + 53.85(\alpha)^4 \tag{4.4}$$

where;

K_Q : conditional or trial K_{IC}

Y : width correction factor

P_Q : load (kN)

B : specimen thickness (m)

W : specimen width (m)

a : crack length (m)

α : (a/W)

The obtained trial values of K_Q were then validated. This was done by calculating $5(K_Q/\sigma_y)^2$ using tensile strength values as σ_y, and this condition must comply with the standard as suggested by ASTM:

i.e;

$$W_{min} > 5(K_Q/\sigma_y)^2 \tag{4.5}$$

If this condition is satisfied, then the value determined for K_Q must be equal to K_{1C}.

4.4 Fatigue Description

The fatigue testing procedures carried out are described below. S-N testing was used to compare the fatigue properties of each lay up. The S-N fatigue testing used two

value of R, namely R=0.1 and R=-1. In order to visualise the damage to the samples especially at the fractured surface due to exposure to fatigue, SEM photographs were taken. In this research, the fibre direction of two lay ups, namely $[90/0]_{2S}$ and $[\pm 45]_4$ have been investigated. It was found that the cloth distorted on impregnation with resin. This distortion clearly happened for $[\pm 45]_4$ lay-ups, possibly during rolling process in laminate preparation. For the environmental fatigue test, the lay ups were tested in air, distilled water and seawater. Moisture absorption tests, as described in Section 4.8 were also used to help explain the results obtained in the environmental S-N testing.

4.4.1 Fatigue Testing

Parallel-sided samples of width 20 mm, length 140 mm or 125 mm and again slightly variable thickness (about 2.5 mm) were fabricated and set up in one of two pneumatic fatigues machines. Initially, the maximum load was taken as 60% of the ultimate tensile strength, (UTS), and adjusted accordingly to the specimen's dimensions. Further tests then took lower percentages of the ultimate tensile strength until the percentage was reached which gave an approximate specimen lifetime of 10^6 cycles. Samples, which had not failed by 10^6 cycles, were removed. For stress ratio R = 0.1 in all tension-tension tests, the minimum load was a tenth of the maximum load. The calculation of stress ratio value, R is as shown below.

$$R = \frac{\text{minimum load}}{\text{maximum load}} \qquad (4.6)$$

The lay-ups were tested in two different fatigue machines (Figure 4.6), which have approximately triangular waveforms. The grips were serrated to ensure a good grip on the sample. Initially, a sample was fixed into bottom set of grips before the load was zeroed. The top set of grips was then tightened. The machine, being pneumatic, worked by the pressure of compressed air on a piston. To load the sample, air was allowed into the chamber above the piston, which forced the piston downward. The samples were then set cycling and the voltages were adjusted with a multimeter until they reached those corresponding to the required maximum and minimum loads. After the loads were

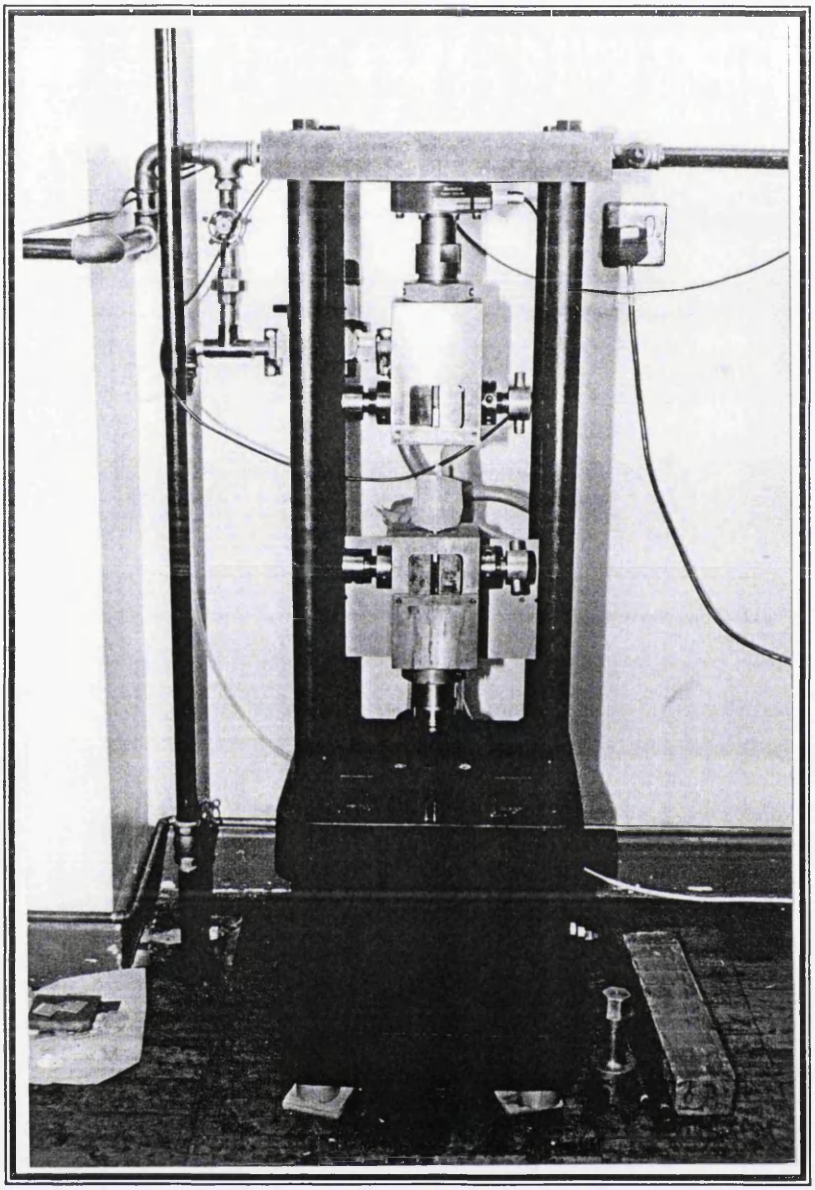

Figure 4.6 : Fatigue machine
(for [90/0] samples)

set, the frequency was adjusted until the samples loading was being cycled at a frequency of 1 Hz by increasing the rate at which air was allowed into the system. The voltages were then rechecked several times during the course of each fatigue test to ensure that the machine was still reaching the set loads. This method ensured that the maximum load was reached before the unloading half of the cycle occurred.

The machines worked by allowing compressed air to push the piston downwards and thus load the sample in tension. Once the voltage from the load cell on the machine reached the set maximum voltage, the solenoid valve was switched off automatically so that no more air could enter the piston chamber and the piston moved upwards. On reaching the minimum voltage, the solenoid valve was again switched allowing compressed air back in to again force the piston downwards. By using this method, the machines only switched after the pre set load had been reached and so any drop in pressure in the compressed air supply had no effect on cycle load, only frequency.

Tests were carried out until either complete failure of the specimen occurred or until 10^6 cycles, the latter being designed the upper boundary of the low cycle fatigue regime. The number of cycles to failure was recorded for each sample and these data were plotted in the form of S-N graphs.

The $[\pm 45]_4$ lay-ups required lower loads, and so these samples were tested on the other pneumatic fatigue machine (Figure 4.7). This machine used a trapezoidal waveform. After the sample was fixed into both sets of grips, the machine was switched on. The pressure on the piston was set to correspond with the maximum load, using data determined from load/pressure calibration curves (Figure 4.8). The calibration was made by attaching a load cell to the machine (Figure 4.9). The pressure was adjusted using the knob on the control panel to get the appropriate pressure for the load. The pressure determined the amount of air available to push the piston downwards and load the sample.

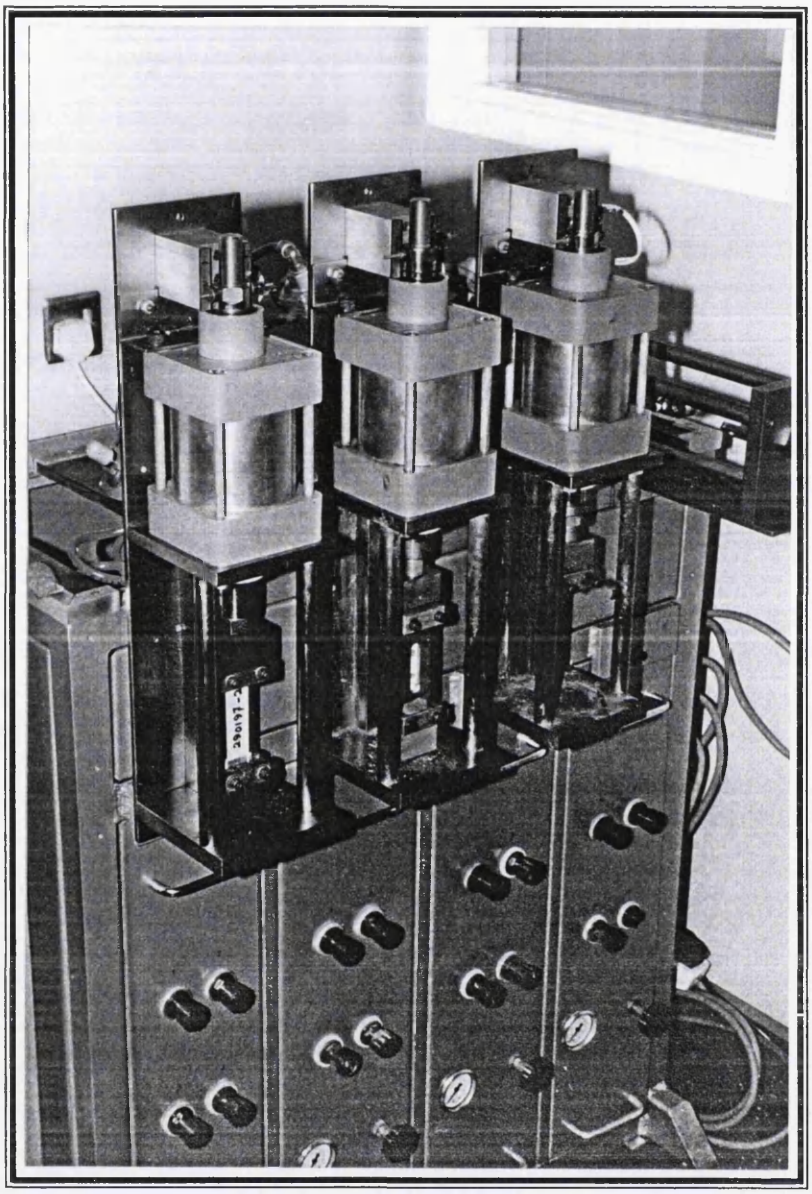

Figure 4.7 : Pneumatic fatigue machine
(for [±45] samples)

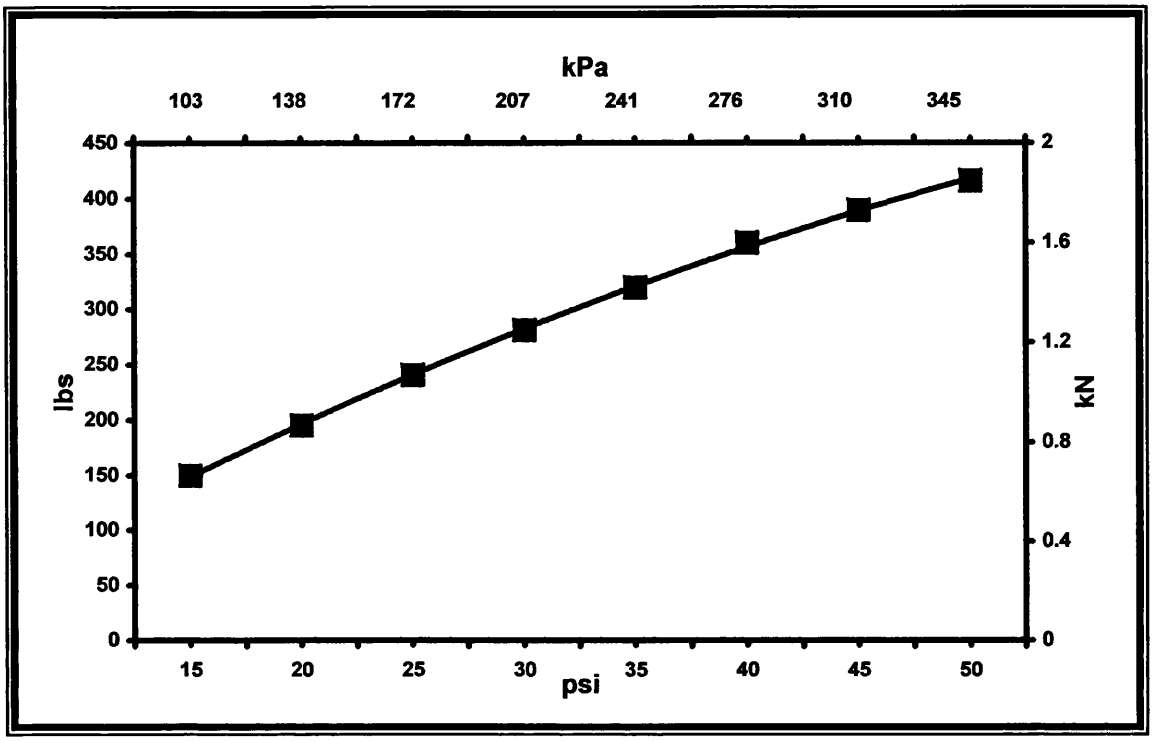

Figure 4.8: The calibrated relation between lbs (load) and psi (pressure)
(For pneumatic fatigue machine on $[\pm 45]_4$ samples)

Figure 4.9: Calibration Set Up using Load Cell
(for ± 45° samples)

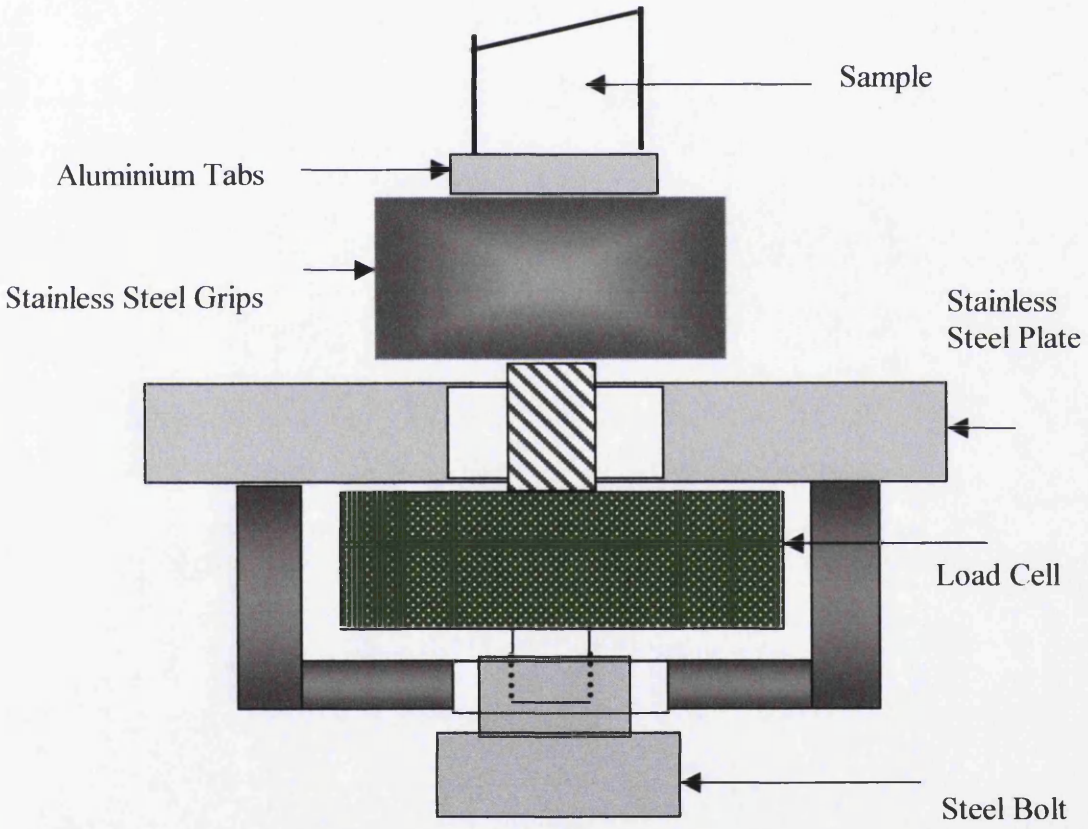

A similar procedure was also used for the S-N fatigue tests, for R= -1 i.e tension-compression testing. However in this case, antibuckling guides had to be used to support the sample during fatigue testing. This reduced the risk of buckling. The anti buckling device is shown in Figure 4.10.

4.5 Microstructural Investigation.

It is important to examine specimens for structures that are representative and relate to the problem and then correlate them with the relevant properties of the material. Samples for viewing both under a scanning electron microscope (SEM) and an AFM were prepared. Fractured surfaces of samples from S-N testing were examined using scanning electron microscopy. Samples for optical microscopic examination were prepared using standard metallographic grinding and polishing techniques. The samples were ground using dry grinding paper of 60 grit and finally polished with fine diamond dust (1 μm diameter). These samples were attached to a stub using collodial silver in acetone solution. The entire sample had to be coated with gold to provide an electrically conductive surface. The coated samples were placed in the vacuum chamber in a JEOL 6100 scanning electron microscope and bombarded with electrons which were accelerated towards to the samples at a voltage of 3 kV or less.

When the electron beam was incident on the sample, secondary electrons were given off and these were collected by a detector, which created an image of the sample. This method allows the morphological features of the sample to be investigated.

4.6 Fibre Direction Measurement

To observe any changes in the properties, fatigue life and strength, which have been carried out before, ten samples from a previous study, Dyer (1996) and ten samples from the present experiments, were analysed. Scanner and Sigma-scan software were used to measure the fibre direction in the laminate. The samples were placed on the scanner and using the sigma scan software, the angle of the fibre direction can be measured as seen in

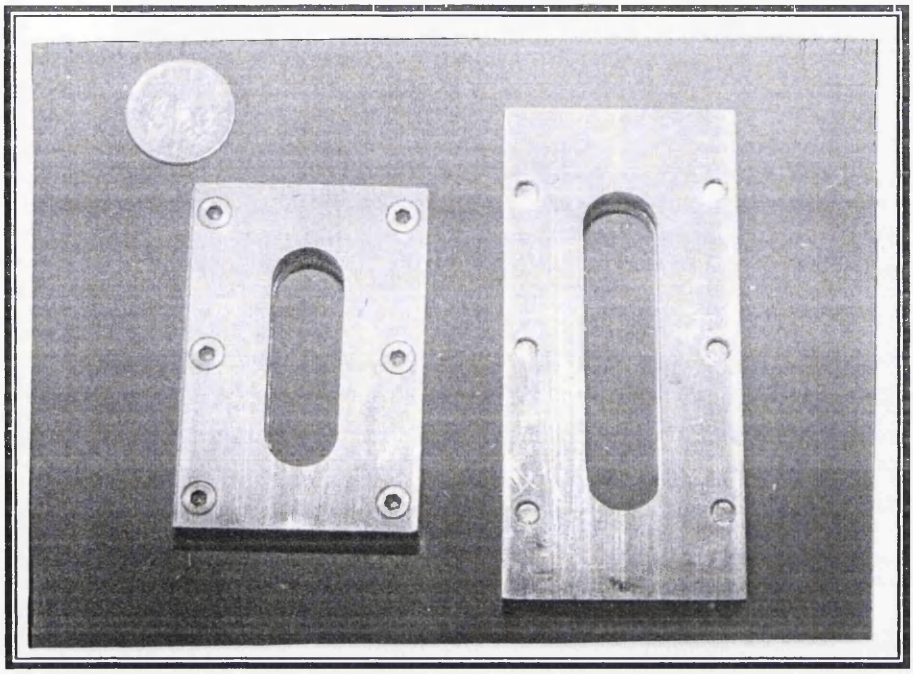

Figure 4.10: Photograph of the antibuckling guides

Figure 5.16. Only the outer part of the laminate can be measured using this equipment. The result for these measurements can be seen in Chapter 5.

4.7 Environmental Effect On Fatigue Test

Numerous tests were performed on the materials used in this research to investigate the effects of air, distilled water and seawater on the properties of all the samples. Seawater tests were perform using a standard sea water preparation which conformed to BS 3900 and BS 2011. All tests were carried out at room temperature 23°C and about 50% humidity condition. The room was equipped with temperature and humidity control equipment.

These environmental fatigue tests were carried out in the same manner and under the same conditions as for the S-N testing, (see Section 4.41) and using both stress ratios, R equal to 0.1 and –1. However, in this part of the investigation, the equipment was modified to include an environmental chamber which held the relevant environment around the sample during testing. For the $[90/0]_{2S}$ lay up the chamber was made from `polypropylene while for the $[\pm 45]_4$ lay up was made from PMMA as illustrated at Figure 4.11. Again parallel-sided samples were used but the length was shortened slightly to accommodate the loss of length from inclusion of the chamber.

4.8 Moisture Absorption Testing

Specimens (of width 45 mm and length 45 mm) were dried out at the start of this part of the investigation. All specimens were preconditioned in an oven at 40°C until the weight loss had stabilised, and no further weight loss could be observed. These specimens, which included pure resins, were referred to as dry. After preconditioning, these specimens were placed in containers of distilled water, air and seawater

Figure 4.11: Environmental Set up

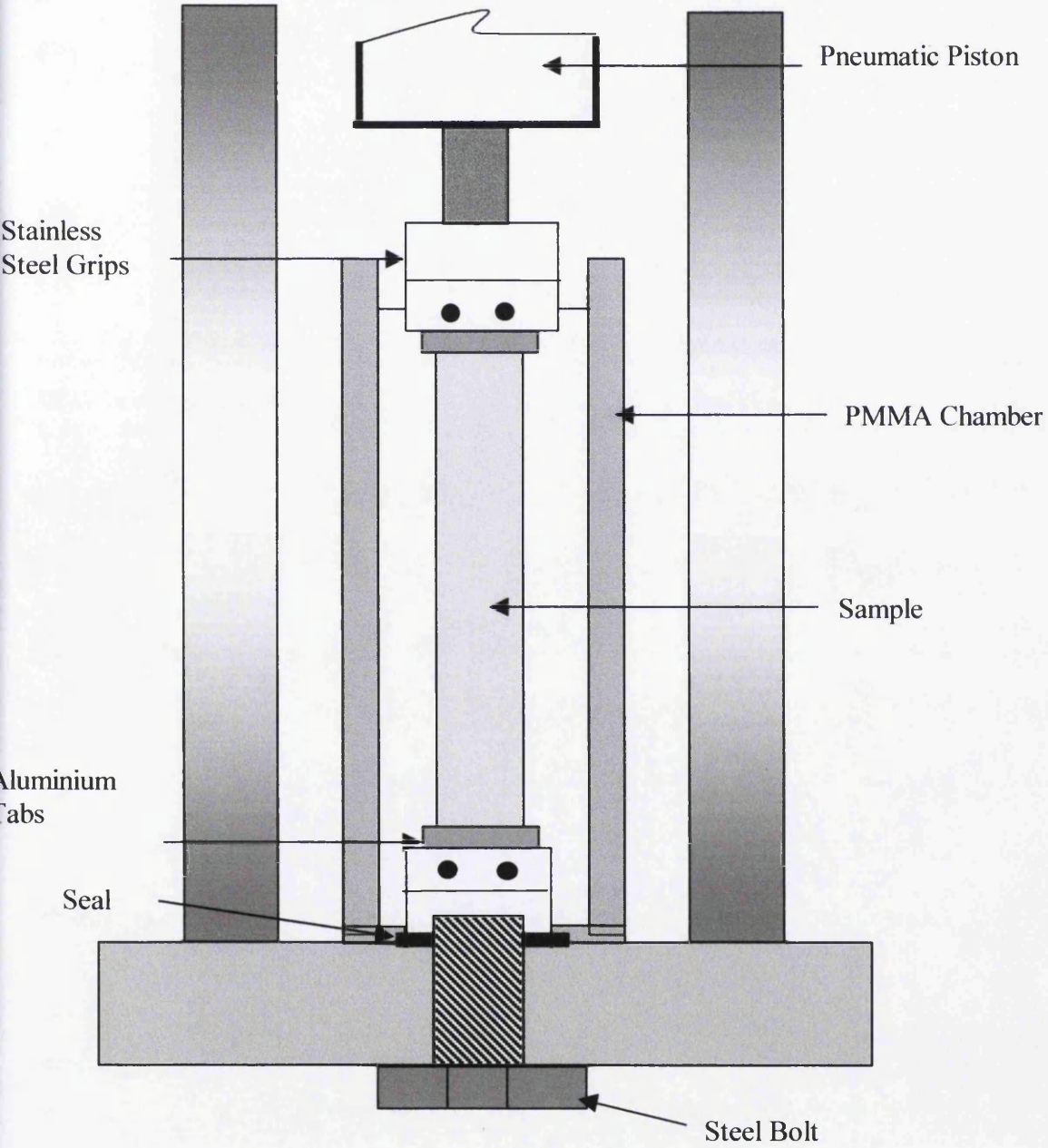

respectively. These tests were conduct at room temperature with 50% humidity condition.

Specimens were removed from the container at various time intervals for weight measurements. In the case of specimens placed in either of the liquids, the surfaces were carefully wiped before weighing. The weight gain process was continued until saturation of the materials. The weight was measured using an analytical balance, and the weight gain was calculated according to the following equation:

$$\text{Moisture content} = \frac{\text{weight of specimen - weight of dry specimen}}{\text{weight of dry specimen}} \times 100\% \qquad (4.7)$$

After the new weights were recorded the samples were replaced in the environments. The data were then plotted as percentage weight gain against time.
The other set of moisture absorption tests were carried out on the same type of lay-up as tested above, but this time all these samples had their edges sealed with silicone sealant in an attempt to prevent moisture uptake through the sample edges. They were used to compare the difference in moisture absorption rates and levels between the samples used in this research.

4.9 Modulus Degradation Testing

Waisted samples, with dimensions shown in Figure 4.4, were fabricated as in previous studies. As before, aluminium tabs were glued at the ends of the sample. There were two indents, 25 mm apart, tapped into the surface of the sample. The indent did not penetrate beyond the first ply. These indents were used to locate the arm pin of the extensometer, which was used to measure the vertical extension of the samples during modulus decay testing. Samples were fixed into the grips on the ESH servo hydraulic machine, and the extensometer located, after which the load, stroke, and strain were zeroed. The waveform which was to run the test, was then set up on the attached

computer. For all tests, a sinusoidal waveform was used with a frequency of 1 Hz and an R value of 0.1 or –1.

At certain interval, in general every 2000 cycles, a slow cycle was incorporated which lasted 50 seconds, during which approximately 85 load/extension data points were recorded. After the waveform had been set up, the maximum and minimum loads were determined and set on the machine. The maximum load was taken as the maximum stress required for each lay –up to last approximately 10^5 cycles (as deduced from the S-N testing), multiplied by the cross sectional area of the sample at the smallest width of the waist. These initial samples, one for each lay up, were cycled to failure. By setting the stroke cut off to a certain point, it was possible to prevent complete separation of some of the samples, allowing the fracture surface of the samples at the point just before failure to be studied. This point, or complete separation of the sample, was designated as specimen failure.

After failure, the recorded load/extension data from the tests were separated into individual hysteresis loops and plotted as stress/strain curves using a graph-plotting package. From the initial slope of each hysteresis loop, the modulus was calculated. It was found the moduli fell with increasing number of cycles. The modulus fall off occurred in stages, with each stage having a different slope suggesting that different damage mechanisms were dominant in each stage.

To study the modulus decay and damage mechanisms that were occurring during each stage, further samples of each lay up were tested under the same conditions i.e. loads, stress ratio and frequency, as for the initial samples. Two tests were run for each lay-up and were stopped after the number of cycles corresponding the end of stage 1 and 2 respectively. The samples were then removed, cut vertically down the centre of the sample; polished to remove mechanical deformation after which they were studied using reflected light microscopy techniques.

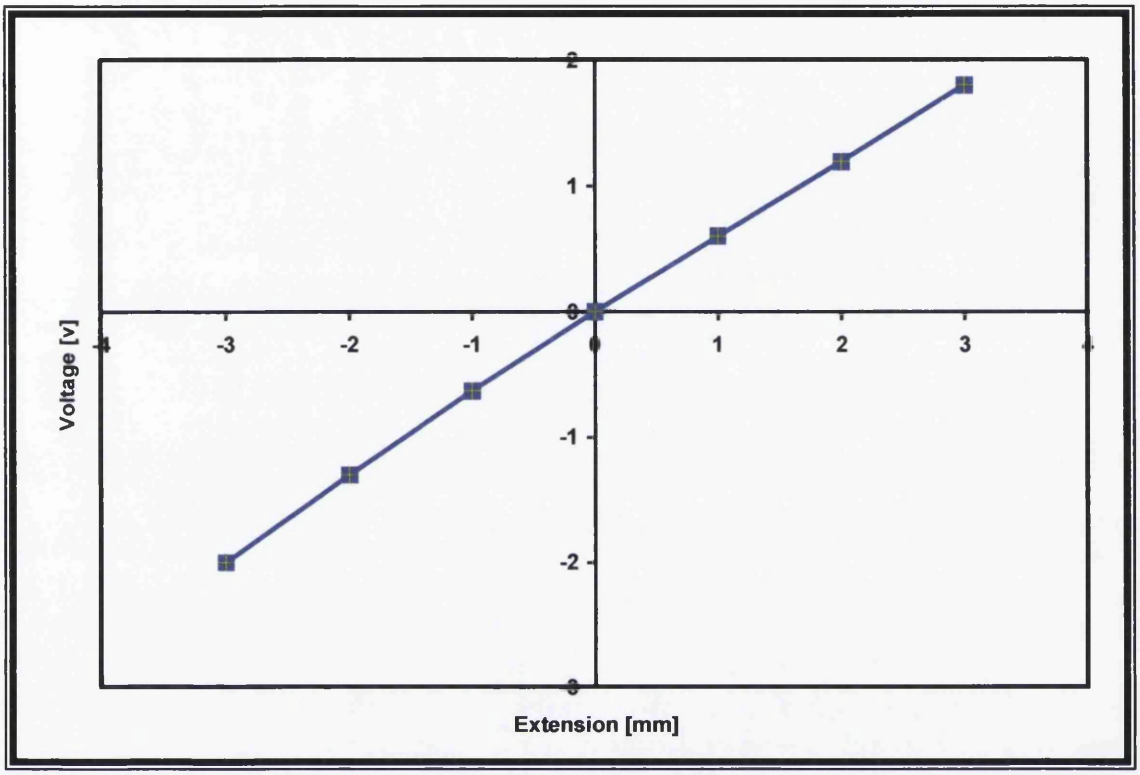

Figure 4.12 : The calibrated relation between voltage and extension

CHAPTER

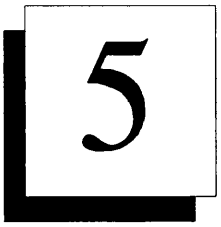

RESULTS and DISCUSSION

5.1 Introduction

In this chapter, the results of the experiments are given. In order to understand the subject better, it is appropriate if this chapter is divided into four topic areas, namely the materials characterisation, the general fatigue properties, the fatigue behaviour of polyurethane acrylate including the environmental effects on fatigue process and the modulus degradation testing.

5.2 Materials Characterisation

The materials used in this study have been described in Section 4.2. In this experiment, parallel sided and waisted specimens were used to generate fatigue life data. The specimens were prepared by cutting, using machines with diamond tools in order to minimise wear and produce a clean cut.

5.2.1 Fibre Weight Fraction

The average values for the fibre weight fractions of the materials used are shown in Table 5.1. Any plaque that deviated more than 5% from the average was rejected. Each plaque was checked to ensure that they gave fairly constant fibre weight fraction. It can be seen from the Table 5.1 that $[0/90]_{2S}$ Ulticloth and woven roving lay-ups have a high percentage of glass fibre compared with Biaxial Ulticloth laminate composites.

Lay-up		Resin	Average fibre weight fraction %
$[0/90]_{2S}$	woven roving	Polyester	64.2±2.4
		Polyurethane vinyl ester	59.6±1.6
		Polyurethane acrylate	60.2±1.3
$[0/90]_{2S}$	Ulticloth	Polyester	63.9±3.0
		Polyurethane vinyl ester	60.9±1.5
		Polyurethane acrylate	60.5±1.4
$[90/0]_{2S}$	Ulticloth	Polyurethane acrylate	61.3±1.8
$[\pm45]_{2S}$	Biaxial Ulticloth	Polyester	50.4±1.7
		Polyurethane vinyl ester	51.3±2.1
		Polyurethane acrylate	50.7±1.4
$[\pm45]_4$	Biaxial Ulticloth	Polyurethane acrylate	50.5±1.6

Table 5.1 Fibre weight fraction

The fibre weight fraction shows that there is little difference between the Ulticloth and woven roving lay-ups. Overall, the woven roving lay-ups have the highest weight fraction (typically about 60%) while the Biaxial Ulticloth $[\pm45]_{2S}$ and $[\pm45]_4$ have a fibre weight fraction (typically about 50%) about 10% lower than that of woven roving.

5.2.2 Tensile Testing

Tensile testing was performed on all eleven lay-ups to give a basic characterisation of their properties. At least three samples from each laminate were tested under tensile conditions. Tensile tests results for all three pure resins are shown in Table 5.2. For the eight composites, the average values for ultimate tensile strength (UTS) and modulus are listed in Table 5.3. Modulus values calculated for this table were based on the curve plotted of stress versus crosshead displacement. This method will give an approximate value for the modulus of the laminate compared with that using an extensometer, which measures the true specimen extension. However, these approximate values are useful for comparative purposes. One other problem with this method is measuring the gradient accurately in order to calculate the modulus, as explained in Section 4.3.2.

Pure Resin	UTS [MPa]	Modulus [GPa]
Polyester	44±3	3.8±0.6
Polyurethane vinyl ester	49±4	3.5±0.9
Polyurethane acrylate	45±4	2.8±0.8

Table 5.2: Pure resin tensile test results

From Table 5.2 and 5.3 it can be seen that the fibres play an important role as the reinforcing material in all the lay-ups. All of the composite lay-ups had higher UTS compared with their pure resin equivalent. For Biaxial Ulticloth laminates, the UTS values were only slightly greater since the orientation of fibres was ±45°, so the matrix plays an important role. Reifsnider and Talug (1980) and Hull (1981) stated that the initial damage was the formation of cracks in the fibre direction in the ply forming the largest angle to the load axis.

Figures 5.1 to 5.6 show stress versus displacement curves, which in the initial part of the curves are linear and begin to bend as stress increases. In the tensile testing, the original sample length of Ulticloth and woven rovings was 90 mm and for Biaxial Ulticloth samples it was 75 mm. The fibres and matrix are extending together and the change in slope is associated with the formation of damage, which leads to stiffness reduction.

Lay-up	Resin	UTS [MPa]	Modulus [GPa]	Normalised UTS	Normalised Modulus
$[0/90]_{2S}$ woven roving	Polyester	320±10	9.8±0.2	5.0	0.15
	Polyurethane vinyl ester	198±5	5.4±0.1	3.3	0.09
	Polyurethane acrylate	351±12	7.5±0.5	5.8	0.12
$[0/90]_{2S}$ Ulticloth	Polyester	375±12	7.2±0.3	5.9	0.11
	Polyurethane vinyl ester	249±4	6.3±0.1	4.1	0.10
	Polyurethane acrylate	374±10	5.8±0.5	6.2	0.10
$[90/0]_{2S}$ Ulticloth	Polyurethane acrylate	373±12	5.6±0.8	6.1	0.09
$[\pm45]_{2S}$ Biaxial-Ulticloth	Polyester	42±3	4.2±0.1	0.8	0.08
	Polyurethane vinyl ester	124±4	3.8±0.1	2.4	0.07
	Polyurethane acrylate	95±4	2.8±0.4	1.9	0.05

Table 5. 3: Composite lay up tensile testing results

Table 5.3 shows the tensile and modulus result. The normalised UTS and modulus have been calculated by divided those values with weight fraction. It can be seen that the $[0/90]_{2S}$ woven roving, polyurethane acrylate lay-ups tend to have a higher strength than their polyester and polyurethane vinyl ester (PUVE) equivalent. The Ulticloth lay-ups have a higher strength than the woven roving, although this difference is slight, especially on the $[0/90]_{2S}$ polyester, $[0/90]_{2S}$ and $[90/0]_{2S}$ polyurethane acrylate lay-ups. This higher

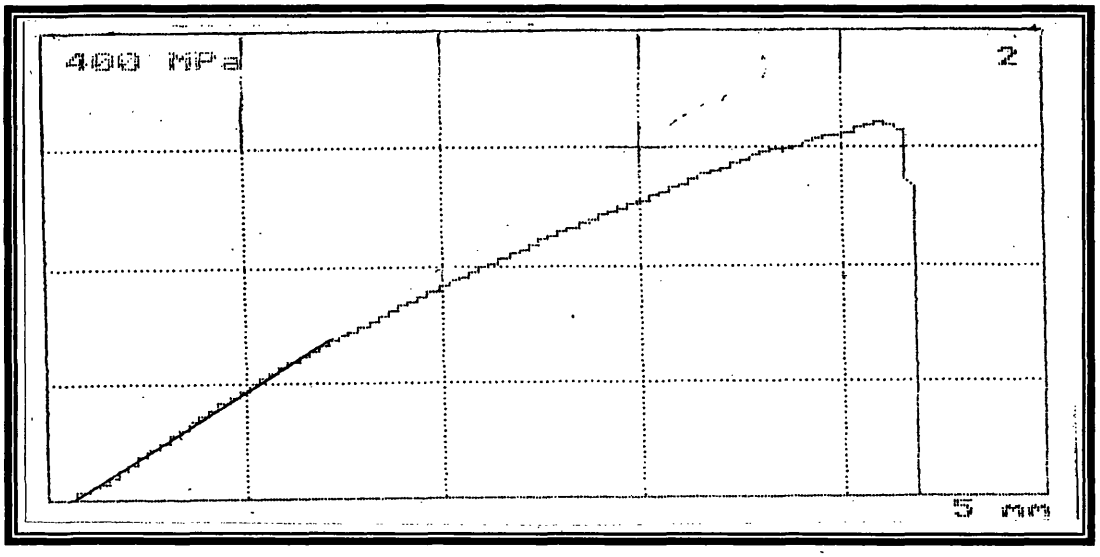

Figure 5.1 Stress-displacement curve at 1 mm/min for Polyester, lay up $[0^{\circ}/90^{\circ}]_{2S}$,woven roving.

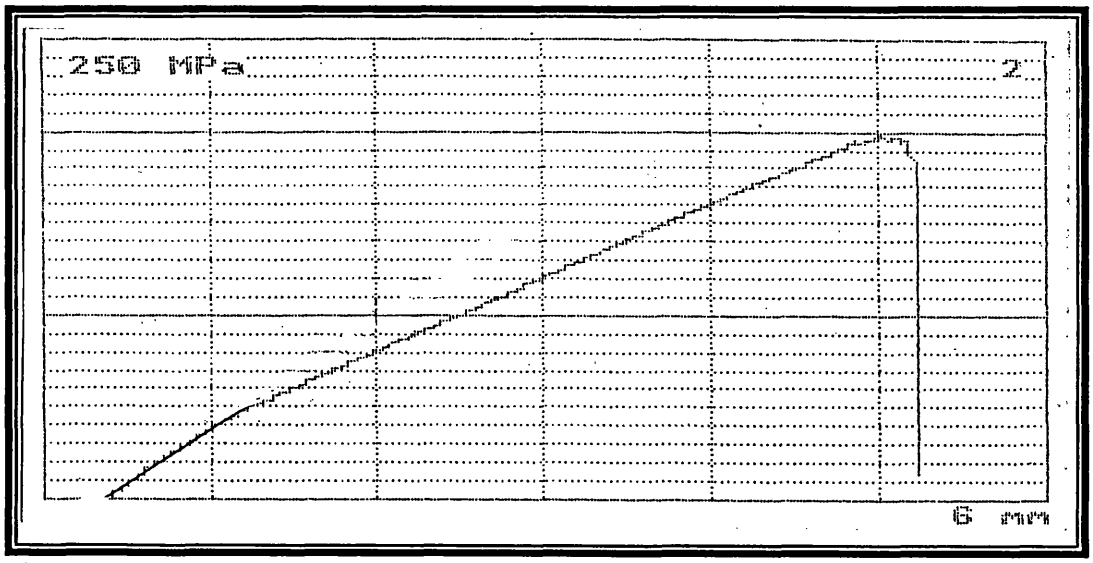

Figure 5.2: Stress-displacement curve at 1 mm/min for Polyurethane vinyl ester, lay up $[0^{\circ}/90^{\circ}]_{2S}$ woven roving.

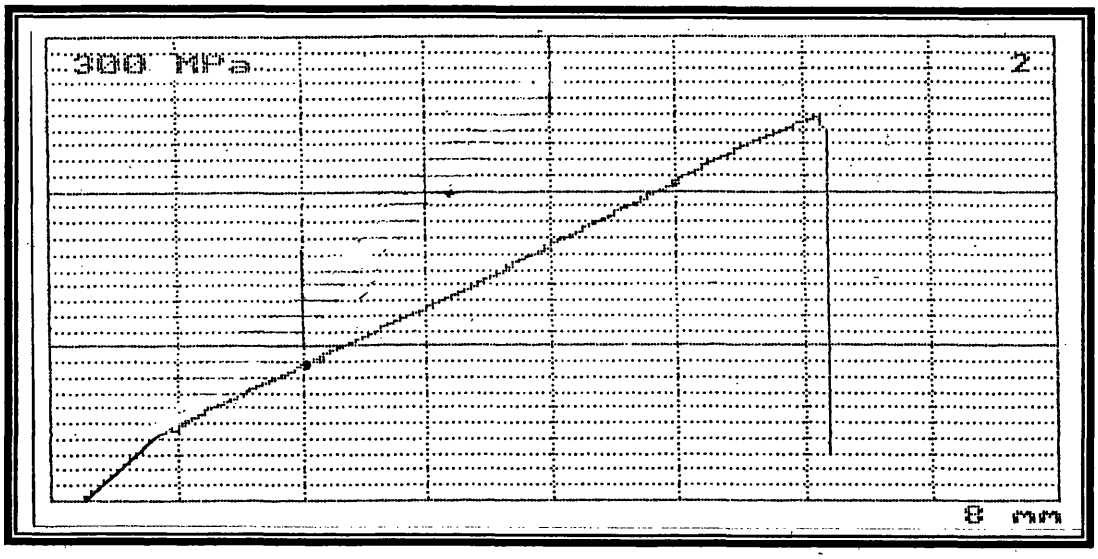

Figure 5.3 Stress-displacement curve at 1 mm/min for Polyurethane vinyl ester, lay up $[0°/90°]_{2S}$,Ulticloth.

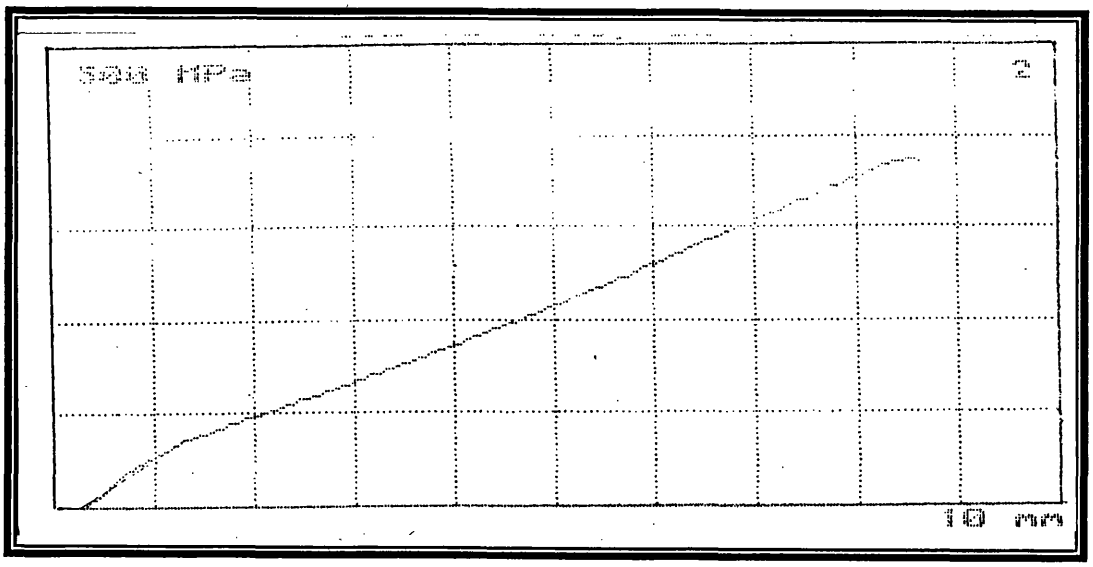

Figure 5.4: Stress-displacement curve at 1 mm/min for Polyurethane acrylate, lay up $[0°/90°]_{2S}$ Ulticloth.

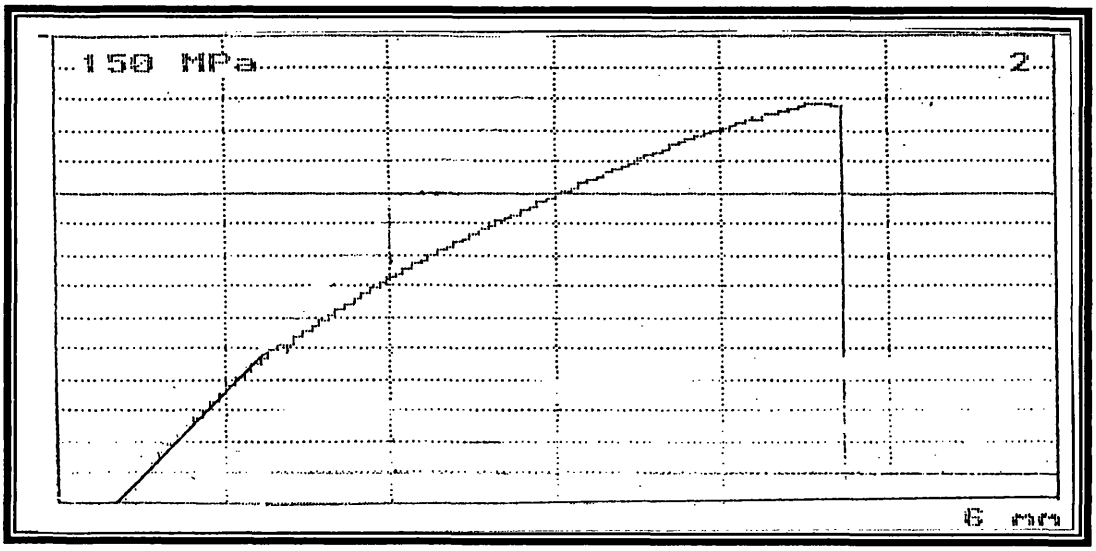

Figure 5.5 Stress-displacement curve at 1 mm/min for Polyurethane vinyl ester, lay up $[\pm 45^{\circ}]_{2S}$,Biaxial-Ulticloth.

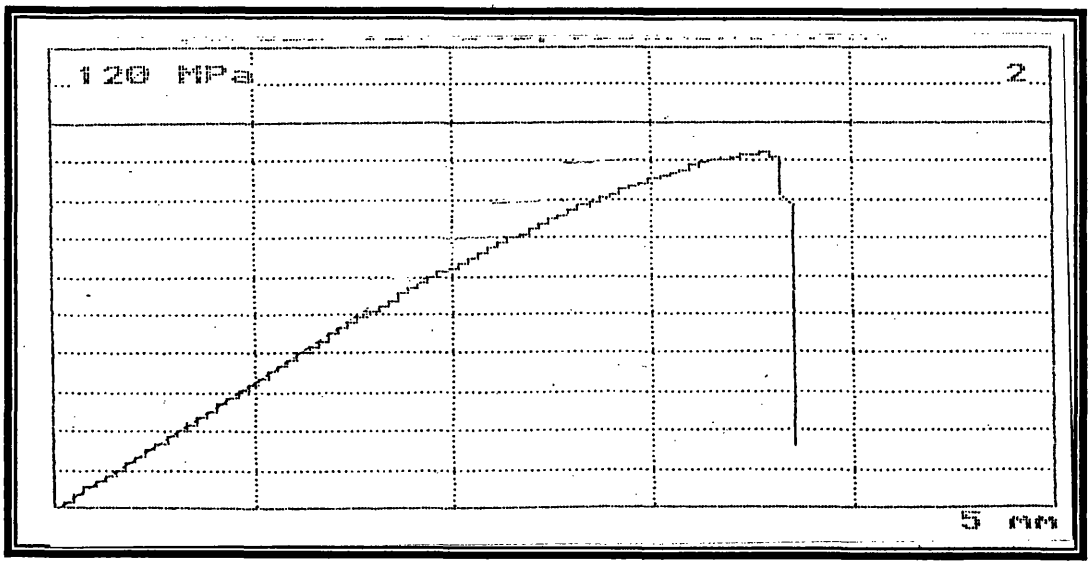

Figure 5.6: Stress-displacement curve at 1 mm/min for Polyurethane acrylate, lay up $[\pm 45^{\circ}]_{2S}$ Biaxial-Ulticloth.

strength is consistent with the higher percentage of fibres in the loading direction for Ulticloth (59%) compared with the woven roving material (50%). The presence of fibres in the loading direction for these lay-ups means that they can be considered to be fibre dominated. These lay-ups have higher strengths than the $[\pm 45]_{2S}$ lay-ups, since the matrix in $[\pm 45]_{2S}$ arrangements carries more load making these lay-ups more matrix dominated.

Comparison of stiffness between the pure resins shows that the polyester has the highest modulus, and it is also seen that polyester resin based composites are the stiffest for all lay-ups followed by polyurethane vinyl ester. However, in the case of $[0/90]_{2S}$ woven roving, the polyurethane acrylate was the second highest in modulus. This may be because the fibre weight fraction for that lay-up was higher than polyurethane vinyl ester lay-up. It is clearly seen from Table 5.1 and Table 5.3 that, although the fibre weight fractions between lay-ups were nearly the same (about 60% for [0/90] lay ups and around 50 % for ±45 lay ups), the moduli of lay-ups show more significant differences. The woven roving and Ulticloth showed higher modulus compared with Biaxial Ulticloth. This is again due to the fibres being arranged in the loading direction. According to Agarwal and Broutman (1990), the contribution of the fibres to the composite properties is a maximum when they are parallel to the loading direction. Composite strength and stiffness will be reduced when the fibres are not parallel to the loading direction.

There is no significant difference in UTS and modulus for $[0/90]_{2S}$ and $[90/0]_{2S}$ polyurethane acrylate lay-ups, and this was as might have been expected since, although the individual lamina are in a different order, the lay-ups have the same proportions of fibres in each direction. The effect of fibre weight fraction of composites on the modulus of the lay-ups can be clearly seen here, where the $[0/90]_{2S}$ woven roving, polyester, which had the highest fibre weight (64.2%) showed highest modulus too. The same effect happened to the lowest fibre weight fraction (59.6%), $[0/90]_{2S}$ woven roving, polyurethane vinyl ester, which showed the lowest modulus in their group.

5.2.3 Fracture Toughness

Fracture toughness tests using three point bend specimen with crack-width (a/w) ratio of 0.2 to 0.3 were used on all twelve samples, four for each matrix. The tests were carried out on a Nene machine at the rate of 1mm/min.

Resin	K_Q ($MNm^{-3/2}$) average
Polyurethane vinyl ester	2.4 ± 0.2
Polyester	1.3 ± 0.4
Polyurethane acrylate	2.3 ± 0.2

Table 5.4: Resin, fracture toughness

As may be seen from Table 5.4, polyurethane vinyl ester had an average fracture toughness (K_Q) of 2.4 ± 0.2 $MNm^{-3/2}$ while polyester had an average fracture toughness of 1.3 ± 0.4 $MNm^{-3/2}$. For the polyurethane acrylate resin, the average fracture toughness was 2.3 ± 0.2 $MNm^{-3/2}$. The above values are higher than expected and may not reflect the absolute materials fracture toughness due to shallow notch used. The state of plane stress could be prevalent near the crack tip instead of plain strain. However these values can be used for comparison purposes only.

These results show that the polyurethane vinyl ester resin has greater fracture toughness and will thus have a greater resistance to matrix cracking and fatigue damage [Joneja (1986)]. Leaity et al. (1992) noted that the presence of the urethane link gave higher toughness to the material. Polyurethane acrylate resin showed values equivalent to the polyurethane vinyl ester for fracture toughness. This means that this resin also has a greater resistance to matrix cracking and fatigue damage. The polyester has a lower value of toughness due to a higher crosslink density, which inhibits the movement of polymer chains leading to increased brittleness.

5.2.4 Fatigue Results

In this research, materials with stacking sequences of $[\pm 45]_{2S}$ and $[0/90]_{2S}$ have been used to generate fatigue life data. To compare the fatigue strengths of the composites, data generated are plotted in Figure 5.7 - 5.12. To illustrate scatter of the points, the scatter band had been drawn on each S-N curves. The scatter lines, lower and upper are drawn at +/- one standard error from the best-fit straight line. The best fit line were calculated by using least square method and the standard error of the estimate S_{YX} were obtained using the following computational formula [(Berenson and Levine (1983) and Mendenhall and Sincich (1994)]:

$$S_{YX} = \sqrt{\frac{\sum Y^2 - a\sum Y - b\sum XY}{n-2}} \qquad (5.1)$$

so the scatter band Y for a given X:

$$Y = \hat{Y} \pm S_{YX} \qquad (5.2)$$

where;

X = independent variables from data

Y = actual value of Y for a given X

$\hat{Y}$ = predicted value of Y for a given X

a = the Y intercept from best fit line equation

b = the sample slope from best fit line equation

n = number of samples

The typical downwards slope shown by all the S-N graphs illustrates that the ability of a material to withstand stress decreases with the number of fatigue cycles it undergoes.

Figure 5.7 shows the S-N curves for $[0/90]_{2S}$ woven rovings with the three different matrix types. It may be seen that all the curves have gradients with large slopes, showing that the fatigue life decreases as the number of cycles increases. Since the polyurethane acrylate samples have a higher static strength (Table 5.2), they might be expected to have higher fatigue strength as well. The best fit straight lines show that all three resins with woven roving lay-ups tend to have a similar pattern and scatter. Here, the fibres play an important role in determining fatigue life since these lay-ups are fibre-dominated. The graphs clearly illustrate that all the matrices generate nearly the same fatigue life since they have similar patterns and scatter.

Figure 5.8 shows the S-N curves for $[0/90]_{2S}$ Ulticloth with the three different matrix types. Again the character of the curves is similar, although there would appear to be some small differences. It appears that the polyester samples have slightly higher fatigue strength than the polyurethane acrylate samples, which in turn are superior to the polyurethane vinyl ester. This is particularly evident at the high stress/low cycles end of the graph and so it may well be related to the relative static strengths of these materials, which display a similar relationship (Table 5.2). At the low stress/high cycles part of the graph the data for the three materials tend to be much closer. It could be that the low fracture toughness of the polyester resin has a more significant effect at higher cycles and this offsets to some extent their relative static strengths.

Figure 5.9 shows the S-N curves for $[\pm 45]_{2S}$ Biaxial Ulticloth with the three different matrix types. It can be seen that with Biaxial Ulticloth, polyurethane vinyl ester and polyurethane acrylate have similar fatigue strengths, and are both significantly superior to the polyester equivalent. This may be correlated with the substantially lower UTS of the polyester-based composite for this particular $[\pm 45]_{2S}$ Biaxial Ulticloth lay-up (Table 5.2) and the low fracture toughness of this resin (Table 5.4).

It is clear from comparison of Figures 5.7, 5.8 and 5.9 that the higher the volume fraction of 0° fibres, the greater the fatigue strength. Thus, the $[0/90]_{2S}$ lay-ups of woven

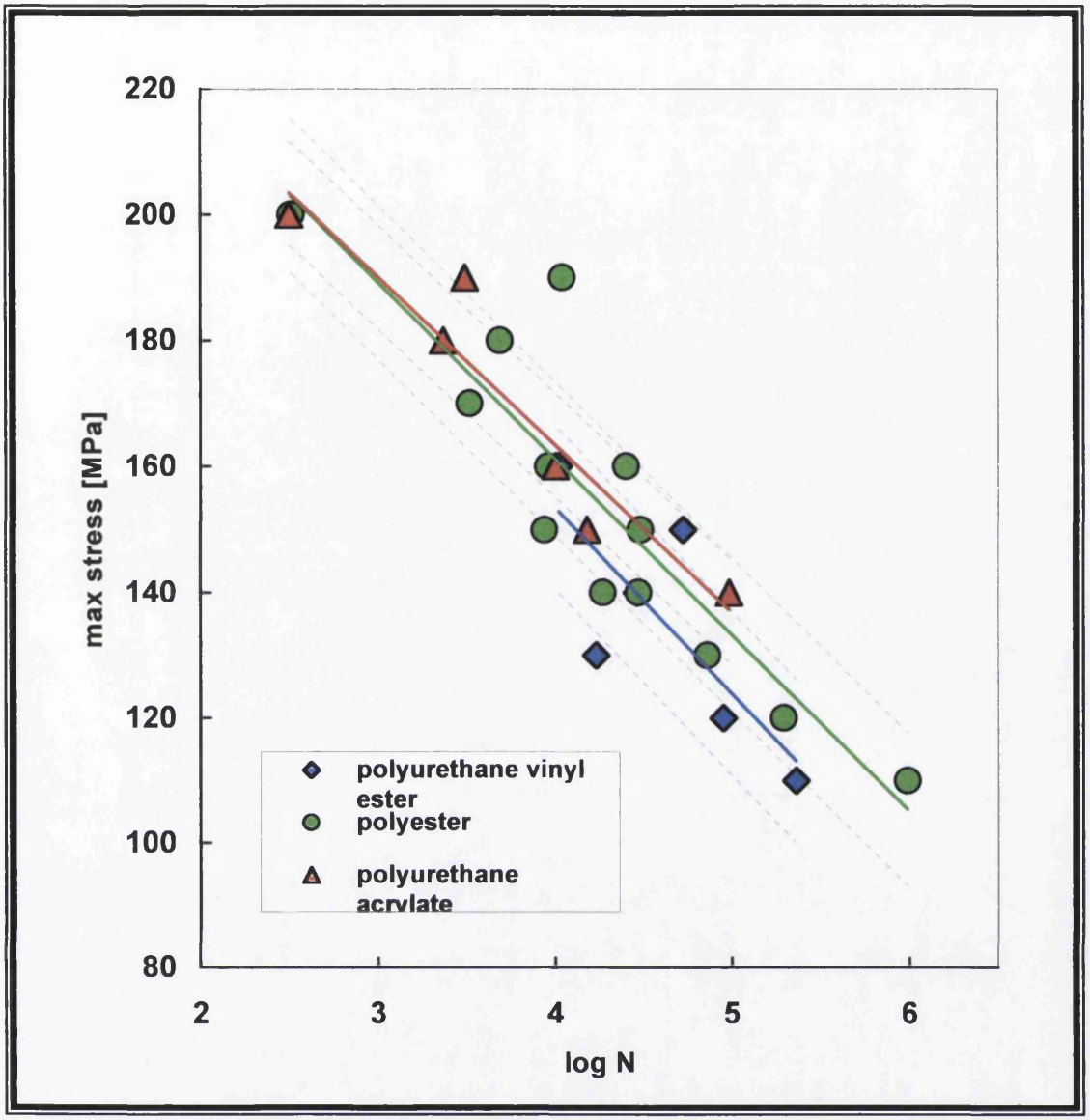

Figure 5.7: The fatigue life performance of $[0^{o}/90^{o}]_{2S}$ Woven Roving

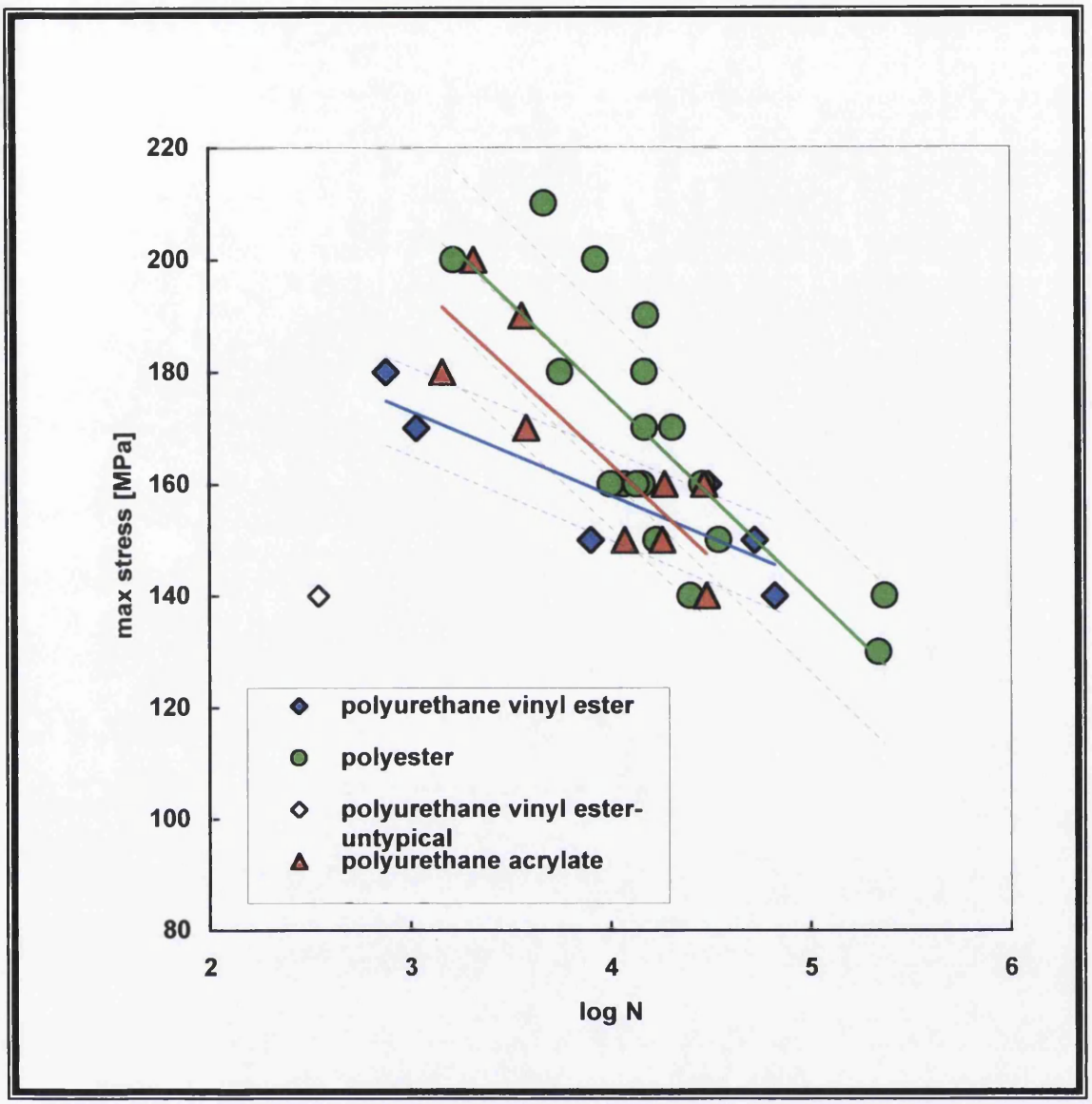

Figure 5.8: The fatigue life performance of $[0^o/90^o]_{2S}$ Ulticloth

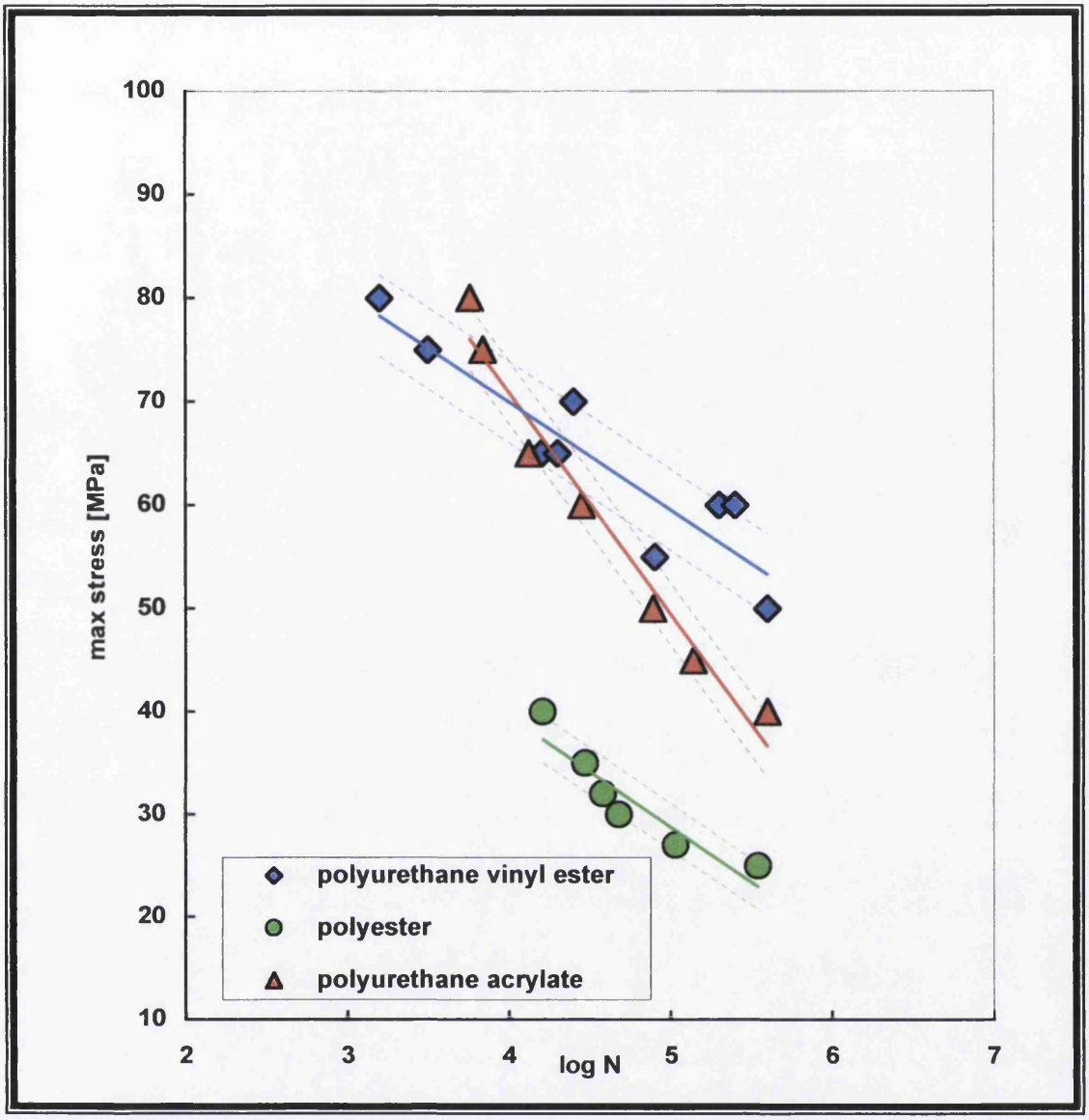

Figure 5.9: The fatigue life performance of $[\pm 45^{o}]_{2S}$ Biaxial Ulticloth

rovings and Ulticloth have similar S-N curves and have significantly higher fatigue strengths than $[\pm 45]_{2S}$ laminates. It is well understood that a higher degree of alignment of the fibres is necessary for the maximum possible reinforcing effect. The effect is seen more clearly in Figures 5.10, 5.11 and 5.12, which compare the three different lay-ups for each of the three resins.

Figure 5.10 shows the fatigue performance of polyester-based composites with the three different fibre lay-ups. This clearly shows that the Biaxial Ulticloth with polyester has a significantly lower fatigue strength (with small slope) than the woven roving and Ulticloth, which have higher strength since they are fibre-dominated laminates. This is consistent with similar data reported by Dyer (1996), that when orientation of the fibre plies was $[\pm 45]_{2S}$ the fatigue strength was low compared with $[0/90]_{2S}$ lay-ups since the latter contained fibres in loading direction. Figure 5.11 and Figure 5.12 show similar trends for the polyurethane vinyl ester and polyurethane acrylate to those seen for polyester composites in Figure 5.10, confirming that matrix dominated, $[\pm 45]_{2S}$ lay-up have low fatigue strength compared with fibre dominated $[0/90]_{2S}$ lay-ups. This set of graphs also shows that the laminate $[\pm 45]_{2S}$ Biaxial Ulticloth with polyester resin had the lowest strength compared with all the other laminates.

An earlier study has been carried out on laminates similar to some of those in the present report. The graphs for comparison can be seen in Figure 5.13, Figure 5.14 and Figure 5.15. From Figure 5.13, it can be seen that the data for the present experiments (for $[0/90]_{2S}$ lay-ups of woven rovings with polyester and polyurethane vinyl ester) are similar to those from the previous report [Dyer (1996)]. If anything the present data are slightly lower, and this may have possibly resulted from small differences in the preparation of the lay-ups and the lower fibre weight fraction in the present samples compared with the earlier data. Another possible reason was the viscosity of the polyester and polyurethane vinyl ester resin that may have varied between the two experiments. This might affect the strength of the lay-up that may give lower strength to the later experiments. This reason agreed with Stinchcomb et al. (1975), Sturgeon

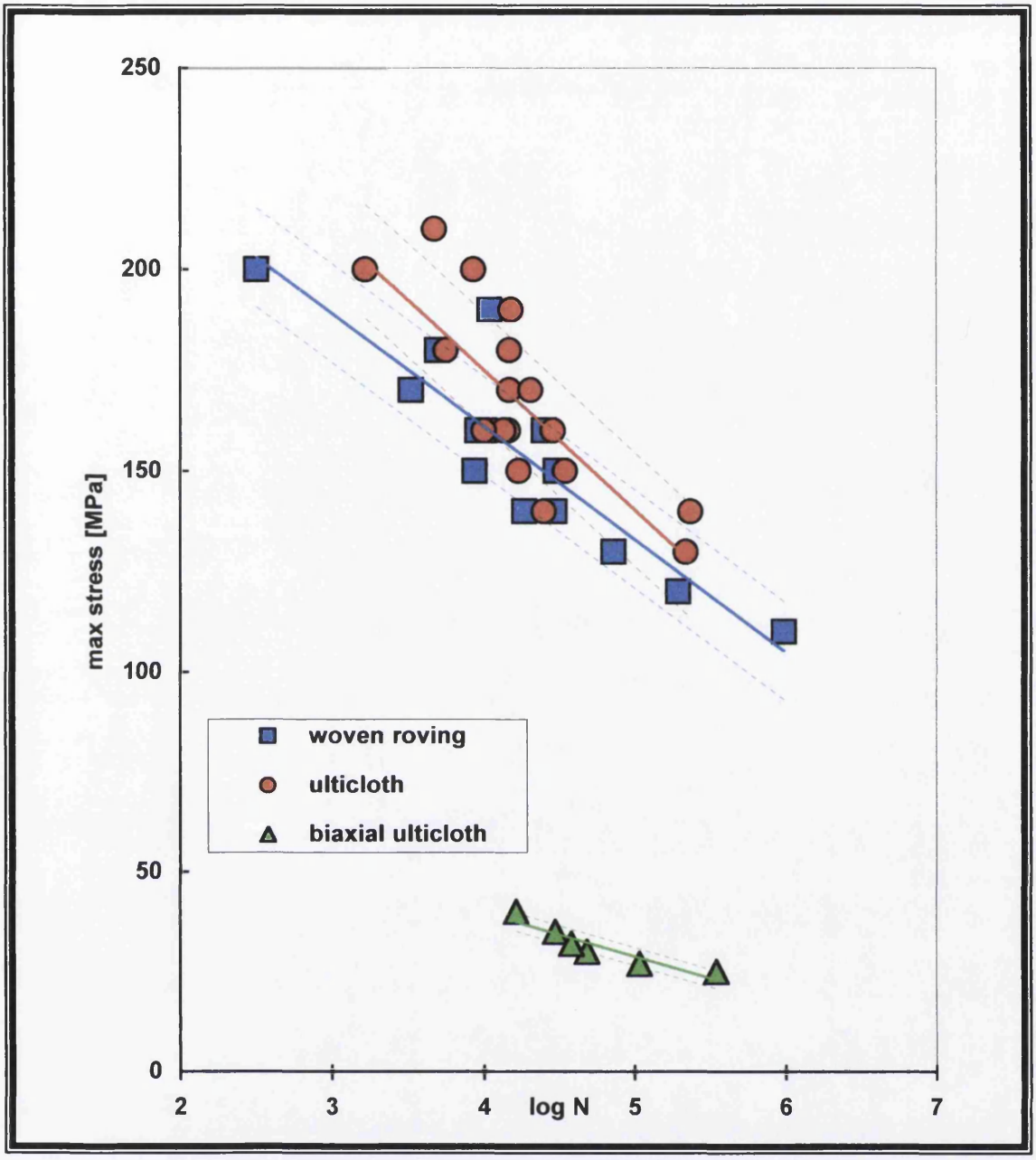

Figure 5.10: The fatigue life performance of Polyester

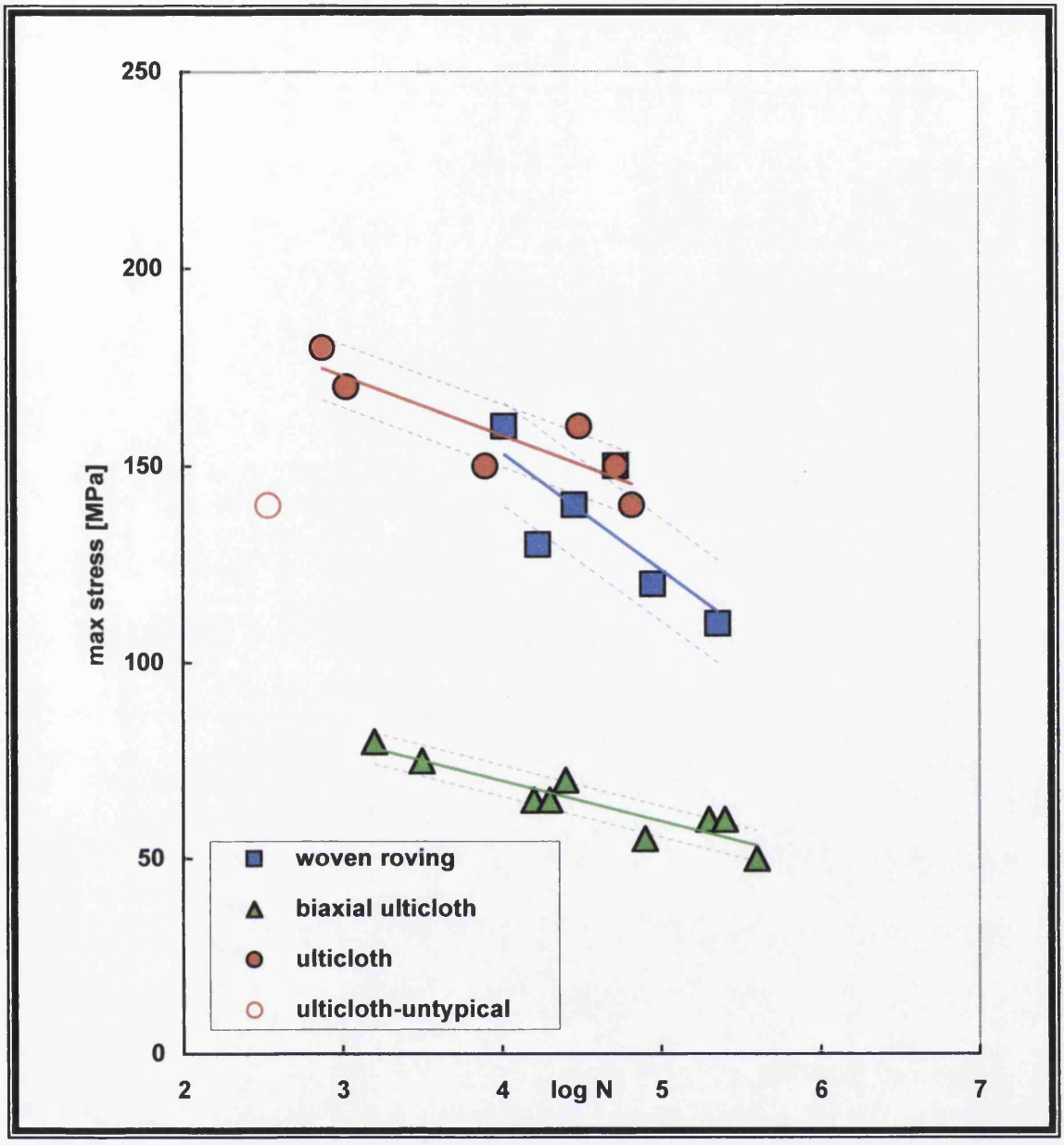

Figure 5.11: The fatigue life performance of Polyurethane Vinyl Ester

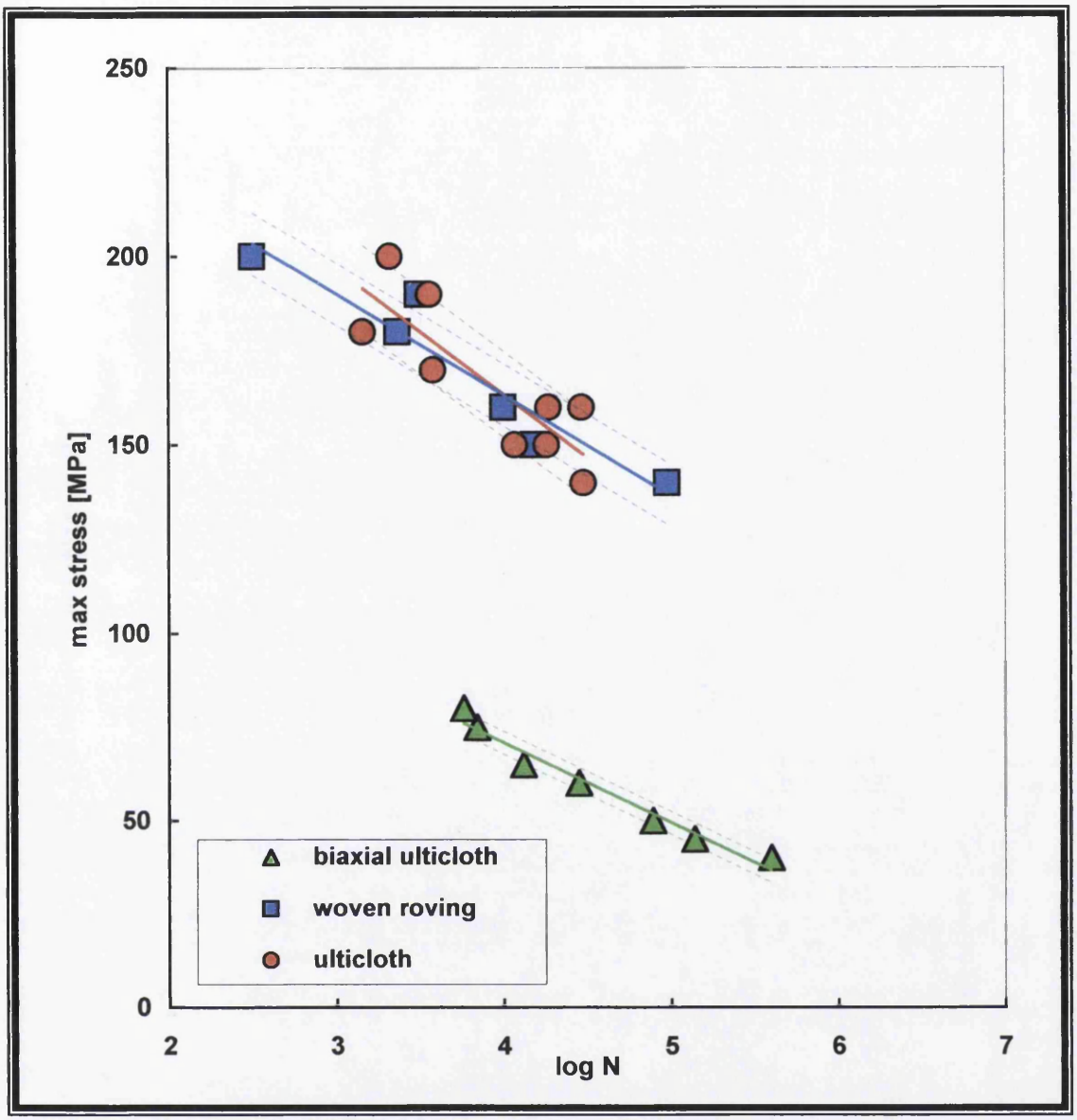

Figure 5.12: The fatigue life performance of Polyurethane Acrylate

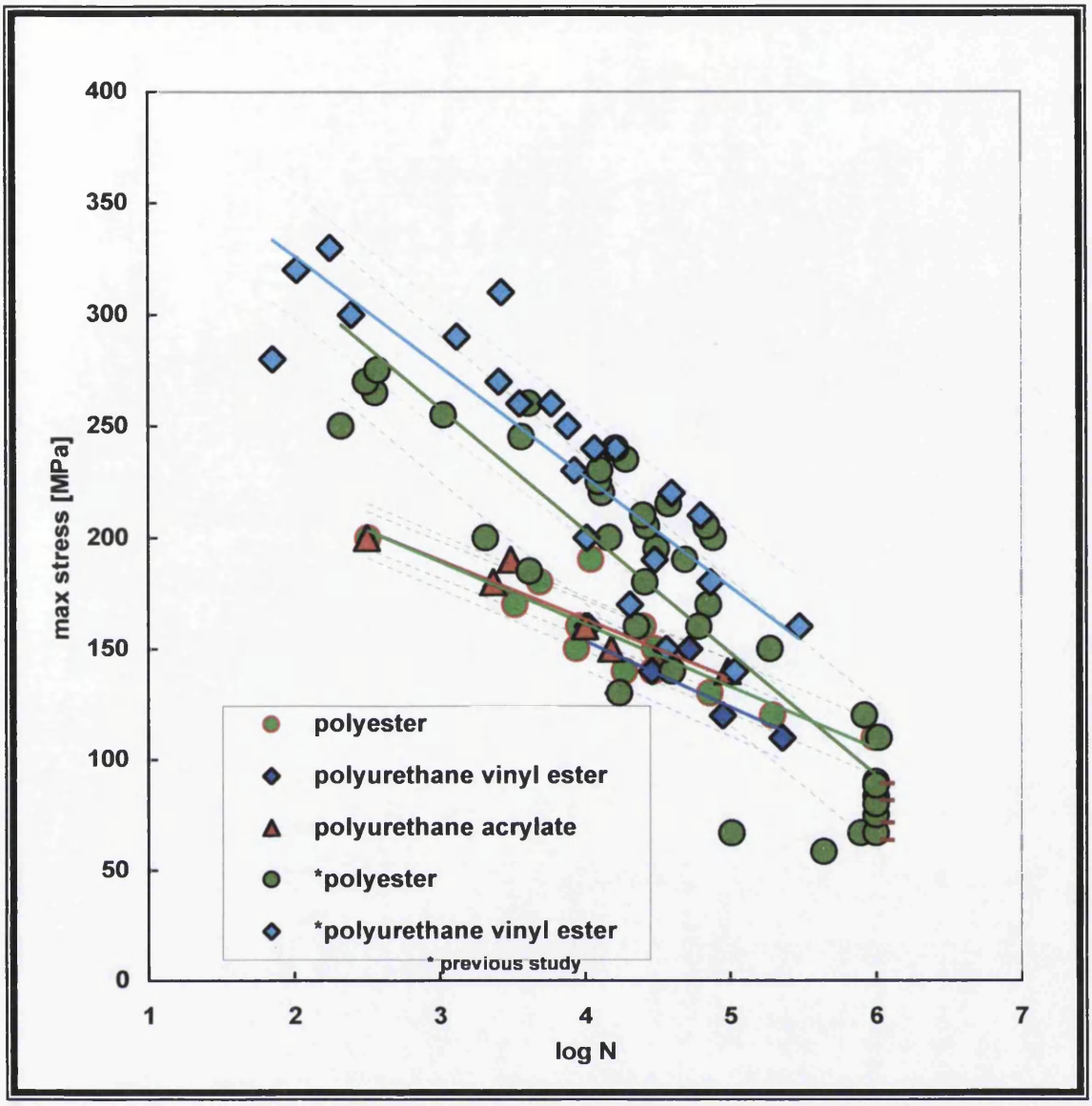

Figure 5.13: The comparison fatigue life performance of $[0^o/90^o]_{2S}$ Woven Roving with previous study

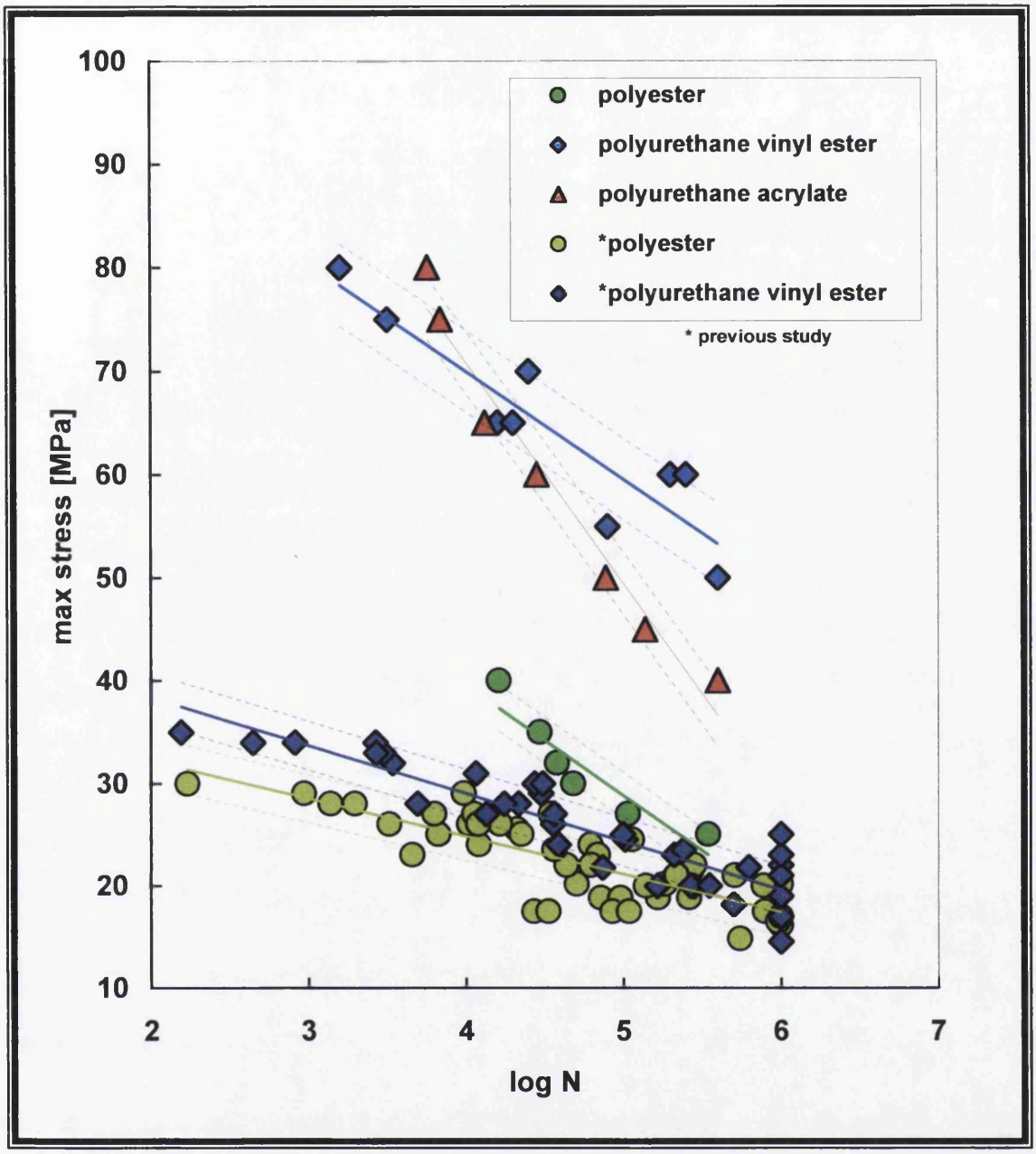

Figure 5.14: The comparison fatigue life performance of $[\pm 45^{o}]_{2S}$ Biaxial Ulticloth with previous study

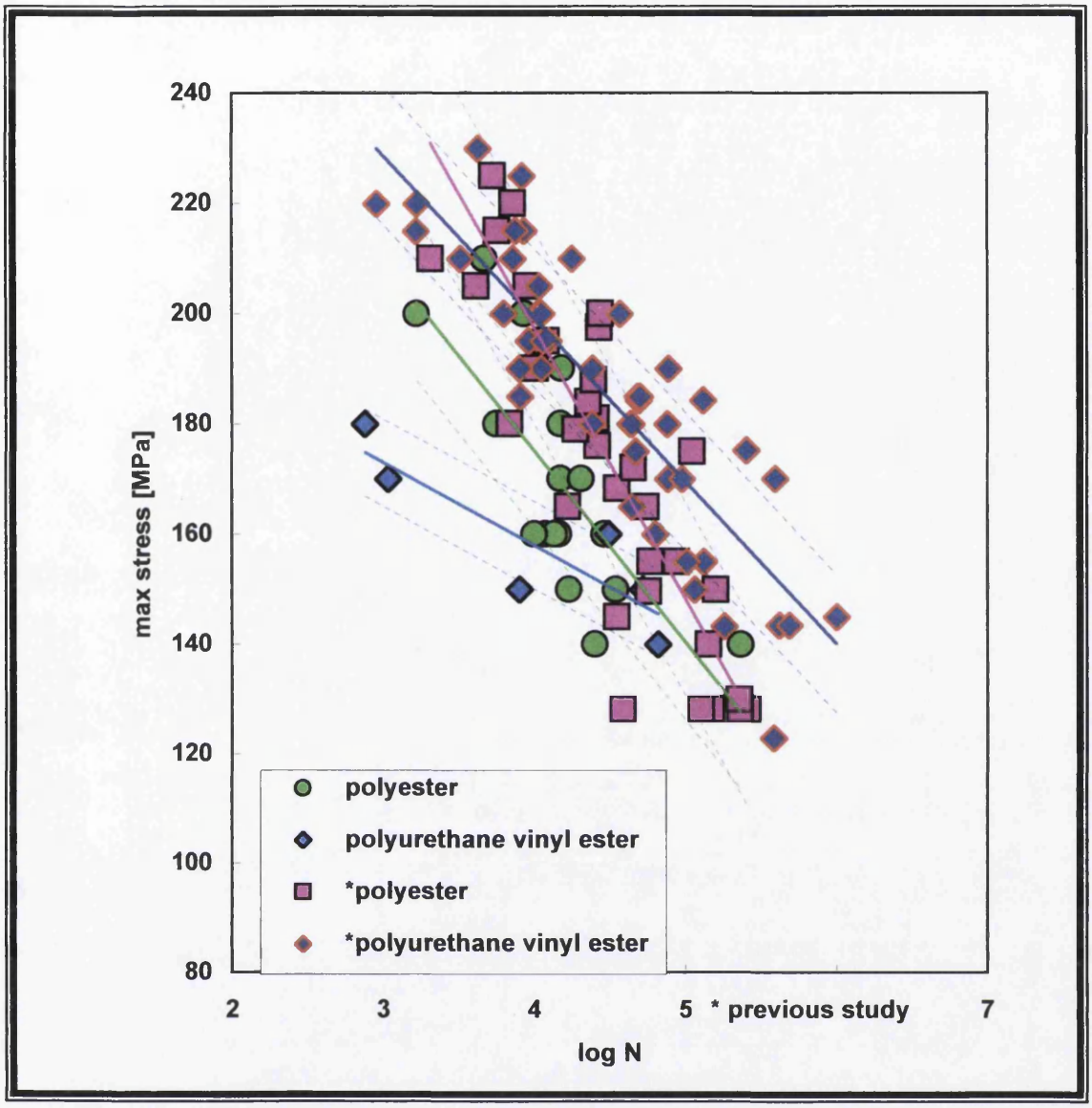

Fiure 5.15: The comparison fatigue life performance of $[0^o/90^o]_{2S}$ Ulticloth with previous study

(1978) and Rotem (1993), who noted that the viscous dependent matrix behaviour plays an essential role in fatigue performance of polymeric composites.

In Figure 5.14 comparison is made with previous results from $[\pm 45]_{2S}$ Biaxial Ulticloth lay-ups in polyester and polyurethane vinyl ester resins. For the polyester resin, the previous results show slightly lower fatigue strength values than the present data, whereas for the polyurethane vinyl ester the differences are more significant. Samples from the previous experiments have been investigated and the results assessed in terms of some microstructural characterisation and this will be discussed in the next section.

Figure 5.15 shows the equivalent comparison with previous data for the $[0/90]_{2S}$ lay-ups of Ulticloth with polyester and polyurethane vinyl ester resins. It may be seen that for the polyester composites the present data show similar but slightly lower fatigue strengths. There is a slightly greater difference for the polyurethane vinyl ester based samples, and again this could probably be explained as resulting from slight differences in the preparation techniques.

5.2.5 Effect of resin and fibre orientation on composites performance

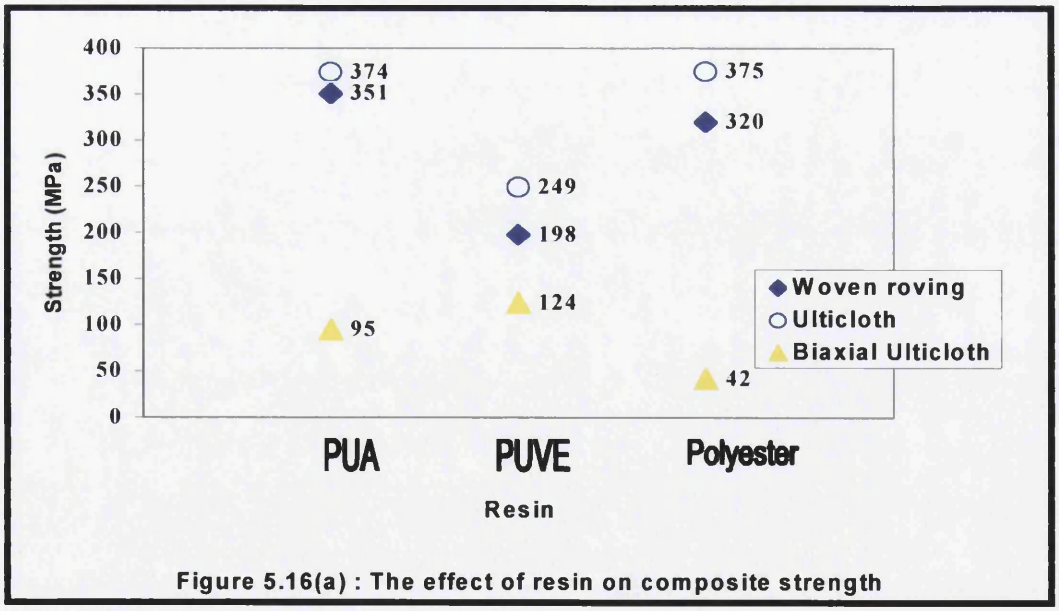

Figure 5.16(a) : The effect of resin on composite strength

Although polyester resin has the highest value of tensile strength, it does not necessarily provides the composites with the highest ultimate tensile strength. In fact

when used as the matrix for the Biaxial Ulticloth it gives the lowest ultimate tensile strength. On the other hand, polyurethane acrylate resin, which has the lowest value of tensile strength, produces composites with high ultimate tensile strength. This strongly indicates that polyurethane acrylate provides better compatibility as a matrix material for the fibres and this is also clearly manifest in the high fatigue strength of the composites.

Figure 5.16(a) shows the effect of resin type on the composite ultimate tensile strength and clearly indicates that polyester and polyurethane acrylate provide excellent tensile strength of composites having similar fibre orientation along and perpendicular to

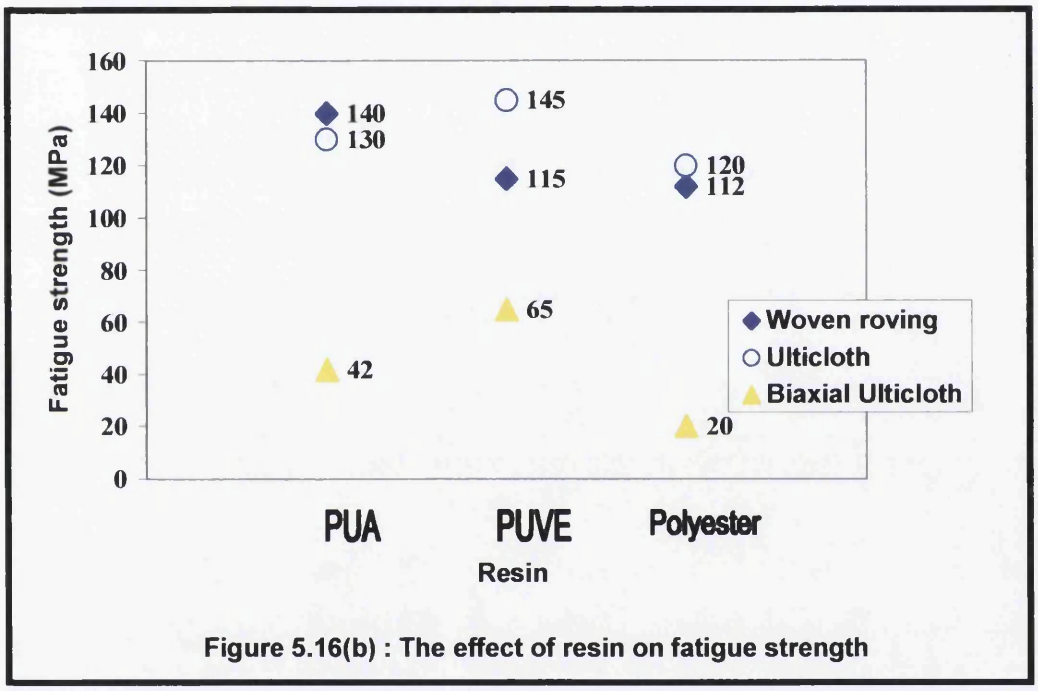

Figure 5.16(b) : The effect of resin on fatigue strength

the loading direction. However, this is not the case for the composite with Biaxial Ulticloth. The fibres orientation thus play an important role in this case. In Biaxial Ulticloth the fibres are aligned at $\pm 45^{o}$ to the applied stress, thus the shear stress exerted in this plane attained its maximum value. The load is distributed and carried both by the matrix and the fibres. Both are relatively weak in exerting the shear stress thus the composites fail at much lower stress compared to the other laminates having fibres aligned along the loading direction.

The effect of resin on the fatigue strength is shown in Figure 5.16(b). In this case the fatigue strength is defined as the lowest value of max. stress in tension-tension fatigue

(R= 0.1) at one million cycles of the composite laminates. Both woven roving and Ulticloth have similar fatigue strength for the same resin type with polyurethane acrylate and polyurethane vinyl ester resins providing greater fatigue strength than polyester resin. The factors that contribute to this effect could be attributed to the low shrinkage during curing thus forming excellent bonding and the inherent toughness of the resin materials. As observed by Bhagwan and Broutman (1990) these factors contribute to high fatigue strength for most glass fibre polymer composites. In this study the inherent toughness of the resins has greater influence on the fatigue strength for composites with similar fibre orientation since all resins used have very similar percentage of volumetric shrinkage.

5.2.6 Fibre Direction Measurement

Table 5.5 shows the results of measurements of the angles that the fibre layer on the outside of individual $[\pm 45]_{2S}$ Biaxial Ulticloth lay-ups made with the tensile axis for comparison between the present experiments and the previous experiments. Ideally these figures should be exactly 45° but in practice it was found that the angle between the two plies was not exactly 90° as it would be if they were precisely ±45°. In fact it was close to 66°. Thus, in the present experiments the angles that the fibres made with the tensile axis were approximately 33° [= 66°/2], whereas in the previous experiments the angle was approximately 57° [= (180-66)°/2]. Therefore the differences in the S-N data can be explained by realising that the composite lay-ups were different.

The variation of angles most probably occurred due to the movement in the cloth during fabrication. As fibre orientation directly affects the distribution of load between the fibres and matrix, the contribution of the fibres to the laminate properties is increased as they get closer to being parallel to the loading direction. The angles between the fibre direction and the tensile axis (as illustrated in Figure 5.16) was approximately 33° as compared with the previous studies, in which the angle was bigger i.e. approximately 57°. The angles measured are for the outer surface only. Although the inner layers were

not measured, for the present experiments they were arranged at the same orientation as the outer layers and it is assumed that this also was the case for the previous experiments. Since the angle between the tensile axis and the fibres was smaller in the present experiment, the strength is thus higher. These difference in the orientations of the fibres help to explain the lower fatigue performance of the samples in the previous study as shown in Figure 5.14

Table 5.5: Fibre direction measurement

Previous sample measurement Angle between fibres and tensile axis (degrees)	Present sample measurement Angle between fibre and tensile axis (degree)
52	33
78	28
57	34
58	35
57	33
57	34
57	34
59	37
48	32
47	31
Average 57 ± 8	Average 33 ± 3

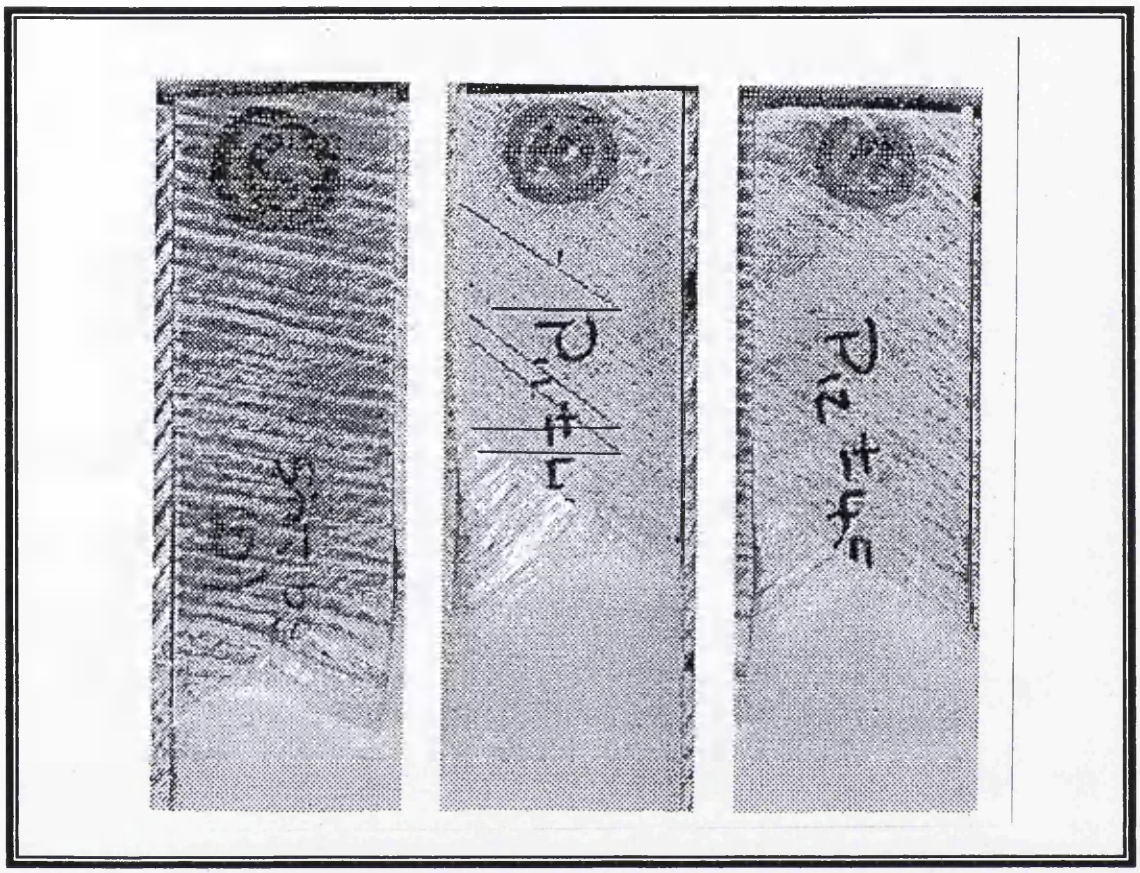

Figure 5.16 : Fibre direction measurement using Sigma Plot Program

5.2.7 SEM Results

A brief study has been made of Ulticloth $[0/90]_{2S}$ polyester and Biaxial Ulticloth $[\pm 45]_{2S}$ polyurethane acrylate which failed in the fatigue tests. On a microscopic scale, the SEM revealed that the samples had also undergone fibre pull out and debonding, many of the debonds having joined to form cracks propagating between fibres.

5.2.7.1 SEM on $[0/90]_{2S}$ Samples

For the $[0/90]_{2S}$ polyester, the first damage was found to be initiated by the transverse cracking. This agreed with the observation made by Agarwal and Broutman

(1990) that large stress and strain concentrations at the fibre matrix interface are responsible for the initiation of these cracks. This was also observed by Takeda et al. (1995). They found that the first damage observed is transverse cracking, which runs through the thickness of the 90° plies. This will followed with separation of fibres from the matrix (debonding) of the plies in which the fibre lie perpendicular to the loading direction, (Figure 5.17). This debonding tends to occur in areas of densely packed fibres that had little polyester resin material between them. Matrix cracks were also observed in areas with fibres perpendicular to the direction of load, (Figure 5.18). Fatigue failures were brittle in nature with both fibres and matrix showing typical brittle fractures.

5.2.7.2 SEM on $[\pm 45]_{2S}$ Samples

For the $[\pm 45]_{2S}$ polyurethane acrylate, the fibres in Figure 5.19 showed irregular, brittle, fast fracture, which suggests that they failed during the final catastrophic failure of the sample. Cracks appeared during the first cycle of loading, and increased as the number of cycles increased. Figure 5.19 shows the interfacial damage that occurred before fibre pull out from matrix. During the fatigue test, when the cycles started, the formation of crazes on the sample surface can be easily observed. Cracks can also be seen on the side of the sample, which is parallel to the fibre ±45° direction. Near to the fractured surface, the crack's direction changes to be perpendicular to loading direction.

5.3 The Effect of Environments on Fatigue Process.

5.3.1 Introduction

The mechanical properties and damage mechanisms during fracture of composite laminates are widely dependent on a variety of factors. These include geometrical factors, environmental factors, the influence of constituent materials and loading conditions.

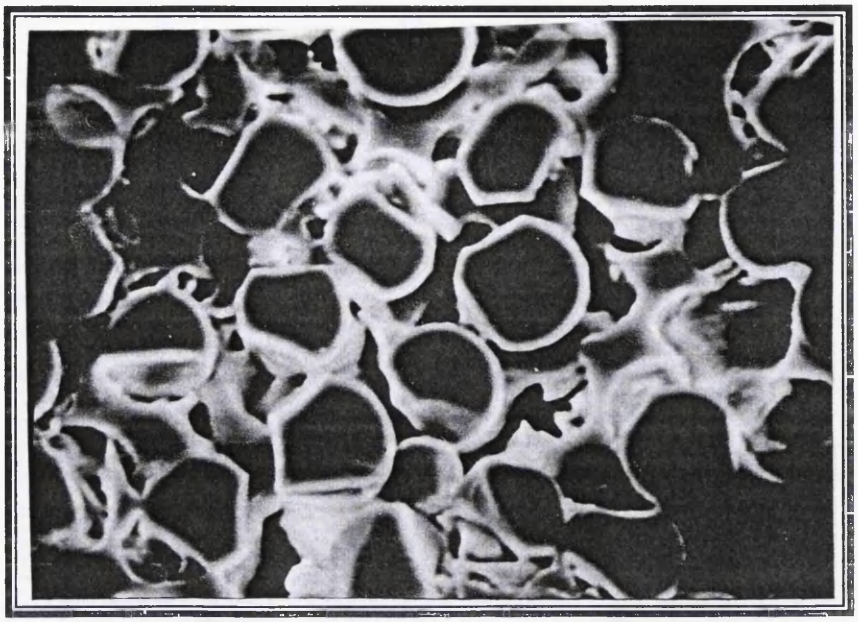

Figure 5.17: The image shows pores on sample.
{Ulticloth $[0/90]_{2S}$ with polyester resin,
N=20573, σ=170 MPa, x 650}

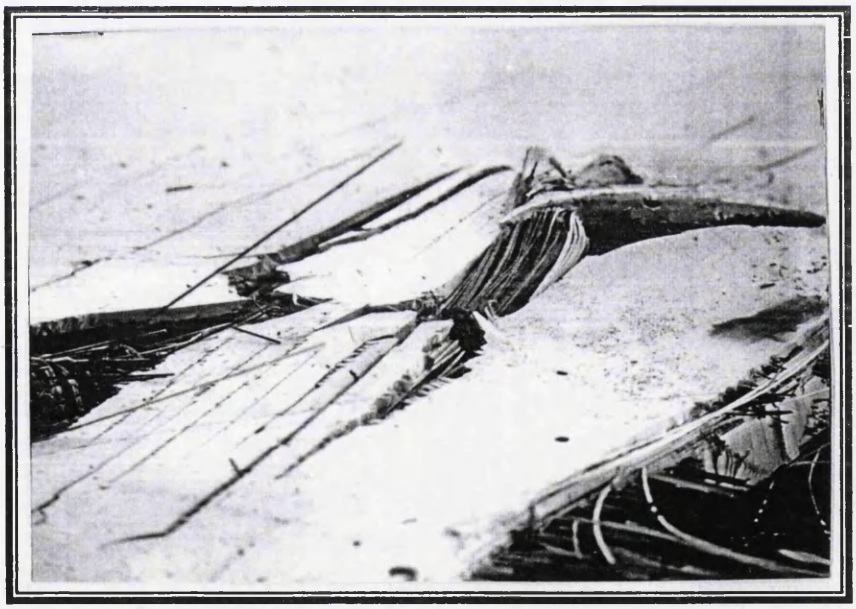

Figure 5.18: Matrix cracks perpendicular to loading direction.
{Ulticloth $[0/90]_{2S}$ with polyester resin, N=20573, σ=170 MPa,
x 20}

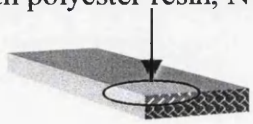

Figure 5.19: Fracture surface: Interfacial damage.
{Biaxial Ulticloth $[\pm 45]_{2S}$ with polyurethane acrylate resin, N=28339, σ=60 MPa, x 1000}

In this section the fatigue characteristics due to the effect of environments on polyurethane acrylate reinforced with Ulticloth and Biaxial Ulticloth with lay-ups, $[90/0]_{2S}$ and $[\pm 45]_4$, will be discussed. Samples were subjected to three types of environments, namely air, distilled water and seawater. S-N testing was carried out on the two lay-ups to characterise their fatigue performance, including strength and resistance to damage.

5.3.2 Fatigue Results in Environments.

The typical downwards slope shown by all the S-N graphs, (Figure 5.20 - 5.23), illustrate that the material's ability to withstand stress decreases with the number of cycles it undergoes.

5.3.2.1 Tension-tension (R=0.1) results.

Figure 5.20 illustrates the S-N data for $[90/0]_{2S}$ Ulticloth in polyurethane acrylate resin. The high slope of the curves indicates that the fatigue life decreases as the number of cycles increases. The lifetime of samples tested in distilled water and seawater is lower than those tested in air. This is consistent with the findings of many researchers, Lekatau et al. (1993), Weitsman and Jackson (1985), Stinchcomb et al. (1982), and Ellis and Found (1983), who all noted a loss of strength for laminates tested in water as compared with air. Hofer et al. (1986) suggested that this could be due to moisture entering the crack network and accelerating the crack growth. It also might be because of the effect of moisture on the formation of cracks. The effects of the water on fatigue performance are seen to be more significant at the low stress/high cycle end of the graph (Figure 5.20), which is consistent with longer immersion times causing more effect.

There is a suggestion that at higher stresses (above about 130 MPa), samples tested in distilled water and seawater may show a small difference but below that stress it seems the differences are minimal. At low stress, below 130MPa no difference in the S-N curves was observed. Sample tested in seawater showed more reduction in strength

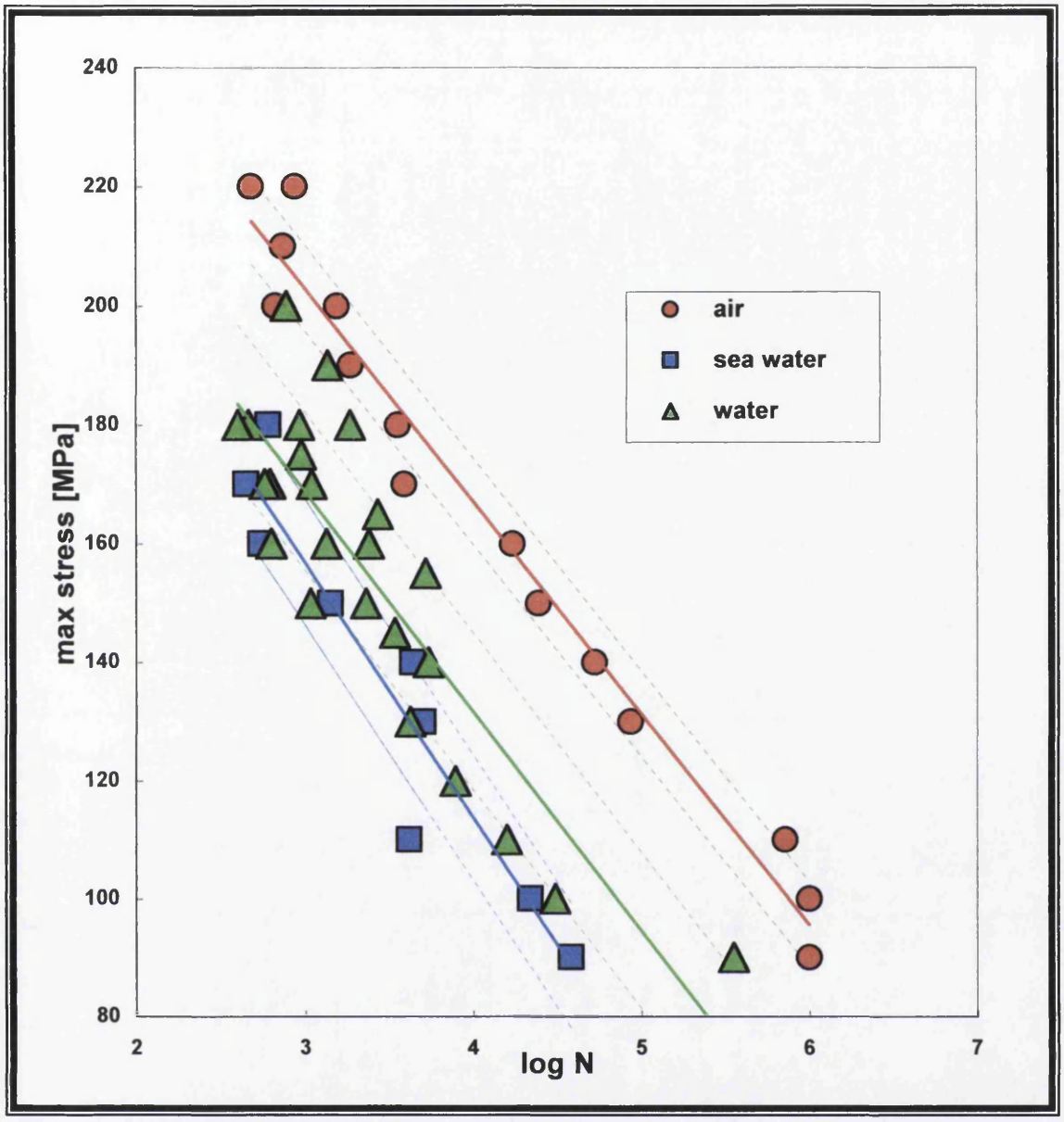

Figure 5.20: The fatigue life performance of Ulticloth $[90^{o}/0^{o}]_{2S}$ Polyurethane Acrylate, R=0.1

compared with those tested in distilled water at these higher stress/lower cycles of fatigue. This suggests that the damage mechanisms from the environment are time dependent that diffusion plays an important role. It was thought that one possible explanation could be that seawater was absorbed more rapidly than distilled water, thus causing the greater deterioration in performance at low cycles/shorter times, and that longer-term absorptions were similar. However, as will be seen from the absorption tests reported later, there were not significant differences between the uptakes of distilled and seawater.

The graph shows that at lower stress level, the difference in fatigue strength increases. Distilled water and seawater have a detrimental effect on materials as they penetrate into the crack network and accelerate their growth until complete failure.

For $[\pm 45]_4$ lay-ups, Figure 5.21 shows lower fatigue strengths compared to $[90/0]_{2S}$, Figure 5.20, since they have no fibres along the load direction. Demonet (1989) suggested that the reduction in strength was due to moisture plasticising the polymer matrix especially in lay-ups with no fibres along the load direction, since in this case matrix properties are important in determining their fatigue performance. However, this figure (Figure 5.21) shows that, there was no significant difference between samples tested in air, distilled water and seawater.

5.3.2.2 Tension-Compression (R=-1) Results.

More scatter was observed for tests at R= -1, (Figure 5.22) than at R = 0.1 (Figure 5.20). The results also indicate that the fatigue life for all samples in different environments is less compare with R=0.1 loading condition. This also can be seen on the reduction of fatigue life from samples tested in air, distilled water and seawater. Lagrange et al. (1991) cited that there was a difference between the results for the distilled water and seawater. At the same stress level, the samples tested in air showed higher lifetimes. Samples tested in seawater seem to have shorter lifetimes due to the effect of seawater entering cracks on the samples.

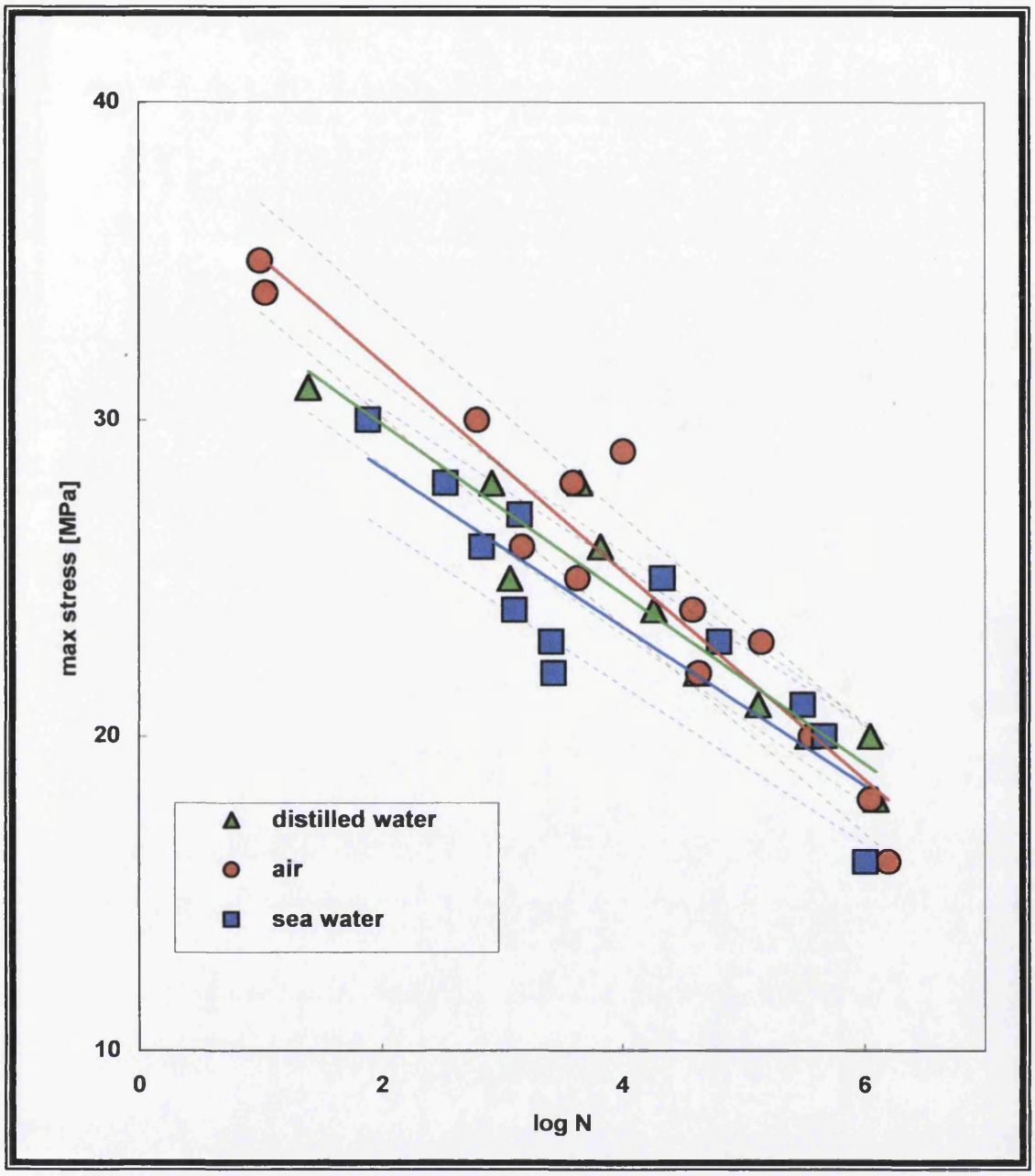

Figure 5.21: The fatigue life performance of Biaxial Ulticloth $[\pm 45^{o}]_4$, Polyurethane Acrylate, R=0.1

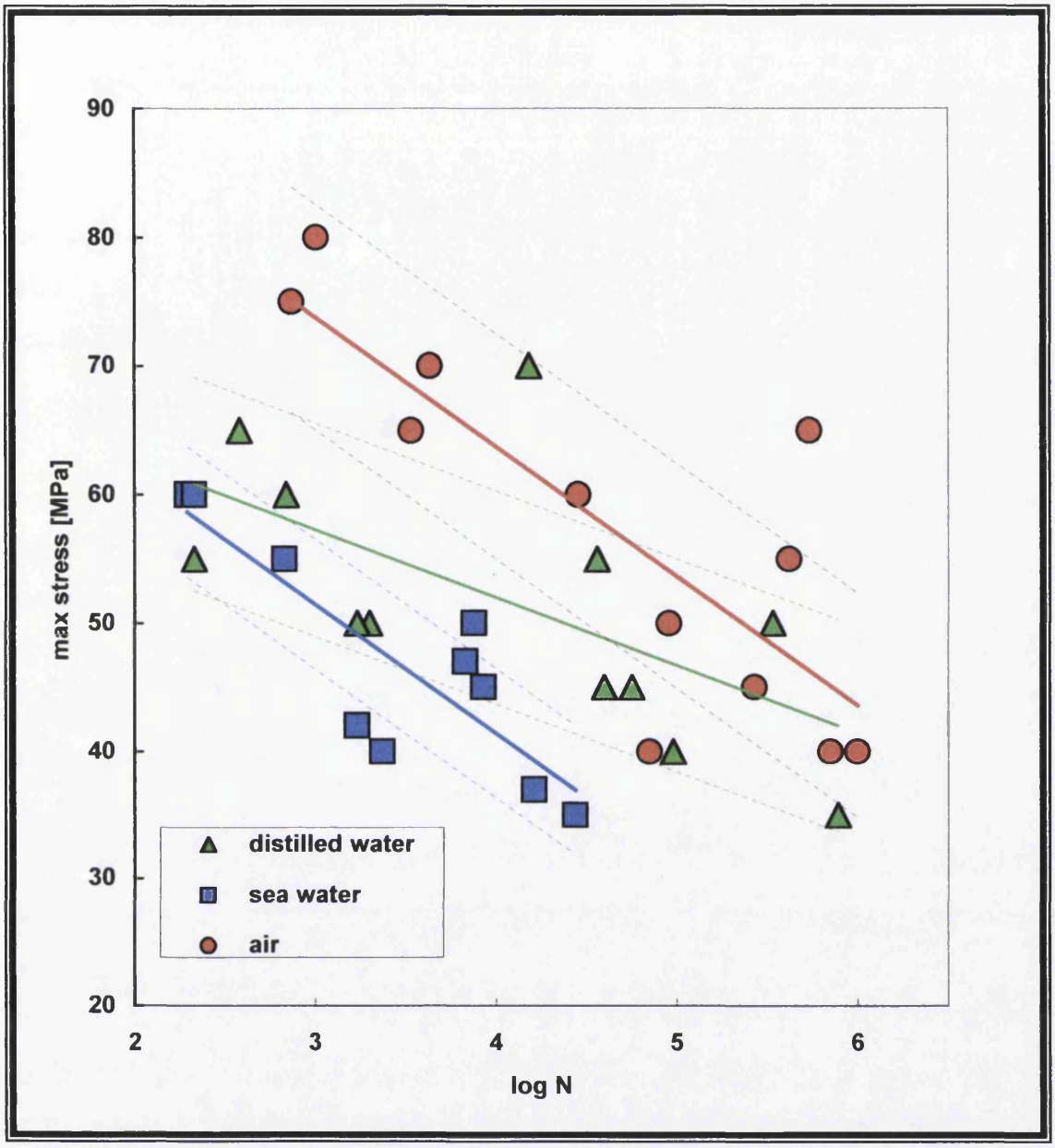

Figure 5.22 The fatigue performance of Ulticloth $[90^{o}/0^{o}]_{2S}$ Polyurethane Acrylate, R=-1

Figure 5.23 shows that the $[\pm 45]_4$ samples tested in distilled water with R=-1 have lower fatigue strength compared with samples tested with R=0.1. This was also observed by Highsmith et al (1984). They mentioned that the interfacial damage under tension-compression loading is greater at a higher rate than under tension-tension loading. They also suggested that the damage modes in laminates subjected to tension-compression loading are both interactive and competitive.

Results for $[90/0]_{2S}$ laminate, (Figure 5.22), are less scattered. This is probably because the $[\pm 45]_4$ lay-ups are matrix dominated, whereas the performance of the $[90/0]_{2S}$ lay-ups is more strongly dependent on the fibres parallel to the stress direction. When fatigue cycling includes compression, this can have significant effects since fibres in compression are notoriously unstable and failure due to buckling can occur in fibres parallel to the compressive stress direction. This might well help to explain the increased scatter in the 90/0 lay-ups when subjected to tension-compression loading.

The graphs comparing the two different values of stress ratio, R=0.1 and R=-1 can be seen in Figures 5.24 to 5.29. Figure 5.24 shows that $[90/0]_{2S}$ samples tested in air with R=0.1 had higher fatigue strength while the samples tested under tension-compression, R=-1 were found to suffer most severe damage. At higher numbers of cycles, so much damage accumulates that the tension-compression stiffness of the samples also drops. This will be discussed later. For $[\pm 45]_4$ samples, the character of the R=0.1 and R=-1 curves in Figure 5.25 is similar. This was probably because this composite was matrix dominated.

Similar characteristics can be seen in Figure 5.26 to Figure 5.29, which show that composites that contain fibres in the loading direction exhibit two different curves depending on the stress ratio. On the other hand, for the matrix-dominated composites, the curves show that the fatigue strength was independent of the stress ratios.

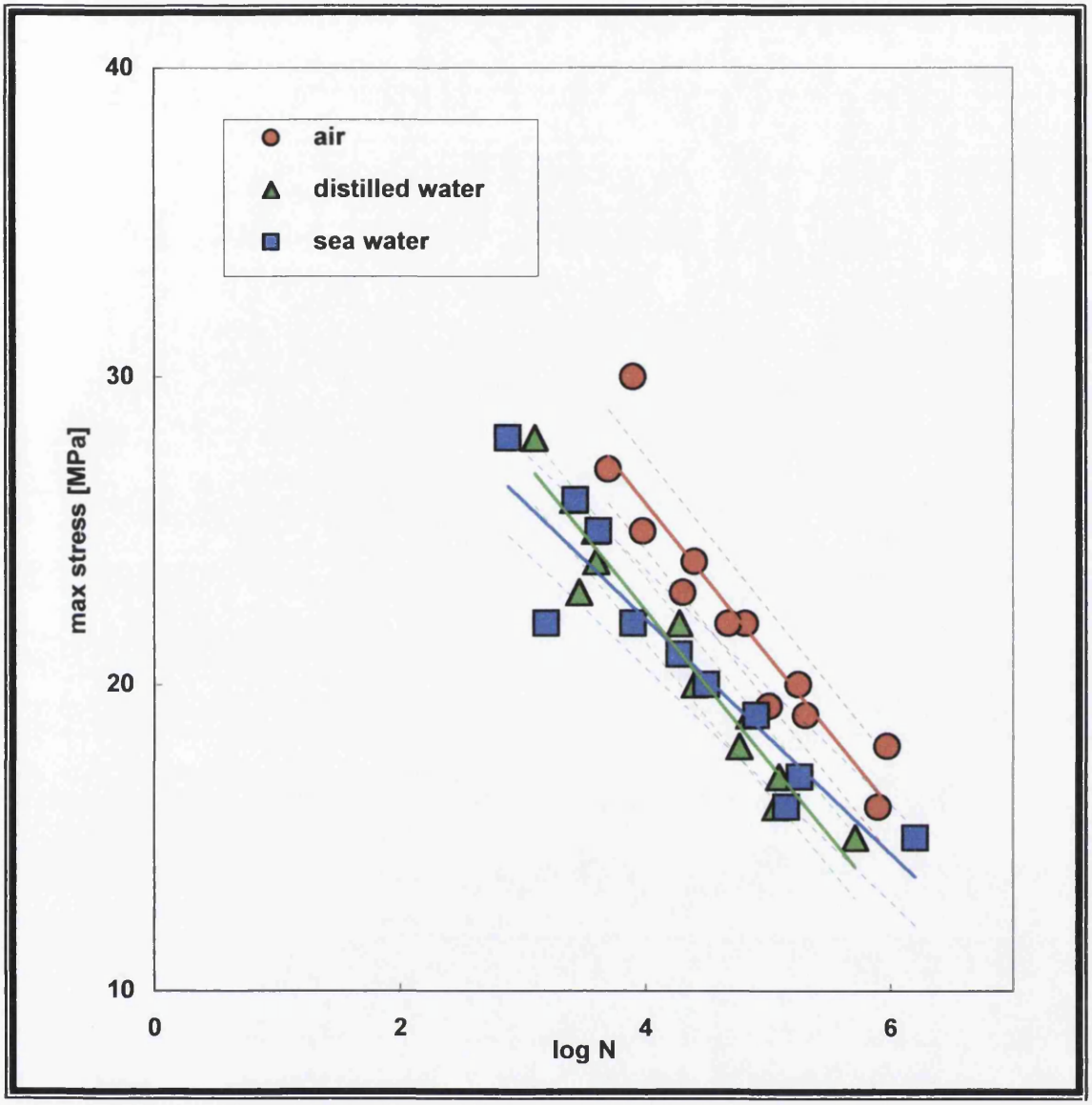

Figure 5.23: The fatigue performance of Biaxial Ulticloth $[\pm 45^{o}]_{4}$, Polyurethane Acrylate, R=-1

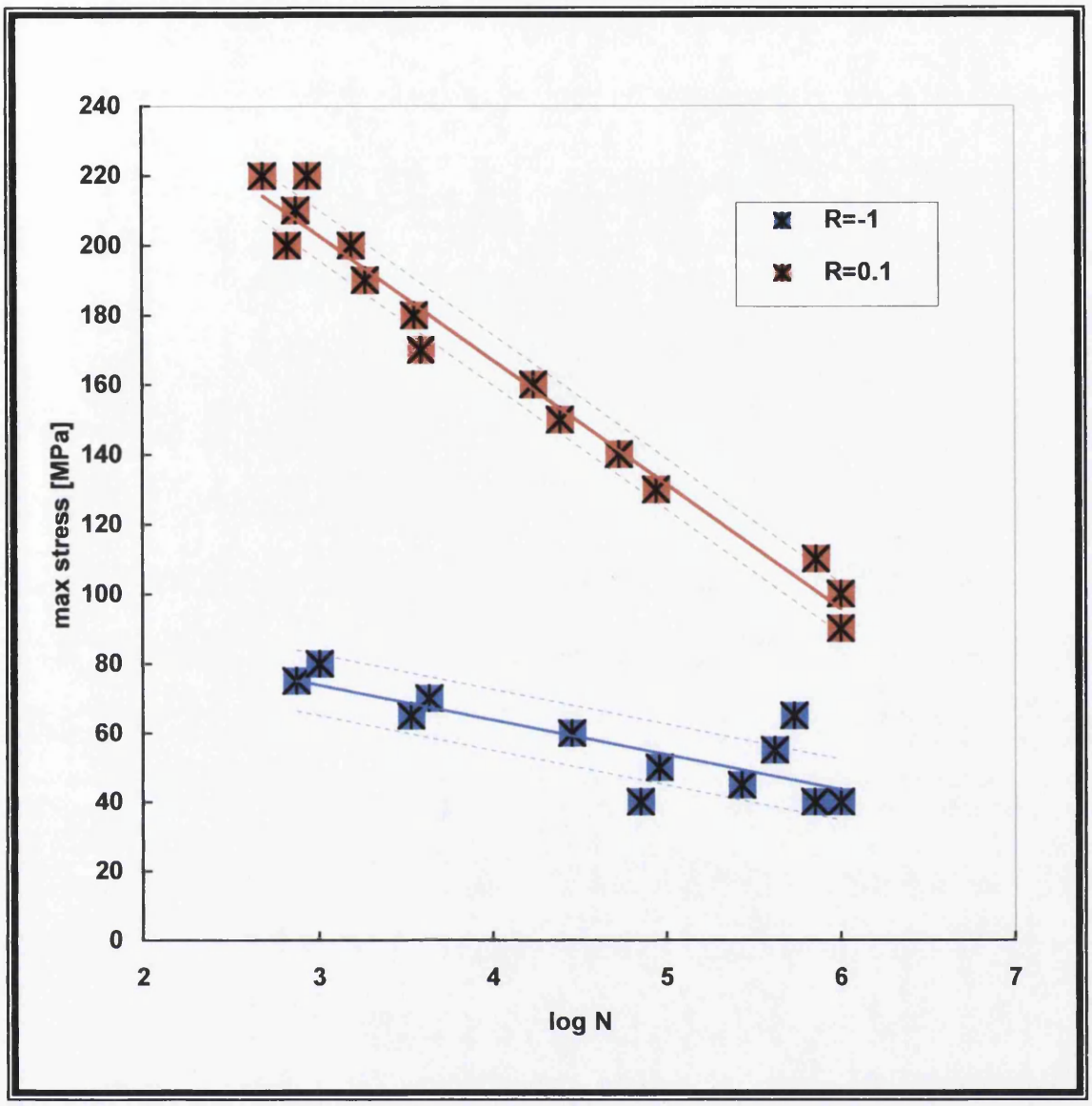

Figure 5.24: The fatigue performance of Ulticloth $[90^{o}/0^{o}]_{2S}$, Polyurethane Acrylate, R=0.1 and R=-1 in air.

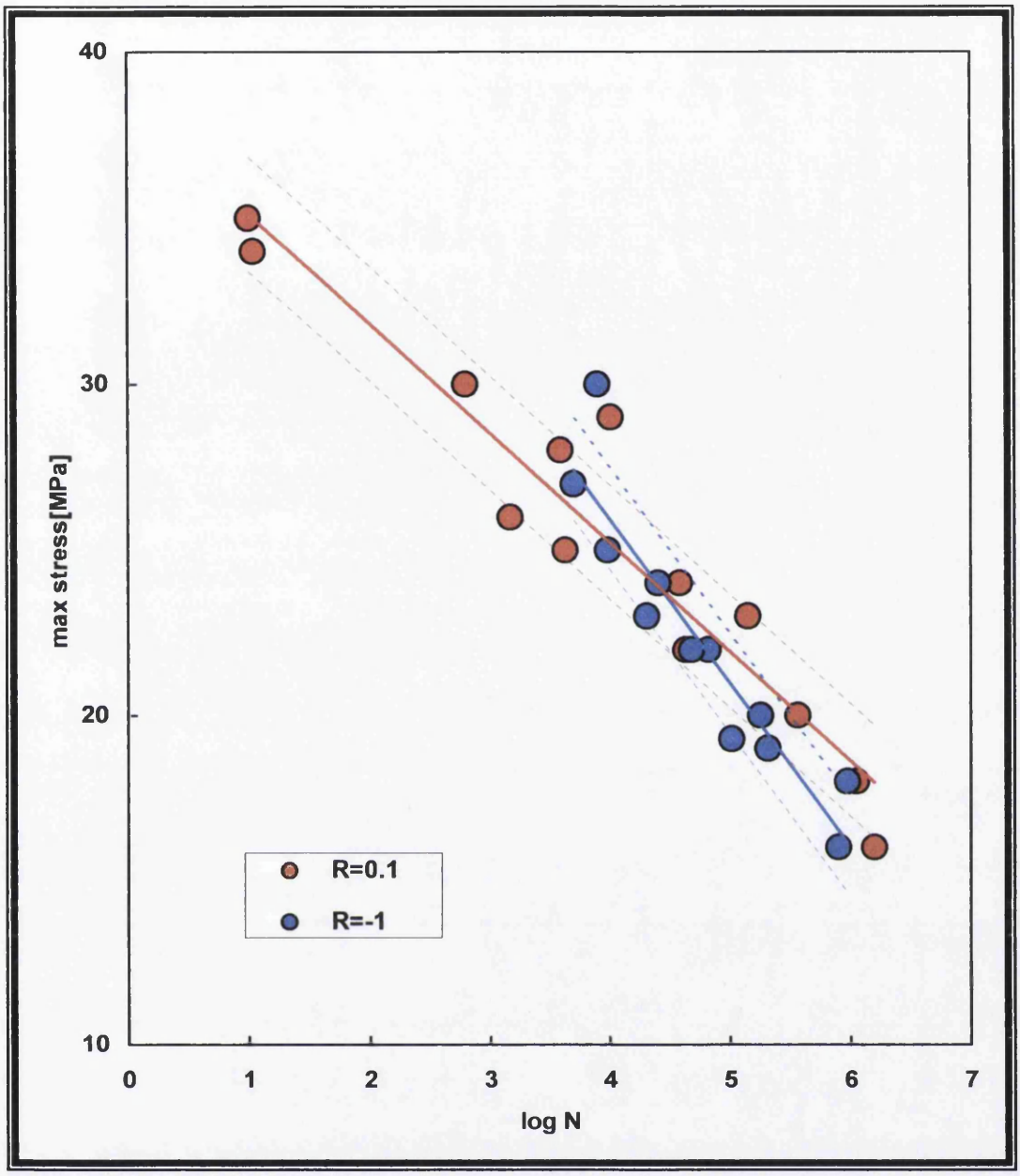

Figure 5.25: The fatigue performance of Biaxial Ulticloth $[\pm 45^{o}]_4$, Polyurethane Acrylate, R=0.1 and R=-1 in air.

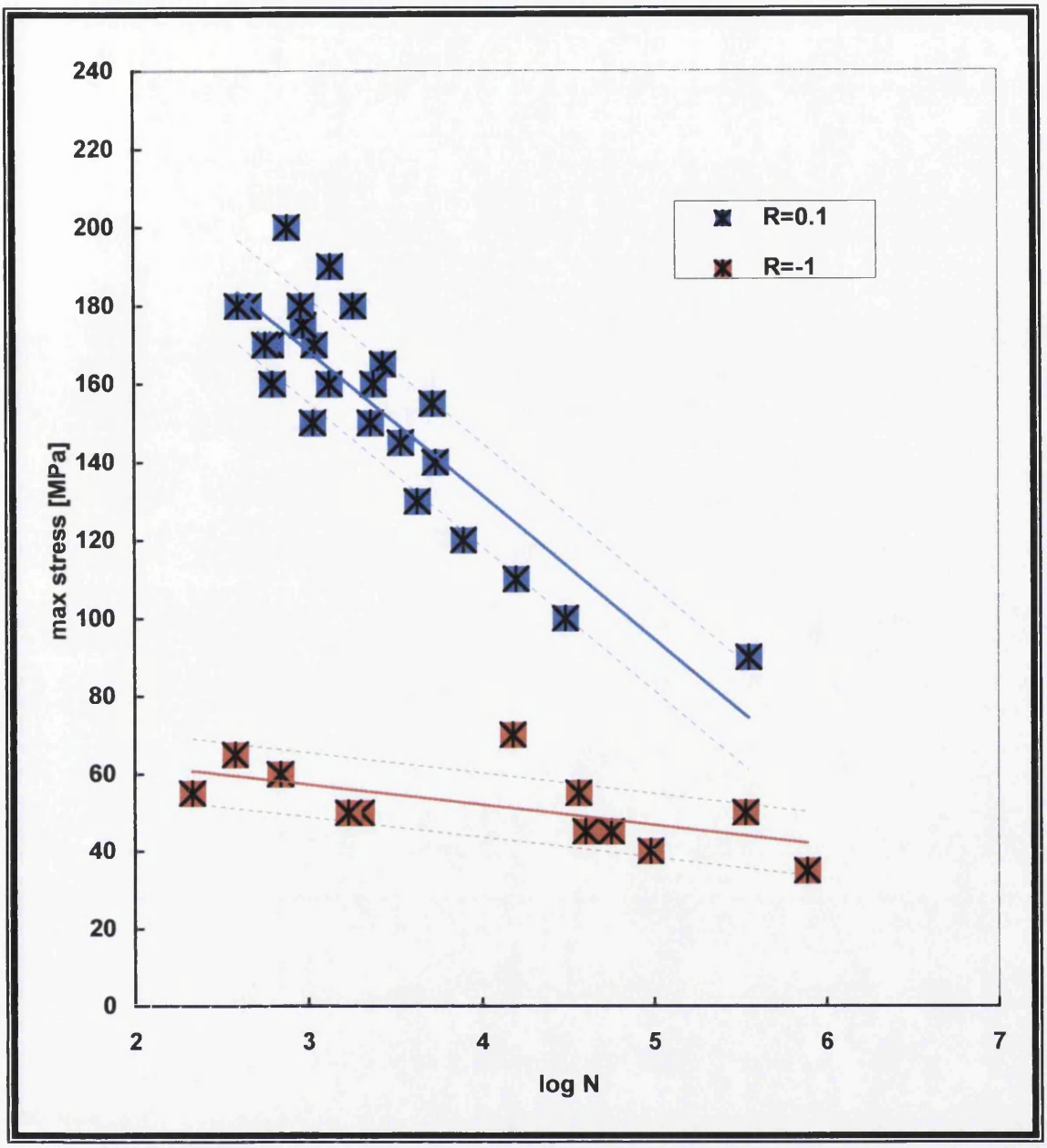

Figure 5.26: The fatigue performance of Ulticloth $[90^o/0^o]_{2S}$, Polyurethane Acrylate, R=0.1 and R=-1 in distilled water.

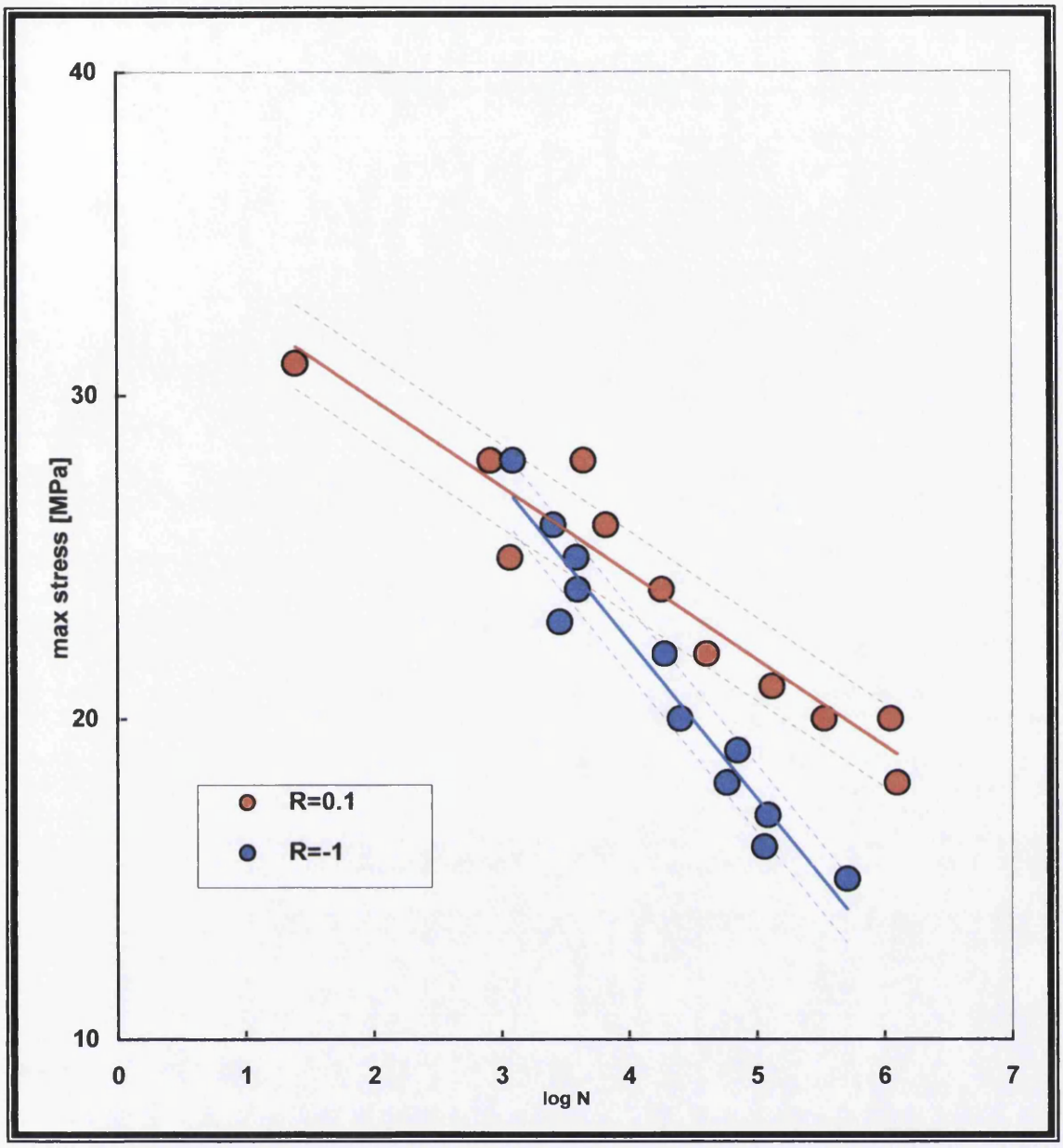

Figure 5.27: The fatigue performance of Biaxial Ulticloth $[\pm 45^{o}]_4$, Polyurethane Acrylate, R=0.1 and R=-1 in distilled water.

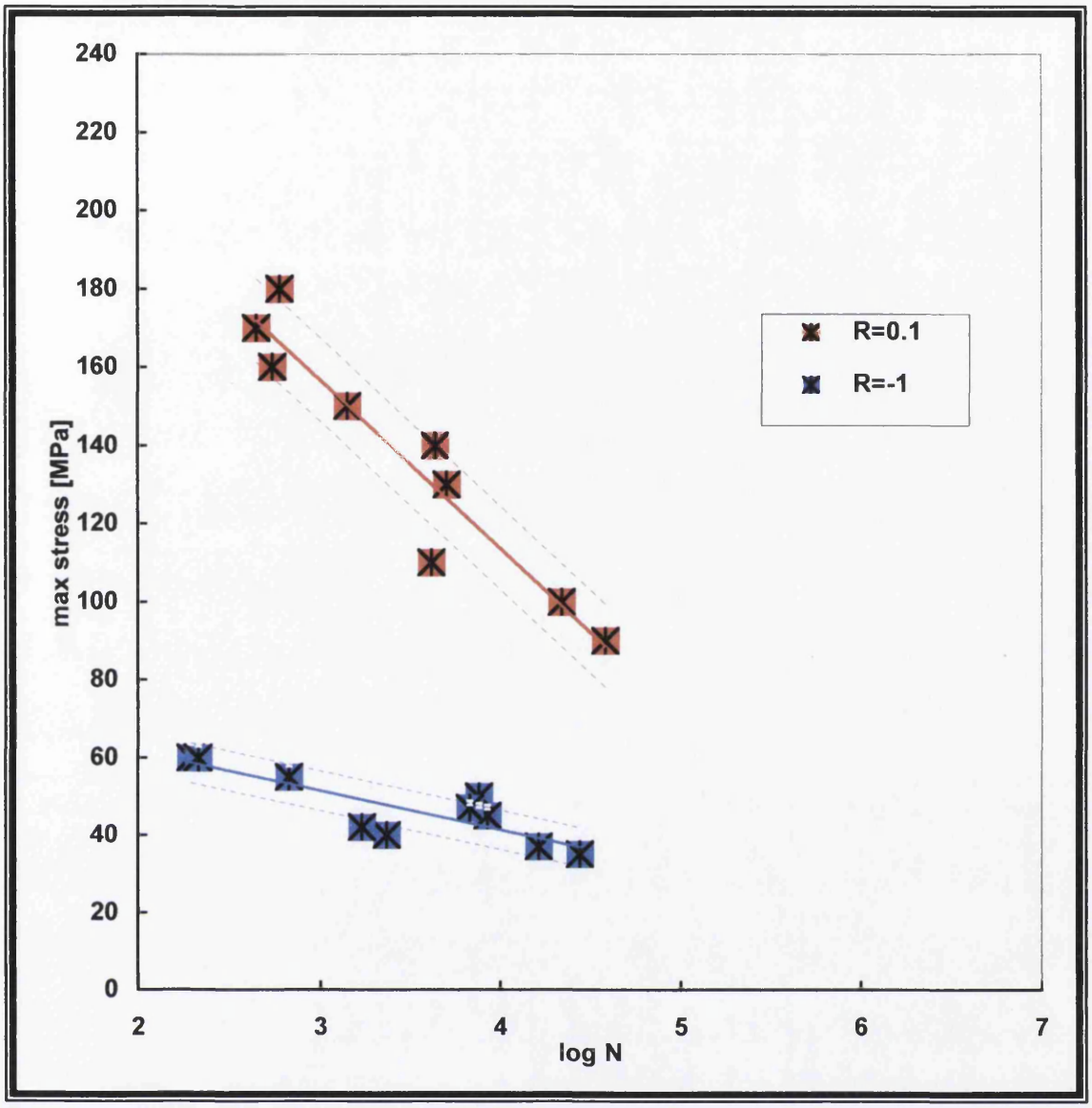

Figure 5.28: The fatigue performance of Ulticloth $[90^{o}/0^{o}]_{2S}$, Polyurethane Acrylate, R=0.1 and R=-1 in seawater.

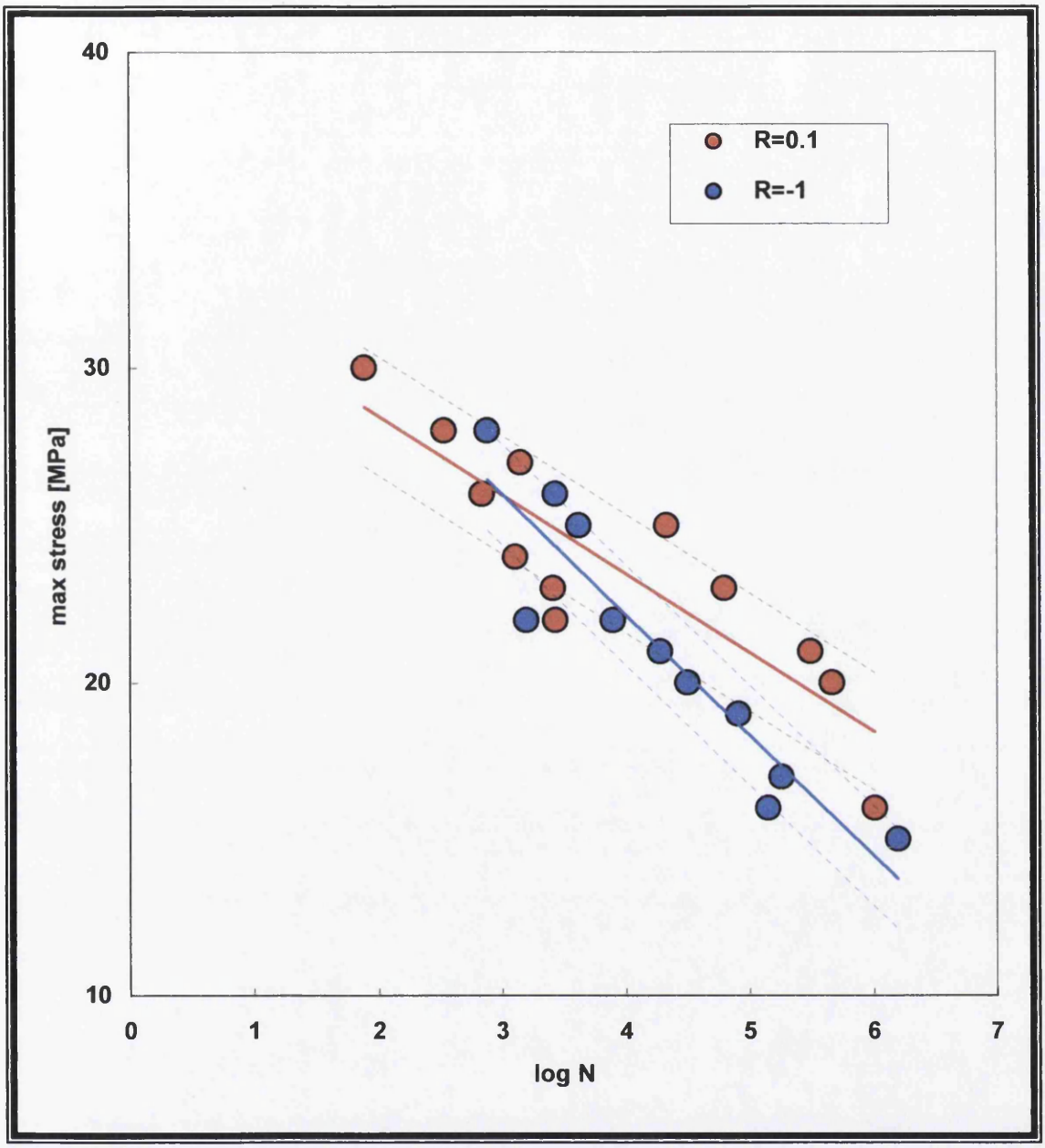

Figure 5.29: The fatigue performance of Biaxial Ulticloth $[\pm 45^{o}]_{4}$, Polyurethane Acrylate, R=0.1 and R=-1 in seawater.

These graphs also clearly show that fatigue lives of the $[90/0]_{2S}$ composite material vary depending on the stress ratios value (-1 and 0.1). It is evident that for the same maximum stress level, the fatigue life increases as R changes from -1 to 0.1.

For a given stress ratio, the composites exhibit longer fatigue lives at lower stress levels. These responses at high stress ratio and low stress level are a consequence of the reduction of stress range on the fatigue damage process [Mandell (1982)] as illustrated in Figure 5.30 to 5.31.

The difference in the fatigue life for a stress- range between R=0.1 and R=-1 is smaller than the difference when plotted in terms of the maximum stress. This indicates that the stress range plays a more important role in determining the fatigue life than the maximum stress in the range of the R-values, particularly when compressive stresses are involved.

5.3.3 Microstructural Observation

Fracture surfaces of all samples tested were first observed visually before further analysis using SEM.

5.3.3.1 $[90/0]_{2S}$ layout at R = 0.1

As a general rule in these fatigue tests, damage was more severe for samples under low stress, high number of cycles than high stress, low cycles. At the higher stress levels, samples tested in air show delamination throughout the entire section while for samples tested in seawater only show delamination near the vicinity of the fracture surface. However, no delamination can be observed for samples tested in distilled water.

Sample tested in air showed fibre pullout and some transverse cracking at the outside of the matrix near the fracture surface. Damage had occurred in the matrices

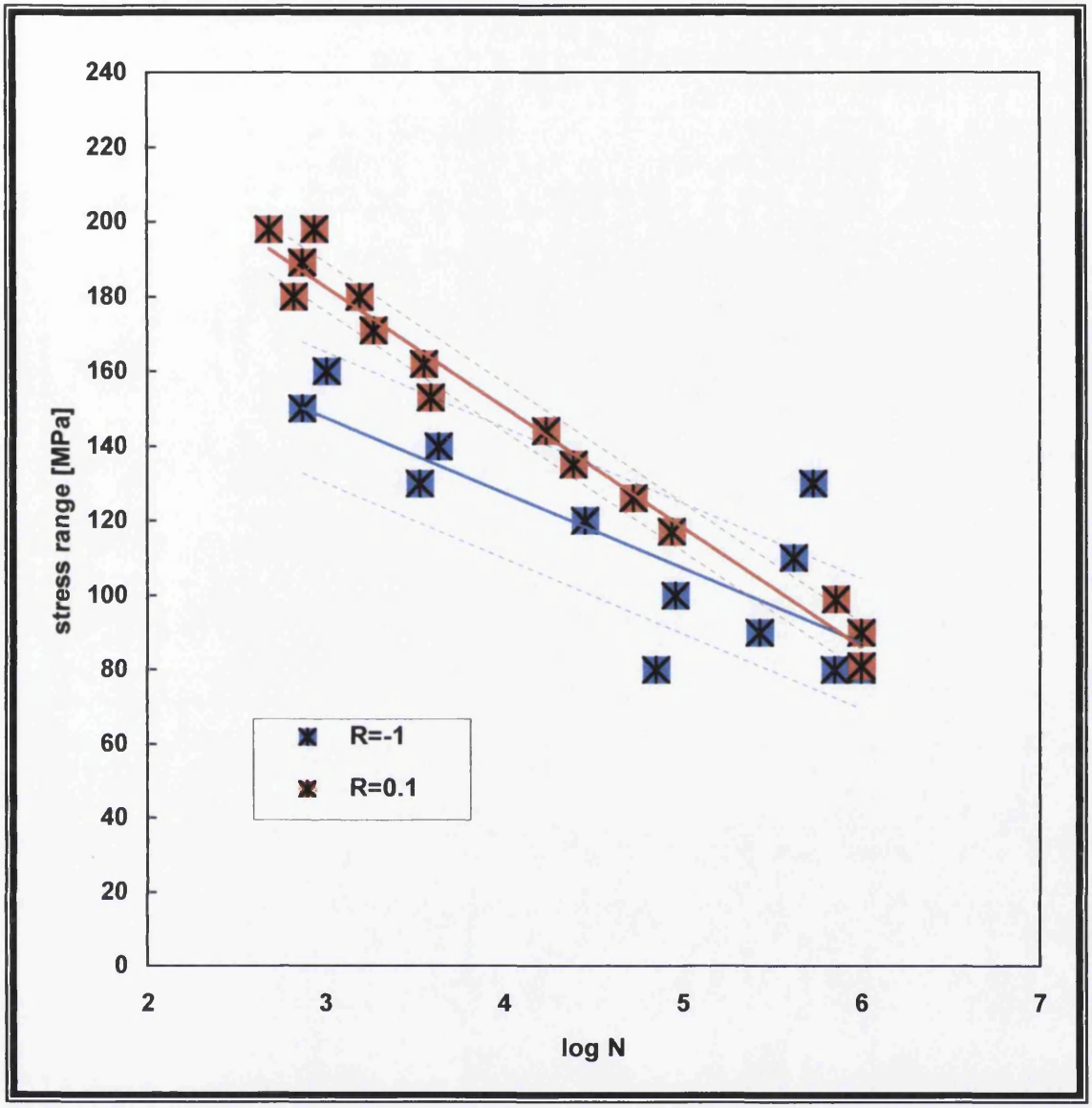

Figure 5.30: The effect of stress range on fatigue performance of Ulticloth $[90^o/0^o]_{2S}$, Polyurethane Acrylate, R=0.1 and R=-1 in air.

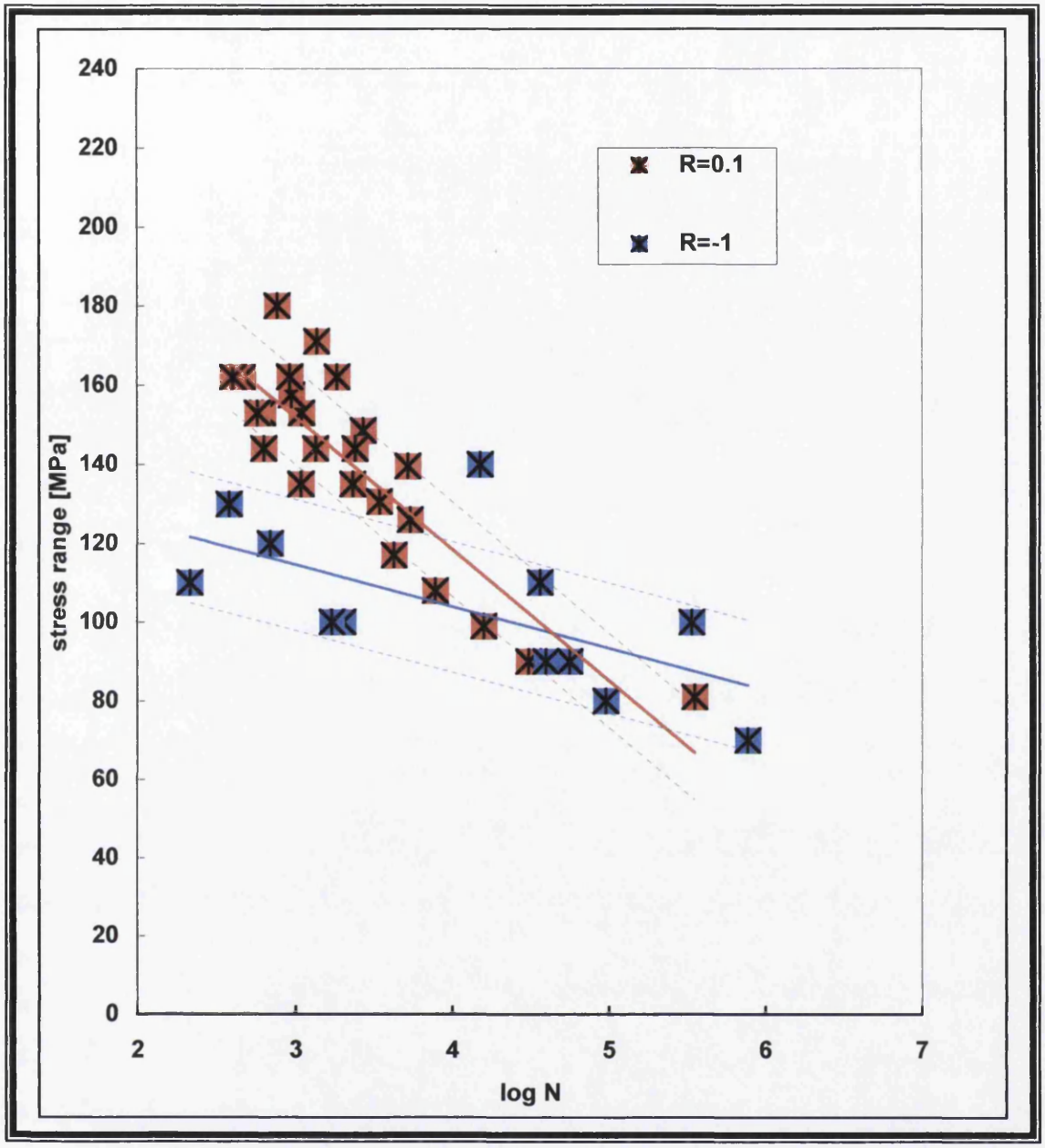

Figure 5.31: The effect of stress range on fatigue performance of Ulticloth $[90^{o}/0^{o}]_{2S}$, Polyurethane Acrylate, R=0.1 and R=-1 in distilled water.

particularly at voids, as illustrated as Figure 5.32 which occurred between fibre bundles and at the ply interfaces, from which cracks had initiated and propagated.

Figure 5.33 depicted broken 90° fibres at the fracture surface of a sample tested in air at a relatively low stress and high cycles to failure. There is evidence of fibre pullout and some transverse cracks. For a relatively high stress, low cycles to failure sample, Figure 5.34 and 5.35 show that cracks along the fibres can be observed through the fracture surface. Damage in the form of crack may have initiated at voids in the matrix, especially between fibre bundles and between plies. Typically, this may explain the mechanism of failure where cracks initiate from such sites and propagate along the 90° fibre direction (Figure 5.36 - 5.37).

Figure 5.38 shows a sample fatigued to failure in distilled water at an intermediate stress level and it explicitly shows the brittle nature of fibre fracture.
At low stress high number of cycles, all samples exhibit delamination. However, samples tested in seawater show more extent of damage and delamination compared with the others. Salt water seemed to affect the surface layer of the matrix and degrade the matrix materials (Figure 5.46). At low stress, the applied load is insufficient to break the fibres, hence, as the matrix material degrades and weakens, fibre-pull out seems the most predominant mechanism of failure. Figure 5.39 illustrates this phenomenon for a sample at intermediate loading in distilled water. Figure 5.33 also shows this mechanism for a sample with low loading in air, illustrating broken 90° fibres.

Seawater and air seem to have greater effect on this composite than distilled water irrespective of the stress levels at this R ratio. Fibre pullout seems to be the main damage mechanism at low stress. At high stress-low cycle damage due to delamination dominates the failure mechanism.

From the above observation, it seems that the samples tested at low stress, high cycles, Figure 5.40, shows more severe damage compared with samples tested with higher stress, low cycles, Figure 5.41.

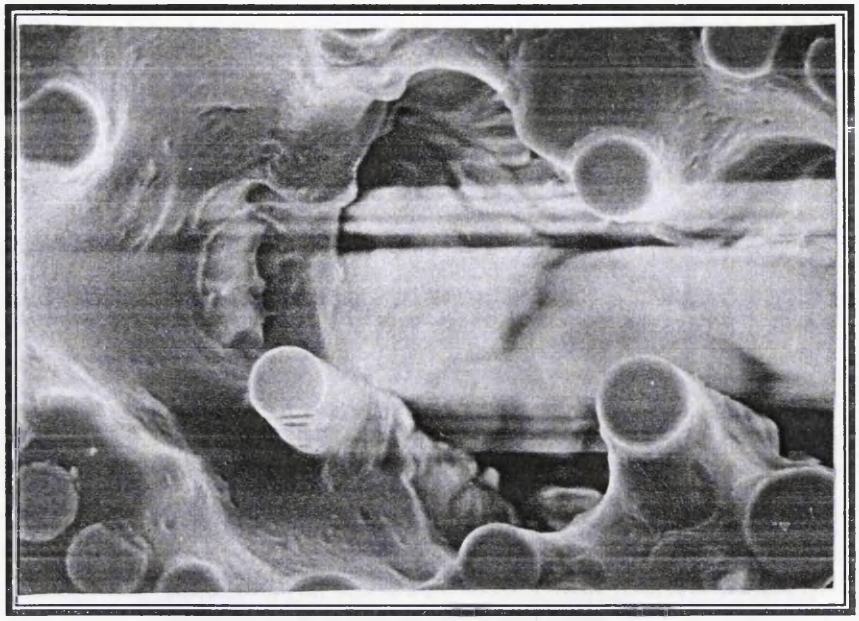

Figure 5.32: Optical micrograph of $[90^o/0^o]_{2S}$ shows a void situated along the surface of the sample. Sample $[90^o/0^o]_{2S,}$ R=0.1, air, 90 MPa, N_f =346736, 500X.

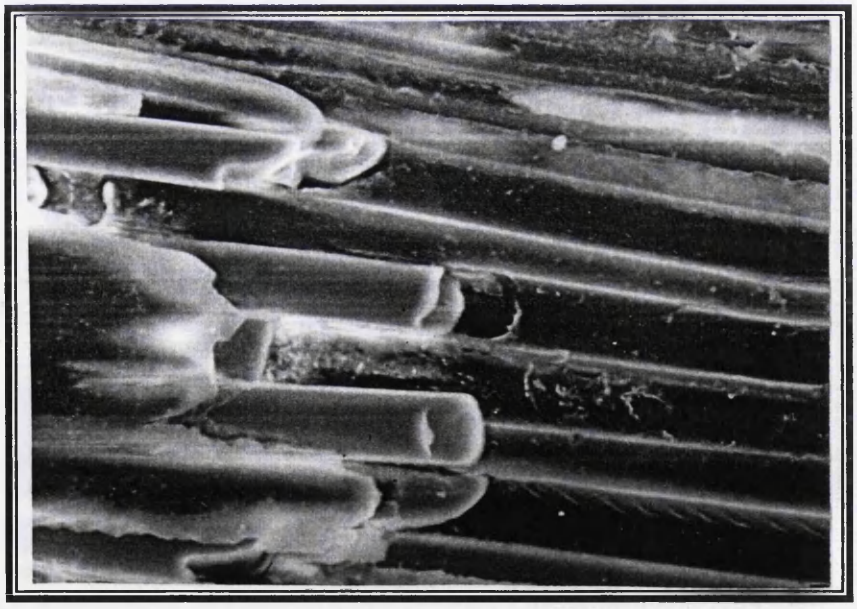

Figure 5.33: Broken 90^o fibre. Sample $[90^o/0^o]_{2S,}$ R=0.1, air, 90 MPa, N_f = 346736, 600X.

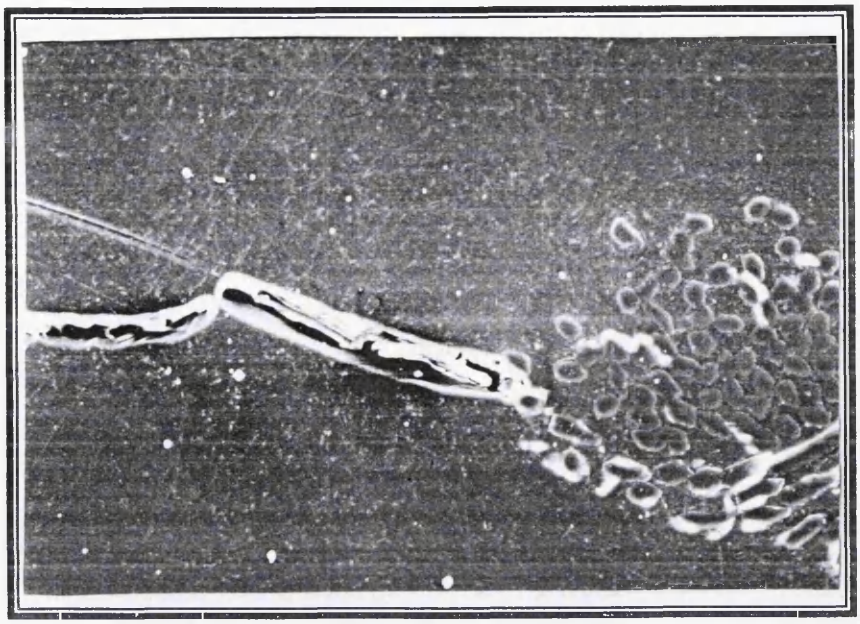

Figure 5.34: Optical micrograph of $[90^{o}/0^{o}]_{2S}$ shows crack observed at the fracture surface of the sample. Sample $[90^{o}/0^{o}]_{2S,}$ R=0.1, air, 200 MPa, N_f =1549, 150X.

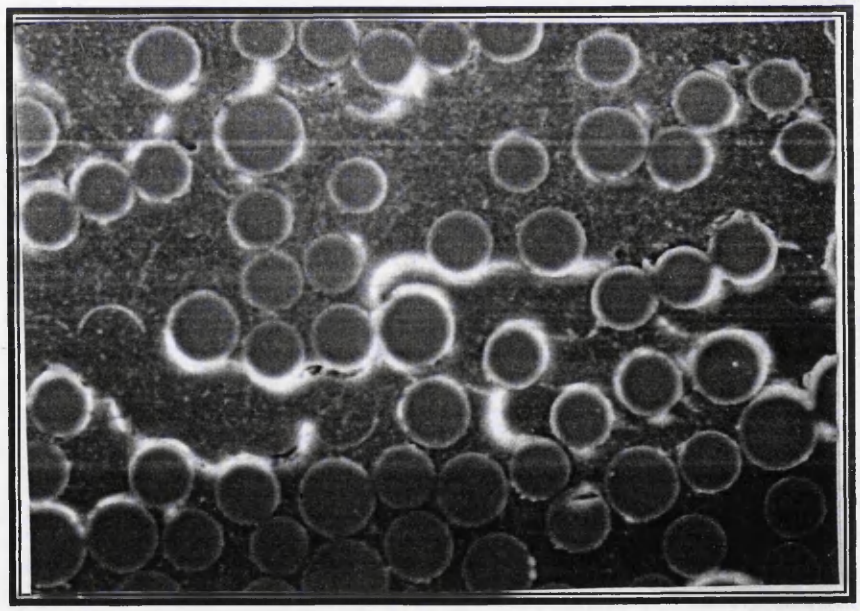

Figure 5.35: The image shows the matrix crack along the fibre. Sample $[90^{o}/0^{o}]_{2S,}$ R=0.1, air, 200 MPa, N_f = 1549, 350X.

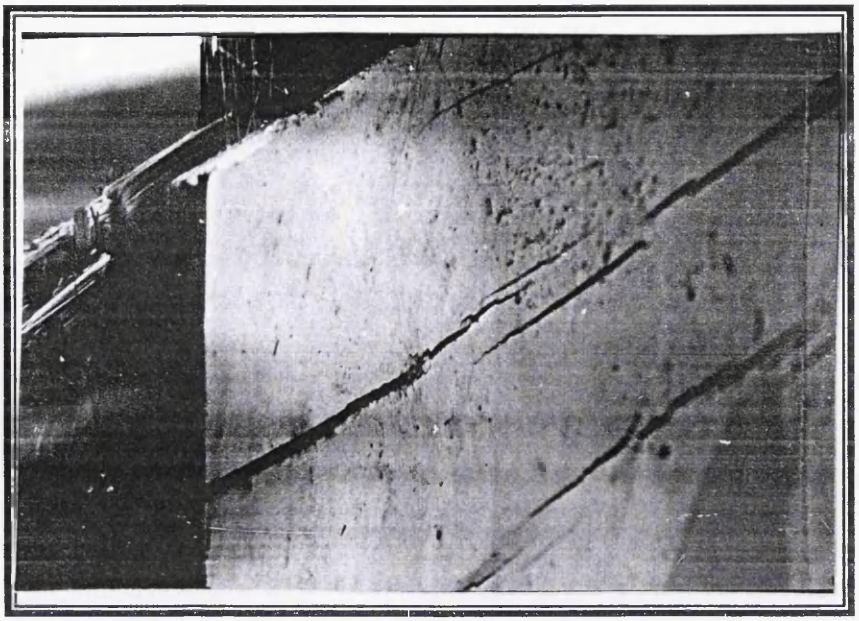

Figure 5.36: Cracks observed near the fracture surface which perpendicular to loading axis. Sample $[90^{o}/0^{o}]_{2S}$, R=0.1, air, 190 MPa, N_f=1354, 15X.

Figure 5.37: The same type of cracks observed near the fracture surface. Sample $[90^{o}/0^{o}]_{2S}$, R=0.1, air, 180 MPa, N_f = 3573, 15X.

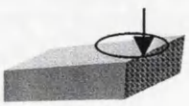

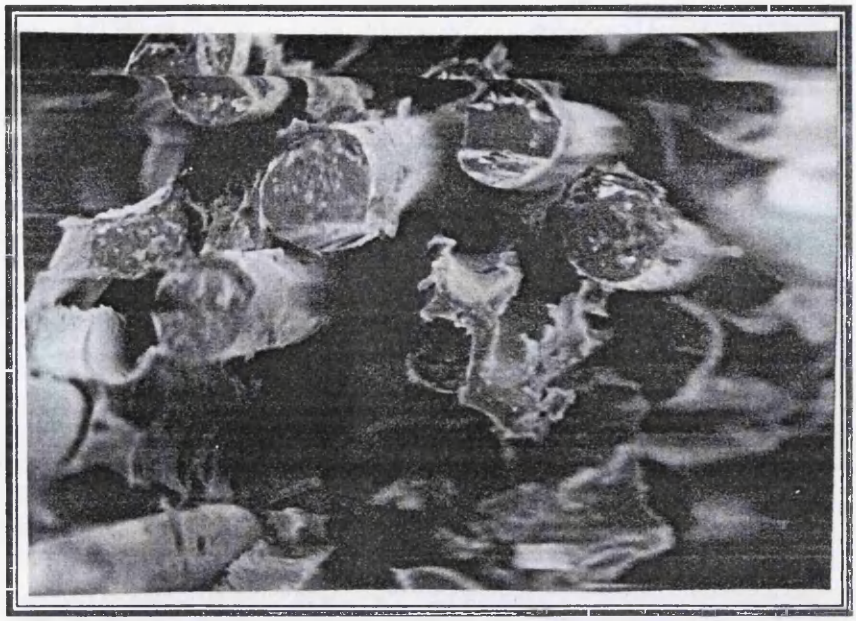

Figure 5.38: The image shows the fibres with brittle fracture with little remaining matrix. Sample $[90/0]_{2S}$, R=0.1, distilled water, 110 MPa, N_f=15849, 600X.

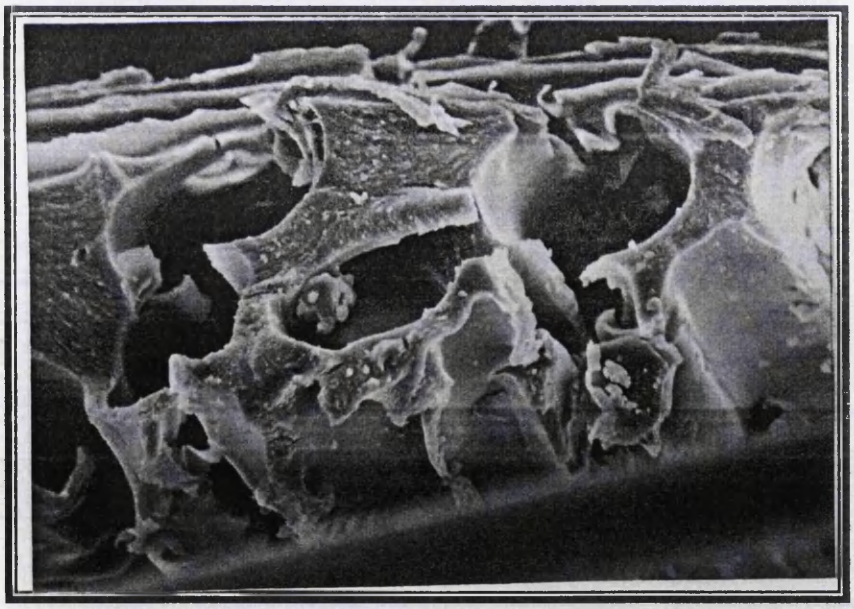

Figure 5.39: Cracks observed from the matrix which fibre pulled out. Sample $[90/0]_{2S}$, R=0.1, distilled water, 110 MPa, N_f = 15849, 950X.

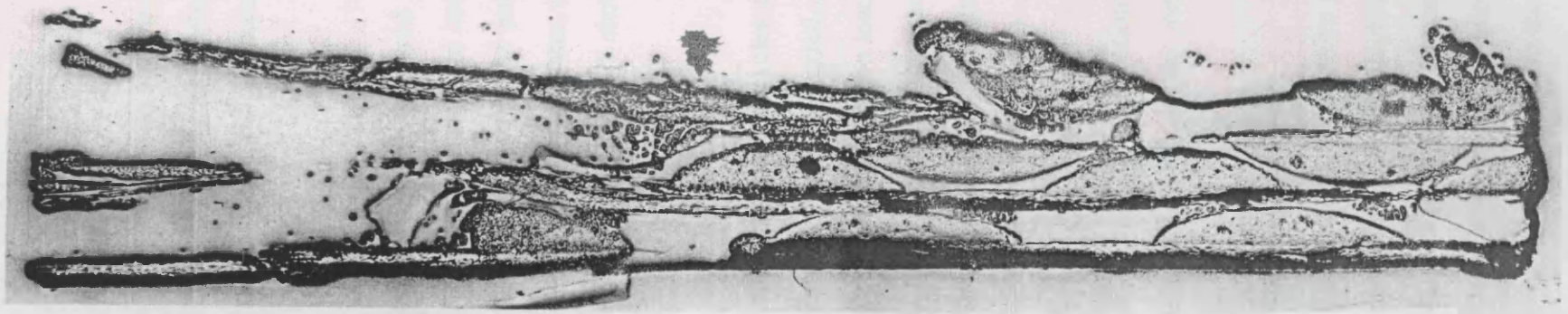

Figure 5.40 : Optical micrograph cross section of fractured surface, severe damage with delamination. Sample $[90/0]_{2S}$, R=0.1, air, 90 MPa, N_f =347736

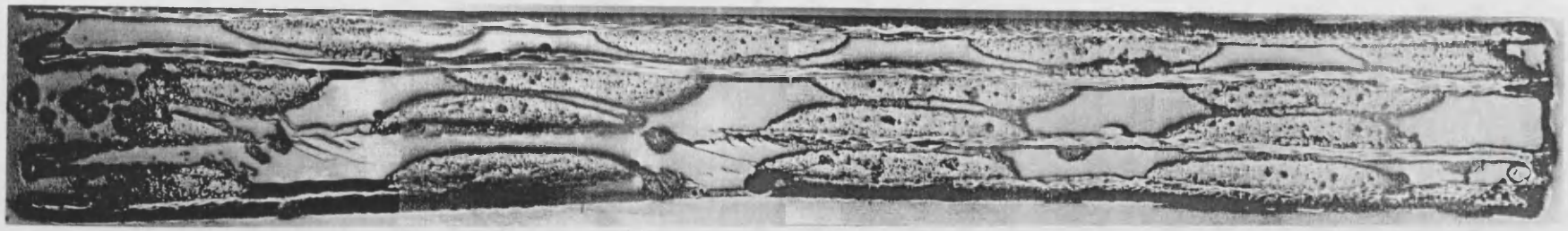

Figure 5.41 : Optical micrograph cross section of fractured surface shows less damage. Also can be seen, crack perpendicular to loading axis. Sample $[90/0]_{2S}$, R=0.1, air, 200 MPa, N_f =1549

5.3.3.2. $[90/0]_{2S}$ Lay-up at R = -1

Microstructural studies were carried out on samples that had been tested with same stress level but had exhibited differences in the number of cycles to failure. Also studied were samples which had been tested at different stress levels but had failed at the same number of cycles.

Tension-compression testing has more effect on samples compared with previous testing with an R ratio of 0.1. The failure mechanisms were more complex, and in addition to delamination and buckling, bundles of transverse fibres pullout are also evident. The most severe damage was seen on samples tested in seawater, less in samples tested in air, and not that critical in samples from distilled water, which show flat fracture surfaces.

On the other hand, the samples with similar number of cycles to failure but difference in the level of stress show that interlaminar fracture occurred on all samples tested. This probably happened as a result of tension and compression loading. Buckling also can more clearly be seen on samples tested in distilled water compared with other tested samples. This may be because distilled water can easily enter through the interface, causing plasticisation along the interfaces while in tension or compression.

At this level of stress (above ~50 MPa), some form of delamination can be easily seen on samples tested in distilled water. Delamination also can be seen on samples tested in air but it is not so obvious.

From the above observations, we can conclude that for the negative stress ratio of R = -1 more damage can be seen in samples tested at the higher stress level (approximately 70 MPa). Buckling and delamination are clearly seen on samples tested in distilled water. Delamination occurred on low level of stress of samples with higher number of cycles. The damage also was not so severe if compared with the samples with

higher stress levels mentioned above. Delamination also can be seen at lower stress but it was not as clear as at higher stress.

5.3.3.3 Samples $[\pm 45]_4$, Lay-up R=0.1

Visual observation of the ±45 samples tested at R = 0.1 in all three environment revealed that all the samples had cracks along the fibre direction, 45° from the loading axis as illustrated in Figure 5.42. Most of these cracks occurred at the first cycle, and rapidly increase near to the fractured surface. All the fractures were angled at approximately 45° to the loading axis and this type of fracture suggests a rapid shear failure [Dyer (1996)]. Samples, which had been tested in air and distilled water showed an overall brush-like failure surface with lots of fibre pull out as seen from Figure 5.43 and 5.44.

One of the effects, when samples were tested in distilled water was that the water plasticised the matrices. However, in the polyurethane acrylate resin, the distilled water was also seen to have affected the fibre surfaces, causing fibre pull out as illustrated in Figure 5.45. This damage occurred at all levels of stress but was much more severe at the higher fatigue life but lower stresses. Samples that had been tested in seawater showed the same failure mechanisms as those tested in distilled water. The plasticisation along the fibre, especially at high stresses has caused the cracks propagating along the interface to be diverted away from the fibre surface. There was less fibre damage (Figure 5. 46) seen in these samples compared to the samples tested in distilled water.

5.3.3.4 Samples $[\pm 45^\circ]_4$, Lay-up R=-1

Matrix cracking along the fibre direction can easily be seen on all the samples tested (Figure 5.47 and Figure 5.48). Compared to samples with tension-tension loading, samples tested in this tension-compression loading showed more severe damage as seen from Figure 5.49 and Figure 5.50.

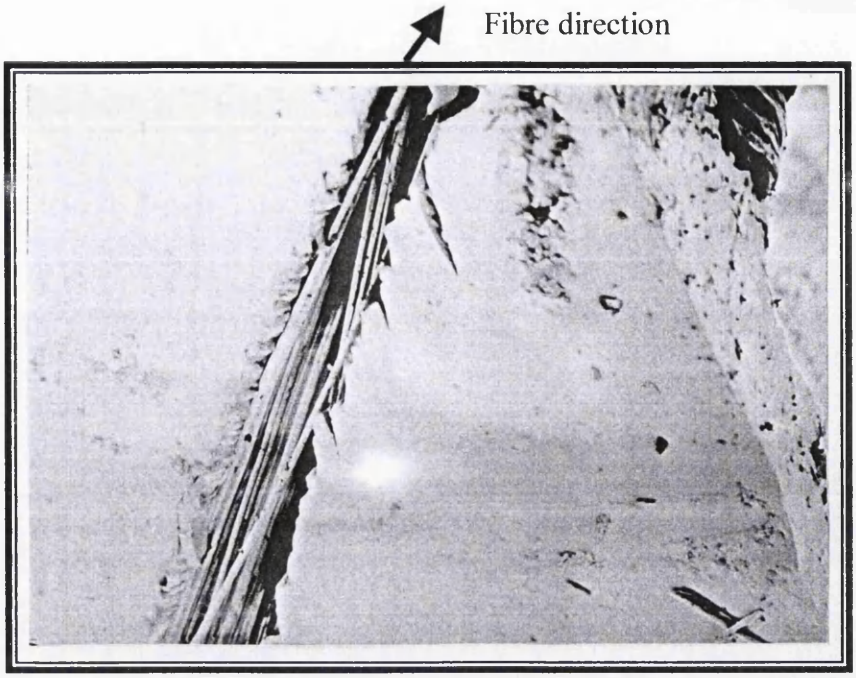

Figure 5.42: The image shows the crack on the side of the sample. Sample $[\pm 45^{o}]_{4,}$ R=0.1, air, 26 MPa, N_f =1491, 40X.

Figure 5.43: Bundle of $\pm 45^{o}$ fibre pull out with remaining matrix. Sample $[\pm 45^{o}]_{4,}$ R=0.1, air, 23 MPa, N_f = 141177, 190X.

Figure 5.44: The image shows brush-like failure at the fracture surface of the sample. Sample $[\pm 45]_4$, R=0.1, distilled water, 26 MPa, N_f =6626, 22X.

Figure 5.45: Bundle of $\pm 45^{o}$ fibre pull out.
Sample $[\pm 45]_4$, R=0.1, distilled water, 21 MPa, N_f = 131825, 170X.

Figure 5.46: Bundle of ±45° fibre pull out. Sample $[\pm 45]_4$, R=0.1, sea water, 21 MPa, N_f =464461, 180X.

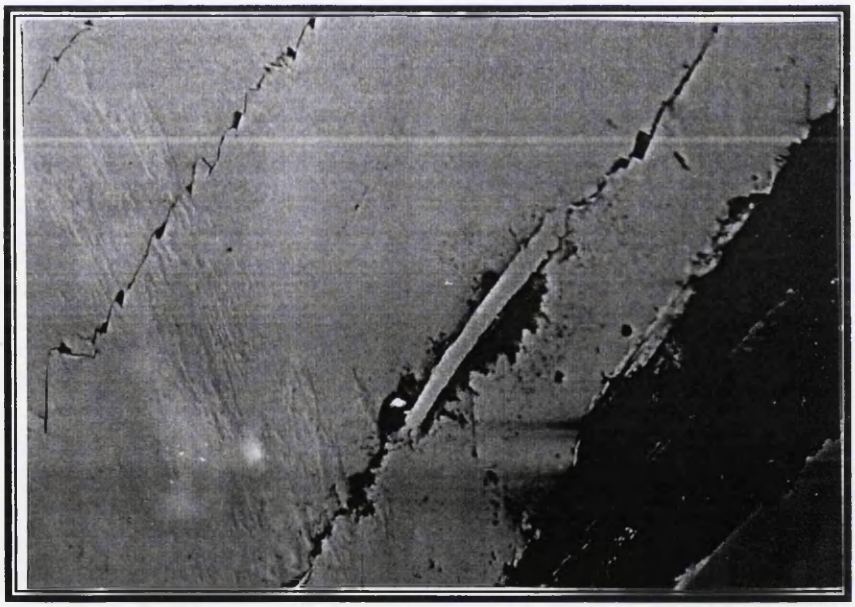

Figure 5.47: Cracks observed perpendicular near the fracture surface. Sample $[\pm 45]_4$, R=-1, distilled water, 16 MPa, N_f = 14815, 13X.

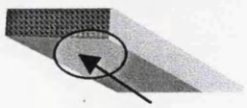

Figure 5.48: Cracks can be seen near the fracture surface. Sample $[\pm 45]_4$, R=-1, sea water, 28 MPa, N_f=755, 25X.

Figure 5.49: Delamination damage observed at the edge of the sample. Sample $[\pm 45]_4$, R=-1, air, 30 MPa, N_f = 8318, 15X.

Samples which had been tested in air showed that the fibres had a brittle failure. This observation can be seen from Figure 5.51. The other damage that can be detected was delamination (Figure 5.49), which occurred at the edges of the samples. This damage accumulates until it reaches failure.

More severe fracture surfaces were observed through SEM for the sample tested in the distilled water. The pulled out fibres crushed by compressive load and this observation was illustrated in Figure 5.52. There was delamination damage seen at the edges of the samples.

In the seawater test, the same damage mechanism occurred. However, more fibres pulled out with bundles which means that the seawater had plasticised the resin to hold the fibres together until it fractured. Figure 5.53 depicts the fracture surface of a sample tested in distilled water at a relatively low stress and high cycles to failure. There is evidence of delamination damage. For a relatively high stress, low cycles to failure, Figure 5.54 shows that the delamination can be observed near the edges of the samples and this damage can easily be seen with the naked eye.

5.3.4 Absorption Test

Tests were conducted both on the pure polyurethane acrylate resin matrix material and composites based on polyurethane acrylate. Specimens were exposed to air, distilled water and seawater under controlled condition. Only two types of lay-ups were studied i.e. Ulticloth $[90/0]_{2S}$ and Biaxial Ulticloth $[\pm 45]_4$. The test results were plotted in different formats as shown in Figures 5.55 - 5.60.

It was seen that the scatter in results increased with increasing weight gain and so error bars are included in Figure 5.55 to 5.59 proportional to weight gain, ±10% error range. Best-fit logarithmic curves show the trend of increasing weight gain with time. Figure 5.55 shows the result of weighing pure (PUA) resin and its composites in air (an air conditioning room at 23°C and 50% relative humidity) at regular time intervals

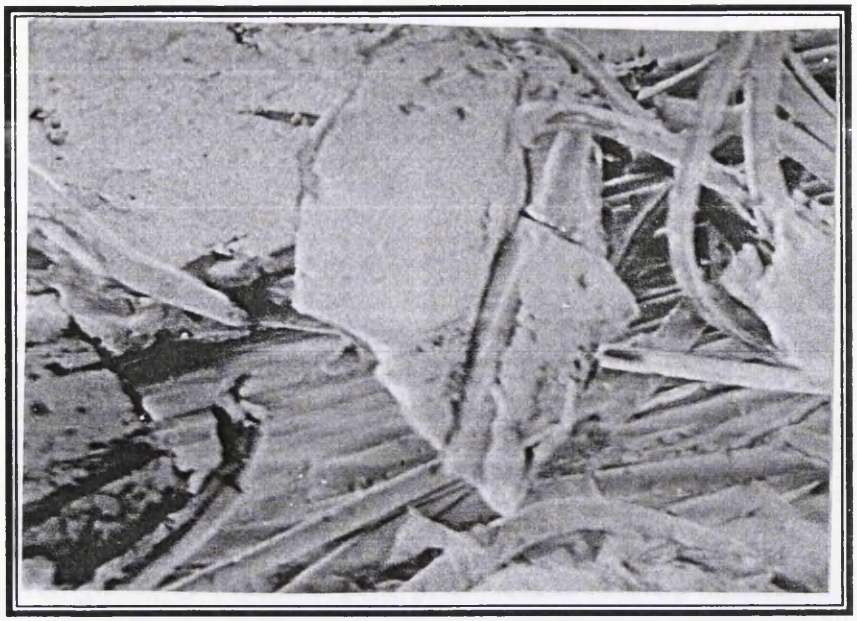

Figure 5.50: Severe damage at the fracture surface. Sample $[\pm 45]_4$, R=-1, distilled water, 16 MPa, N_f =114815, 170X.

Figure 5.51: The image shows brittle fibres fracture. Sample $[\pm 45]_4$, R=-1, air, 60 MPa, N_f = 195, 1000X.

Figure 5.52: Pull out fibre-crushed by compression.
Sample $[\pm 45^{o}]_{4,}$ R=-1, distilled water, 28 MPa,
N_f =1259, 220X.

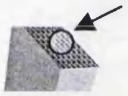

Figure 5.53: Delamination damage.
Sample $[\pm 45^{o}]_{4,}$ R=-1, sea water, 16 MPa,
N_f = 134896, 20X.

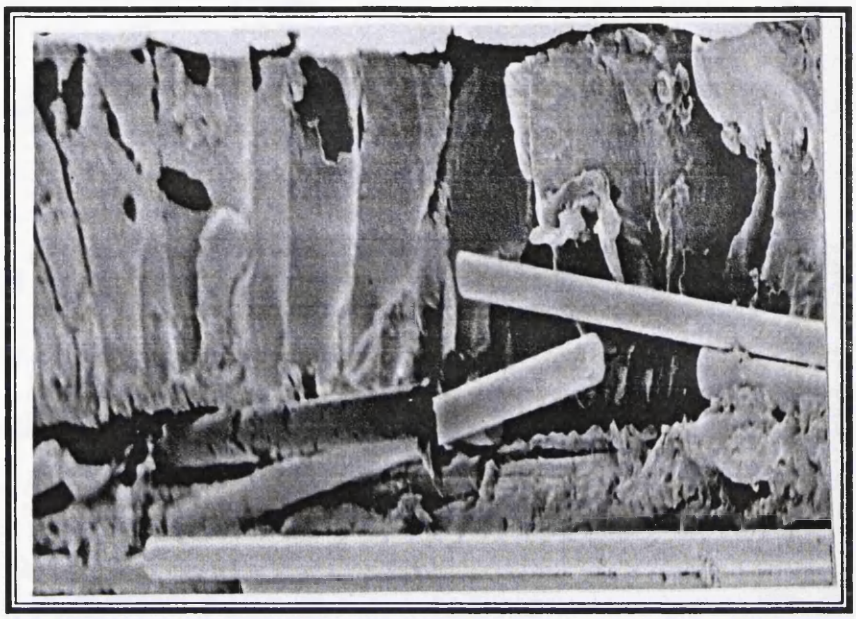

Figure 5.54: Delamination damage and fibres fracture.
Sample $[\pm 45]_4$, R=-1, sea water, 28 MPa,
N_f =758, 150X.

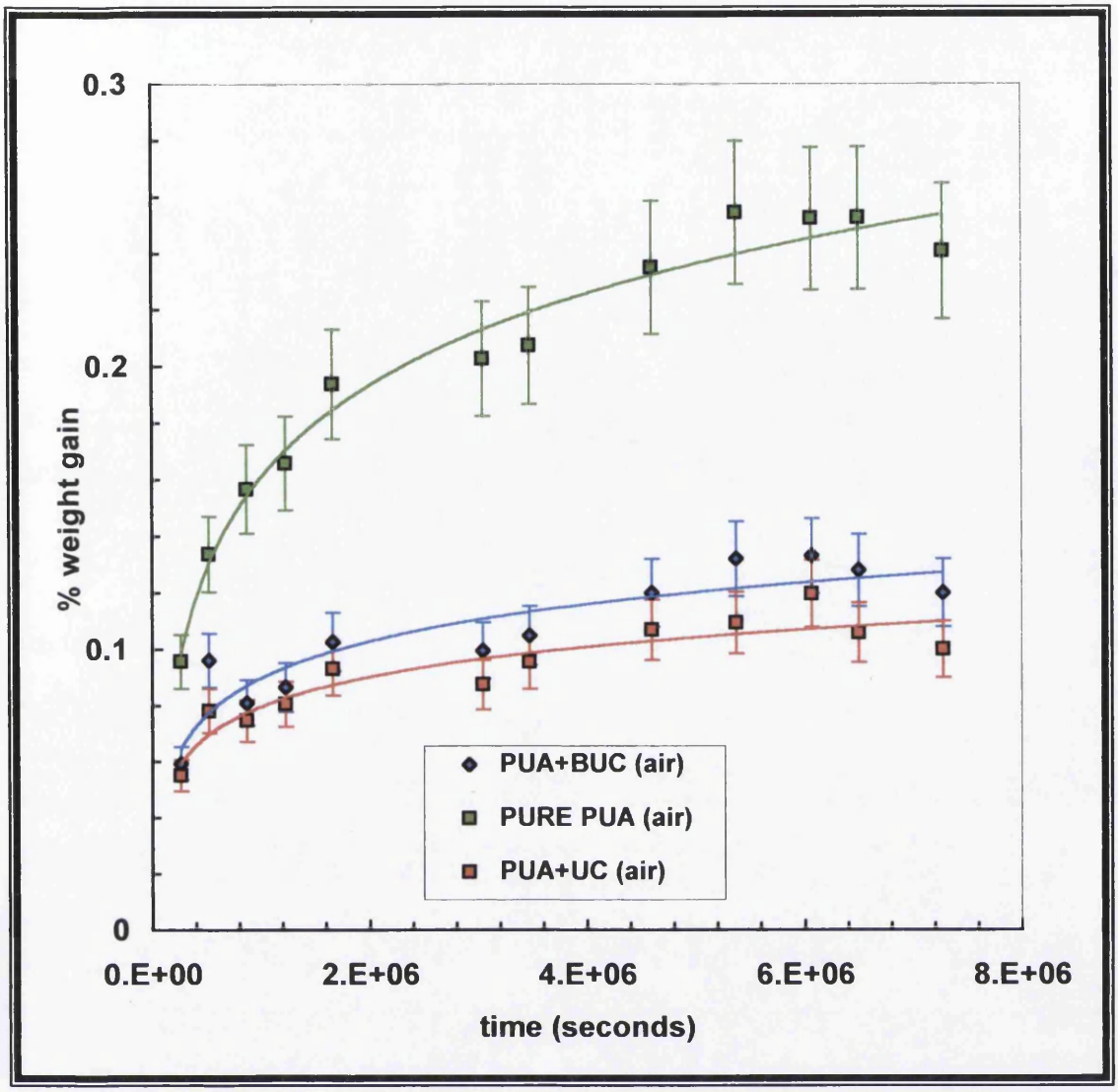

Figure 5.55: Moisture absorption for lay-up $[90^{o}/0^{o}]_{2S}$, $[\pm 45^{o}]_{4}$ and pure resin Polyurethane Acrylate in air.

following oven drying. It may be seen that (PUA) resin has a higher percentage weight gain than its composites. The percentage weight gain by PUA was 0.26% whereas the weight gain of both composite lay-ups (Biaxial Ulticloth and Ulticloth) was almost the same at about 0.12% and 0.1% respectively. This is consistent with uptake of water into the resin regions, rather than the glass fibres or the interfaces. The weight fractions of resin in pure polyurethane acrylate, Biaxial Ulticloth composite and 0/90 Ulticloth composite are 100%, ~50% and ~40% respectively which match quite closely the relative amounts of water uptake. From Figure 5.55, it also can be concluded that all the three curves, points measurement were in acceptable of 10% range error bar.

The absorption test on the $[90/0]_{2S}$ composites both in distilled water and seawater are compared in Figure 5.56. For the two composites without sealed edges, the samples in distilled water had a larger weight gain than that in seawater. For the composites with sealed edges also there was a higher weight gain in distilled water than in seawater. However, although the sealing of the edges was tried in order to prevent water ingress through the cut edges where it could be transported into the composite by capillary action along the fibre matrix interface, the effect of using silicon sealant was to increase the overall water uptake rather than reduce it. This must have arisen from some absorption of water by the sealant or at the sealant sample interface. This was confirmed by carrying out absorption tests on the sealant material alone. Thus subsequent testing was continued using samples without sealing the edges.

The absorption tests on Biaxial Ulticloth composites both in seawater and distilled water for unsealed laminates are shown in Figure 5.57. Again there was a higher increase in weight for samples in distilled water than those in seawater, rising to figures of about 0.95% and 0.6% respectively.

Figure 5.58 shows the result of absorption tests for pure PUA resin and its composites in distilled water. All samples exhibit almost equal percentage of weight gains at about 1%. Similarly, Figure 5.59 shows the effect of immersion of the same materials in seawater. In this case, pure polyurethane acrylate resin was found to have a greater

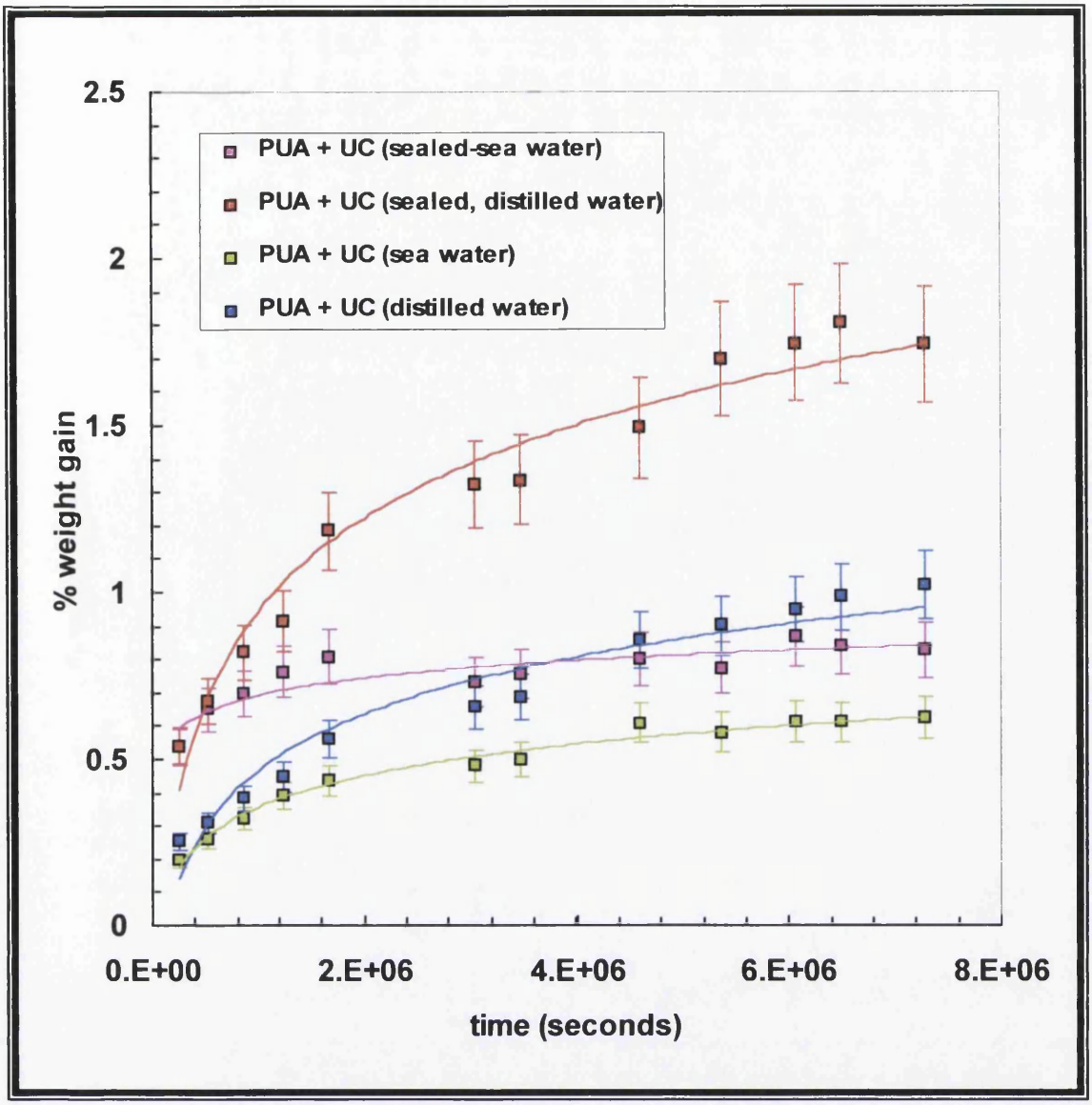

Figure 5.56: Moisture absorption for lay-up $[90^{o}/0^{o}]_{2S}$, Polyurethane Acrylate.

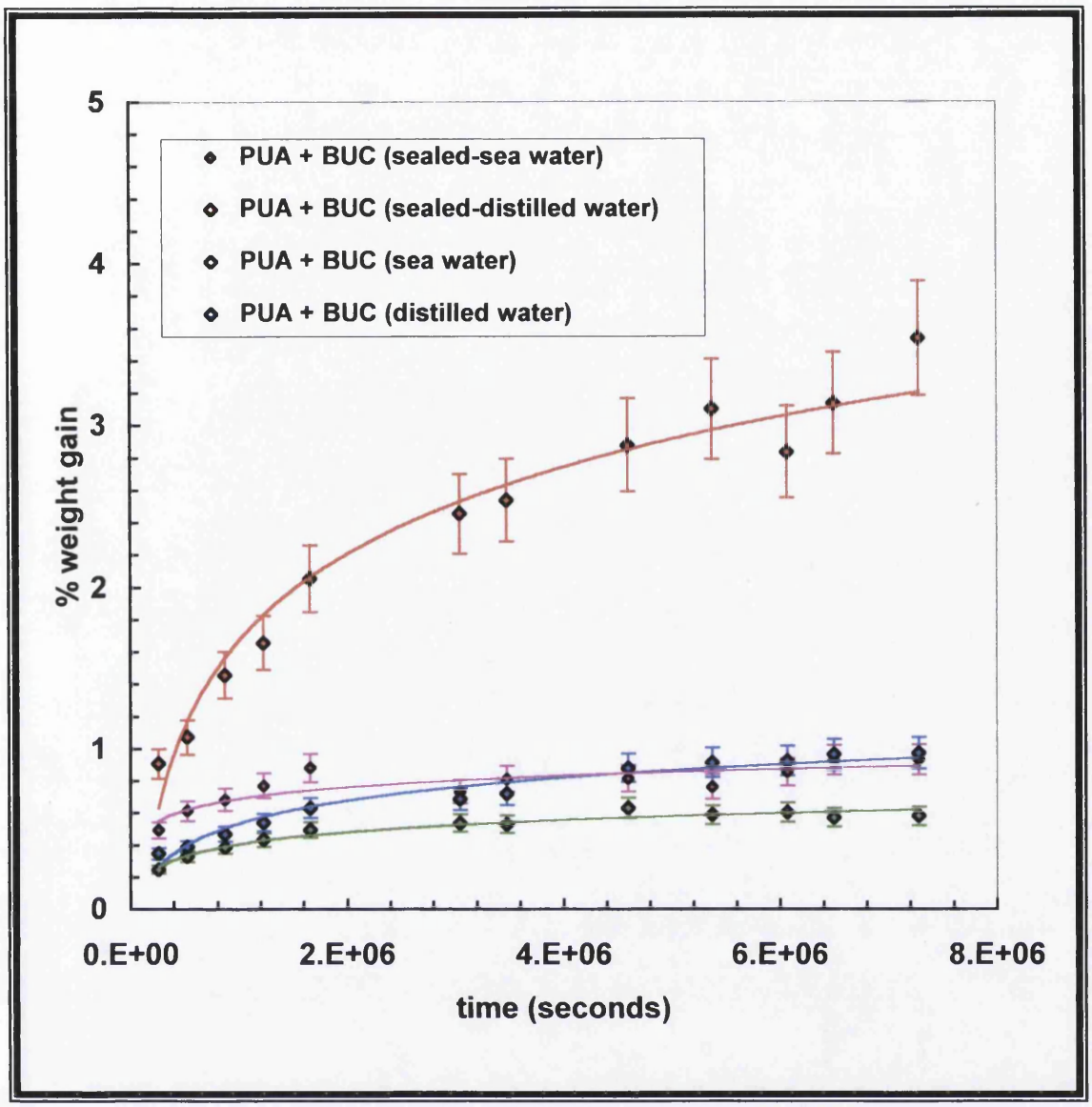

Figure 5.57: Moisture absorption for lay uyp $[\pm 45^{o}]_4$, Polyurethane Acrylate.

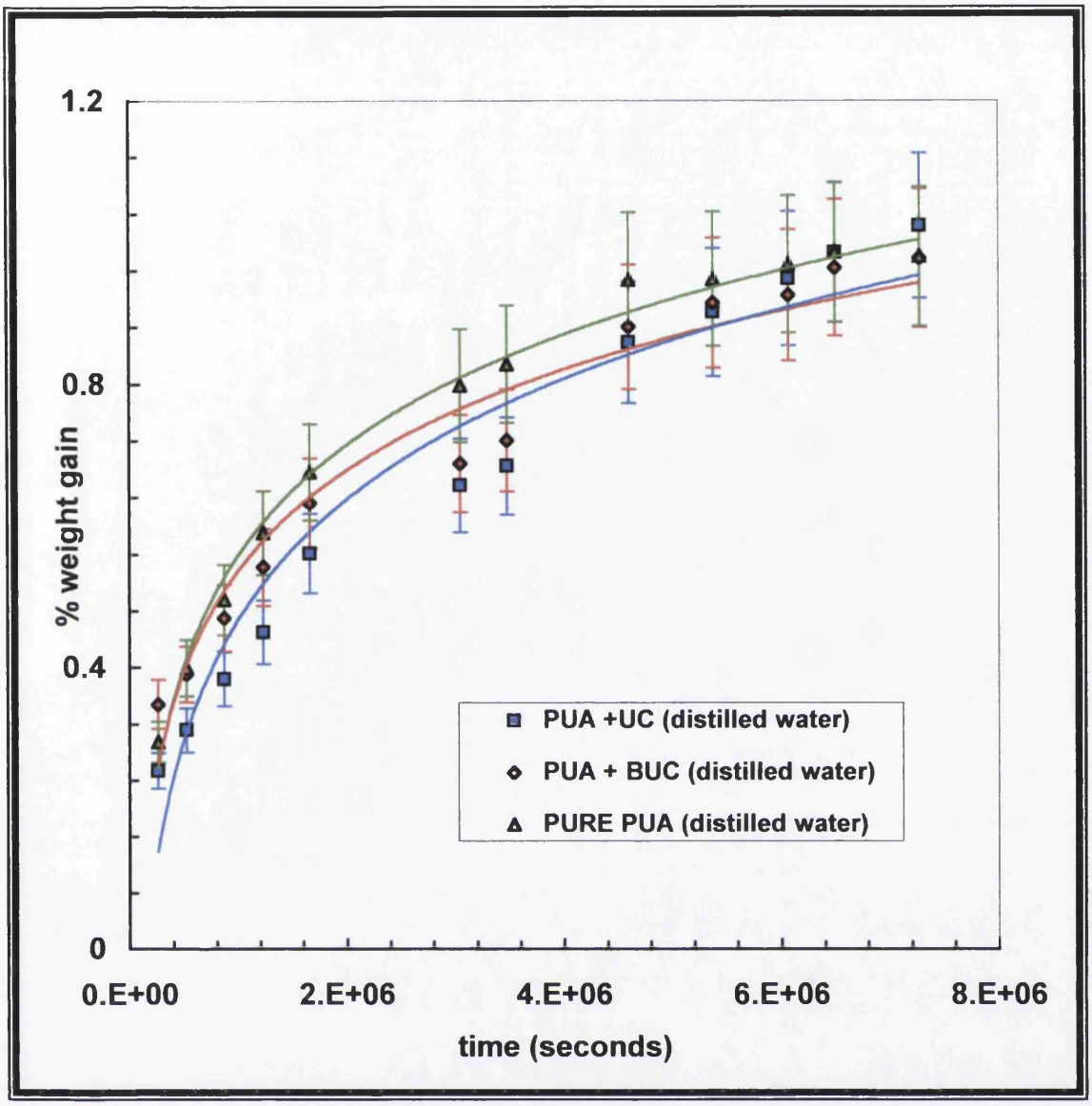

Figure 5.58: Moisture absorption for lay up $[90^{o}/0^{o}]_{2S}$, $[\pm 45^{o}]_{4}$, Polyurethane Acrylate in distilled water.

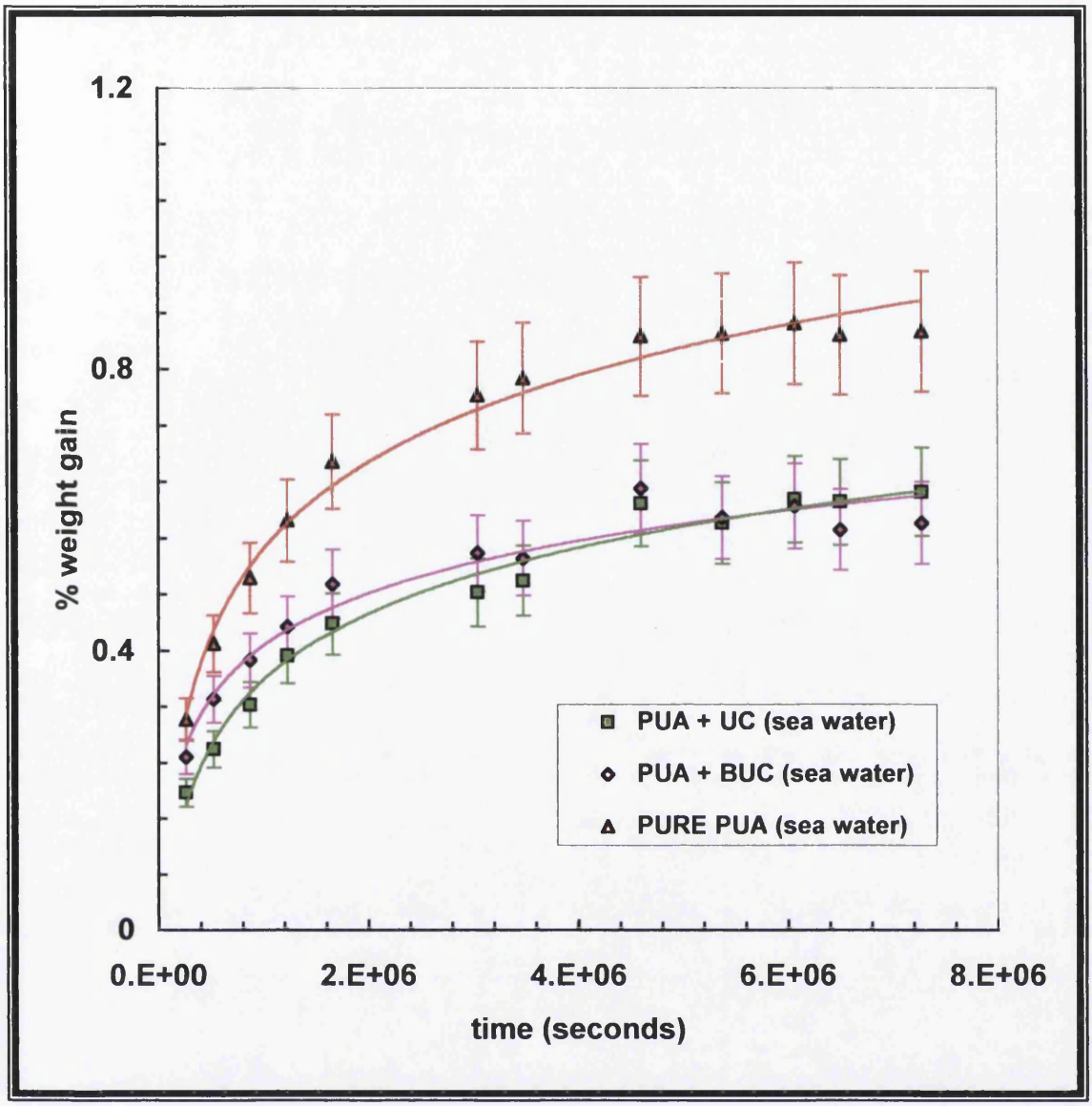

Figure 5.59: Moisture absorption for lay up $[90^{o}/0^{o}]_{2S}$, $[\pm 45^{o}]_{4}$, Polyurethane Acrylate in sea water.

percentage weight gain than its composites. The percentage weight gain of the pure resin is about 0.25% greater than $[90/0]_{2S}$ composite and about 0.3% greater than the Biaxial Ulticloth composite.

The results of the above tests are tabulated below in terms of the long-term weight gain, that is, the point at which the weight has stabilised. For the weight gains in air, there is every indication that the water uptake is into the resin, since the percentage weight increases are quite closely linked to the proportions of resin in the pure resin and the composite samples. Such differences are not so evident in the data for samples tested in distilled water, for which both the pure resin and the composite samples produced weight gains of approximately 1%. It seems likely that, when immersed in water, capillary action will cause water penetration along the fibre matrix interface, and it could well be that this transport mechanism in the composites added to the absorption into the resin component (~50-60% by weight) balances the water absorption into the 100% resin.

In the case of the seawater, absorption into the pure resin (0.9%) is similar to that seen in distilled water, but the absorption into the composite samples is significantly less (~0.6%). These lower values for the composites may be due to differences in the glass wetting properties of seawater compared with distilled water, or possibly an osmosis effect on the water at the fibre matrix interface.

Percentage weight gain due to silicon sealant suggests that the sealant materials is pervious to distilled water more than seawater probably due to distilled water containing smaller molecules. Dyer (1996) observed similar phenomenon using the same sealant type but on other composites.

Material	Unsealed % weight gain			Sealed % weight gain		
	Seawater	Dist. water	air	Seawater	dist. water	air
PUA resin	0.90	0.90	0.26	_	_	_
Biaxial	0.60	0.95	0.12	0.95	3.90	_
Ulticloth	0.65	1.10	0.10	0.85	1.65	_

Table 5.6: Stabilised percentage weight gains for PUA based samples in various environment.

5.4 Modulus Degradation.

5.4.1 Introduction

Modulus degradation tests have been carried out to investigate the damage progression of composite laminates during the fatigue process. Composite laminates under fatigue loading were shown to exhibit an accumulation of damage mechanisms, consisting of matrix cracking in off axis plies, delamination, fibre pull out, breakage and fibre-matrix debonding. All these damage mechanisms will affect the material mechanical properties such as stiffness and strength.

5.4.2 Normalised Modulus

In order to understand the effect of loading conditions on the modulus degradation of composite materials, the elastic modulus was normalised to its initial value on the first cycle (E/E_o), while the number of cycle was normalised to the cycle number at failure (N/N_f). The use of normalised modulus facilitated the comparison of different materials under various loading conditions as well as providing a similar base for all the tests. This

allowed comparison of the influences of lay-up, stress level and stress ratio on the modulus degradation of the materials.

In order to identify the progress of modulus degradation, two series of samples; waisted $[90/0]_{2S}$ and $[\pm 45]_4$ lay-ups, were studied under two stress ratios. The stress ratios used were R= 0.1 and R= -1.

5.4.3 Tension-Tension Loading, R=0.1

5.4.3.1 Samples $[90/0]_{2S}$

For polyurethane acrylate composite samples with $[90/0]_{2S}$ lay-ups, the effect of maximum stress on the normalised modulus at R = 0.1 is illustrated in Figure 5.60. The modulus degradation curves can be divided into three stages. Stage 1 is characterised by a rapid decrease in modulus and lasts for about 10 percent of the fatigue life. During stage 2, the modulus degradation is quite steady and slow and this stage typically lasts about until 90 percent of fatigue life. In stage 3, the modulus decreases much more rapidly and this stage typically accounts for the final 10% of the fatigue life. The second stage since it accounts for the region from 10% to 90% of the life time can be surmised as the most important stage for failure prediction and design purposes.

Although these tests depicted in Figure 5.60 were all conducted at the same stress ratio, the effect of maximum stress cannot be disregarded. The results indicate that when the maximum stress was less than 60% UTS of the material (~370 MPa), there was little modulus degradation until stage 3. Generally, at higher stress levels, there were greater modulus reductions in stage 1. Also, as a percentage of their total lifetimes, the lower stressed samples had a shorter stage 3, or in other words, they failed more suddenly relative to their lifetimes, hence it can be concluded that there is no significant modulus degradation for $[90/0]_{2S}$ samples tested at low stress until final failure is approached.

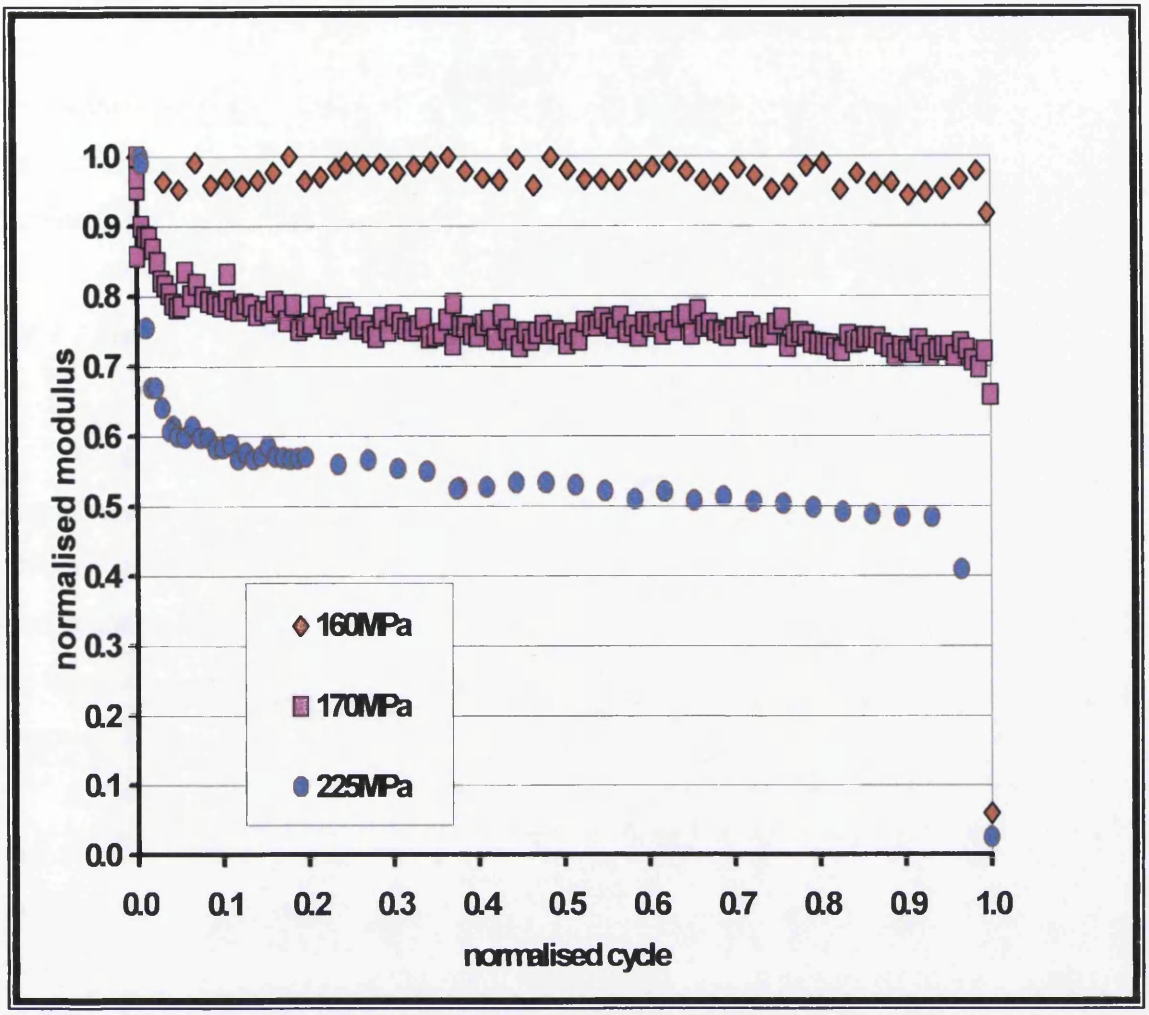

Figure 5.60 : Modulus degradation for $[90^{o}/0^{o}]_{2S}$, R=0.1

At higher stress levels, there were significant reductions in modulus during stage 1, with values in some cases down to 60% of the initial value. The changes in modulus degradation result from damage initiation and development such as matrix cracking, interfacial damage, and fibre pull out and these mechanisms are discussed further in Section 5.4.7.

5.4.3.2 Samples $[\pm 45]_4$

For polyurethane acrylate composite samples with $[\pm 45]_4$ lay-ups, the modulus degrades significantly from the first cycle until failure for all values of maximum stress. This is indicated in Figure 5.61, where rapid decreases in modulus mostly occurred during the first 50 percent of the lifetime. The degradation was such that the modulus of all samples fell to less than half the initial value during the first 50% of the lifetime. Degradation was then slower but steadier for the next half of the fatigue life.

Although stages 1 and 2 were not so easily differentiated with $[\pm 45]_4$ samples they did tend to exhibit a stage 3 as modulus degradation accelerated towards eventual failure. There did not appear to be a significant dependence of modulus degradation with stress level, since all the curves were fairly similar. It may be that degradation during the middle stage is less at lower stress levels, since the gradients of the curves from the lower stressed samples tend to be less, but to assess this dependence would require further experimental data.

During the first halves of the lifetimes, modulus values drop drastically corresponding to damage development mostly dominated by matrix cracking and delamination. Matrix cracking has been observed to appear at $N/N_f = 0.1$. Delaminations appear at a later stage as N/N_f increases. Near the end of the life, damage become more extensive mostly consisting of combined matrix cracking and delamination and these mechanisms are discussed more fully in Section 5.4.7.1.

5.4.4 Tension-Compression Loading, R=-1

5.4.4.1 Samples $[90/0]_{2S}$

According to Echtermeyer (1995), glass/polyester laminates regained their original static modulus completely during compressive stresses beyond the fatigue knee point. He used five layers of Rovimat 800/100 from Chomarat. This is a combination of a woven roving of 800 g m^{-2} and chopped strand mat of 100 g m^{-2}. Fibres were oriented in the 0/90 direction during testing, i.e. running in the load direction and perpendicular to it.

Also the combination of stiffness of the 0° fibres and the toughness of the polyurethane acrylate matrix may account for the much smaller changes in the fatigue response of this $[90/0]_{2S}$ lay-up when tested at R = -1. This is clearly depicted in Figure 5.62, which shows that no significant modulus degradation occurred for $[90/0]_{2S}$ lay-up in tension-compression loading until very close to final failure. From this study the modulus decay amounted to less than 30 percent of its initial value before final failure.

There are no distinct stages for the modulus degradation of this specimen. From visual observation, first damage seemed to be attributed to transverse matrix cracking. However, as the damage progressed the mechanism of failure tended to favour fibre pull out. This reduces the local stiffness component and causes microbuckling. The combined effect of the compressive loading and microbuckling further accelerate damage growth and finally lead to local failure.

5.4.4.2 Samples $[\pm 45]_4$

Figure 5.63 shows that there is a much more steady degradation of modulus for $[\pm 45]_4$ samples at R = -1 than for the other lay-ups and R-values. There is an approximately linear fall off in modulus to about 30% of the initial value by about 85% of the lifetime, at which point there is a more rapid degradation to final failure. This pattern of modulus reduction is very similar for the various different stress levels.

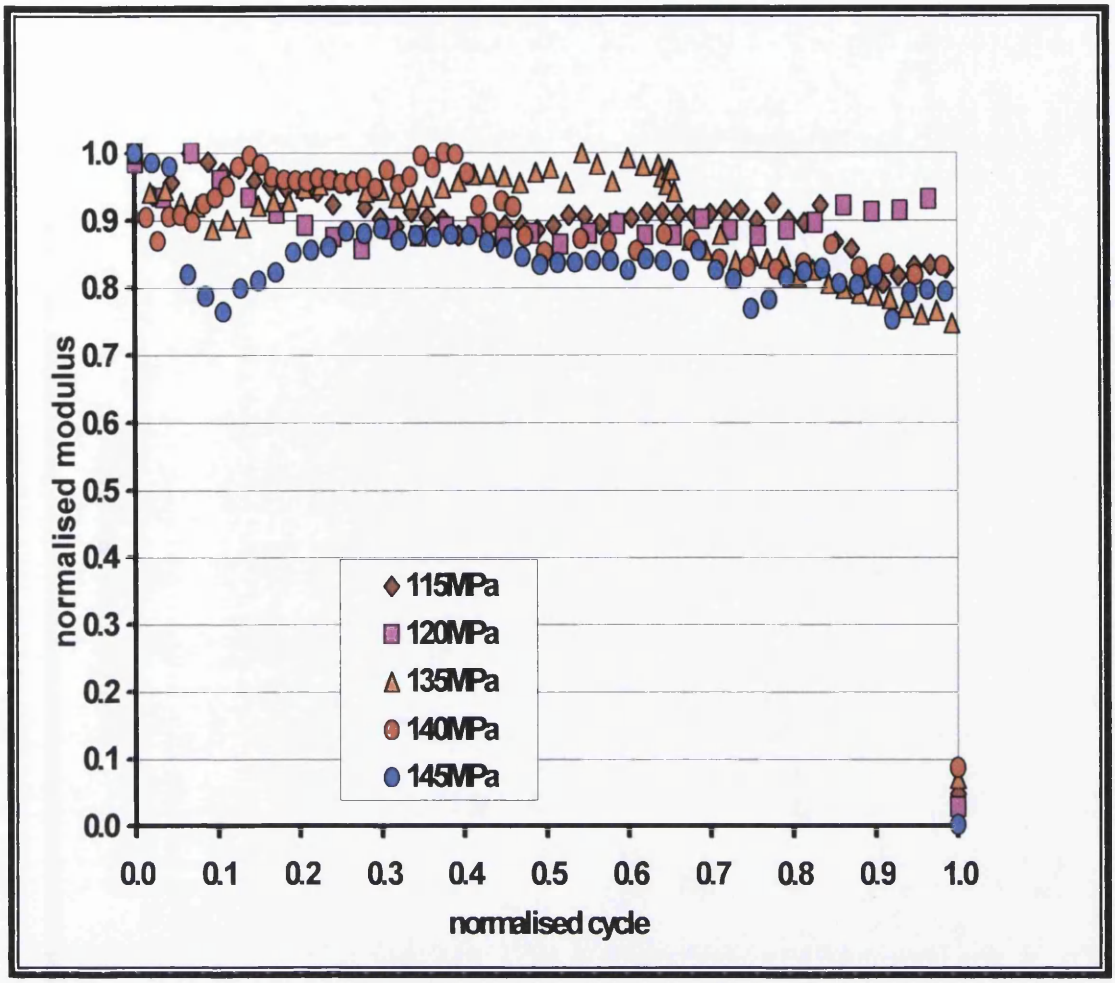

Figure 5.62 : Modulus degradation for $[90^{o}/0^{o}]_{2S}$, R=-1

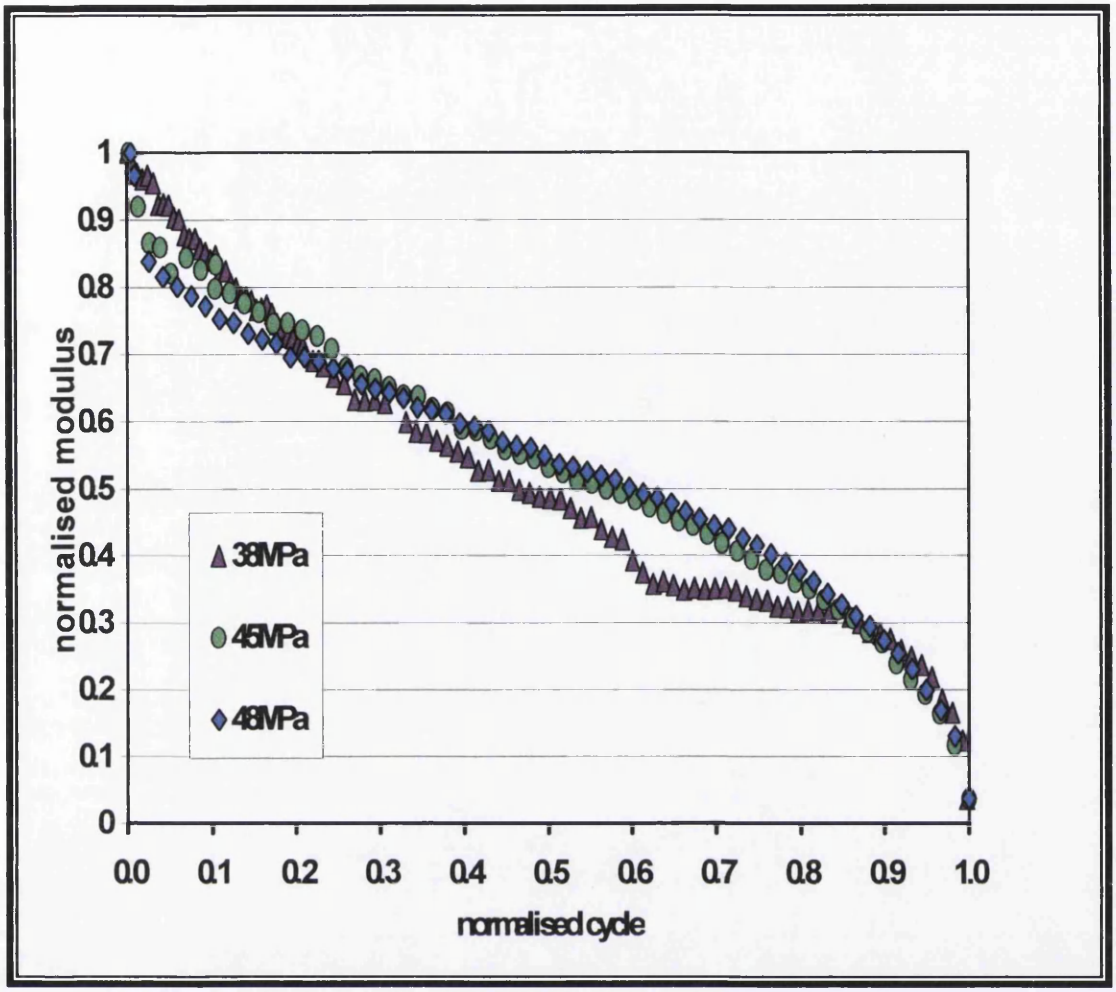

Figure 5.63: Modulus degradation for $[\pm 45^{o}]_4$, R=-1

Buckling of outside plies although not so obvious as for the $[90/0]_{2S}$ lay-up, was observed. The changes in modulus degradation in this case were due to damage accumulation resulting from matrix cracking, fibre pull out and delamination and these intensified as the test progressed. Matrix cracking and delamination seemed to be the dominating damage mechanism during the final stage. Visual observation showed that interfacial damage also occurred in this test as shown in Figure 5.78.

5.4.5 The effect of lay-up on modulus degradation at the same number of cycle to failure N_f.

In this study, comparisons are made based on the same number of cycles to failure. Two maximum stress levels were selected, one representing the high N_f and the other for low N_f.

5.4.5.1 Stress ratio, R= 0.1

From Figure 5.64 for low N_f (high stress), the [90/0] lay-up shows a initial rapid fall in modulus followed by a levelling out at about half the initial value, whereas the $[\pm 45]_4$ lay-up continuously degrades reaching a level of about 20% by 90% of its lifetime. The effect is that the two curves meet at 20% of the life, after which the modulus of the [90/0] sample levels off whilst that of the $[\pm 45]_4$ sample continues to reduce. Modulus reduction in both samples accelerates during the last 10% of their lives.

At high N_f (low stress), during the first 10% of life the fall in normalised modulus is similar. As the cycling continues the normalised modulus of the $[90/0]_{2S}$ lay-up remains almost constant until close to failure whereas normalised modulus of the $[\pm 45]_4$ sample continues to fall until about 40% of its life before remaining steady until about the last 10% of its lifetime.

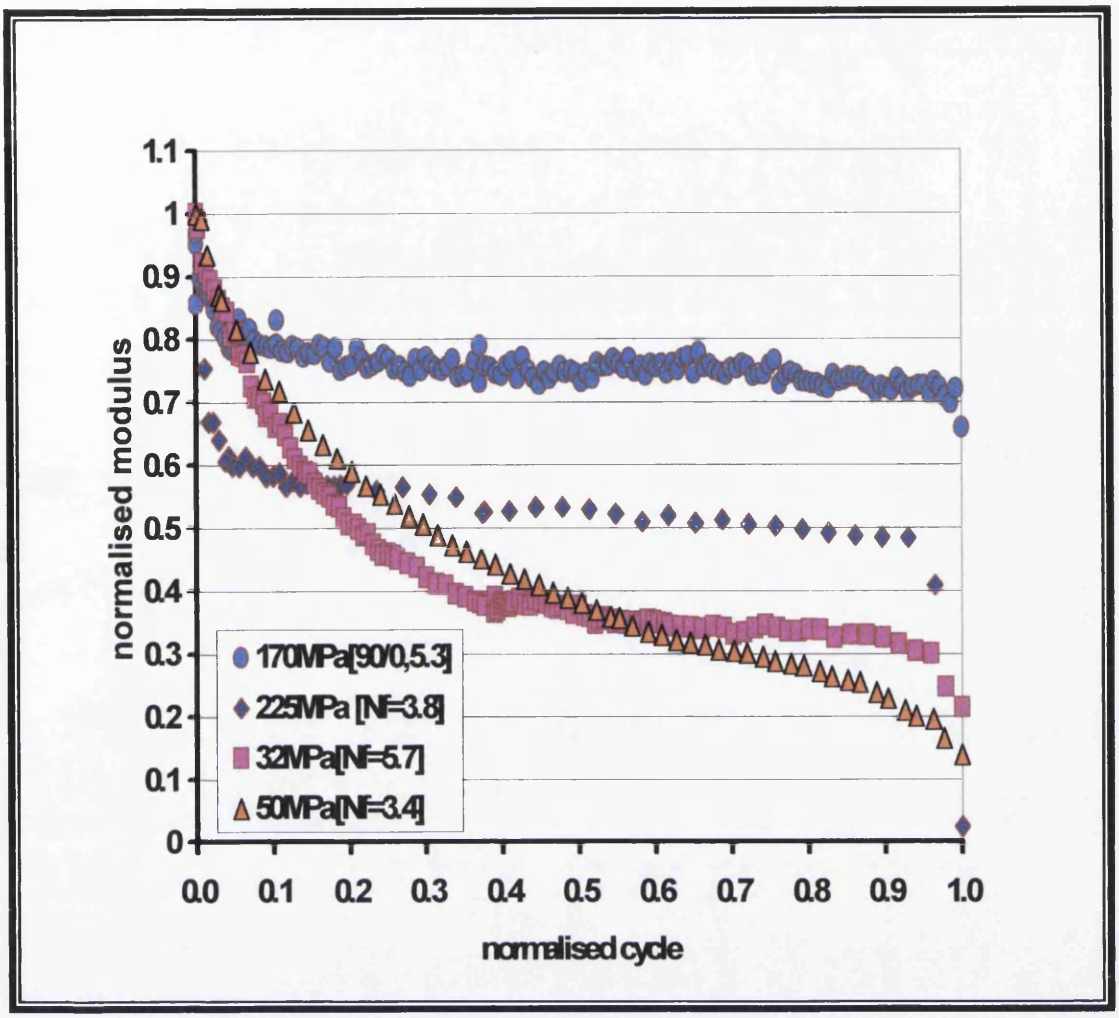

Figure 5.64: Comparison of modulus degradation for $[90^{o}/0^{o}]_{2S}$ and $[\pm 45^{o}]_{4}$, R=0.1 at the same no of cycle.

5.4.5.2 Stress ratio, R=-1

For R = -1 fatigue testing, at both low N_f (high stress) and high N_f (low stress) the two curves for each of the lay-ups show similar trends. The difference in normalised modulus degradation widens as the cycling continued. This is demonstrated in Figure 5.65. Whereas there is very little modulus degradation in either of the $[90/0]_{2S}$ samples, the modulus of the $[\pm 45]_4$ samples falls approximately linearly for most of the lifetime.

5.4.6 The Effect of Stress Ratio on Modulus Degradation.

5.4.6.1 $[90/0]_{2S}$ lay-up

Figure 5.66 illustrates the effect of stress ratio on modulus degradation for the $[90/0]_{2S}$ specimens. Two were subjected to cyclic stresses of 170 MPa and 225 MPa respectively at R = 0.1, whilst the other two were subjected to stresses of 115 MPa and 140 MPa at R = -1. Both curves for R=0.1 can be divided into three stages, showing similar patterns of degradation, namely an initial rapid fall in modulus for about 10% of the lifetime, followed by a levelling off and a further rapid reduction to failure in the final 10% of life. However for samples tested at R = -1 the curves cannot be divided into three stages and the modulus of those samples only degraded very slightly. Even very close to failure there was no sudden fall in modulus and there was very little warning of final failure.

5.4.6.2 $[\pm 45]_4$ lay-up

Four samples have been chosen for comparison, two from tension-tension loading, R = 0.1, and another two from tension-compression loading R = -1. Two samples were subjected to high N_f (low stress) and two to low N_f (high stress) as in the previous sections.

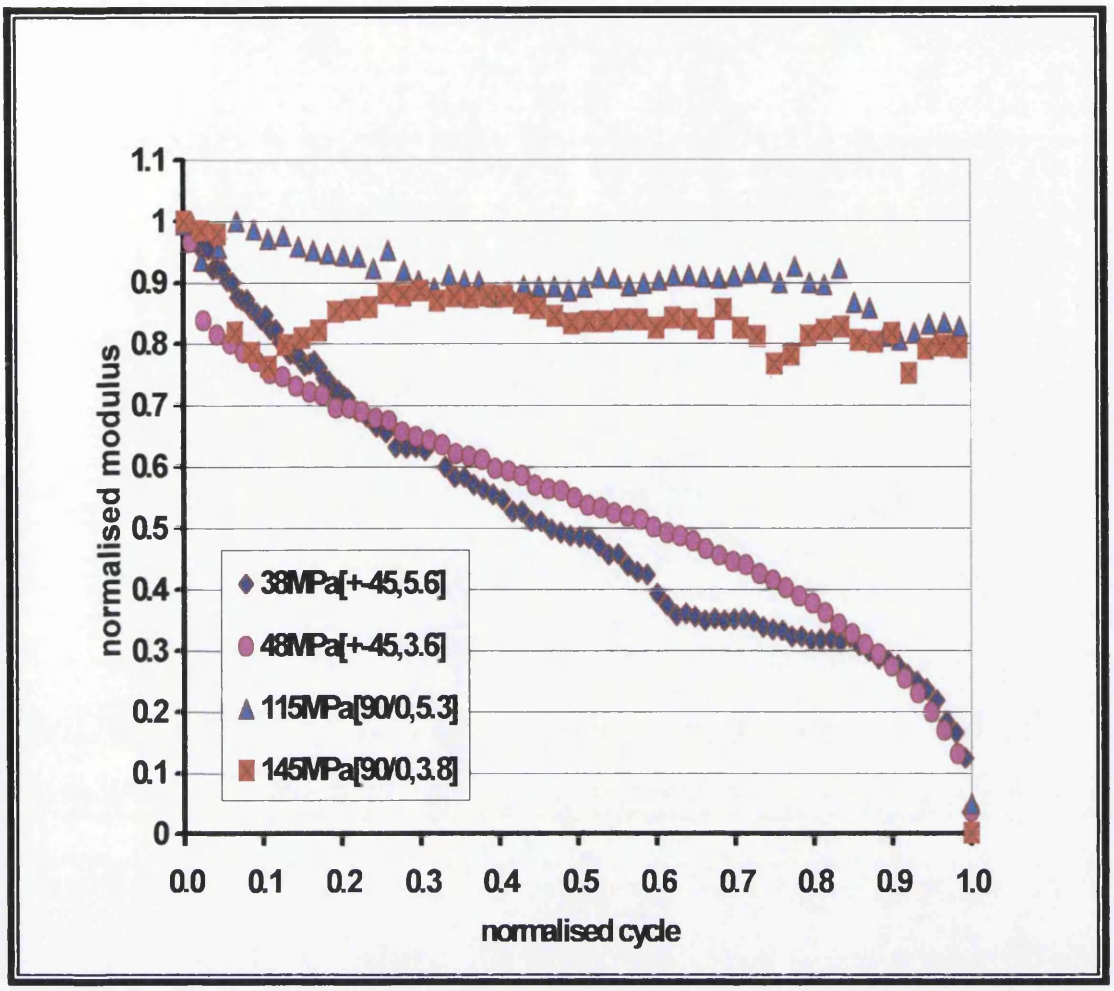

Figure 5.65: Comparison of modulus degradation for $[90^{o}/0^{o}]_{2S}$ and $[\pm 45^{o}]_{4}$, R=-1 at the same no of cycle.

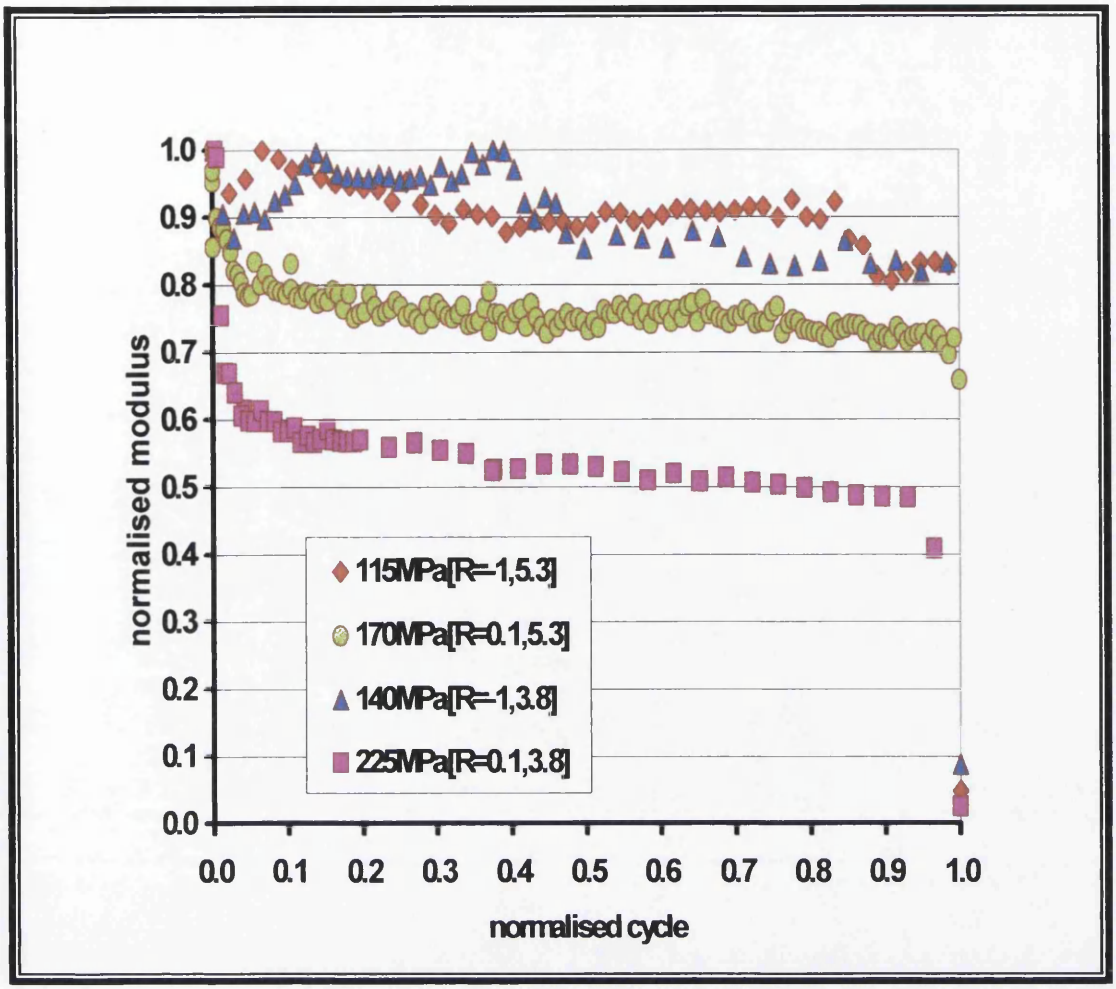

Figure 5.66: Comparison of modulus degradation for $[90^o/0^o]_{2S}$, R=0.1 and R=-1 at the same no of cycle.

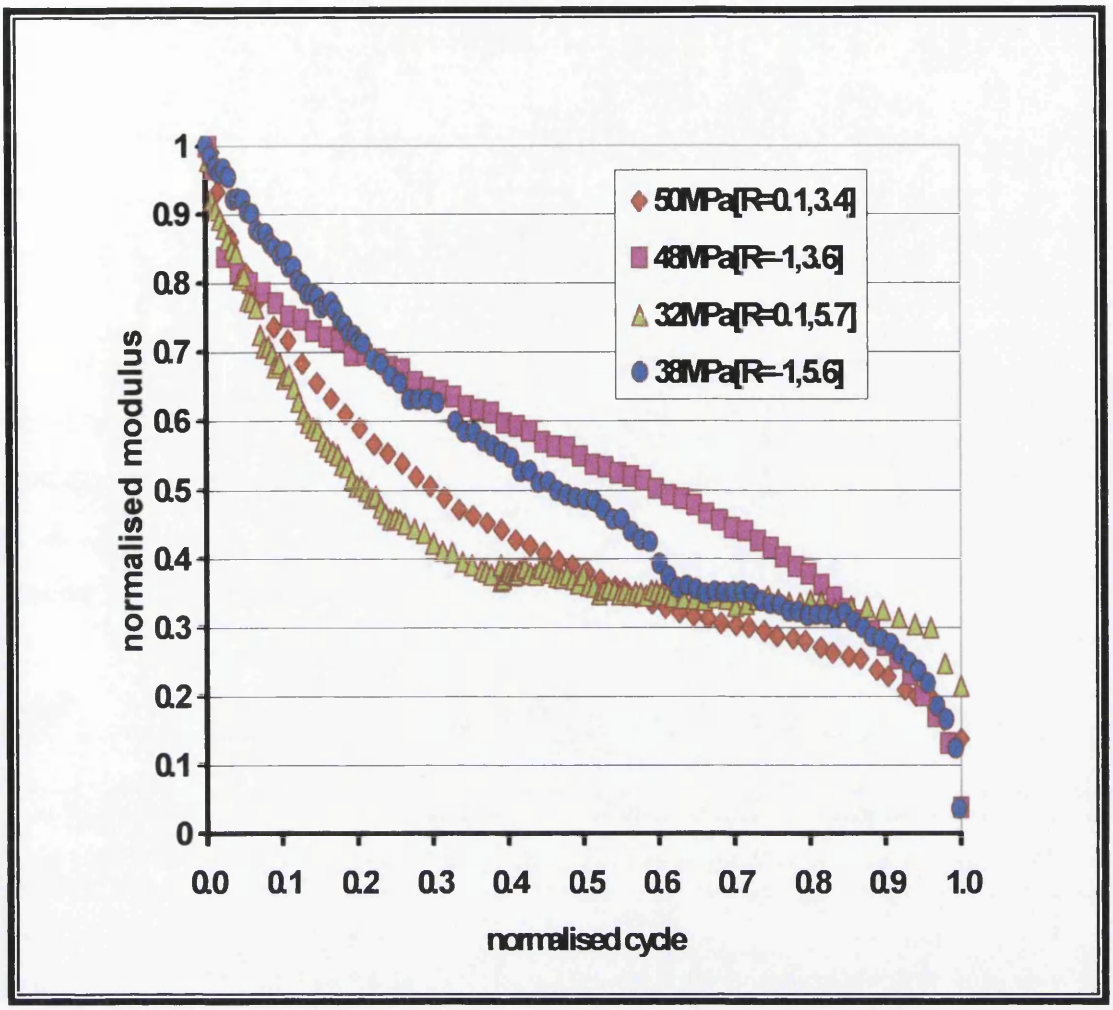

Figure 5.67 : Comparison of modulus degradation for $[\pm 45^{o}]_4$, R=0.1 and R=-1 at the same no of cycle.

Figure 5.67 illustrates that the R-value is a more significant factor than the stress level in determining the pattern of modulus reduction. Thus the initial modulus reduction is greater for R = 0.1 samples than for R = -1 samples. However the R = 0.1 curves tend to level off during the second half of their lifetimes, so that by about 90% of lifetimes the modulus of all the samples had reduced to about 25% of the initial values.

Although, the modulus degradation for both groups were similar, the damage that occurred in R = -1 samples was more severe compared with samples in tension-tension loading, as confirmed in the SEM observations discussed in Section 5.4.7.1 Echtermeyer et al. (1995) also noted that fatigue tests performed on other composites under reverse loading (R = -1) caused more severe damage than other loading conditions.

5.4.7 Microstructural Observations and SEM

Samples tested in tension-compression loading may produce a crushing of the appearance of the fractured surface if the sample is compressed following failure. Thus displacement trip control was used throughout the study to minimise the effect of post failure damage. The effect of this was that when the extension of the fatiguing sample was so great that failure must have occurred, then cycling was stopped before the next compressive part of the cycle took place. The tested samples were examined visually before SEM observation of the fractured surfaces.

Figure 5.68 illustrates the two types of lay-up used in the modulus degradation test, which are $[90/0]_{2S}$ and $[\pm 45]_4$. All the samples tested fractured in the waisted area.

5.4.7.1 $[\pm 45]_4$ lay-up.

All the $[\pm 45]_4$ samples failed in the waisted area, within the gauge length and the progression of damage can be seen from Figure 5.69. Visual observation of the tested samples revealed that all the samples had cracks along the fibre direction, at 45° to the loading axis. Samples show that the matrix cracks at the area of the waist, where the

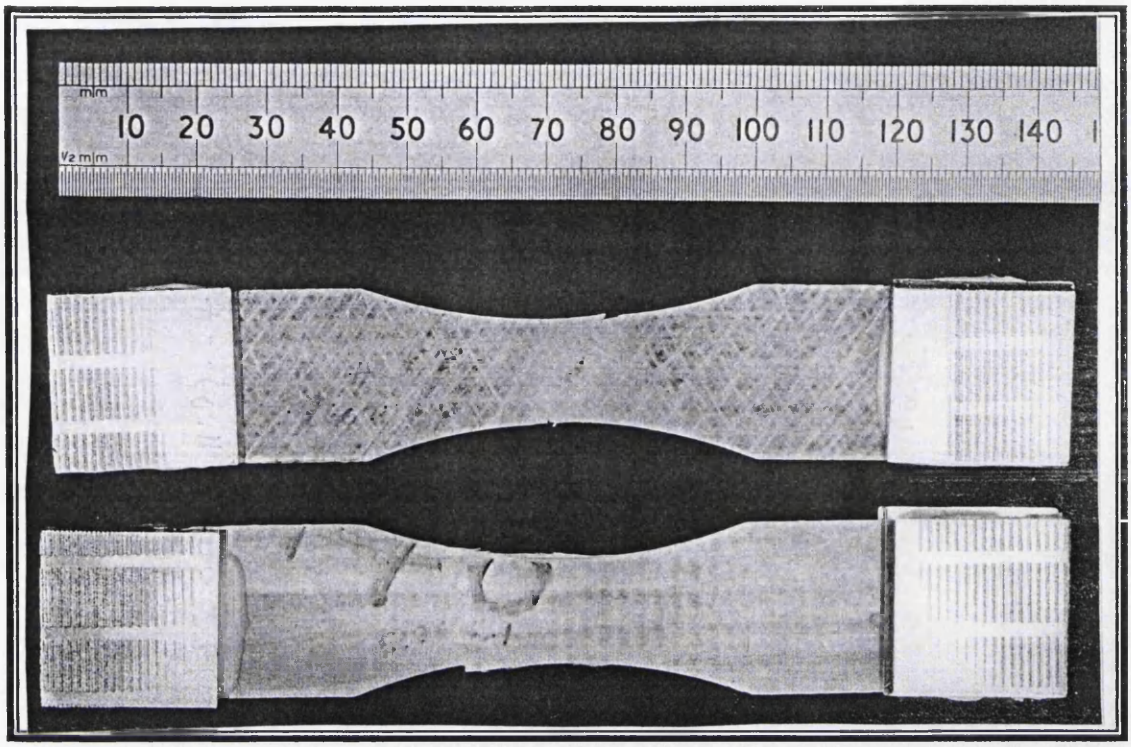

Figure 5.68: Samples Used In Modulus Degradation Test: $[90/0]_{2S}$ (top) and $[\pm 45]_4$ (bottom)

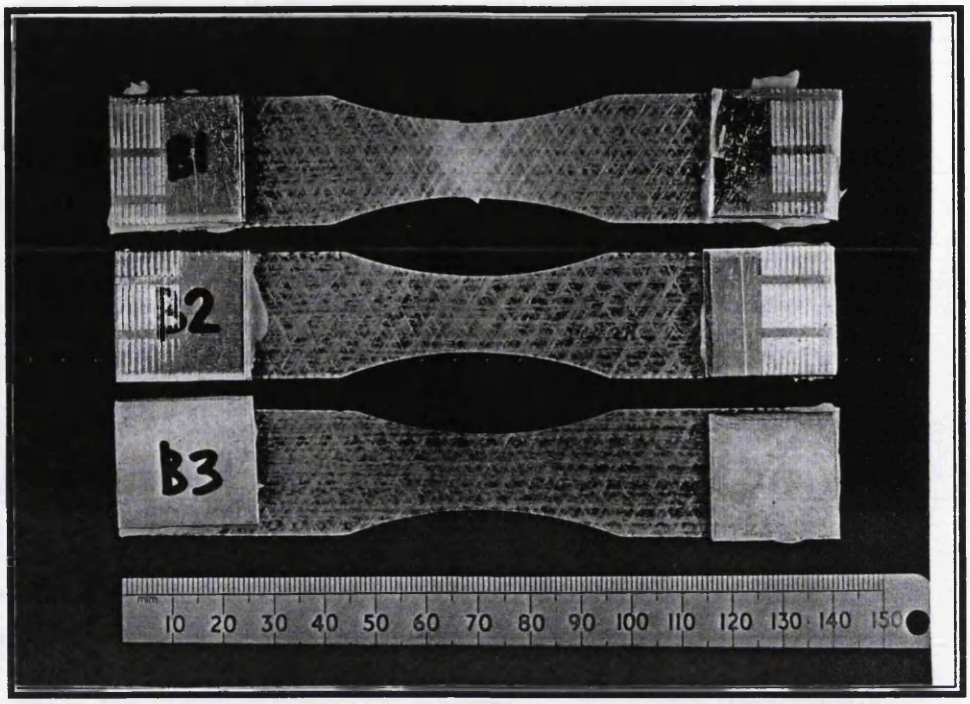

Figure 5.69 : Photograph of three $[\pm 45^{o}]_4$ modulus degradation samples. The samples show the progression of damage at the waist from a sample without any test (bottom), at the middle of the test (middle) and a fractured sample (top)

Figure 5.70 : SEM : Crack can be seen from side of the sample, near to the fractured surface. Modulus Degradation Test sample $[\pm 45^{o}]_4$, R=-1, 38 MPa, N_f = 398107, 15X

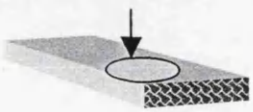

stress concentration was greatest. Cracks also can be seen in other areas but they are most clearly seen at the waist. Most of these cracks occurred during the first cycle whether it was on tension-tension or tension-compression loading. Figure 5.70 confirmed these crack observations.

The final damage from tension-tension loading (Figure 5.71 and 5.72) is less compared with samples tested in tension-compression (Figure 5.73 and 5.74) and quasi-static tensile loading (Figure 5.75 and 5.76). In quasistatic tensile loading the samples also exhibit white bands indicating severe damage. It seems that in quasistatic tensile tests, damage covered a larger area around the fracture surface more than for the R = -1 sample and much greater than the R= 0.1 sample. Perhaps this behaviour is linked to the level of applied stress, since in the tensile test, the whole sample would have been subjected to stresses closer to the ultimate tensile strength than others.

Samples subjected to tension-compression loading, also showed fibre pull out due to matrix cracks, which enhanced further crack growth. This is illustrated in Figure 5.77, SEM examination (Figure 5.78) shows that the matrix cracks and interface cracking contribute more damage to grow. The interface crack or longitudinal splitting, would be expected to reduce stiffness in the $[\pm 45]_4$ lay-up. Other significant contributors to modulus reduction are fibre pull out and delamination, which can be seen from Figure 5.79 and Figure 5.80.

Delamination reduces the ability of laminates to transfer stress away from damaged sections. The observation on the edge surface, (Figure 5.80), indicates a separation of fibre from matrix. This evidence suggests that interlaminar fracture, particularly associated with the damage near the interface, be involved in the failure process. It also can be seen that polyurethane acrylate matrix remains on the fibres in the fracture, indicating a strong interface between the matrix and fibres.

If Figure 5.78 and Figure 5.81 are compared, it is clearly seen that the sample tested with R = -1 had more severe damage. Figure 5.81 shows the interfacial damage and

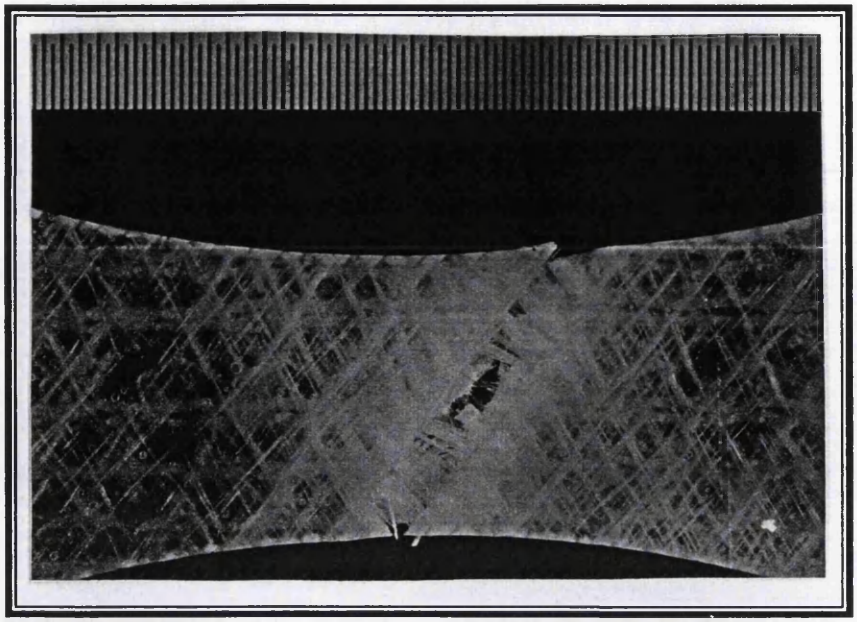

Figure 5.71 : Modulus Degradation Test sample $[\pm 45]_4$, R=0.1, 32 MPa, $N_f = 566400$.

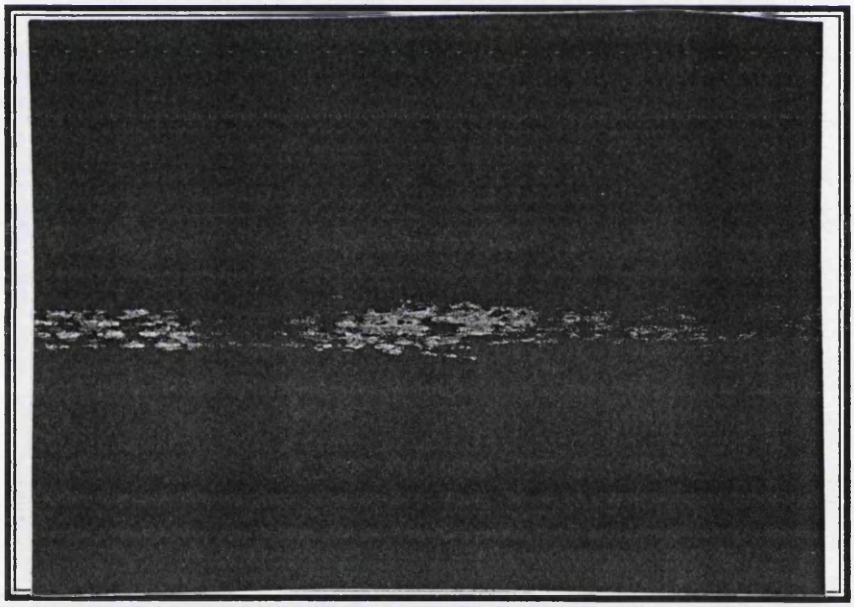

Figure 5.72 : Same sample as in 5.71 from a different view.

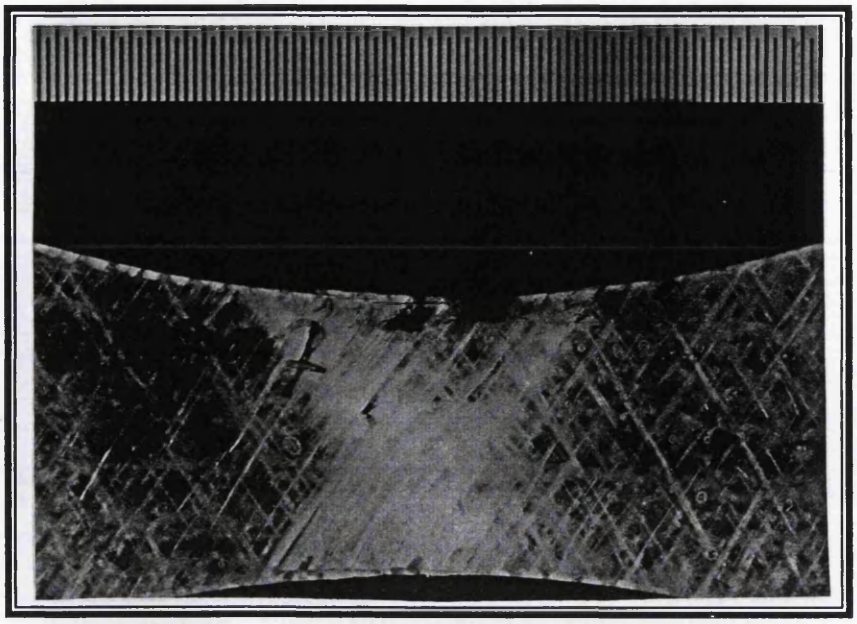

Figure 5.73 : Modulus Degradation Test sample $[\pm 45]_4$, R=-1, 38 MPa, N_f=408200.

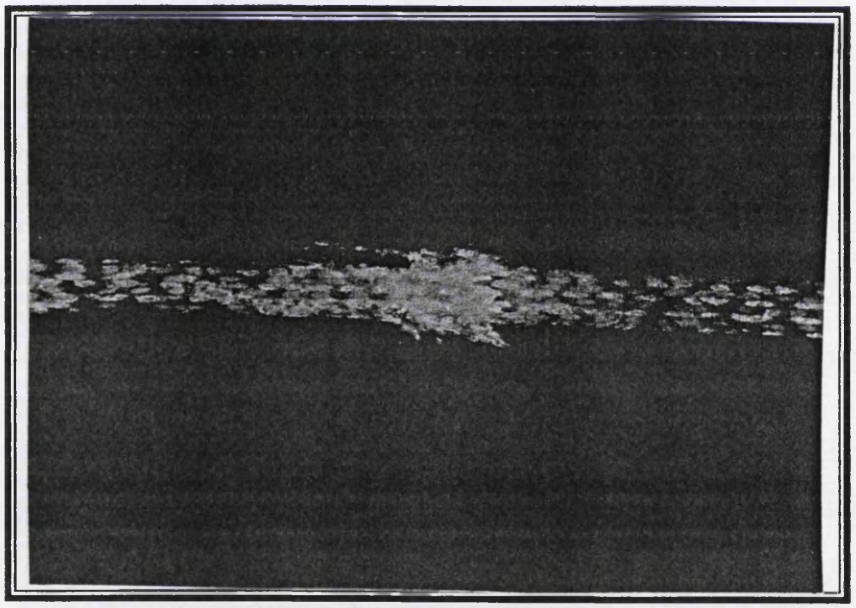

Figure 5.74 : Same sample as in 5.73 from a different view.

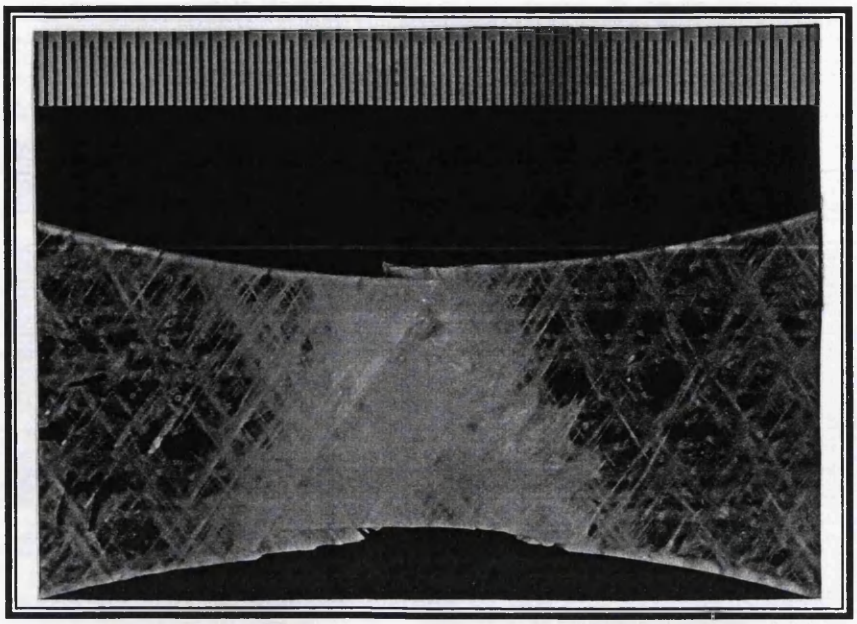

Figure 5.75 : Damage for the $[\pm 45]_4$, lay up fractured by tensile loading. White mark can be seen around the fracture and it break as the direction of fibre.

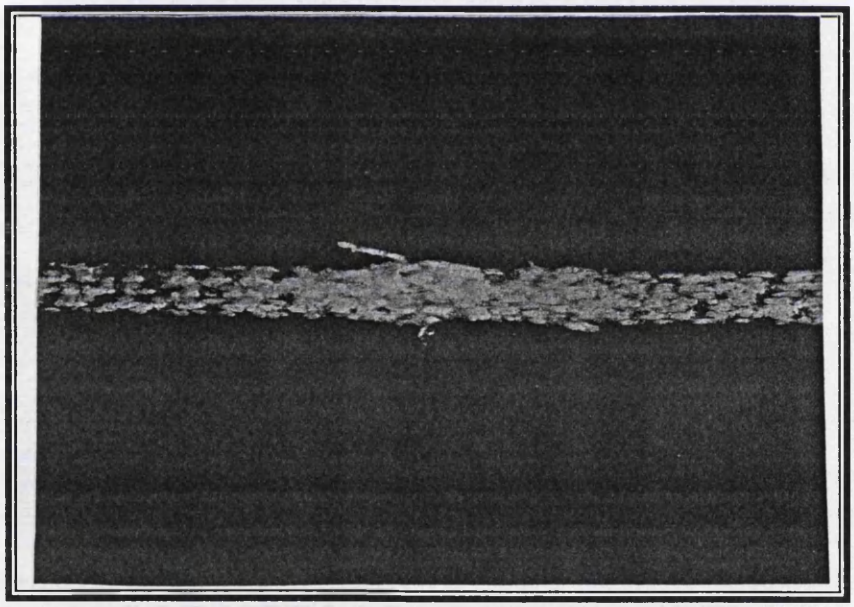

Figure 5.76 : Same sample as in 5.75 from a different view.

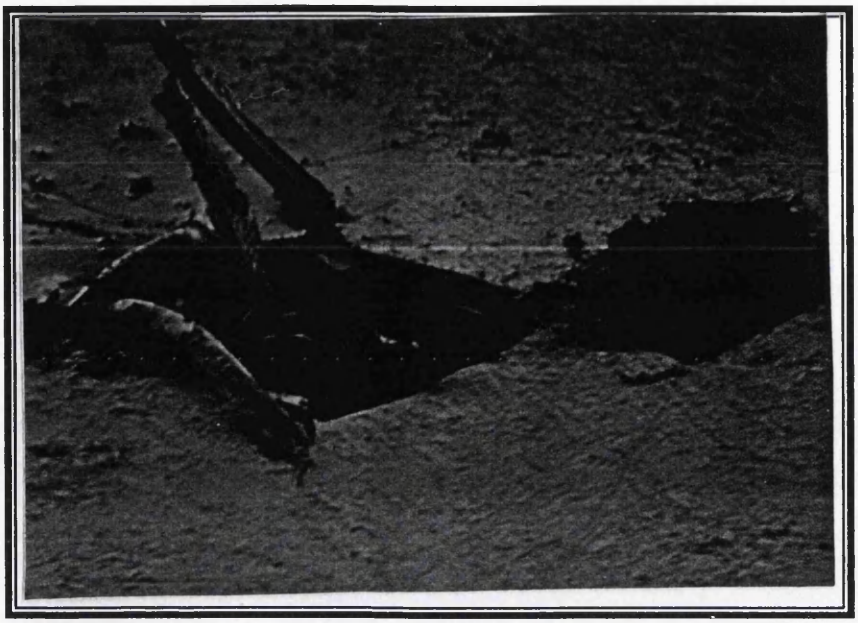

Figure 5.77 : Side of the sample, crack which was parallel to fibre direction. Also seen the fibre pull out. Modulus Degradation Test sample $[\pm 45]_4$, R=-1, 38 MPa, N_f = 398107, 200X.

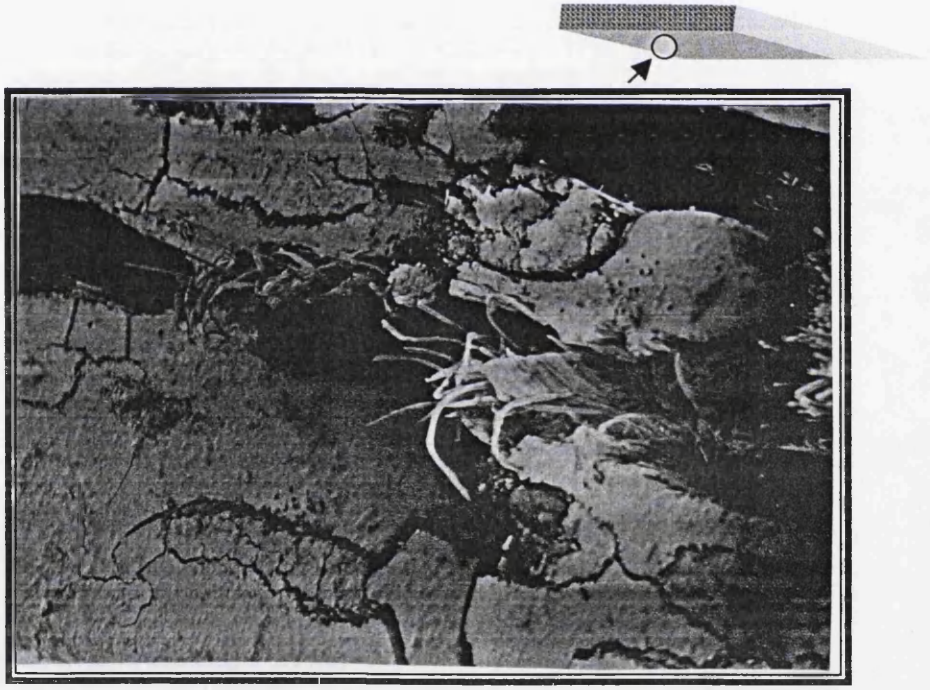

Figure 5.78 : Interfacial Damage can be seen from side of the sample. Modulus Degradation Test sample $[\pm 45]_4$, R=-1, 40MPa, N_f = 16218, 30X.

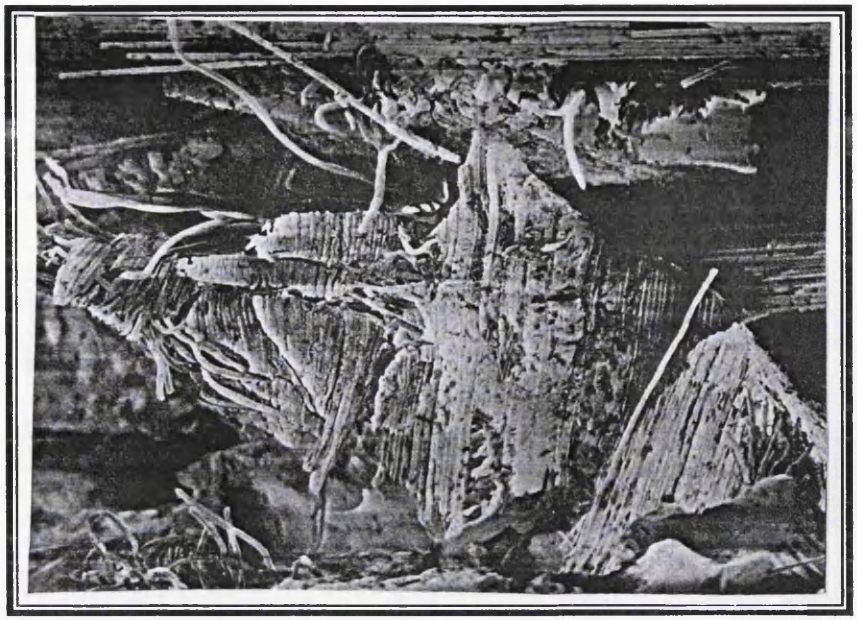

Figure 5.79 : SEM :Delamination observed from modulus degradation test sample. Matrix damage with fibre pull out. Sample $[\pm 45]_4$, R=-1, 48MPa, N_f=3981, 40X.

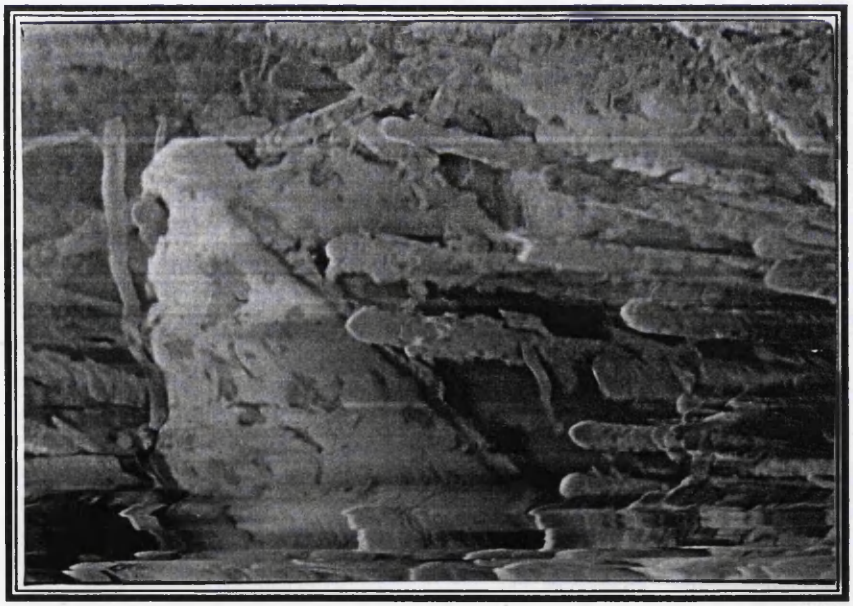

Figure 5.80 : SEM: Modulus degradation fracture surface showing fibre pull out and some matrix still attached to fibre. Sample $[\pm 45]_4$, R=-1, 40 MPa, N_f = 16218, 200X.

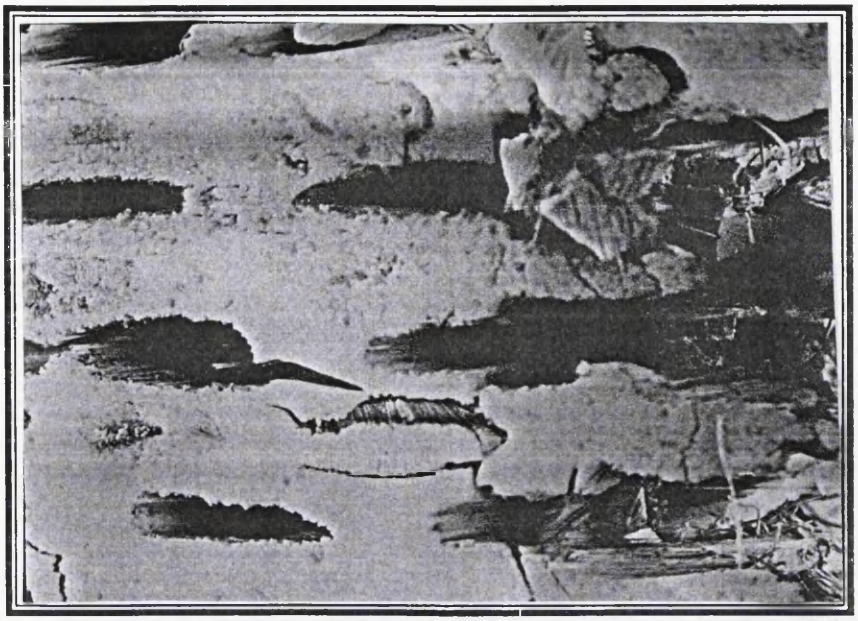

Figure 5.81 : SEM : At the side of the sample showing interfacial damage. Sample $[\pm 45^{o}]_{4,}$ R=0.1, 32MPa, N_f =501187, 20X.

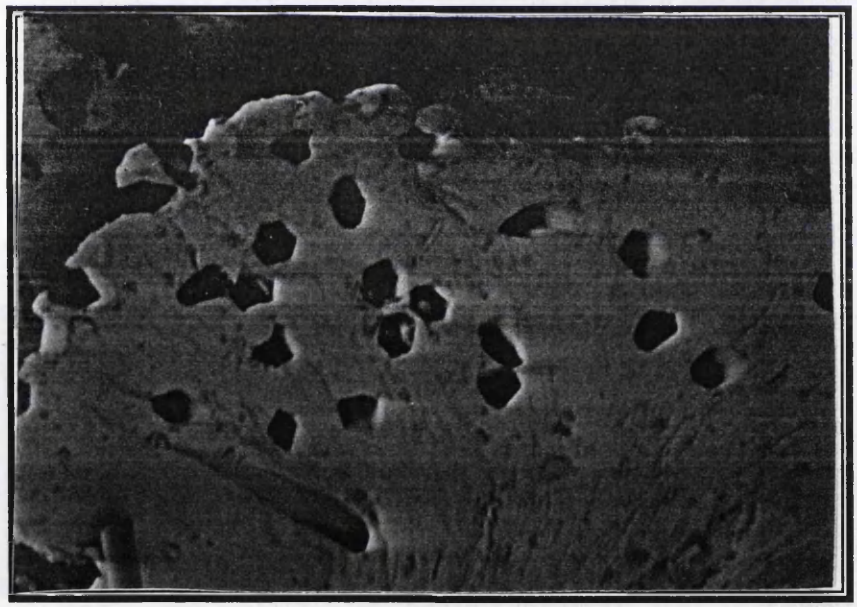

Figure 5.82 : SEM: Holes which fibre pulled out. Sample $[\pm 45^{o}]_{4,}$ R=0.1, 32 MPa, N_f = 501187, 270X.

cracks along the fibre direction at 45° to the stress axis, which propagates, into the delaminations and final fracture. Holes of fibre pull out (Figures 5.82 and 5.83), which occurred extensively during the testing, also accelerated the samples to failure.

From the above observations, the conclusion can be drawn that although the lays up have been tested at two different types of stress ratio, the same damage mechanism occurred in each type of sample. The difference between the two was only the degree of damage where one was more severely damaged than the other.

5.4.7.2 $[90/0]_{2S}$ lay-up.

All $[90/0]_{2S}$ samples failed in the waisted area. Figure 5.84 shows the progression of damage at the waist of a sample, from the beginning to the fractured sample. The type of fracture that occurred for this lay-up is shown in Figure 5.85 - Figure 5.90. Matrix cracking can be seen on the outside plies of the $[90/0]_{2S}$ sample. It occurs in the early part of loading and increases as the cycle number increases.

From visual observation, transverse cracking can be clearly seen on both samples tested at R = -1 and R = 0.1. It was suspected that debonding happened on these samples since the white band can be clearly seen along the fibre. Figure 5.88 and Figure 5.90 reveal that the delamination also occurs in both loading, which was followed by fibre fracture. The first damage observed is matrix cracking in off axis plies. A matrix crack extends completely through the thickness of the cracked ply and follows the general fibre direction of ply across the width of the sample. The small amount of delamination develops because of interlaminar stresses that arise due to the presence of transverse matrix cracks, longitudinal splits and fibre direction cross cracks in the laminate.

For samples tested at R = -1, matrix cracking along the transverse fibres can be seen at 5 to 10% of the cycles to failure for all samples at any stress level. It follows with the appearance of a white band on the sample surface, which can be clearly seen especially

Figure 5.83 : SEM: The image shows a bundle of ±45 fibres pull out with matrix still on them. Sample $[\pm 45]_{4,}$ R=0.1, 32 MPa, N_f =501187, 170X.

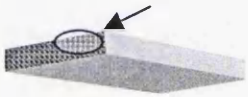

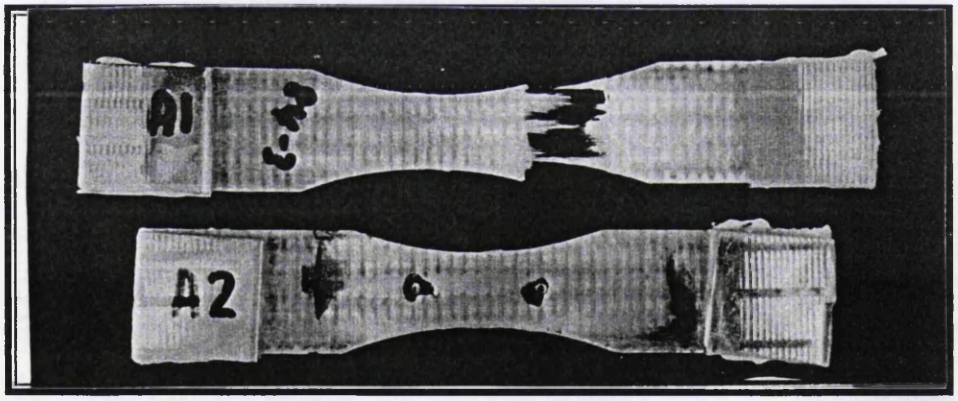

Figure 5.84 : Photographs of two $[90/0]_{2S}$ modulus degradation samples. The samples show the progression of damage at the waist from a sample at the beginning and a fractured sample (top)

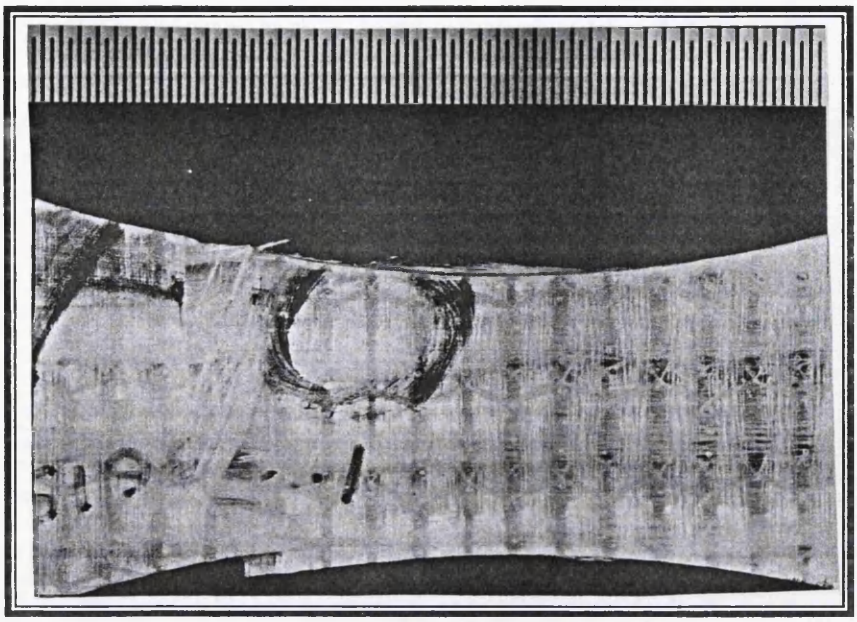

Figure 5.85 : Photograph: damage for the $[90^{o}/0^{o}]_{2S,}$ lay up Fractured by tensile loading.

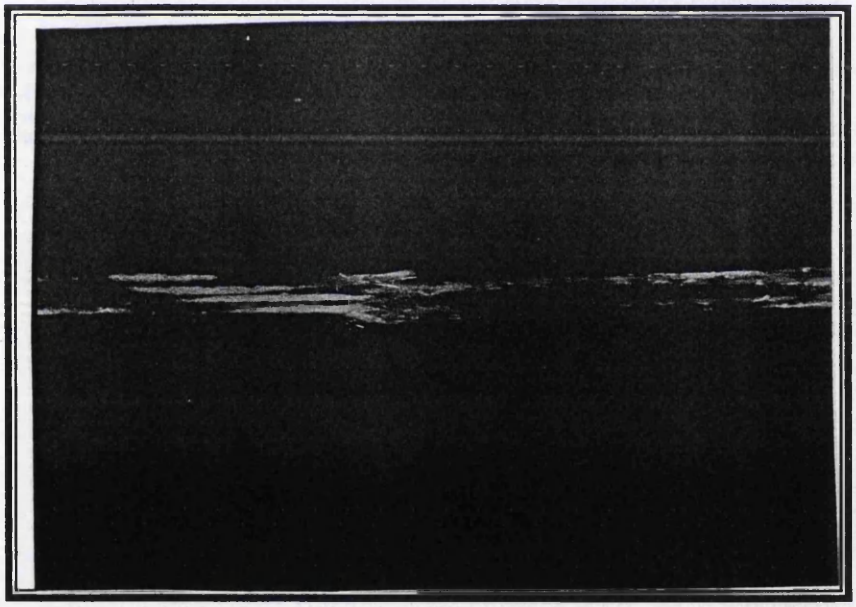

Figure 5.86 : Same sample as in 5.85 from a different view.

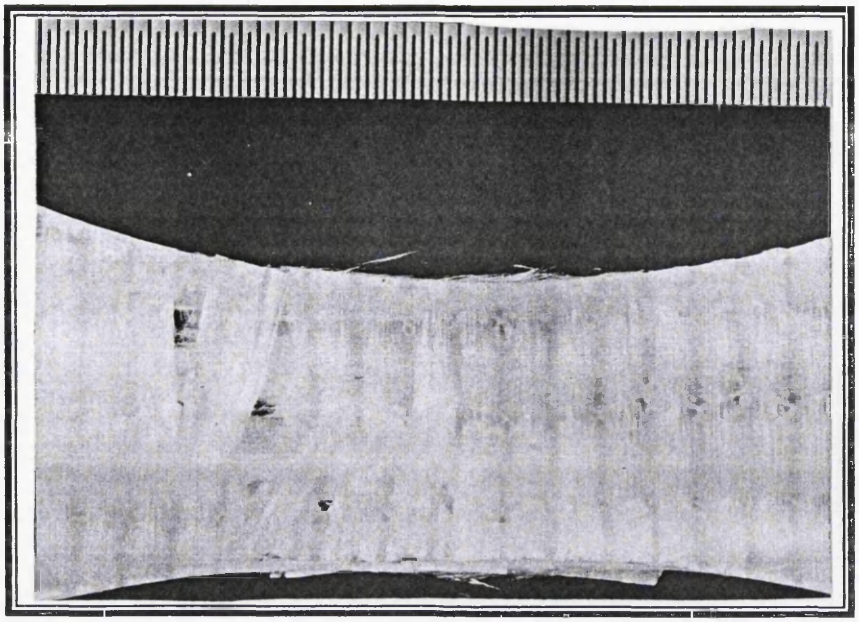

Figure 5.87 : Photograph: Modulus Degradation Test sample $[90/0]_{2S,}$ R=- 1, 120 MPa, N_f = 29040.

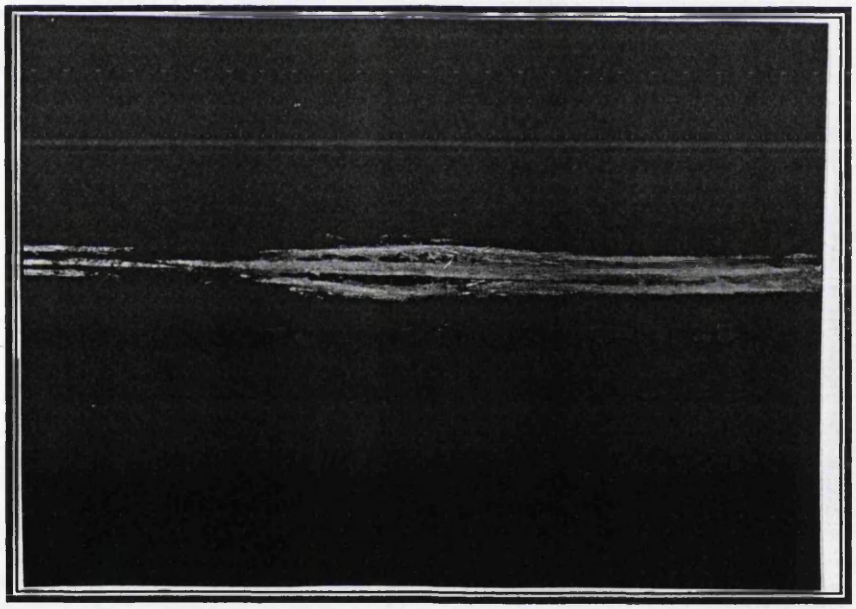

Figure 5.88 : Same sample as in 5.87 from a different view.

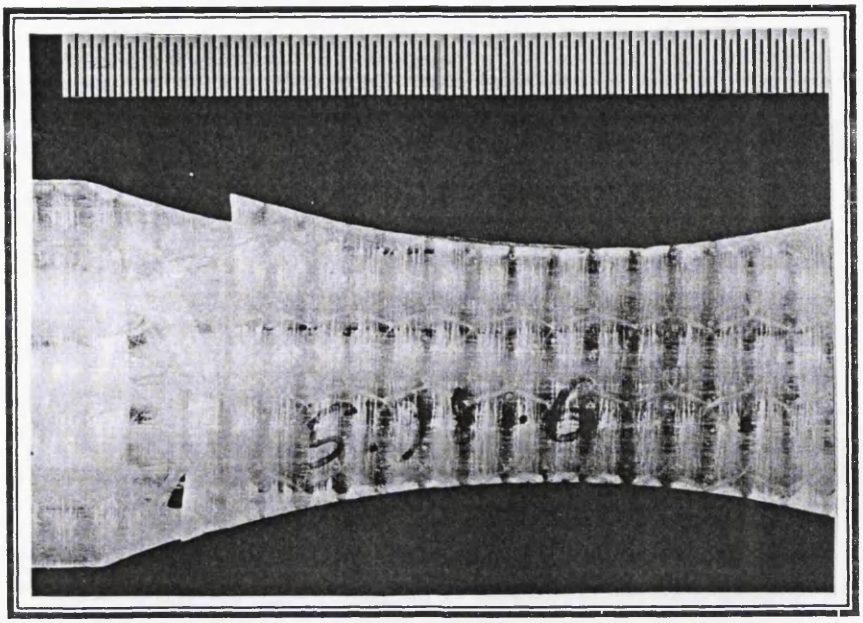

Figure 5.89 : Photograph: Modulus Degradation Test sample $[90/0]_{2S,}$ R=0.1, 220 MPa, $N_f = 10530$.

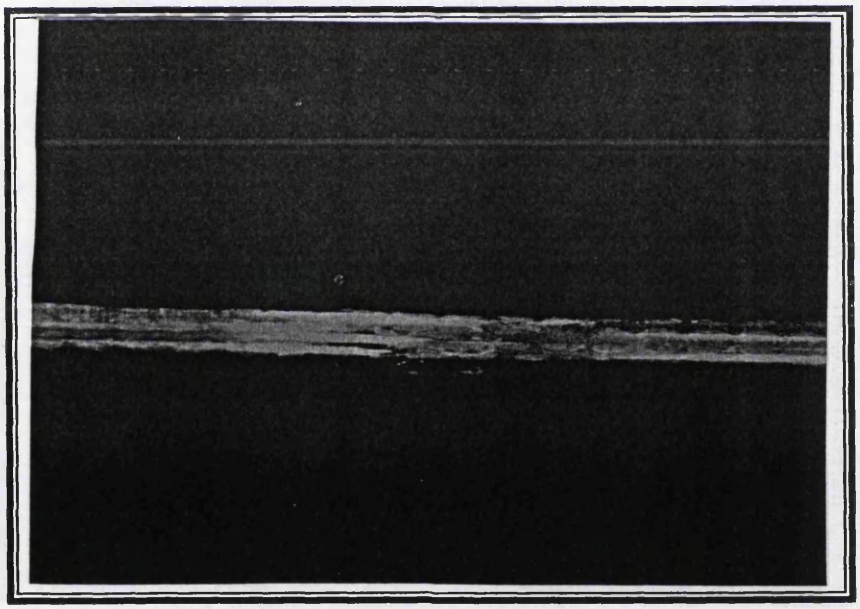

Figure 5.90 : Same sample as in 5.89 from side view.

when it was in tension mode. Debonding also was suspected to have occurred on this sample. The developing damage will degrade the local stiffness, around the waist area and cause microbuckling and formation of kink band, (Figure 5.91). The combined effect of the compressive loading and microbuckling will accelerate damage growth and lead to local failure. Damage mechanisms started with matrix cracking followed by debonding, fibre pull out and fibre break. In can seen from the Figure 5.92 that the fibres pull out with little matrix still attached to them.

SEM observation also reveals that at higher numbers of cycles ripple like layers can be seen in the matrix as shown in Figure 5.93. In the tension-compression loading, transverse cracks propagate, causing some of the 90° fibres to break (Figure 5.94). The continuous tension and compression process will cause the lay-up more damage at the edges of the sample. Figure 5.95 illustrates this point more clearly and shows that delamination occurred with R value equal to -1. The damage continued to accumulate and it appears that these stiffness reducing mechanisms progress until a critical point is reached, at which point specimen failure occurs. The damage on the fractured surface can be seen in Figure 5.96 and Figure 5.97.

Similar damage mechanisms occurred in tension-tension loading of the $[90/0]_{2S}$ lay-up. The only difference in damage mechanisms was the microbuckling effect which only occurred on lay-ups tested at R = -1. The most clear damage occurring in the test was off axis internal and external matrix cracking which can be observed by visual observation as seen in Figure 5.98 and Figure 5.99. As mentioned before in section 5.3.3.1, the tension-tension loading with lower stress will give more severe damage to the fractured surface. This damage accumulates through stage 3 and the damage will reduce the modulus until a critical point is reached, at which the sample will break into two halves.

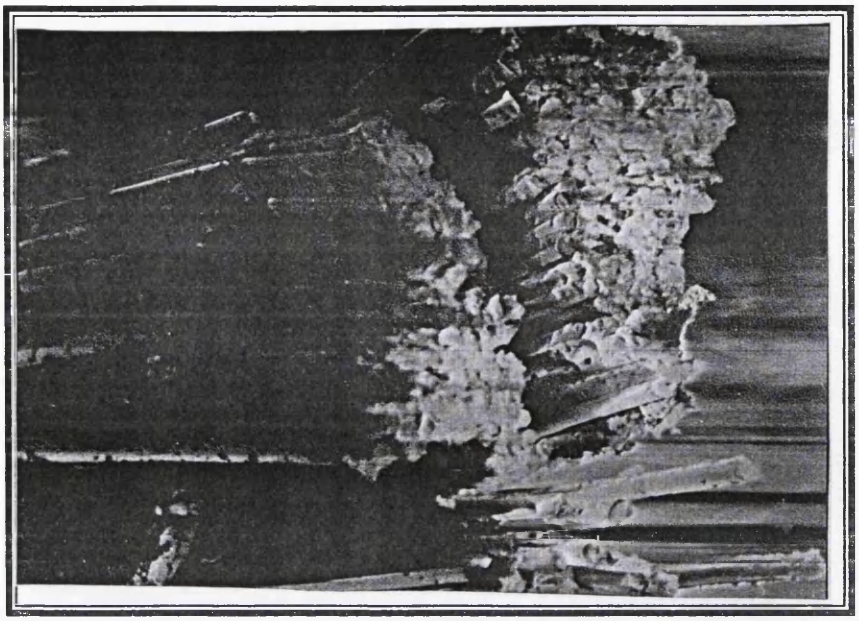

Figure 5.91 : SEM: The image shows microbuckling of fibres and formation of a kink band. Sample $[90/0]_{2S,}$ R=-1, 115 MPa, N_f =199526, 120X.

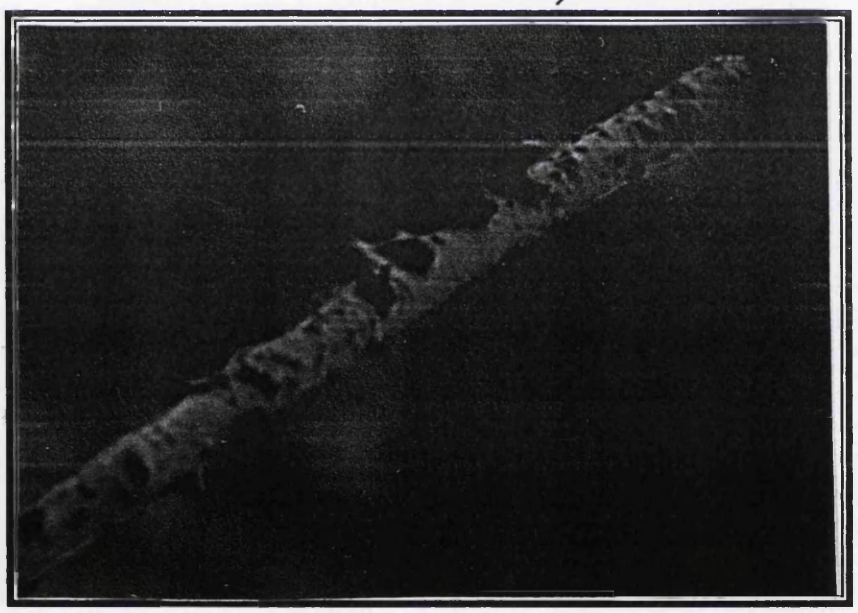

Figure 5.92 : SEM: Single fibre with matrix still on it. Sample $[90/0]_{2S,}$ R=-1, 115 MPa, N_f = 199526, 270X.

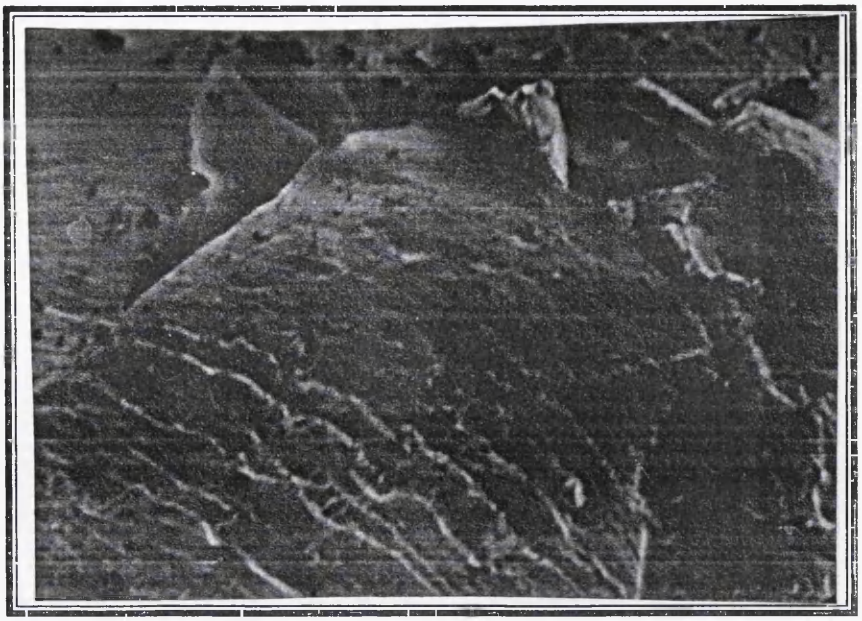

Figure 5.93 : SEM: The image shows a matrix like a ripple.
Sample $[90/0]_{2S,}$ R=-1, 115 MPa, N_f =199526, 300X.

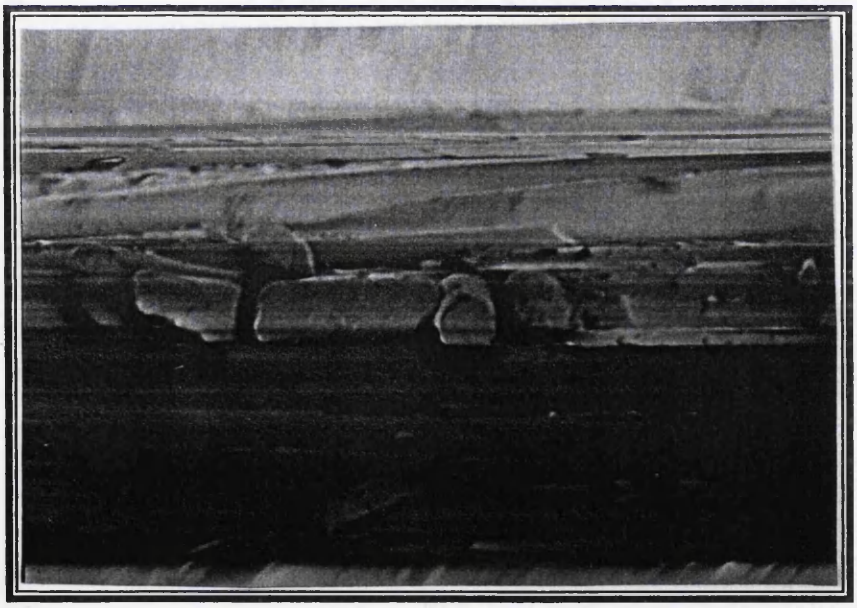

Figure 5.94 : SEM: Broken 90° fibre. Sample $[90/0]_{2S,}$ R=-1,
115 MPa, N_f = 199526, 330X.

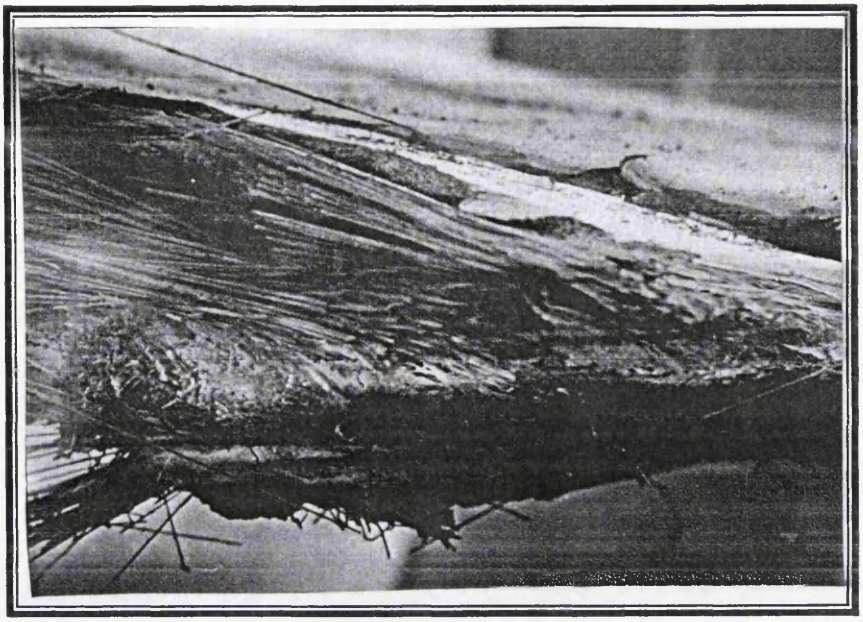

Figure 5.95 : SEM: The image shows a fracture surface with delamination damage.
Sample $[90/0]_{2S,}$ R=-1, 140 MPa, N_f =6309, 15X.

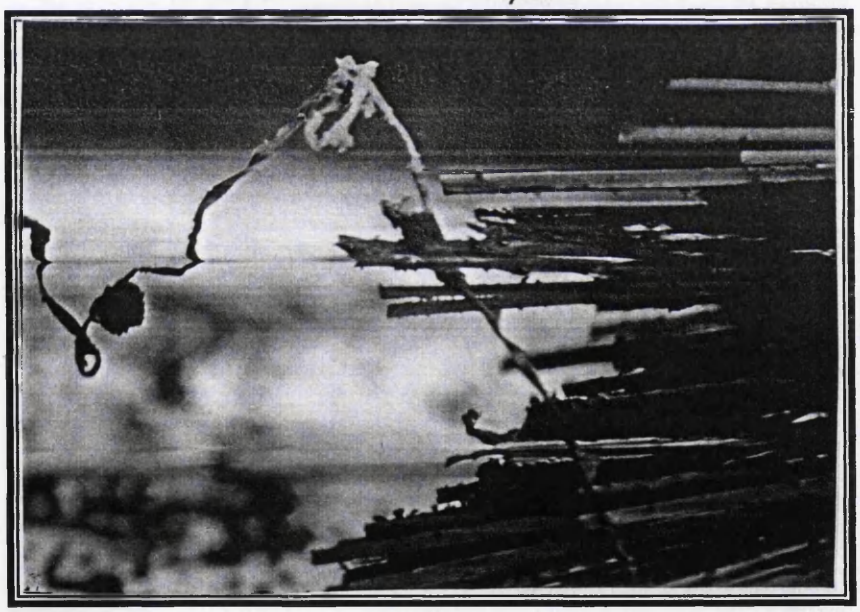

Figure 5.96 : SEM: The image shows fibre pull out at fracture surface.
Sample $[90/0]_{2S,}$ R=-1, 140 MPa, N_f =6309, 130X

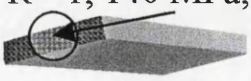

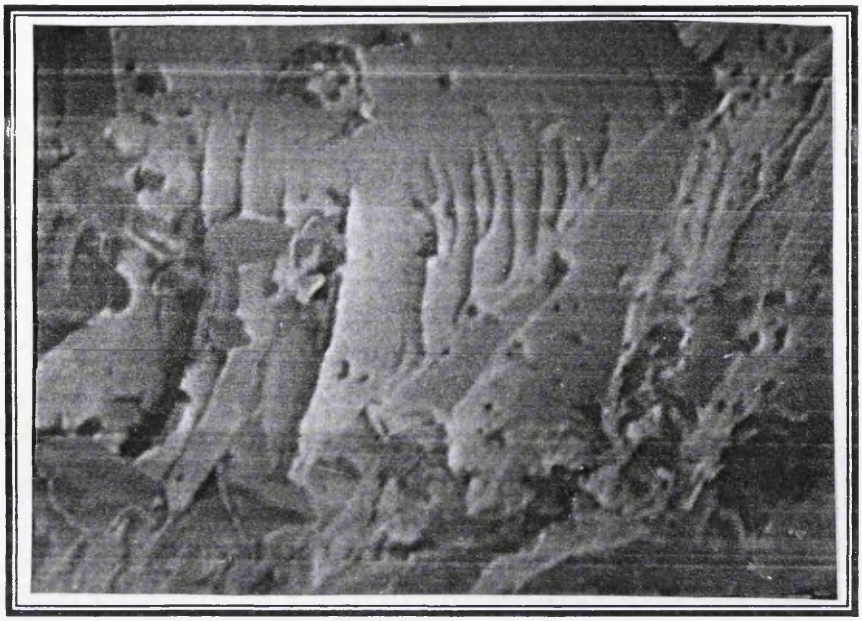

Figure 5.97 : SEM: The image shows the matrix with the effect of fibre pulled out at fractured surface.
Sample $[90/0]_{2S,}$ R=-1, 140 MPa, N_f = 6309, 400X.

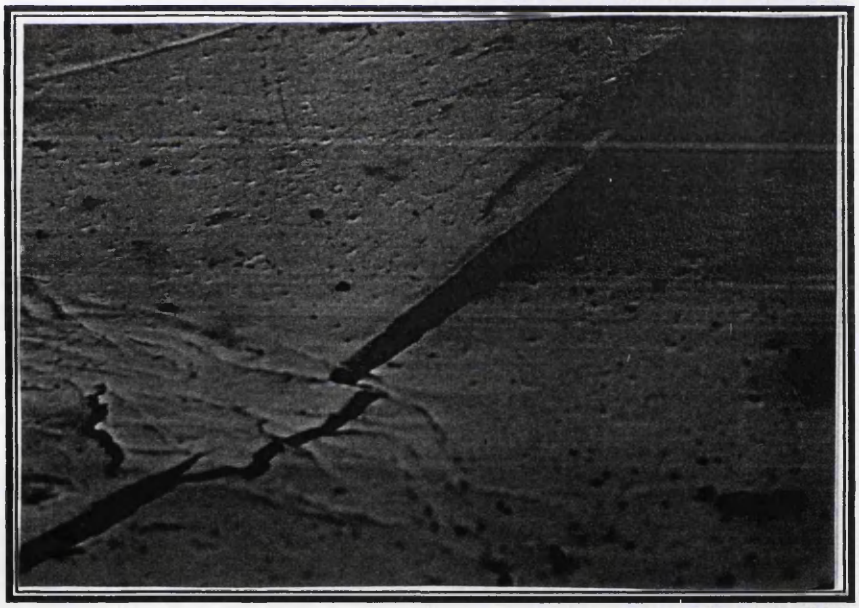

Figure 5.98 : SEM: External matrix cracking observed at the side of the sample which is parallel to fibre direction.
Sample [90/0]2S, 225 MPa, Nf=5754, 55X.

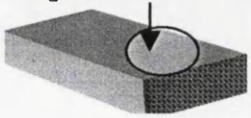

5.4.8 Damage At Final Failure

5.4.8.1 $[90/0]_{2S}$ lay-up, R=0.1

Larger modulus reduction is associated with higher maximum stress for R=0.1 However samples with most damage are those that showed least modulus reduction during the progression of fatigue. Echtermeyer et al (1995) reported that at low cycles to failure (high stress) the fatigue matrix has more influence, and at high cycles (low stress) fibres dominate the fatigue properties.

At low stress the matrix stays intact longer causing the fibre strain to remain longer at the initial level before finally the modulus drops to the critical fatigue modulus. However, the fibre strains do not increase anymore, therefore the fibres experience smaller strain increases over their lifetime. At high applied stress the matrix fails early therefore the fibre strain increases continuously causing high stress concentration around the fibre bundles. This will transfer high stresses into the fibres and ultimately reduce the fatigue life. Dharan (1975) noted that the applied stress level also affected the damage mechanism of the samples. High stresses cause matrix cracking and large numbers of fibre failures whilst low stresses produce matrix cracking and random fibre breaks followed by delamination and further increase in fibre breakage.

Optical micrographs (Figures 5.40 and 5.41) of fracture surfaces for the sample clearly illustrate this hypothesis.

5.4.8.2 $[90/0]_{2S}$ lay-up, R= -1

The final damage surfaces of sample at R=-1, for both low maximum stress (115MPa) and high maximum stress (140MPa) show little difference. This is also evident as the normalised modulus cycle curves for both low and high maximum stress coincide.

The applied stress levels are therefore sufficient to initiate similar damage mechanisms for the lay-up.

Comparing these final fracture surfaces for R=0.1 (maximum stress 220MPa) and R=-1, (maximum stress 120MPa) (Figure 5.88 and Figure 5.90), clearly indicates more extensive damages occur in sample with R = -1, although the maximum stress is much lower. It seems that all the mechanisms of damage initiation and growth for R = 0.1 also occurred at R = -1, but the compression-tension mode of R = -1 contributed to the severity of the damage by the existence of microbuckling, kink bands and the formation of an abrasive region (Figure 5.100) [Purslow and Potter (1984)]. In one study [Dillion and Buggy (1995)], the effect of the compressive load during the fatigue test has the abraded region covered with debris, also to be the site of compressive crack.

5.4.8.3 [± 45] lay-up, R=0.1

Many investigators [Dharan (1975), Reifsnider and Talug (1980), Hull (1981), Zhuo (1995) and Dyer (1996) have studied the effect of tension-tension mode on the [±45] lay-up. In the absence of compressive load, shear stress plays the dominant role. Matrix cracks initiate in the resin-rich region propagates along the fibre directions, and ultimately causes failure of fibre bundles at the end of its lifetime.

Delamination is also noted to occur where these cracks meet the ply interface and the interlaminar tensile stress separated the plies. This agreed well with Reifsnider et al (1983). Dyer (1996) also noted that the crack would halt upon reaching the specimen edge thus localisation of damage is evident at the central region of the waist. Cracking along the fibre interface resulted in longitudinal splitting which reduced the specimen stiffness until a critical point was reached at which the specimen failed.

5.4.8.4 [± 45] lay-up, R = -1

Referring to the modulus degradation curve (Figure 5.63), it may be divided into two main stages. The modulus degrades gradually in the first stage (85%) of the lifetime before falling rapidly in the last 15% of its lifetime (second stage). During the first stage damage in the sample is manifested by the development of a whitening region at the waist section (Figure 5.73). Fujii and Maekawa (1981) noted that this whitening is due to the initiation of cracks in the matrix as they propagates along the fibre causing splitting. High interlaminar stresses are involved in this situation [Lagace and Narendra (1992)]

Delamination is also observed to initiate at the edge (Figure 5.79) in the presence of matrix cracking and is due to a free edge effect [Fish and O'Brien (1992)]. As the cycling progresses the damage becomes more extensive causing interfacial failure (peeling away of matrix from fibre) and even causing fibre breakage (Figure 5.80).The damage in the [± 45] lay-up can be generalised as damage dominated by the matrix in the form of delamination and cracking.

5.5 Fatigue Life Prediction

Data obtained from modulus degradation testing were substituted into the life prediction model proposed by Mahfuz et al. (2000) to evaluate the fit of the model to experimental data from this study.

In this case, normalised fatigue modulus values, $F(n)/F_0$ were determined for $[90/0]_{2S}$ and $[\pm 45]_4$ polyurethane acrylate (as seen in Figure 5.60 and Figure 5.61 respectively) at two cycle number (at 30% and 90% of the cycles to failure). The values of C and B were calculated by substituting these values into the equations below (Equations 2.28 and 2.32). The values determined for B and C are shown in Table 5.7a and Table 5.7b. The variations of B and C with r (normalised stress level) are shown in Figures 5.101, 5.102 and Figures 5.103, 5.104 respectively.

$$C = \frac{\ln\left(\dfrac{\dfrac{F(n_2)}{F_0}-1}{\dfrac{F(n_1)}{F_0}-1}\right)}{\ln\left(\dfrac{\dfrac{n_2}{n_f}}{\dfrac{n_1}{n_f}}\right)}$$

from Equation (2.28)

$$B = \frac{{n_f}^C\left[\left(\dfrac{n_2}{n_f}\right)^C - \left(\dfrac{n_1}{n_f}\right)^C\right]}{\dfrac{F(n_1)}{F_0} - \dfrac{F(n_2)}{F_0}}$$

from Equation (2.32)

Table 5.7a: The values (from experimental data $[90/0]_{2S}$) used to find the values of B and C

Stress [MPa]	$\frac{n_1}{n_f}$	$\frac{n_2}{n_f}$	$\frac{F(n_1)}{F_0}$	$\frac{F(n_2)}{F_0}$	B	C
160	0.3	0.90	0.98	0.94	7945572	1.0331
170	0.3	0.90	0.80	0.70	297.77	0.3691
225	0.3	0.90	0.60	0.50	11.37	0.2031

Table 5.7b: The values (from experimental data $[\pm 45]_4$) used to find the values of B and C

Stress [MPa]	$\frac{n_1}{n_f}$	$\frac{n_2}{n_f}$	$\frac{F(n_1)}{F_0}$	$\frac{F(n_2)}{F_0}$	B	C
32	0.3	0.90	0.42	0.32	9.86	0.1448
35	0.3	0.90	0.30	0.17	6.62	0.1551
50	0.3	0.90	0.38	0.23	6.05	0.1972

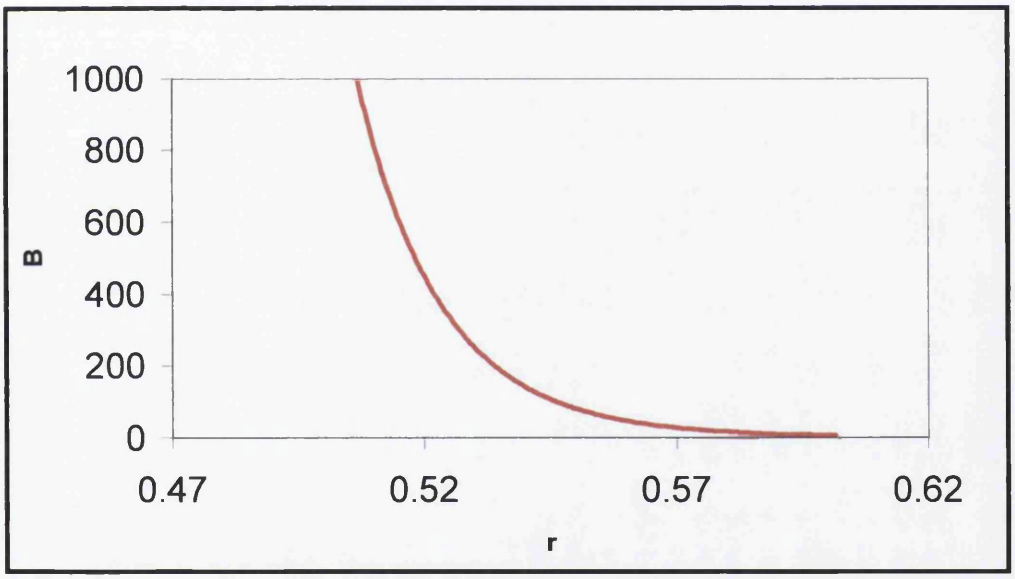

Figure 5.101: The relationship between B and r for the $[90/0]_{2s}$ data

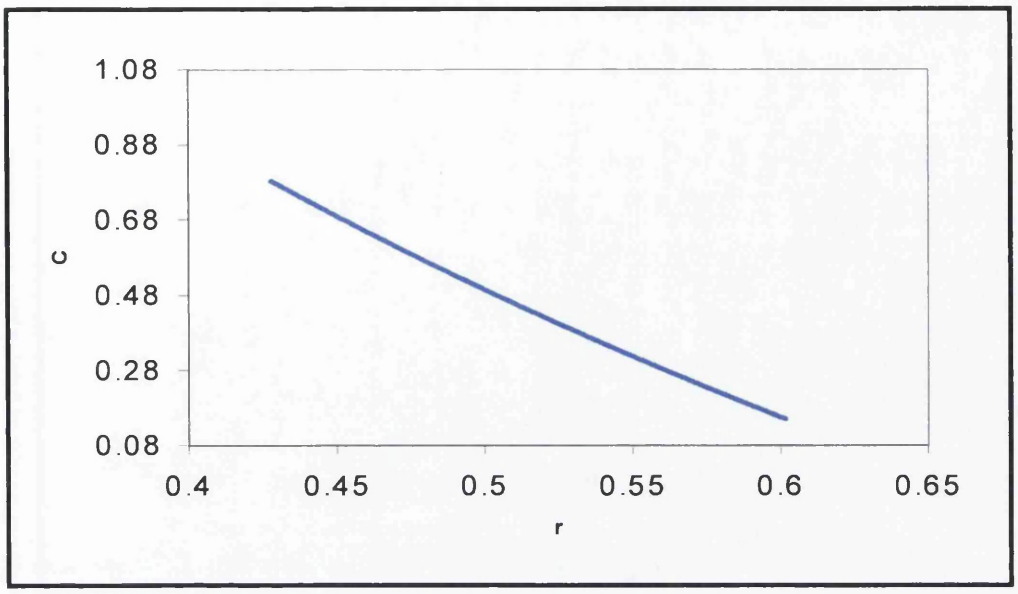

Figure 5.102: The relationship between C and r for the $[90/0]_{2s}$ data

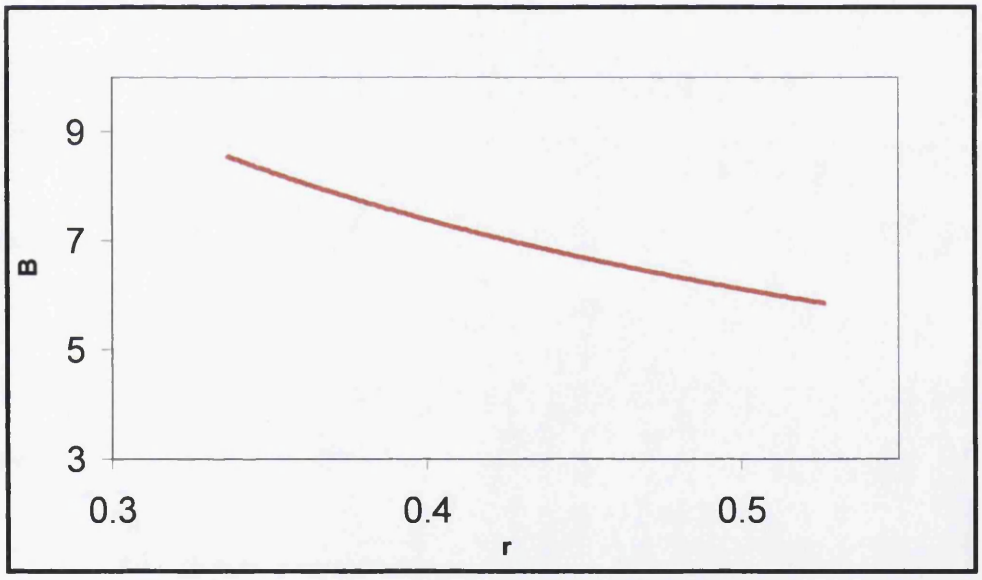

Figure 5.103: The relationship between B and r for the $[\pm 45]_4$ data

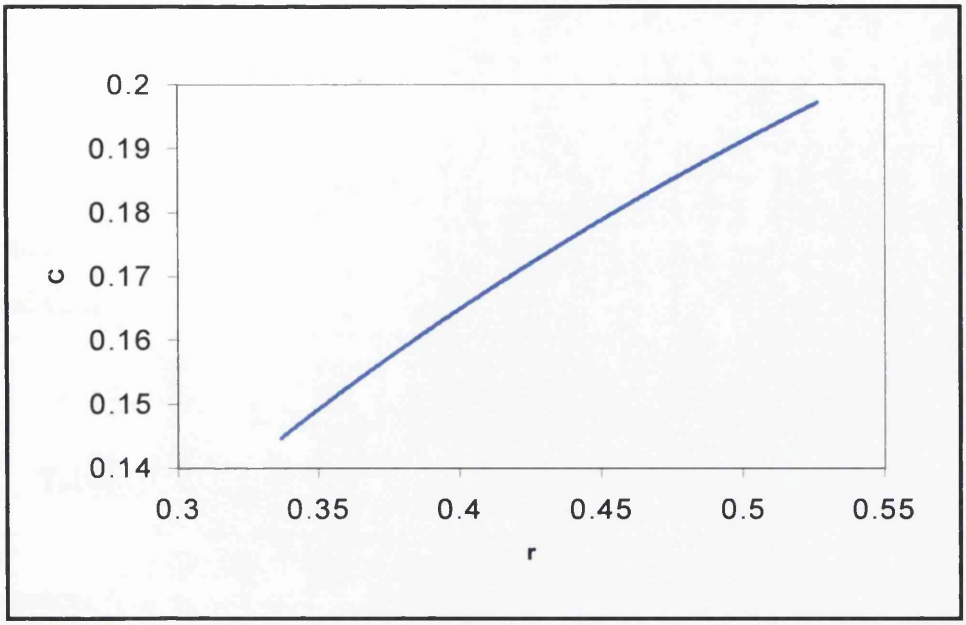

Figure 5.104: The relationship between C and r for the $[\pm 45]_4$ data

From the above figures, the equations relating B and C to r for each lay-up were found by fitting appropriate functions to the data points. These equations are shown below and they enable the values of B and C to be obtained for other stress levels.

For $[90/0]_{2S}$,

$$B = 8\text{x}10^{-7}\, r^{-30.831}$$

$$C = -1.8624 \ln(r) - 0.797$$

And for $[\pm 45]_4$,

$$B = 3.3724\, r^{-0.8545}$$

$$C = 0.1176 \ln(r) + 0.2726$$

Values of B and C appropriate to the stress level (r) may then be used in Equation 2.21,

$$N_f = [\, B\,(1 - r)\,]^{\frac{1}{C}} \qquad \textit{from Equation (2.21)}$$

to predict the fatigue life at any stress level. Comparisons between the predicted and experimental values are shown in Table 5.8a and Table 5.8b.

Table 5.8a: A comparison between the experimental and predicted fatigue lives after fitting curves for $[90/0]_{2S}$

Stress [MPa]	Experimental Log N_f	Predicted log N_f using B and C curves and Equation 2.21
130	4.94	6.72
140	4.73	6.63
150	4.40	6.53
160	4.24	6.41
170	3.59	6.25
180	3.55	6.03
190	3.27	5.74
200	3.19	5.29
210	2.87	4.58
220	2.68	3.26

Table 5.8b: A comparison between the experimental and predicted fatigue lives after fitting curves for $[\pm 45]_4$

Stress [MPa]	Experimental Log N_f	Predicted log N_f using B and C curves and Equation 2.21
22	4.63	9.51
23	5.15	8.83
24	4.58	8.23
25	3.63	7.71
26	3.17	7.24
28	3.59	6.43
29	4.01	6.09
30	2.80	5.77
32	-	5.21
34	1.04	4.72
35	1.00	4.50

S-N curves for both experimental and predicted data for $[90/0]_{2S}$ and $[\pm 45]_4$ were plotted in Figure 5.105a and Figure 5.105b respectively. It can be observed that the predicted life time model does not fit very well but shows the trend. The graphs show that there are differences between the two results. The predicted life time results show much longer cycle numbers compared with the experimental results. This may be because the model proposed by Mahfuz et al. related the number of cycles to failure to applied stress level and the thickness of the laminates.

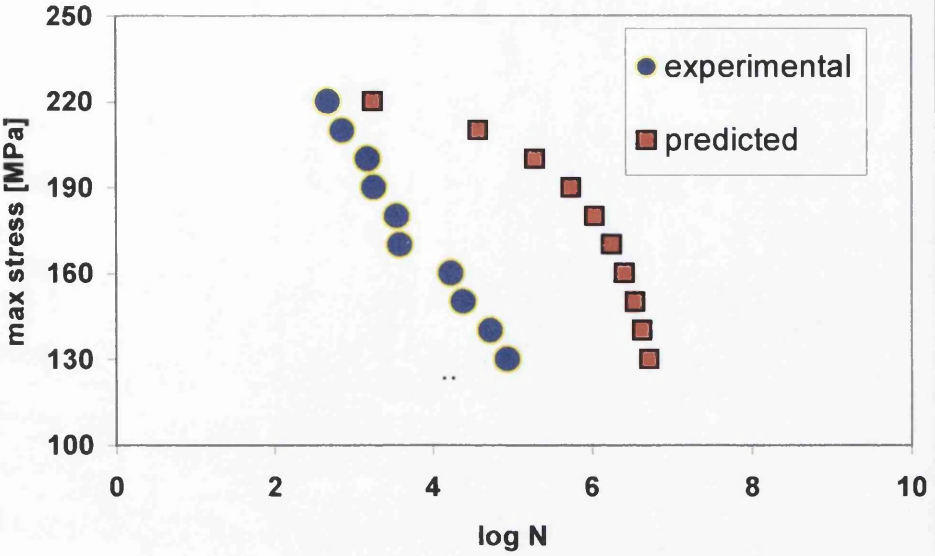

Figure 5.105a: S-N curves for experimental and predicted life for $[90/0]_{2S}$

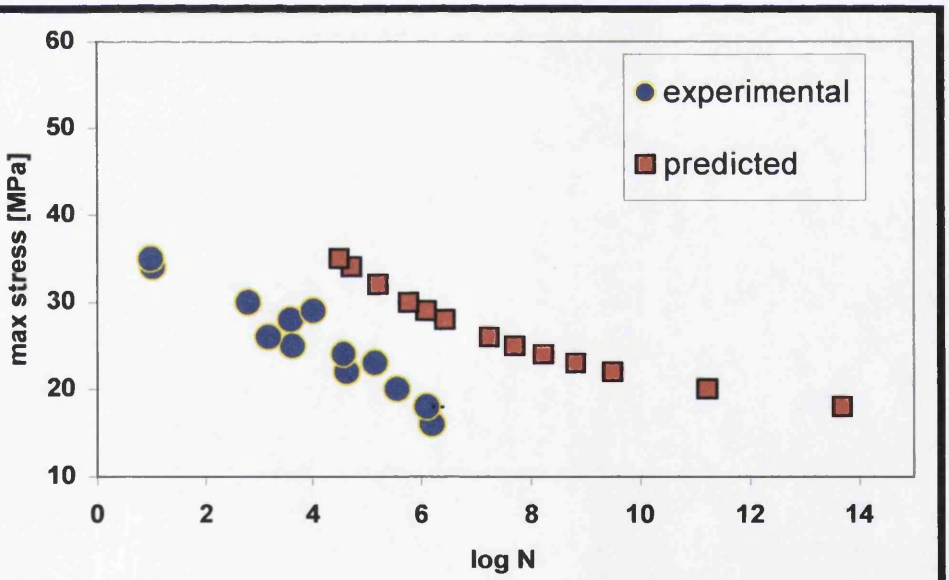

Figure 5.105b: S-N curves for experimental and predicted life for $[+/-45]_4$

This model was successfully applied by Mahfuz et al. to laminates with thicknesses of 12.7mm to 18.03 mm. The thickness of the laminate also plays an important role due to different dominating mechanisms involved between thin and thick laminates. The data collected for experimental and predicted lifetimes in this study suggest that the model proposed by Mahfuz et al. cannot be used directly in this experimental work. It may need some modification to be useful for this glass/polyurethane acrylate resin composite. Although various other algebraic functions were tried for the curve fitting of B against r and C against r none could be found that gave any better fit than those shown. However, it is difficult to make any firm conclusions concerning the validity of the model, due to the relatively small amount of experimental data being used to fit the model in this study. With only three points on the B against r and C against r graphs, it is difficult to have high confidence in the fitted curves. More data are required in order to provide a more rigorous test of the model.

CHAPTER

6

CONCLUSIONS

6.1 Materials Characterisation and General Fatigue Properties

From studies of the static tensile behaviour and the fatigue life performance of polyester, polyurethane vinyl ester and polyurethane acrylate resins, reinforced with Ulticloth ($[0/90]_{2S}$ stitch bonded fibres), Biaxial Ulticloth ($[\pm 45]_4$ stitch bonded fibres) and woven roving ($[0/90]_{2S}$) glass fibres, the following conclusions can be drawn:

Factors affecting the ultimate tensile strength, UTS:

- The $[\pm 45]_{2S}$ (Biaxial Ulticloth) lay ups gave the lowest values for the UTS and modulus. This was as expected since for these lay ups there were no fibres parallel to the tensile stress direction whereas the laminates based on Ulticloth and woven rovings contained a high proportion of fibres along the tensile direction.
- For the $[0/90]_{2S}$ lay ups, the Ulticloth had slightly superior UTS to the woven rovings reinforced samples, probably due to the higher proportion of fibres parallel to the tensile axis.

- For the $[0/90]_{2S}$ lay ups, the polyester and polyurethane acrylate resins gave similar UTS values, and were significantly superior in strength to the equivalent samples based on polyurethane vinyl ester. On the other hand, for the $[\pm 45]_{2S}$ lay ups the polyurethane vinyl ester resin gave the highest UTS and the polyester was significantly lower than the other two resins.

Factors affecting the fatigue life;

- Although the higher proportion of axial fibres for the Ulticloth gave rise to higher UTS than the woven rovings, there was much less difference in their fatigue performance. This may mean that the woven roving arrangement of fibres generally has slightly superior fatigue resistance to stitch bonded fibres when similar numbers of fibres are parallel to the axis.
- Just as the UTS values of $[\pm 45]_4$ lay ups with polyurethane acrylate and polyurethane vinyl ester are higher than those with the polyester resin, these two resins also provide superior fatigue life to samples based on the polyester resin. Studies indicate that the higher toughness values measured for these two resins inhibit matrix cracking during fatigue loading, hence contributing to the higher fatigue strength.

Damage mechanism;

From the SEM analysis of damage mechanisms in $[0/90]_{2S}$ polyester and $[\pm 45]_4$ polyurethane acrylate samples, the following conclusions could be drawn:

- In the $[0/90]_{2S}$ polyester samples, damage was initiated by transverse cracking followed by fibre-matrix debonding in plies containing transverse fibres, which is consistent with previous reports.
- In the $[\pm 45]_4$ polyurethane acrylate samples, interfacial damage occurred before final failure by fibre pull-out from the matrix.

6.2 The Effects of Environment on the Fatigue Process

Studies of polyurethane acrylate reinforced by $[90/0]_{2S}$ Ulticloth and $[\pm 45]_4$ Biaxial Ulticloth glass fibres composites and subjected to fatigue loading in air, distilled water and sea water at R-values of 0.1 and –1 have shown the following:

- The $[90/0]_{2S}$ lay ups are very much more sensitive to compression loading than the $[\pm 45]_4$ lay ups. Thus, for the $[90/0]_{2S}$ samples, maximum stress levels for similar lifetimes at R = -1 are less than half those of R = 0.1 (i.e. the stress range is more of a guide to fatigue lifetime than the maximum stress) On the other hand, with $[\pm 45]_4$ samples, plots of maximum stress against log (cycles to failure) for R = 0.1 and R = -1 almost superimpose.
- The effects of distilled water and sea water on the fatigue lifetimes of polyurethane acrylate samples with $[\pm 45]_4$ lay ups is negligible when R = 0.1, although at R = -1 (i.e. tension compression cycling) a small effect is evident.
- In contrast, for $[90/0]_{2S}$ lay ups, the environment plays a significant role. Although there are not significant differences between the effects of distilled water and sea water, both these environments significantly reduce the fatigue lifetimes in both tension-tension fatigue (R = 0.1) and tension-compression fatigue (R = -1)

Damage mechanism;

$[90/0]_{2S}$ lay ups

- More severe damage occurs for specimens tested at low stress-high cycles than at high stress-low cycles to failure.
- At R = -1, damage mechanisms are more complex than at R = 0.1. In addition to delamination and buckling of bundles, transverse pull-out is evident as a main failure mechanism.

$[\pm 45]_4$ lay ups

- Fibre pull-out was the dominant mechanism at an R ratio of 0.1 in all environments. At R = -1, matrix cracking along the fibre direction dominates the damage mechanisms. Damage to specimens was generally more severe than at R = 0.1

6.3 Modulus Degradation

Studies conducted on waisted samples of polyurethane acrylate with $[90/0]_{2S}$ and $[\pm 45]_4$ lay-ups and at R values of 0.1 and –1 showed that the way in which the modulus changed with fatigue cycling was clearly dependent on the fibre lay-up. The following conclusions could be drawn:

$[90/0]_{2S}$ lay up

- At R=0.1 modulus degradation curves are characterised by three stages, namely an initial reduction, followed by a region of very gradual reduction between ~10% and ~90% of lifetime and finally a rapid reduction to failure in the last 10% of lifetime. It was also evident that the level of the initial reduction increased with increasing stress levels (shorter times to failure). At the lowest stress level there was very little modulus degradation until close to the final failure. Results at a stress ratio R of -1 showed much smaller modulus degradations before failure at all of the stress levels tested (the absolute values of the stress levels being significantly lower than those in the R = 0.1 tests).

$[\pm 45]_4$ lay-up

- For $[\pm 45]_4$ lay ups, the modulus degradation curves show similar trends for all the stress levels and at both R-ratios. Modulus values fall most rapidly early in the fatigue cycling and continue falling through the majority of the cycling (albeit at a reducing rate) and then the rate increases when nearing final failure.

6.4 Fatigue Life Prediction

- Fatigue life prediction models, as proposed by Mahfuz et al. (2000), failed to fit the results in the present studies. It is thought that they would need further modification to take into account effects such as the free edges for thin specimens.

6.5 Future Works

It has been shown that the effects of distilled water and sea water on the fatigue performance of polyurethane acrylate reinforced by Ulticloth and Biaxial Ulticloth glass fibres can be detrimental. If this material is to be successfully applied in marine applications, then other factors such as the effect of temperature and other hostile environments need to be investigated.

A more comprehensive study should be made of the effect of fibre orientations on the fatigue life and modulus degradation. Although covered to some extend in this work, it would be valuable to include a wider range of fibres orientation along the loading direction, particularly considering some more versatile lay ups such as quasi-isotropic laminates.

Fractographic analysis has been shown to be very useful in helping further understanding of the fatigue processes. Further work in this area would be most beneficial, in particular, monitoring the fracture morphology throughout the entire modulus degradation curve should be very useful in establishing the details of the damage progression and failure mechanisms.

A modified fatigue life prediction model using the present formulation requires further work. The proposed formulation requires the determination of two materials constants that vary with the stress levels. These factors need to be determined empirically for a larger spectrum of stress levels and at various specimen thicknesses, in order to provide more confidence in the model.

CHAPTER

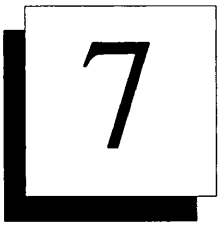

REFERENCES

Bakis C.E. and Stinchcomb W.W., "Response of Thick, Notched Laminates Subjected to Tension-Compression Cyclic Loads", Composite Materials: Fatigue and Fracture, ASTM STP 907, H.T. Hahn. Ed., American Society for Testing and Materials, Philadelphia, (1986),314-334.

Bakis C.E., Simond R.A., Vick L.W. and Stinchcomb W.W., "Matrix Toughness, Long-term Behaviour and Damage Tolerance of Notched Graphite Fiber Reinforced Composite Materials", Fiber Reinforced Composite Materials, Composites Material: Testing and Design, (1990)349-370.

Berenson M.L. and Levine D.M, "Basic Business Statistics: Concept and Applications", second edition, Prentice Hall, 1983,492-512

Bhagwan D.A and Broutman L.J, "Analysis and Performance of Fiber Composite, 2 Edition, John Wiley and Sons, Inc.,(1990).

Botsis J. and Zhao D., "Fatigue Fracture Process in a Model Composite", Composites 28A(1997)657-666.

Boudreau R.J. " Proceedings of 37th. SPI Conference", 2-A(1982).

Broutman L.J and Sohu S., "Progressive Damage of A Glass Reinforced Plastic During Fatigue", Presented at the 24th. Annual Reinforced Plastics Composites Industry Conference Society of Plastic Industry, Sec. 11-b,(1969).

Brown W.F. Jr. and Srawley J.E., "Plane Strain Crack Toughness Testing of High Strength metallic Materials", ASTM STP 140, American Society for Testing and Materials, Phliladelphia (1966)

Buxton A. and Baillie C., " A Study of The influence of the Environment of the Measurement of Interfacial Properties of Carbon Fibre/Epoxy Resin Composites", Composite, Volume 25,no7,(1994)607.

Camponeschi, E.T., and Stinchcomb, W.W., Composite Materials:Testing and Design, Sixth Conference, ASTM STP 787, American Society for Testing and Materials, Phliladelphia (1982)

Cervenka A., Polymer Composites, 9(1988)263.

Charewicz A. and Daniel I.M., "Composite Materials: Fatigue and Fracture", ASTM STP 907, American Society for Testing and Materials, Philadelphia, PA, (1986)274-297.

Chester R.J. and Baker A.A., "Environmental Durability of F/A-18 graphite/Epoxy Composite", Polymer and Composites, (1996)315-323.

Chiou P. and Bradley W.L., "Effects of Seawater Absorption on Fatigue Crack Development in Carbon/Epoxy EDT Specimens", Composites, 26(1995)869-876.

Cox H.L. , J. Apply Physics, 3(1952)72.

Curtis D.C., Davies M., Moore D.R., Slater B., "Composite Materials: Fatigue and Fracture (3rd. vol), ASTM STP 1110, T.K. O'Brien, Ed, American Society for Testing and Materials, Philadelphia, (1991)581-595.

David A.R. and Jamie C.H., "Proceeding SAE Fatigue Conference", Fatigue Considerations For FRP Composites, (1982) 237-247.

Demonet C.M., "Interaction of Moisture with Resin Matrix Composites", 21st. Int. SAMPE tech. Conf., Atlantic City, N.J., (1989)231-238.

Denial I.M. and Ishai O., "Engineering Mechanics of Composite Materials", Oxford Uni. Press, (1994).

Dharan C.K.H., "Fatigue Failure Mechanisms in a Unidirectionally Reinforced Composite Material," ASTM STP 569, American Society for Testing and Materials, Philadelphia, pp 171-188 (1975)

Dillon G and Buggy M., "Damage Development Dduring Flexural Fatigue of Carbon Fibre Reinforced PEEK Laminates," Composites,Volume 26,no 5,(1995), 303-308

Donat R.C., J. Composite Materials, 4(1970)124.

Dyer K.P., "Fatigue of Composite Materials", PhD Thesis, University of Wales, Swansea, (1996).

Echtermeyer A.T, Engh B. and Buene L., "Lifetime and Young's Modulus Change of Glass/Phenolics and Glass/Polyester Composites under fatigue", 26(1995)10-16.

Echtermeyer A.T., Buene L., Engh B. and Sund O.E., "8th. Conf. On Composite Materials", ICCM VIII, Honolulu, Hawaii, (1991)38.

Ellis B. and Found M.S., "The Effects of Water Absorption on a Polyester/Chopped Strand Mat Laminate", Composites vol. 14, 3(1983)237-243.

Emadipour H., Chiang P. and Koenig J.L., Res. Mech, 5(1982)165.

Evans W.J., Isaac D.H. and Saib K.S., "The Effect of Short Carbon Fibre Reinforced On Fatigue Crack Growth in PEEK", Composite Part A, Elservier Science Ltd. 27A(1996)547-554.

Fish J.C. and O'Brien T.K., Composite Materials, Testing and Design, ASTM STP 1120,348 (1992)

Fujii T. and Maekawa Z., "Fatigue Properties of Fibrous Composite Materials and Some Considerations on the Process of Fatigue," Proc. Of Conf. On Composites Materials. Pp. 155-162 (1981)

Goetchius G.M., " Fatigue of Composites Materials", Conference on Advanced Composites 3 (1987)289-298.

Haener J., Ashbaugh N., Chia C.Y. and Feng M.Y., "Investigation of Micromechanical Behaviour of Fibre Reinforced Plastics", US Army Aviation, Materials Laboratories Tech. Report (1967)67.

Hahn H.T. and Kim R.Y., "Fatigue Behaviour of Composites Laminates", J, Composite Materials 10(1976)156-180.

Hearle J.W.S., Sparrow J.T. and Cross P.M., The Use of the Scanning Electron Microscope, Pergamon Press, Oxford, (1972).

Hemsley D.A., "The Light Microscopy of Polymers", Oxford University Press, Oxford,(1984).

Highsmith A.L., Stinchcomb W.W. and Reifsnider K.L., "Effect of Fatigue-Induced Defects on the Residual Response of Composite Laminates", ASTM STP 836, American Society for Testing and Materials, (1984)194-216

Hitchen S.A., Ogin S.L., and Smith P.A., "Effect of Fibre Length on Fatigue of Short Carbon Fibre/Epoxy Composites", Composites 26(1995)303-308.

Hofer K.E., Skaper G.N., Rao N. and Bennet L.C., "Effect of Moisture on Fatigue and Residual Strength Losses for Various Composites", 41st. Annual Conf. Of Reinforced Plastics/Composites Ints. Soc. Plast. Ind. Inc., New York, (1986)149-155.

Hull D, "Introduction to Composite Materials", Cambridge University Press, (1981).

Hull D. and Clyne T.W., "An Introduction To Composite Material" 2nd. Edition, Cambridge University Press, (1996).

Ishai O., Polymer Engineering Sci., 15(1975)491.

Jamison R.D. and Reifsnider K.L., AFWAL-TR-82-3103, (1982)

Jang B.Z., "Advanced Polymer Composites: Principles and Application", The Materials Information Society, ASM.,US, (1994).

Joneja S.K., "Matrix Contribution to Fatigue Behaviour of Glass Reinforced Polyester Composites", 41st. Annual Conference of Reinforced Plastics/Composites Inst., Soc. Plast. Ind. Inc, New York, (1986)215-220.

Karam G.N., "Effect of Fibre Volume on Tensile Properties of Real Unidirectional Fibre Reinforced Composites", Composite Vol 22, 2(1991)84-88.

Kelly A. and Tyson W.R., J. Mech. Phys. 13(1965)329.

Kujawski D. and Ellyin F., "Rate/Frequency Dependent Behaviour of Fibreglass/Epoxy Laminates in Tensile and Cyclic Loading", Composites, 26(1995)719-723.

Lagace Paul A., Ed., Composites Materials, Fatigue and Fracture, 2nd Edition (1989).

Lagace P.A. and Narendra Bhat, Composite Materials, Testing and Design, ASTM STP 1120,384 (1992)

Lagrange A., Melenea C.H. and Jacquanet R.," Influence of Various Stress Conditions in Distilled Water and in Natural Sea Water", Cardon A.H and Verchery G. (Ed.), Elsevier Science, (1991)385-392.

Leach D.C. and Grover R.l., "Proceedings, 14th. National SAMPE Conference", Society For Advancement of Materials and Process Engineering, (1982).

Leaity M.A., Smith P.A., Bader M.G. and Curtis P.T., " The Behaviour of Cross Ply Hybrid Matrix Composite Laminates", Composite Vol 23, 6(1992).

Lee B.L. and Holl M.W., "Effect of Moisture and Thermal Cycling on in Plane Shear Properties of Graphite Fibre-reinforced Cyanate Ester Resin Composites", Composites 27A(1996)1015-1022.

Lee B.L., Lewis R.W. and Sacher R.E., "Effects of Static Immersion in Water on The Tensile Strength of Cross Ply Laminates", Proc. 2nd. Int. Conf. On composites materials (1978)1560-1583.

Lee J.W., Daniels C.M. and Yanir G., "Composite Materials: Fatigue and Fracture", ASTM STP 1012, American Society For Testing and Materials, Philadelphia, 2(1989)19-28.

Lee M.C. and Peppas N.A., J. Appl. Polymer Science, 47(1983)1349.

Lekatau A., Qian Y., Faidi S.E., Lyon S.B., Islam N. and Newman R.C., "Interfacial Water Transport and Embrittlement in Polymer matrix Composite", Polymer/Inorganic Interfaces, 34(1993)27-32.

Macabder A., Silvergleit M. and Edestein H.P., " Proc. ICM 3, Vol 3", Cambridge, UK, (1979)333-343.

MacKague E.L., Halkias J.E. and Reynolds J.D., "Moisture in Composites: The Effect of Supersonic Service on Diffusion", J. Composite Materials Vol. 9 (1975)2

Madayag A.F., Metal Fatigue, Theory and Design, John Wiley and Son, London, (1969).

Mahfuz H., Zaman K., Haque A., Foy C., Mohamed H. and Jeelani S., "Fatigue Life Prediction of Thick-Section S2-Glass/Vinyl Ester Composites Under Flexural Loading", Journal of Engineering Material and Technology, volume 122, No 4, (2000)402-408.

Mallick P.K., "Fiber Reinforced Composites", Marcel Dekker, Inc., Basel and New York, (1988)214-248.

Mandell J.F., "Long Term Behaviour of Composites", ASTM STP 813, (1982)551.

Marom G., "Application of Fracture Mechanics to Composites Materials", K.Friedrich, Ed., Elsevier, Amsterdam, (1989) chap. 10.

Mashall J.M., Mashall G.P. and Pinzelli R.F. , "Proc. 37th. SPI Conf." Section 9-C(1982).

Mashall P. and Price J., Composite 22(1991)53.

Matthew F.L and Rawlings R.D, "Composite Materials; Engineering and Science", Chapman and Hall Ltd., London, (1994).

McClintock F.A, Journal Applied Mechanics, 22, (1955),3.

McConnell V.P., "Tough Promises From Cyanate Ester", Adv. Composites, 7(1992)28.

Mendenhall W. and Sincich T., "Statistics For Engineering and the Sciences", Fourth Edition, Prentice Hall, 1994,561-568

Morgan R.J., "Environmental Induced Degradation Mechanism of Polymer Matrix Composites", Proceedings of The American Society for Composites, (1987), 250-256.

O'Brien T.K. and Reifsnider K.L. , "Fatigue Damage Evaluation Through Stiffness Measurements in Boron-Epoxy Laminates, J. Composites Material, 15(1981)55-70.

O'Brien T.K., "Towards a Damage Tolerance Philosophy for Composite Materials and Structure, Composites Materials: Testing and Design", vol. 9 ASTM STP 1059 (1990)7-33.

Owen M.J. and Morris S., "Carbon Fibres: Their Composites and Applications", Plastics Institute , London, (1971)292.

Parkyn B., Ed., "Glass Reinforced Plastics", London, ILIFFE Books, (1970).

Phillips E. P., "Fatigue of Fibrous Composite Materials", ASTM STP 723, American Society for Testing and Materials, Philadelphia, (1981)197-212.

Plueddemann E.P., "Silane Coupling Agents ", Plenum Press, New York,(1983).

Purslow D. and Potter R.T., Composites,15,112(1984)

Puškár A. and Golovin S.A.,"Fatigue in Materials: Cumulative damage processes", Materials Sciences Monographs 24, Elsevier, (1985).

Razvan A. and Reifsnider K.L., "Theoretical Application in Fractured Mechanics", 16(1991)81.

Reifsnider K.L., Ed., "Fatigue of Composite Materials", Composite Materials Series, Elsevier, 4(1991)29.

Reifsnider K.L. and Talug A., "Analysis of Fatigue Damage in Composite Laminates", International Journal Fatigue, (1980)3-11.

Reifsnider K.L., Heneke E.G., Stinchcomb W.W. and Duke J.C., "Mechanics of Composite Materials, Recent Advances", American Society For Testing and Materials, Philadelphia, (1983)399-420.

Reifsnider K.L., Modelling of The Interphase in Polymer Matrix Composite Material System", 25(1994)468.

Reifsnider K.L., Schulte K., and Duke J.C, "Long Term Fatigue Behaviour of Composite Materials", ASTM STP 813, O'Brien T.K, Ed., American Society for Testing and Materials, Philadelphia, (1983)136-159.

Rotem A., Composites Science Technology, 46(1993)129.

Roulin-Moloney A. C. Editor, Fractography and Failure Mechanisms of Polymers and Composites, Elsevier Applied Science, London (1989)

Russell A.J., "Micromechanics of Interlaminar Fracture and Fatigue ", Polymer Composites, 8(1987)342-351.

Saib K.S., "The Effects of Microstucture on the Fatigue Behaviour of Short Fibre Reinforced PEEK Composites", PhD, University of Wales, Swansea, (1991).

Sandifier J., "Proc. Progress in Science and Engineering of Composites: ICCM-IV", Tokyo, Japan, (1982)979-986.

Scott Bader Technical Sheets: Crystic 272 (1991), Crestomer 650 & 651 (1995) and Crestomer 1220PA (1996).

Selzer R. and Friedrich K., "Mechanical Properties and Failure Behaviour of Carbon Fibre Reinforced Polymer Composites Under The Influence of Moisture", Composites, Elsevier Science Ltd., 28A(1997)595-604.

Shah Khan M.Z. and Mouritz A.P., "Fatigue Behaviour of Stitched GRP laminates", Composites Science and Technology 56(1996)695-701

Sloan F.E., and Seymour R.J., J. Composite Materials, 26(1992)2655.

Smith K., Hal M.G. and Hay J.N, J. Polymer Sci. Polymer Phy. Ed.,14(1976)751

Springer G.S., Ed., "Environmental Effects on Composite Materials" Vol 1, Technomic Publishing Co., Wesport, CT, (1981).

Stinchcomb W.W. and Bakis C.E., " Fatigue Behaviour of Composite Laminates", Reifsnider K.L. Ed., Vol 4 Composite Materials Series. (1990),105-178

Stinchcomb W.W. and Kriz R.D., " Effects of Moisture, Residual Thermal Curing Stresses and Mechanical Load on The Damage Development in Quasi Isotropic Laminates", ASTM STP 775, Reifsnider K., Ed., American Society for Testing and Materials, Philadelphia, (1982)63-80.

Stinchcomb W.W., Reifsnider K.l., Marcus L.A. and Williams K.S., " Fatigue of Composite Materials", ASTM STP 569, American Society for Testing and Materials, Philadelphia, PA, (1975)115.

Sturgeon J.B., J. Material Science, 13(1978)1490.

Subramaniam S., Elmore J.S., Stinhcomb W.W. and Reifsnider K.L., "The Influence of Fiber Matrix Interphase on The Long Term Behaviour of Graphite/Epoxy Composites", Pergamon Press, New York, (1997).

Subramaniam S., Reifsnider K.L. and Stinchcomb W.W., " A Cumulative Damage Model to Predict The Fatigue Life of Composite Laminates Including The Effect of a Fibre Matrix Interphase", Int. J. Fatigue, 17(1995)343-351.

Swain R.E., PhD Thesis, Virginia Polytechnic Institute and State University, (1992).

Takeda N. and Ogihara S., "Microscopic Fatigue Damage Progress in CFRP Cross-ply Laminates", Composites, 26(1995)859-867.

Talreja R., "Fatigue of Composite Materials", Technomic Publishing Company Inc., (1987).

Thomason J.L., "The Interface Region in Glass Fibre Reinforced Epoxy Resin Composites; Sample Preparation, Void Content and Interfacial Strength, Composites, 26(1995a)467-475.

Thomason J.L., "The Interface Region in Glass Fibre Reinforced Epoxy Resin Composites; Water Absorption, Voids and The Interface, Composites, 26(1995b)477-485.

Wang S.S. and Chim E.S., "Fatigue Damage and Degradation in Random Short-Fibre SMC Compound", J. Composites Material, 17(1983)114-134.

Weitsman Y. and Jackson S.P., "Moisture Effects and Moisture Induced Defects in Composites", 5th. International Conference on Composite Materials, (1985)1435-1452.

Wolff E.G., "Moisture Effects on Polymer Matrix Composites" SAMPE, J., 29(1993)11.

Woo M. and Piggott M.R., J. Composite Technology, 10(1988)20.

Yang J.N., Meskini A., and Yang S.H., School of Engineering and Applied Science, The George Washington University, Washington DC, 20052 USA, "Prediction of Stiffness Degradation of Composite Laminates under Fatigue Loading", International Conference On Advanced Composites Materials and Structures, (1987)467-477.

Yaniv G., Lee J.W. and Daniel I.M., "Damage Development and Shear Modulus Degradation in Graphite/Epoxy Laminates," Composite Materials: Testing and Design (Ninth Volume), ASTM STP 1059, (1990)404-416

Zhuo N., "Fatigue Behaviour and Damage Mechanisms of PEEK/ASA Composites", PhD Thesis, University Of Wales, Swansea, (1995).